

Index

Abstract	5
1 Fundamentals of the Sol–Gel Process	11
1.1 Introduction	11
1.2 Hydrolysis and Condensation Reactions	12
1.2.1 Silica-Based Materials	12
1.2.2 Precursors	17
1.2.3 pH effect	18
1.2.4 Alkoxo Group/H ₂ O Ratio (R _w)	18
1.2.5 Solvent	19
1.2.6 Electrolytes	19
1.3 Metal Oxide-Based Materials	19
1.4 Sol–Gel Transition (Gelation)	21
1.4.1 Hydrolytic Sol–Gel Processes	21
1.4.2 Nonhydrolytic Sol–Gel Processes	24
1.5 Monodisperse Silica Particles via Stöber Process	25
1.5.1 One-step process	26
1.5.2 Two-step process	28
1.5.3 Morphological variations: mesoporous silica	28
1.6 Inorganic–Organic Hybrid Materials	30
1.7 Aging and Drying	30
2 In Situ Sol-gel Synthesis of Hybrid Inorganic–Polymer Nanocomposites	31
2.1 Formation of the Organic Network and Crosslinks between the Organic and Inorganic Components in Hybrids	31
2.2 Nanocomposite Fabrication via Sol–Gel Processes	33
2.3 Epoxy Nanocomposites	33
2.3.1 Effect of Synthesis Procedure and pH on the Structure and Morphology of Nanocomposites	35
2.3.2 The Effect of Silane Coupling Agents	37
3 Flame retardants (FRs) and thermal degradation of epoxy resin	37
3.1 Thermal Degradation of Epoxy Resins	39
3.2 The Use of Flame Retardants	40
3.3 Halogenated Flame Retardants	41
3.4 Alternatives to Halogen Flame Retardants	42
3.4.1 Metal Hydroxides	42
3.4.2 Melamine Polyphosphate	43
3.4.3 Phosphorus Flame Retardants	43
3.4.4 Additive Flame Retardants	45

3.4.5 Reactive Phosphorus Flame Retardants.....	49
4 State of art, major drawbacks and objectives.....	51
4.1 Sol-gel treatments for the surface modification of natural fibers	52
4.1.1 Fire retardancy of biocomposite materials	52
4.1.2 Production and functionalization of natural fibers	56
4.2 Hybrid epoxy nanocomposites	57
4.2.1 Thermal and fire behavior of hybrid silica/epoxy nanocomposites.....	57
4.2.2 Fire retardancy of phosphorous-based in-situ generated silica/epoxy composite materials.....	60
5 Experimental and Methods.....	63
5.1 Materials	63
5.2 Synthesis of the investigated samples and sol-gel methodologies	63
5.2.1 Hemp fabric silica coating.....	63
5.2.2 Manufacturing of hemp fabric/epoxy composites	64
5.2.3 Hemp particles production.....	65
5.2.4 Particles functionalization	65
5.2.5 Synthesis of epoxy composites epoxy/APTS functionalized hemp fibers.....	65
5.2.6 Preparation of the epoxy/silica hybrid nanocomposites	66
5.2.7 Preparation of the in-situ silica/epoxy composites added by phosphorous based flame retardants	67
5.3.1 Scanning electron microscope (SEM-EDX) and inductively coupled plasma optical emission spectroscopy (ICP-OES).....	71
5.3.2 Transmission electron microscope (TEM)	72
5.3.3 Nuclear magnetic resonance (NMR)	74
5.3.4 Fourier transform infra-red (FTIR).....	75
5.3.5 Thermogravimetric analysis (TGA).....	76
5.3.6 Differential scanning calorimetry (DSC) and dynamic mechanical analysis (DMA)	77
5.3.7 Small-angle x-ray scattering (SAXS).....	80
5.3.8 Three-point bending test.....	81
5.3.9 Standard test method for tensile properties of plastics	82
5.3.10 UL94 VB - vertical burning test.....	83
5.3.11 Cone calorimeter.....	85
5.3.12 Pyrolysis combustion flow calorimeter (PCFC).....	86
5.3.13 Pyrolysis–gas chromatography–mass spectrometry (Py-GC-MS) and Direct inlet probe mass spectroscopy (DIP-MS).....	87
6 Results and discussion.....	89
6.1 Development of a sol-gel method for the improvement of the flame retardancy of hemp fabric/epoxy composites	89
6.1.1 Characterization of the silica coating	89
6.1.2 Solid-state NMR spectroscopy of the hemp fibers	91
6.1.3 Thermogravimetric Analysis of hemp fabric/epoxy composites	93

6.1.4 Cone Calorimetry Tests of hemp fabric/epoxy composites.....	95
6.1.5 Three-Point Bending Tests of hemp fabric/epoxy composites.....	98
6.2 A new sol-gel method for the production of hemp fibers through a waterglass based green process .	100
6.2.1 Sol-gel preparation and characterization of hemp fibers	100
6.2.2 Scanning Electron Microscopy observations of epoxy/APTS functionalized hemp fibers composites	104
6.2.3 Dynamic Mechanical Analysis of epoxy/APTS functionalized hemp fibers composites	105
6.3 Fire behavior study of in-situ generated silica/epoxy hybrids.....	107
6.3.1 Characterization of the epoxy/silica hybrid nanocomposites	107
6.3.2 Morphology of the epoxy/silica hybrid systems.....	109
6.3.3 Small Angle X-ray diffraction analysis of the epoxy/silica hybrid nanocomposites.....	111
6.3.4 Dynamic Mechanical Analysis of the epoxy/silica hybrid nanocomposites	112
6.3.5 Solid-state NMR spectroscopy of the epoxy/silica hybrid systems.....	115
6.3.6 Fire behavior of the epoxy/silica hybrid systems	117
6.4 Phosphorous-based in-situ generated silica/epoxy materials	120
6.4.1 Chemical, thermal and mechanical characterization of the in-situ silica/epoxy composites.....	120
6.4.2 Fire behavior of the in-situ generated silica/epoxy materials	127
6.4.3 Thermogravimetric Analysis (TGA), Pyrolysis Combustion Flow Caloremeter (PCFC), Pyrolysis– Gas Chromatography–Mass (PY-GC-MS) and Direct Insertion Probe–Mass Spectrometry (DIP-MS) and analysis of the char produced in the UL test.....	140
Conclusions	160
References	163

Abstract

The sol–gel synthesis route has been extensively exploited since the 1970s, in combination with polymer synthesis methodologies, to produce not only inorganic materials (glassy or ceramic) but also hybrid organic/inorganic composites in the form of aerogels, monoliths, coatings, fibers, and particles. The strategy takes advantage of the fact that almost all the important oxides MO_n (where M is a metal or semimetal and n is not necessarily an integer), as well as many mixed oxides, have been prepared by the sol–gel process through reactions occurring at low temperatures starting from precursors that are commercially available at high purity. Moreover, a great number of organometallic compounds are available, allowing easy surface functionalization and interface tailoring. Sol–gel synthesis also allows the easy production of particles at the nanoscale, where materials properties change [Dehghanhadikolaei 2018]. Moreover, the sol–gel process has been extensively employed as the most important route in tailoring textile surfaces and in forming new hybrid inorganic–organic materials. This is because this process can modify the chemical nature of material surfaces and introduce ceramic phases into composites through chemistry. Very mild reaction conditions and low reaction temperatures are particularly useful for incorporating inorganic moieties into organic materials or organic materials into inorganic matrices. The author of this PhD thesis has applied the sol-gel methodology to solve industrial and technological problems inherent to the use of polymer based bio-composites. These composites can show severe limitations due to the easy flammability of the polymer matrix: this behavior can significantly restrict the application fields of these materials, especially when the possibility of the use of the composites is strictly related to specific regulatory fire tests that have to be passed, hence ensuring public safety (e.g., in the aerospace industry). Additional limitations descend from the mechanical properties of the above mentioned bio-composites, which may be due to a low interfacial adhesion between the filler (e.g., natural fibers) and the polymer matrix. Sol-gel methodologies can improve the fire behavior and the mechanical properties of bio-composites through the in-situ synthesis of ceramic domains in the polymer network or the tailoring of the interphase between filler and matrix.

In the last ten years, the interest in natural fiber-reinforced polymer composites exhibited a significant growth as far as fundamental research and their industrial applications are considered: indeed, these materials are cheap, fully or partially recyclable and also biodegradable. Apart from wood, such plants as flax, jute, sisal, kenaf, cotton, hemp, bamboo, banana, pineapple, ramie, etc., have been utilized as a source of lignocellulosic fibers and very often exploited as the reinforcement of composites. Their convenience, renewability, low density and price, as well as acceptable mechanical features make them very attractive “green” alternatives to glass, carbon and man-made

fibers, commonly employed for the manufacturing of composites. One of the major drawbacks of the aforementioned composites, including those containing hemp, is their ease of flammability when exposed to a heat flux or a flame source: this behavior can significantly restrict the application fields of these materials, especially when the possibility of the use of the composites is strictly related to specific regulatory fire tests that have to be passed, hence ensuring public safety. The fire retardancy of composite materials can be enhanced exploiting different strategies [Grexa 2001, Grexa 2003, Lazko 2013]. In this PhD thesis, a new, inexpensive, simple and ecofriendly sol-gel chemical strategy will be shown to coat hemp fabrics with a silica-based fire retardant layer, obtained by using a waterglass coating prepared in acidic conditions. Hemp fabric/epoxy composites are prepared by using vacuum bag molding. In parallel, Ammonium Polyphosphate (APP), a very well-known flame retardant, is added to epoxy resin, aiming at assessing the possible joint effects of the flame retardant with the waterglass treatment. The exploitation of the hemp surface treatment and Ammonium Polyphosphate (APP) addition to epoxy favors a remarkable decrease of the Heat Release Rate (HRR), Total Heat Release (THR), Total Smoke Release (TSR) and Specific Extinction Area (SEA) (respectively by 83%, 35%, 45% and 44%) as compared to untreated hemp/epoxy composites, favoring the formation of a very stable char. The fire behavior of the obtained composites and the effect of the modification of hemp fabrics with the waterglass treatment are assessed through fire tests and several chemical analysis methods.

Natural fibers and nanocellulose materials are used as reinforcement for polymer composites. Nanocellulose materials can be mainly of three types: nano- or microfibrillated cellulose, nanocrystalline cellulose, bacterial nano-cellulose [Sharma 2019]. These reinforcements are produced from various sources mainly through four mechanical methods: homogenization, microfluidization, microgrinding and cryocrushing. The drawbacks of the production processes are fibers entanglement and clogging of the mechanical apparatus and mechanical energy consumption. The mechanical energy consumption is obviously a function of the degree of fibrillation. Recently the detection of biological and chemical pre-treatment methods allowing an easier mechanical disintegration. However, the research keeps on looking for new synthesis methods allowing, also, if possible, to have products of superior properties. Another challenge in the use of microfibrillated cellulose comes from the hydrophilic character of cellulose and the tendency to form strong network held together by hydrogen bonds. Many methods of surface modification to have them well dispersed in non-polar polymer matrices (e.g., epoxy resin) were proposed and discussed in the literature [Hubbe 2008, Missoum 2013, Nechyporchuk 2016]. In this PhD thesis, a new pretreatment that allows to have hemp fibers with diameters from tens of microns to tens of nanometers with the aid of a low power mixer will be shown. The pretreatment creates, also, a silica

layer that allows easy surface modification with the so many organometallic silanes commercially available. The method exploits the sol-gel chemical strategy used by the author to coat hemp fabrics with a silica-based fire retardant layer. It is shown that when properly prolonging this eco-friendly process the hemp fabric becomes brittle and easily gives silica coated hemp fibers with the aid of a low power mixer. The silica based coating present on them allows easy functionalization with (3-Aminopropyl)triethoxysilane (APTS). The functionalized fibers are easily dispersed in epoxy resin and, in a concentration of 5%, strongly affects the glass transformation temperature and the storage modulus of the pristine resin. The obtained silica coated hemp fibers and the effect of the functionalization with the coupling agent are assessed through several chemical analysis methods.

Many synthesis routes have been proposed in the literature to produce not only composites but also organic/inorganic hybrid particles where sol-gel chemistry gives the inorganic phase or plays a fundamental role in the coupling: heterocoagulation, layer-by-layer assembly, molecular recognition assembly, grafting through coupling agents, polymerization in multiphase systems, surface-initiated polymerization, sol-gel nanocoating. The mild sol-gel synthesis conditions also allow the inherent difficulty in combining organic with glass and ceramic chemistries due to the traditional wide gap in the typical process temperatures to be overcome. In particular new perspectives are opened by the so-called in situ processes where the inorganic phase is produced in the presence of a polymer or a monomer [Pandey 2011].

It is known that polymeric materials do possess limited properties for many industrial applications. Nowadays, epoxy resins cured with various aliphatic amines are mostly exploited in the field of coatings, adhesives, casting, potting, composites, laminates, and for encapsulating semiconductor devices. These applications are mainly due to the excellent heat, moisture, and chemical resistance and good adhesion to many substrates of the epoxy resins. One of the major drawbacks of the epoxy systems cured with aliphatic amines, is their ease of flammability when exposed to a heat flux or a flame source: this behavior can significantly restrict the application fields of these materials. The use of aromatic hardeners, instead of the aliphatic ones, allow to confer an increased thermal stability and an improved fire behavior to the epoxy resin. However, it is well known that both the use of traditional halogen-based flame-retardants than the use of aromatic hardener lead to generate corrosive/toxic problems for the environment and the workers in the Industry. In this prospect, in-situ generated silica/epoxy hybrid materials (cured with aliphatic amines), i.e., polymer matrices filled with specific, finely dispersed nanofillers, are considered to pave the way for the future combining physico-chemical and thermo-mechanical performances with enhanced flame retardant (FR) behavior. Organic/inorganic systems based on silica/epoxy systems are the most widely

utilized [Matějka 1999, Pandey 2011]. It is known that the thermal stability of epoxy nanocomposites (cured with aliphatic amines) can be improved through the inclusion of silica into the matrix, which favors the char formation and increases its yield: the carbonaceous residue layer acts as a thermal insulator and a barrier to oxygen diffusion. In this PhD thesis, the preparation of new hybrid silica/epoxy composites (with an aliphatic amine as hardener) will be shown. The new hybrid structures consist of very fine silica nanoparticles, homogeneously dispersed in a silica/epoxy hybrid network. The presence of the silica domains prevents melt dripping phenomena in vertical flame spread tests. As assessed by forced-combustion test (Cone Calorimeter), the inorganic domains acts as a thermal protective layer, hence improving the heat and smoke-related parameters. Moreover, a non-isothermal post curing treatment beyond the glass transition temperature of the neat epoxy affects the thermal and mechanical features of the obtained hybrid materials. The fire behavior of the obtained hybrid composites and the morphology treatment silica/epoxy hybrid network are investigated through fire tests and several chemical analysis methods.

In-situ silica/epoxy composite materials (cured with aliphatic amines), added with suitable green phosphorus-based flame retardant allow to combine the absence of dripping phenomena with very good performances in terms of flame retardancy. Phosphorous compounds are considered as potential replacement for toxic flame-retardants (FRs) (i.e., halogen-based FRs), hence they have been synthesized by many researchers [Wendels 2017]. It is well known that phosphorous-based flame retardants may act through a flame inhibition mechanism or by promoting the formation of a carbonaceous char layer which acts as thermal shield and oxygen barrier for the underlying polymer. Among the phosphorus based FRs, development of 9,10-dihydro-9-oxa-10-phosphaphenanthrene-10-oxide (DOPO) and its derivatives:

- 3-(6-oxidodibenzo[c,e][1,2]oxaphosphinin-6-yl)propanamide (DA),
- 6H-dibenz[c,e][1,2]oxaphosphorin,6-[(1-oxido-2,6,7-trioxa-1-phosphabicyclo[2.2.2]oct-4-yl)methoxy]-, 6-oxide (DP),

have gained much attention in the research and industrial community due to their efficient flame retardant action and green properties [Hirsch 2017]. However, the use of additive flame-retardants, such as DOPO and its derivatives, requires high loadings or the addition of a synergist or the use of an aromatic hardener, in the field of the epoxy resins applications, to impart flame retardancy to epoxy resins. The author of this PhD thesis spent six months at Empa Research Institute (St. Gallen, Switzerland) by investigating a new methodology to obtain self-extinguishing in-situ silica/epoxy materials (cured with a cycloaliphatic amine as hardener) and by characterizing the fire behavior of

the prepared materials. This methodology exploits the experience in the field of sol-gel chemistry of the Chemistry Group (University of Naples Federico II) [Branda 2011, Costantini 2009] and the expertise in the flame retardancy field of the Additive and Chemistry Group (Empa Research Institute) [Gaan 2015, Samleia 2018]. Therefore, in this PhD thesis, a new strategy for the preparation of self-extinguishing in-situ silica/epoxy materials will be shown. The strategy exploits the procedure used by the author for the synthesis of the above mentioned hybrid silica/epoxy composites. The classic synthesis route is modified by adding DA or DP (phosphorous-based flame retardants) and eventually melamine just before the addition of the cycloaliphatic hardener. Melamine is added as a source of nitrogen that could play a role of blowing agent. The addition of DA with or without melamine strongly improves the fire behavior of the studied epoxy system until to achieve self-extinguishing capacity, when only 2 wt. % of P-loading is present. Additionally, the presence of only 2% silica guarantees the absence of dripping phenomena during the burning of the epoxy resin. Conversely, DP guarantees absence of dripping phenomena with or without silica but the self-extinguishing is possible only in combination with silica and melamine, and when 2 wt. % of P-loading is present. The fire behavior of the obtained in-situ silica/epoxy composites and the fire retardant mechanisms of the two phosphorous-based additives (DA and DP) are investigated through fire tests and several chemical analysis methods.

References

- Branda, F. (2011). *The sol-gel route to nanocomposites. Advances in Nanocomposites–Synthesis, Characterization and Industrial Applications; Reddy, B., Ed, 323-340.*
- Costantini, A., Luciani, G., Silvestri, B., Tescione, F., & Branda, F. (2009). *From nanocomposite to blend hybrid pHEMA/SiO₂ hydrogels: the effect of chemical coupling on thermal stability, swelling and bioactivity. In Solid State Phenomena (Vol. 151, pp. 118-122). Trans Tech Publications.*
- Dehghanghadikolaei, A., Ansary, J., & Ghoreishi, R. (2018). *Sol-gel process applications: A mini-review. Proceedings of the Nature Research Society, 2(1), 02008.*
- Gaan, S., Liang, S., Mispreuve, H., Perler, H., Naescher, R., & Neisius, M. (2015). *Flame retardant flexible polyurethane foams from novel DOPO-phosphoramidate additives. Polymer degradation and stability, 113, 180-188.*
- Grexa, O., & Lübke, H. (2001). *Flammability parameters of wood tested on a cone calorimeter. Polymer Degradation and Stability, 74(3), 427-432.*
- Grexa, O., Poutch, F., Manikova, D., Martvonova, H., & Bartekova, A. (2003). *Intumescence in fire retardancy of lignocellulosic panels. Polymer degradation and stability, 82(2), 373-377.*
- Hirsch, C., Striegl, B., Mathes, S., Adlhart, C., Edelmann, M., Bono, E., ... & Nyffeler, J. (2017). *Multiparameter toxicity assessment of novel DOPO-derived organophosphorus flame retardants. Archives of toxicology, 91(1), 407-425.*
- Hubbe, M. A., Rojas, O. J., Lucia, L. A., & Sain, M. (2008). *Cellulosic nanocomposites: a review. BioResources, 3(3), 929-980.*
- Lazko, J., Landercy, N., Laoutid, F., Dangreau, L., Huguët, M. H., & Talon, O. (2013). *Flame retardant treatments of insulating agro-materials from flax short fibres. Polymer degradation and stability, 98(5), 1043-1051.*
- Matějka, L., Dušek, K., Pleštil, J., Kříž, J., & Lednický, F. (1999). *Formation and structure of the epoxy-silica hybrids. Polymer, 40(1), 171-181.*

- *Missoum, K., Belgacem, M. N., & Bras, J. (2013). Nanofibrillated cellulose surface modification: a review. Materials, 6(5), 1745-1766.*
- *Nechyporchuk, O., Belgacem, M. N., & Bras, J. (2016). Production of cellulose nanofibrils: A review of recent advances. Industrial Crops and Products, 93, 2-25.*
- *Pandey, S., & Mishra, S. B. (2011). Sol–gel derived organic–inorganic hybrid materials: synthesis, characterizations and applications. Journal of sol-gel science and technology, 59(1), 73-94.*
- *Salmeia, K. A., Gooneie, A., Simonetti, P., Nazir, R., Kaiser, J. P., Rippl, A., ... & Gaan, S. (2018). Comprehensive study on flame retardant polyesters from phosphorus additives. Polymer degradation and stability, 155, 22-34.*
- *Sharma, A., Thakur, M., Bhattacharya, M., Mandal, T., & Goswami, S. (2019). Commercial application of cellulose nano-composites-A review. Biotechnology Reports, e00316.*
- *Wendels, S., Chavez, T., Bonnet, M., Salmeia, K. A., & Gaan, S. (2017). Recent developments in organophosphorus flame retardants containing PC bond and their applications. Materials, 10(7), 784.*

1 Fundamentals of the Sol–Gel Process

1.1 Introduction

Sol–gel materials are therefore metastable solids that are formed in kinetically controlled reactions from molecular precursors, which constitute the building blocks for the later materials. An immediate consequence is that all reaction parameters, including the precursor properties, have a decisive influence on the structure and thus the properties of sol–gel materials [Brinker 2013]:

- A sol is a stable suspension of colloidal particles (nanoparticles) in a liquid. The particles can be amorphous or crystalline, and may have dense, porous, or polymeric substructures. The latter can be due to aggregation of subcolloidal chemical units.
- A gel consists of a porous, three-dimensionally continuous solid network surrounding and supporting a continuous liquid phase (“wet gel”). In most sol–gel systems for the synthesis of oxide materials, gelation (i.e., formation of the gels) is due to the formation of covalent bonds between the sol particles. Gel formation can be reversible when other bonds are involved, such as van der Waals forces or hydrogen bonds. The structure of a gel network depends to a large extent on the size and shape of the sol particles.

The easy agglomeration or aggregation of fine particles (sol particles) is caused by attractive van der Waals forces and/or minimization of the total surface or interfacial energy of the system. In order to prevent aggregation (i.e., to stabilize the sols), repulsive forces of comparable dimensions are required that must be overcome during gelation. Stabilization can be achieved by adsorbing an organic layer (“steric barrier”) or by creating electrostatic repulsion between the particles. This shows the great influence of organic additives and especially ionic species on the gelation behavior, as will be discussed later in more detail. The stability and coagulation of sols is of utmost importance to sol–gel chemistry. Gelation can also be induced by rapid evaporation of the solvent, which is especially important for the preparation of films or fibers. Drying of the initially obtained wet gels by evaporation of the pore liquid gives rise to capillary forces that cause shrinkage of the gel network, often by a factor of 5–10. The resulting dried gels are called xerogels. Due to the drying stress, monolithic gel bodies are often destroyed, and powders are obtained. When a wet gel is dried in a way that the pore and network structure of the gel is retained, the resulting dried gel is called an aerogel.

In the following, the chemical and physical principles behind the individual steps of sol–gel processing will be discussed in more detail.

1.2 Hydrolysis and Condensation Reactions

1.2.1 Silica-Based Materials

The basic chemical principle behind sol–gel processing of silica-based materials is the transformation of Si-OR and Si-OH containing species to siloxane compounds by condensation reactions. From a structural point of view, this corresponds to connecting SiO₄ tetrahedra (or RSiO₃ tetrahedra in hybrid materials) by corner sharing. To obtain a stable gel, the number of siloxane bonds (Si-O-Si) must be maximized and consequently the number of silanol (Si-OH) and alkoxy (Si-OR) groups has to be minimized.

The most common precursors are aqueous solutions of silicates (“water glass”) and silicon alkoxides, Si(OR)₄, mostly tetramethoxysilane (TMOS) or tetraethoxysilane (TEOS). Water glass solutions contain complex mixtures of different monomeric and oligomeric silicate species (i.e., species with negatively charged, nonbridging oxygen atoms), with an approximate average composition of M₂SiO₃ (M=Na, K). The equilibrium compositions of such “metasilicate” solutions are highly dependent on the concentration, pH, metal counterion, temperature, and so on. The point of zero charge (PZC) of Si-OH-containing species is between pH 1.5 and 4.5; the higher the degree of condensation of the silica species, the lower the PZC (the acidity of surface M-OH groups generally depends somewhat on the particle size). Acidifying a solution to a pH below the PZC means that the siliceous species are positively charged, and increasing the pH above the PZC means that the species are negatively charged (Eq. (1.1) and Eq. (1.2)). The silicate species in water glass solutions are stable only under strongly alkaline conditions, because the anionic species reject each other.



The chemical reactions during sol–gel processing can be formally described by three equations (Eq. (1.3), Eq. (1.4) and Eq. (1.5)). In alkoxide-based systems, hydrolysis reactions of Si-OR groups must precede condensation to generate the Si-OH groups, which are necessary for condensation. The fact that the reactive groups must be created in the first place is an important difference to typical organic polymerization reactions. Condensation (i.e., formation of Si-O-Si units) takes place by either alcohol or (more often) water elimination.





The most important differences between the two precursor types are the following:

- Gelation is initiated in aqueous silicate systems by pH changes, and in alkoxide precursor systems by addition of water (hydrolysis reactions to generate Si-OH groups).
- A mixture of a Si(OR)_4 in water and alcohol would react very slowly. Therefore, acid or base catalysis is necessary to start the hydrolysis and condensation reactions of alkoxysilanes.
- The solvent in water glass-based reactions is always water, while the alkoxides are employed either neat or dissolved in an organic solvent. Since many alkoxysilanes are immiscible with water, alcohols are often used to homogenize the reaction mixture (mostly the same alcohol as liberated by the hydrolysis reactions to avoid alcohol exchange reactions).
- Alkoxide-based systems are more complex because more parameters influence the sol–gel reactions. This gives more possibilities to control the texture and properties of the obtained materials.

The use of silicon alkoxides also allows introducing organic groups, by means of organo-substituted derivatives. While sol–gel processing of tetraalkoxysilanes, Si(OR)_4 , results in the formation of silica, SiO_2 , alkoxysilanes of the type $\text{R}'\text{Si(OR)}_3$ ($\text{R}' =$ any hydrolytically stable organic moiety) result in the so-called silsesquioxanes, $\text{R}'\text{SiO}_{3/2}$. In practice, however, alkoxysilane mixtures are processed in most cases, by which any proportion of the organic group(s) R' can be introduced.

The reaction mechanisms are the same for both silicate and alkoxysilane precursors. However, from a mechanistic point of view, reactions under acidic or basic conditions have to be considered separately.

Under acidic conditions, that is, at a pH below the PZC, the oxygen atom of a $\equiv\text{Si-O}^-$, $\equiv\text{Si-OH}$, or $\equiv\text{Si-OR}$ group is protonated in a rapid first step (see Figure 1). A good leaving group (water or alcohol) is thus created. In addition, electron density is withdrawn from the central silicon atom, rendering it more electrophilic and thus more susceptible to attack by water (in hydrolysis reactions) or silanol groups (in condensation reactions).

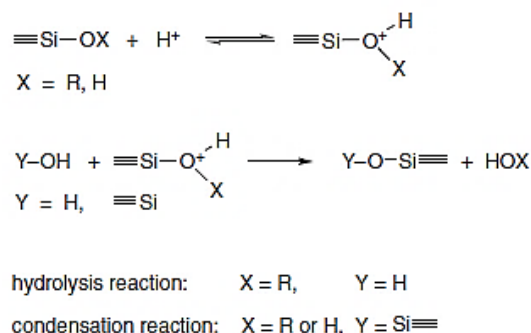


Figure 1: Sol-gel reactions under acid operative conditions [Brinker 2013].

Under basic conditions, the reaction proceeds by nucleophilic attack of either an OH^- (in hydrolysis reactions) or a $\equiv\text{Si-O}^-$ ion (in condensation reactions) to the silicon atom with an $\text{S}_{\text{N}}2$ -type mechanism (see Figure 2). The entering OH^- or $\equiv\text{SiO}^-$ group is formed by deprotonation of water or a $\equiv\text{Si-OH}$ group. Under strongly alkaline conditions, the Si-O-Si bonds can be cleaved again by OH^- .

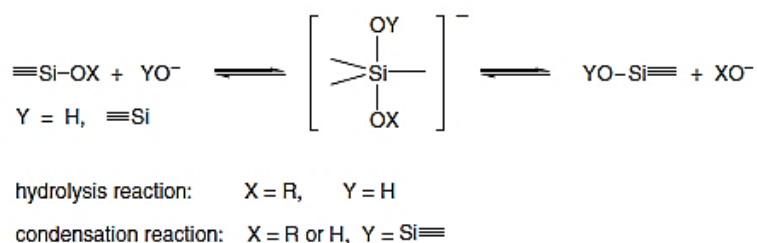


Figure 2: Sol-gel reactions under basic operative conditions [Brinker 2013].

Inductive effects of the substituents attached to a silicon atom are very important, because they stabilize or destabilize the transition states or intermediates during hydrolysis and condensation. The electron density at the silicon atom decreases in the following order:

$$\equiv\text{SiO}-\text{R}' > \equiv\text{SiO}-\text{OR} > \equiv\text{SiO}-\text{OH} > \equiv\text{Si}-\text{O}-\text{Si} \quad (1.6)$$

For acid catalysis, the electron density at the silicon atom should be high because the positive charge of the transition state (Figure 1) is then stabilized best. Therefore, the reaction rates for hydrolysis and condensation under acidic conditions increase in the same order as the electron density. For base catalysis, a negatively charged intermediate has to be stabilized (Figure 2). Therefore, the reaction rates for hydrolysis and condensation increase in the reverse order of the electron density.

This has several consequences, for example:

- As hydrolysis and condensation proceed (increasing number of OH and OSi units attached to a specific silicon atom), the silicon atom becomes more electrophilic. This means, for example, that in acidic media monomeric $\text{Si}(\text{OR})_4$ hydrolyzes faster than partially hydrolyzed $\text{Si}(\text{OR})_{4-x}(\text{OH})_x$ or oligomeric species (which have more Si-O-Si bonds), and vice versa in basic media.
- More branched (i.e., more highly condensed) networks are obtained under basic conditions and chain-like networks under acidic conditions, because reactions at central silicon atoms (i.e., atoms with two or three Si-O-Si bonds) are favored under acidic conditions, and reactions at terminal silicon atoms (i.e., atoms with only one Si-O-Si bond) under basic conditions.
- Organically substituted alkoxy silanes $\text{R}'\text{Si}(\text{OR})_3$ react faster than the corresponding $\text{Si}(\text{OR})_4$ under acidic conditions and slower under basic conditions.
- The acidity of a silanol group increases with the number of Si-O-Si bonds at the silicon atom. This is one of the reasons why the PZC changes with the degree of condensation.

An important feature of the chemistry of silicon alkoxides is that *hydrolysis and condensation reactions* compete during all steps of the sol–gel process. Figure 3 shows the reaction possibilities of a hypothetical trisiloxane intermediate as an example. It can react by either hydrolysis or condensation, and these reactions can occur on chemically different silicon atoms. Note that monomeric species (“cluster–monomer” aggregation leading to extension by one Si-O unit), oligomeric species (“cluster–cluster” aggregation), or even siliceous structures can be involved in the intermolecular condensation reactions

($\equiv\text{Si}$ - in Figure 1.1d and e can be the silicon atom of a monomeric or oligomeric species or of a particle). The situation is even more complex, since each possibility shown in Figure 3 has a different reaction rate, which is influenced to a different degree by the reaction parameters. The same is true for the different intermediates that are formed as hydrolysis and condensation reactions proceed; that is, each intermediate has its own set of kinetic parameters.

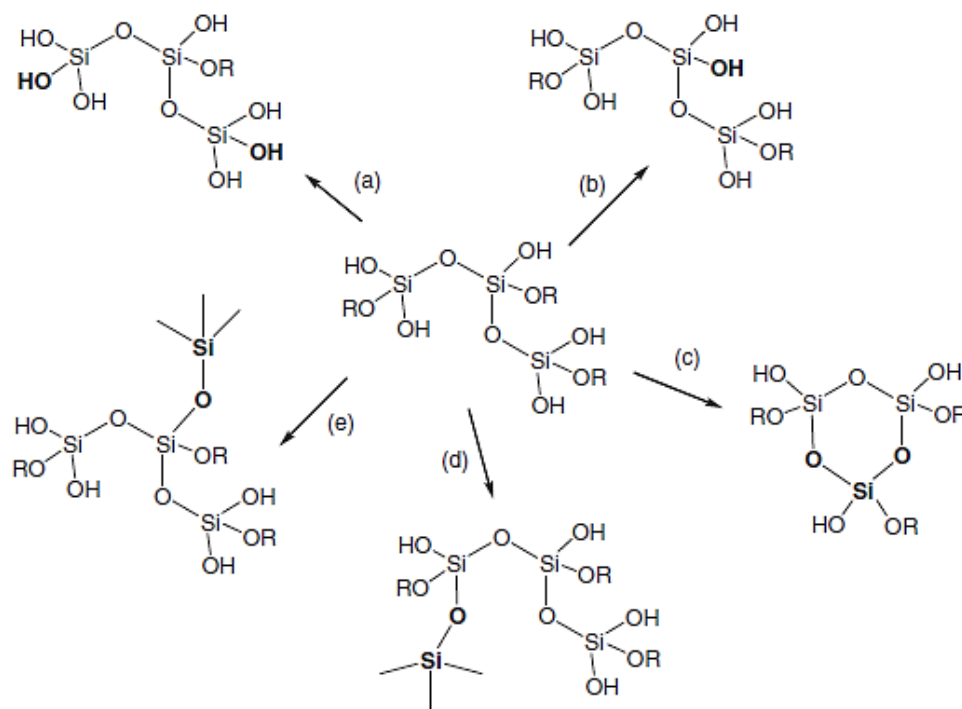


Figure 3: Reaction possibilities of a hypothetical linear trisiloxane intermediate during sol-gel processing of $\text{Si}(\text{OR})_4$: (a) further hydrolysis at terminal positions; (b) further hydrolysis at the central silicon atom; (c) intramolecular condensation leading to a cyclic trisiloxane; (d) intermolecular condensation of a monomeric or oligomeric silicate species at a terminal position; and (e) intermolecular condensation of a monomeric or oligomeric silicate species at the central position.

As indicated in Figure 1.1c, not only linear or branched structures can be formed, but closed structures as well. Many three-dimensional cage compounds, the so-called spherosilicates (Figure 4), with either closed or partially open cages, have been isolated. Such structures can also be substructures of the networks formed during sol-gel processing. Cage compounds $(\text{RSiO}_{1.5})_n$, the so called POSS (polyhedral oligomeric silsesquioxanes), can be similarly obtained from $\text{R}'\text{Si}(\text{OR})_3$. Both POSS and spherosilicates are interesting building blocks for materials syntheses for their own [Pielichowski 2006].

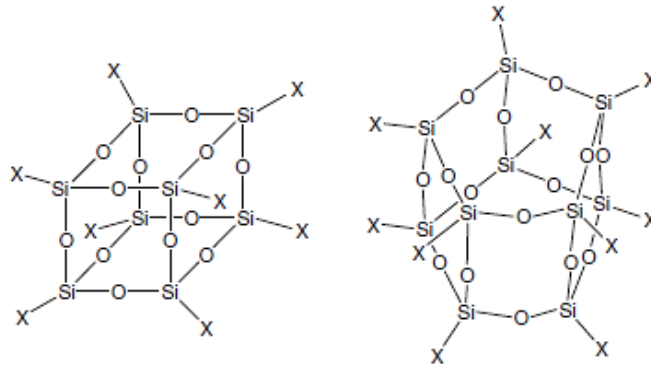


Figure 4: Molecular structures of $(XSiO_{1.5})_n$ cages for $n= 8, 10$; $X=R, H$ (POSS), OH, OR, O^- (sphaerosilicates).

From what has been said, it is obvious that the systems are very complex and many different routes from the molecular precursor to the final silica gel are possible. The chemical parameters discussed in the following determine which route is taken. Because of this complexity, a detailed understanding (and awareness) of the parameters influencing the reaction rates and thus the structure evolution is necessary in order to tailor the texture and properties of sol–gel materials. The most important parameters influencing hydrolysis and condensation (and their relative rate) are:

- the kind of precursor(s),
- the pH (OH^- or H^+ catalysis), or other catalysts,
- the alkoxy group to water ratio (R_w) for alkoxide precursors,
- the kind of solvent,
- the presence of electrolytes,
- the temperature,
- the relative and absolute concentration of the components in the precursor
- mixtures, and other parameters.

1.2.2 Precursors

Different from water glass as a precursor, the Si-OR groups of silicon alkoxides must first be hydrolyzed before condensation reactions can take place. In addition to the inductive effects discussed above, the hydrolysis rates of alkoxysilanes are also influenced by steric factors. Any branching of the alkoxy group or increasing of the chain length lowers the hydrolysis rate of the alkoxysilanes.

1.2.3 pH effect

As discussed above, the reaction mechanisms for acid or base catalysis are very different. Furthermore, the reaction rates for hydrolysis and condensation of silicon alkoxides have different pH dependence (Figure 5).

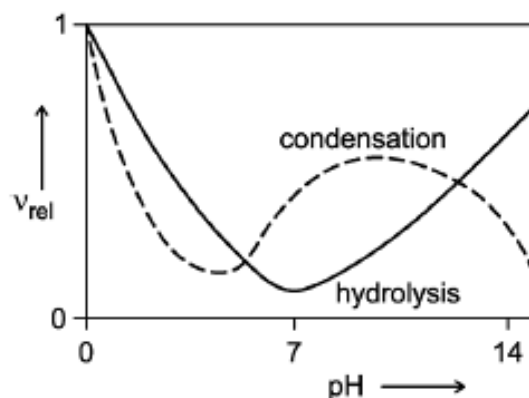


Figure 5: Dependence of the relative rates of Si(OR)₄ hydrolysis and of condensation reactions on the pH.

The minimal reaction rate for hydrolysis is at pH 7, and for condensation at around pH 4.5. The latter corresponds to the PZC of silica. At pH < 5, hydrolysis is favored, and condensation is the rate-determining step. Many monomers or small oligomers with reactive Si-OH groups are simultaneously formed. In contrast, hydrolysis is the rate-determining step at pH > 5, and hydrolyzed species are immediately consumed because of the faster condensation. Catalysis by fluoride ions is similar to that of hydroxide ions (basic conditions). The pH is an especially important parameter to control the texture of gels from water glass solutions. At intermediate pH, the reaction rate of condensation is proportional to the concentration of the OH⁻ ions (see Figure 2). At pH lower than about 2, the silicic acid species are positively charged, and according to the mechanism given in Figure 2, the reaction rate of the condensation is proportional to the concentration of H⁺. Under strongly alkaline conditions, the solutions contain mainly anionic species. For this reason, the rate of Si-O-Si cleavage or redissolution of particles is high at high pH (see Figure 5).

1.2.4 Alkoxo Group/H₂O Ratio (R_w)

The overall reaction for sol-gel processing of tetraalkoxysilanes implies that two equivalents of water (R_w=2) are needed to convert Si(OR)₄ to SiO₂. Four equivalents of water (R_w=1) are needed for the complete hydrolysis of Si(OR)₄ if no condensation would take place. Increasing the water

proportion (i.e., lowering R_w) generally favors the formation of silanol groups over Si-O-Si groups. The R_w , together with the kind of catalyst, thus strongly influences the properties of the silica gels.

1.2.5 Solvent

A solvent may be necessary to homogenize the reaction mixture of alkoxidebased systems, especially at the beginning of the reaction. Polarity, dipole moment, viscosity, and protic or nonprotic behavior of the solvent influence the reaction rates and thus the structure of the final sol-gel material.

1.2.6 Electrolytes

Increasing the electrolyte concentration in a colloidal dispersion compresses the electrical double layer around the particles, because the number of charges required to balance the surface charge is now available in a smaller volume surrounding the particle. The colloid will eventually coagulate because the attractive force between the particles is unchanged, while the repulsive barrier is reduced.

Therefore, the presence of electrolytes (salts) has a strong influence on the gelation behavior. To render sol-gel processes reproducible, special care has to be taken (especially in alkoxide-based systems) not to introduce unwanted salt contaminations in the system, for example, through the water used for hydrolysis of alkoxides. An often-neglected source of ionic species is the counterions of the acids or bases needed for catalysis. The reason why ammonia is mostly used as a base is that it is not ionic. Acids are more problematic, because anionic species (the counterions) are inevitably introduced and influence the reaction rates and the gelation behavior.

1.3 Metal Oxide-Based Materials

Any metal oxide can, in principle, be prepared by sol-gel processing. There are two important differences between silicon (as a semimetal) and typical main group or transition metals that are highly relevant for sol-gel chemistry [Schubert 2003]:

- Metals are more electropositive (Lewis acidic) than silicon and therefore more susceptible to a nucleophilic attack.
- The preferred coordination number of silicon is 4, and is thus equal to its valence (+IV). For metals, especially transition metals, on the other hand, the preferred coordination number is higher than their valence. The increase of the coordination number beyond the valence is

reached by interaction with any nucleophilic (Lewis basic) entity in the system, as will be discussed in more detail below.

As in silicate sol-gel processes, inorganic or metal-organic (alkoxide) precursors can be used. Many metal salts are hydrolytically unstable; that is, they form oxide/hydroxide precipitates from aqueous solutions upon pH changes. This is due to the fact that water molecules coordinated to metal ions are more acidic than those in the noncoordinated state due to charge transfer from the oxygen to the metal atom. The series of equilibria shown in Figure 6 is more easily shifted to the right than in water itself when the pH is increased (i.e., if a base is added).

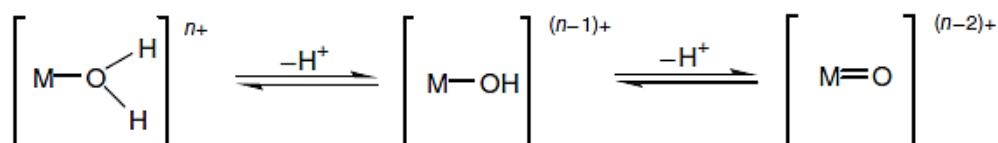


Figure 6: Series of equilibria.

Condensation reactions, that is, formation of M-O-M links with concomitant cleavage of H₂O, require the presence of M-OH units (as for silica, Figures 1 and 2). This means that the equilibria in Figure 6 must be shifted in the M-OH regime, which depends on the valence of the metal and the pH. This is schematically shown in Figure 7. There are three possibilities to shift the equilibria in the M-OH regime:

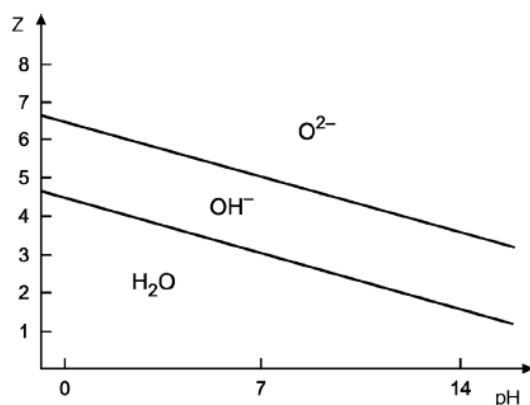


Figure 7: Charge (Z) versus pH diagram indicating the domains of aquo, hydroxo, and oxo species. Note that the lines only roughly indicate transitions between the corresponding domains.

1. Raising the pH corresponds to moving from left to right in Figure 7 for a given valence (Z). For example, when aluminum salts are dissolved in water, the hydrated cation $[\text{Al}(\text{H}_2\text{O})_6]^{3+}$ exists only below pH 3. As the pH is increased, the water ligands are deprotonated, and the

ions $[\text{Al}(\text{OH})_x(\text{H}_2\text{O})_{6-x}]^{(3-x)+}$ are formed. Mononuclear species with $x = 0-4$ are stable only in very dilute solutions; at higher concentrations, polynuclear species are formed by condensation reactions, that is, by formation of Al-O-Al links. Alternatively, the solution can simply be aged at elevated temperatures. A higher temperature promotes dissociation of protons from the hydrated metal ions.

2. Solutions of metallate ions, such as titanates, vanadates, niobates, tantalates, or tungstates, form gels when acidified (right to left in Figure 7 for a given valence).
3. Solutions of oxide species with the metal in high oxidation states can be reduced to give gels (top-down in Figure 7 at a given pH); one of the best-known examples is the formation of MnO_2 gels from MnO_4^- .

As in the case of silica-based sol-gel processes, M-OH groups can also be created by hydrolysis of M-OR groups, that is, by addition of water to metal alkoxides. As outlined above, metal alkoxides are stronger Lewis acids than silicon alkoxides, and the formation of higher coordinated species is easier. Nucleophilic attack at the metal is thus facilitated, and the hydrolysis rates are strongly increased.

1.4 Sol-Gel Transition (Gelation)

1.4.1 Hydrolytic Sol-Gel Processes

The crystalline state of a solid compound is thermodynamically more favorable than the amorphous state. In order that crystallization can occur, however, (crystalline) nuclei must be formed and growth of the nuclei must be possible. If either nucleation or crystal growth is inhibited under a given set of experimental conditions, amorphous materials are formed, which include glass-like materials and gels. The formation of amorphous networks (i.e., networks without a three-dimensional order) is particularly favored if there are many degrees of freedom for the mutual arrangement of the building blocks.

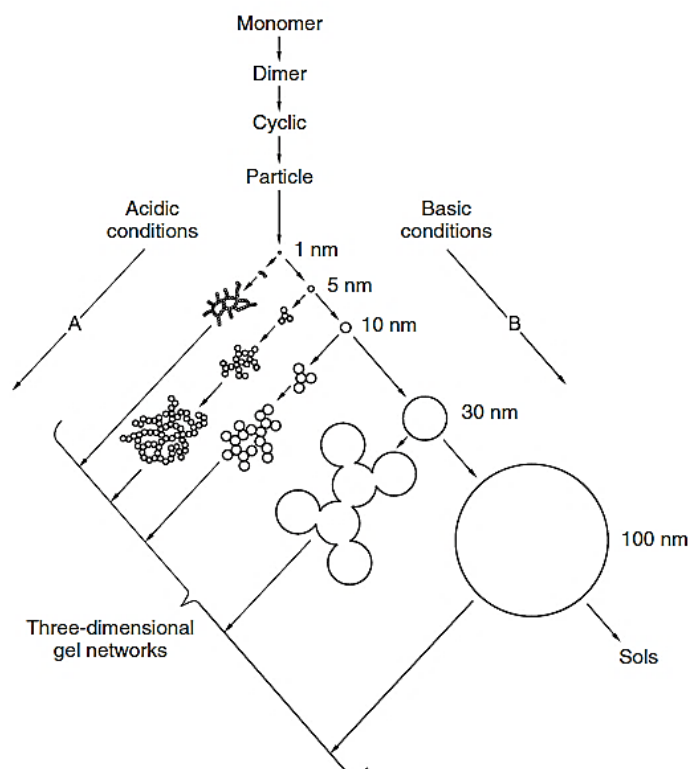


Figure 8: Structural development of silica gels [Iler 1979].

This is the reason why silica-based materials form gels more easily than other oxides, and consequently the chemistry of silica gels is particularly well investigated. The following discussion of gelation is thus focused on silica, but is analogous for other materials. In the initial stage of sol–gel reactions, small three-dimensional oligomeric particles are formed. Figure 8 schematically shows the structural development of silica gels from molecular precursors. Whether the initially formed primary (nano)particles aggregate once they have reached a certain size or continue to grow depends on the experimental conditions. Aggregation of the primary particles may lead to (larger) secondary particles (features at the descending branches in the left part of Figure 8). Whether the particles (with a polymeric or dense substructure) may remain suspended in solution (i.e., form a stable sol) or aggregate to form a three-dimensional network (i.e., a wet gel) again depends on the system and the experimental conditions. The basic chemical processes (hydrolysis and condensation), however, are the same. In nonsilicate systems, the network-forming (nano)particles may be crystalline or semicrystalline.

As the sol particles aggregate and condense, the viscosity of the sol gradually increases. The sol–gel transition (gel point) is reached when a continuous network is formed. Before the gel point has been reached, the colloidal dispersion behaves like a more or less viscous liquid. At the gel point, the viscosity increases sharply, and a form-stable, elastic gel body is obtained. From a practical point of

view, the gel time (t_{gel} =time at which the gel point is reached after starting hydrolysis and condensation reactions) is determined by turning the reaction vessel upside down. Since all liquid is retained in the gel body, no liquid can flow out of the vessel. For the same reason, the volume of the gel in this stage is the same as that of the original precursor solution.

Typical t_{gel} values for $\text{Si}(\text{OEt})_4$ are 92h with 0.05 mol of HCl or 107h with 0.05 mol of NH_4OH as the catalyst. Without a catalyst, t_{gel} would be about 1000h [Pope 1986]. The t_{gel} is generally lowered by all parameters that increase the rate of condensation reactions, as discussed above. These parameters thus allow to deliberately influence the gel times.

A wet gel, by definition, consists of a continuous solid network, the pores of which contain a liquid phase. At the gel point, however, unbound oligomers of various sizes or even monomeric species are still dissolved or dispersed in the pore liquid. This is important for the aging of gels (see below).

The simplest picture of gelation is that the particles grow by aggregation or condensation until they collide to give clusters of particles. (Note that in the models describing gelation, the term “cluster” is used equivalent to “particle” or “oligomeric species.”) The clusters become bigger and bigger by repeated collisions. This process produces clusters of various sizes. In this picture, which is mathematically described by the percolation theory, the gel is formed when the last link between two giant clusters of particles is formed. This is called the “spanning cluster,” that is, a cluster that reaches across the vessel that contains it. Note that the bond resulting in the formation of the spanning cluster is not different from the previously formed bonds; that is, gelation is not a special thermodynamic event.

An alternative description of gelation is given by kinetic growth models. These also explain the different microstructures upon changing the reaction conditions. Depending on the conditions, growth in silicate systems may occur predominantly by condensation of clusters with monomers or with other clusters. The rate of the condensation reactions may be diffusion or reaction limited. As has been discussed before, hydrolysis of silicon alkoxides is faster than condensation under acidic conditions. Since all species are hydrolyzed at an early stage of the reaction, they can condense to form small oligomeric species (clusters) with reactive Si-OH groups. Under these conditions, reactions at terminal silicon atoms are favored (see above). This results in polymer-like gels; that is, small clusters undergo condensation reactions with each other to give a polymer-like network with small pores. Monomer-cluster growth, on the other hand, requires a continuous source of monomers. Hydrolysis is the rate-determining step under basic conditions. The hydrolyzed species are immediately consumed by reaction with existing clusters because of the faster condensation

reactions. Furthermore, the rate of hydrolytic cleavage of (terminal) Si-O-Si bonds is much higher than that under acidic conditions. This additionally ensures that a source of monomers is available.

Condensation of clusters among each other under these conditions is relatively unfavorable because this process requires inversion of one of the silicon atoms involved in the reaction. Reaction at central silicon atoms of an oligomer unit is favored under basic conditions (see above). The resulting network therefore has a particulate character with big particles and large pores (colloidal gels). The formation of larger particles, mainly in aqueous systems, is also favored by Ostwald ripening by which small particles dissolve and larger particles grow by condensation of the dissolved species. Solubility of a particle is inversely proportional to its radius. The solubility of nanoparticles (<5 nm) therefore is rather high. Growth stops when the difference in solubility between the smallest and the largest particles in the system becomes only a few ppm. Solubility depends on the given conditions (temperature, pH of the solution, etc.). At higher temperatures, larger particles are obtained because the solubility of silica is higher. Therefore, materials with a different structure will be obtained by working in solutions of different pH [Hüsing 1998].

1.4.2 Nonhydrolytic Sol–Gel Processes

The conventional (hydrolytic) sol–gel process is based on the hydrolysis and condensation of molecular precursors, leading to oxide networks. The oxo ions originate from water that is added as a reagent or may be formed in situ by water-producing reactions, such as ester formation and aldol condensation [Mutin 2013].

Variations of these reactions have been developed, in which the oxo groups are formed by alkyl chloride, ether, or ester elimination instead of water or alcohol elimination (Eqs. (1.3), (1.4) and (1.5)) in the traditional sol–gel process. This process has been termed the nonhydrolytic sol–gel process because no water is added and the oxygen atoms originate from an organic O-donor. The basic reactions are given in Figure 9.

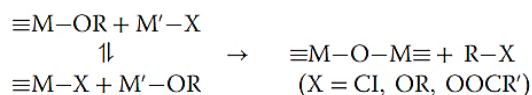


Figure 9: Basic reaction of the nonhydrolytic sol–gel process.

Condensation occurs at temperatures between 20 and 100°C; sometimes, a catalyst is needed (FeCl₃ is often used). The kinetics of nonhydrolytic sol–gel processes depends on the nature of the metal, the nature of the oxygen donor, electronic effects of the group R, and the composition of the initial metal alkoxide/metal chloride (carboxylate) mixture, but is generally slower than that for aqueous

processes. Noteworthy features of this method are that nonhydrated oxides without residual hydroxo groups are obtained, due to the aprotic conditions, and that in bimetallic systems the metals M and M' have an alternate order (no phase separation), due to the reaction mechanism (Figure 9). A limitation of nonhydrolytic processes is that the M/M' ratio is not freely selectable if fully condensed products are targeted. For this reason, sol-gel processes of mixed metal systems are sometimes initiated by nonhydrolytic reactions (to obtain a high homogeneity) and then completed by hydrolytic reactions (to obtain complete hydrolysis and condensation).

1.5 Monodisperse Silica Particles via Stöber Process

The Stöber process is a sol-gel chemical process used to prepare silica (SiO₂) particles [Stöber 1968] of controllable and uniform size [Bogush 1988] for applications in materials science. It was pioneering [Drašar 2016] when it was reported by Werner Stöber and his team in 1968, [Stöber 1968] and remains today the most widely used wet chemistry synthetic approach to silica nanoparticles [Drašar 2016]. It is an example of a sol-gel process wherein a molecular precursor (typically TEOS) is first reacted with water in an alcoholic solution, the resulting molecules then joining together to build larger structures. The reaction produces silica particles with diameters ranging from *50 to 2000 nm*, depending on conditions. The process has been actively researched since its discovery, including efforts to understand its kinetics and mechanism – a particle aggregation model was found to be a better fit for the experimental data [Bogush 1991] than the initially hypothesized LaMer model [LaMer 1950]. The newly acquired understanding has enabled researchers to exert a high degree of control over particle size and distribution and to fine-tune the physical properties of the resulting material in order to suit intended applications.

In 1999 a two-stage modification was reported [Boissière 1999], that allowed the controlled formation of silica particles with small holes [Boissière 2000]. The process is undertaken at low pH in the presence of a surface-active molecule. The hydrolysis step is completed with the formation of a microemulsion [Prouzet 2005] before adding sodium fluoride to start the condensation process. The non-ionic surfactant is burned away to produce empty pores, increasing the surface area and altering the surface characteristics of the resulting particles, allowing for much greater control over the physical properties of the material [Boissière 1999]. Development work has also been undertaken for larger pore structures such as macroporous monoliths [Cademartiri 2009], shell-core particles based on polystyrene [Ding 2004], cyclen [Masse 2009], or polyamines [Masse 2008], and carbon spheres [Liu 2011].

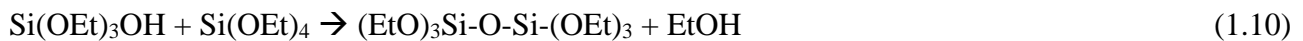
Silica produced using the Stöber process is an ideal material to serve as a model for studying colloid phenomena [Berg 2010] because of the monodispersity (uniformity) of its particle sizes [Boday 2015]. Nanoparticles prepared using the Stöber process have found applications including in the delivery of medications to within cellular structures [Prokop 2014] and in the preparation of biosensors [Ju 2011]. Porous silica Stöber materials have applications in catalysis [Ramirez 2003] and liquid chromatography [Kruk 1999] due to their high surface area and their uniform, tunable, and highly ordered pore structures. Highly effective thermal insulators known as aerogels can also be prepared using Stöber methods [Berg 2010], and Stöber techniques have been applied to prepare non-silica aerogel systems [Qiu 2015]. NASA has prepared silica aerogels with a Stöber-process approach for both the Mars Pathfinder and Stardust missions [Nixon 2012].

1.5.1 One-step process

The Stöber process is a sol-gel approach to preparing monodisperse (uniform) spherical silica (SiO₂) materials that was developed by a team led by Werner Stöber and reported in 1968 [Stöber 1968]. The process, an evolution and extension of research described in Gerhard Kolbe's 1956 Ph.D. dissertation [Kolbe 1956], was an innovative discovery that still has wide applications more than 50 years later [Drašar 2016]. Silica precursor TEOS is hydrolyzed in alcohol (typically methanol or ethanol) in the presence of ammonia as a catalyst [Stöber 1968].



The reaction produces ethanol and a mixture of ethoxysilanols (such as Si(OEt)₃OH, Si(OEt)₂(OH)₂, and even Si(OH)₄), which can then condense with either TEOS or another silanol with loss of alcohol or water [Van Blaaderen 1992] (see Figure 10).



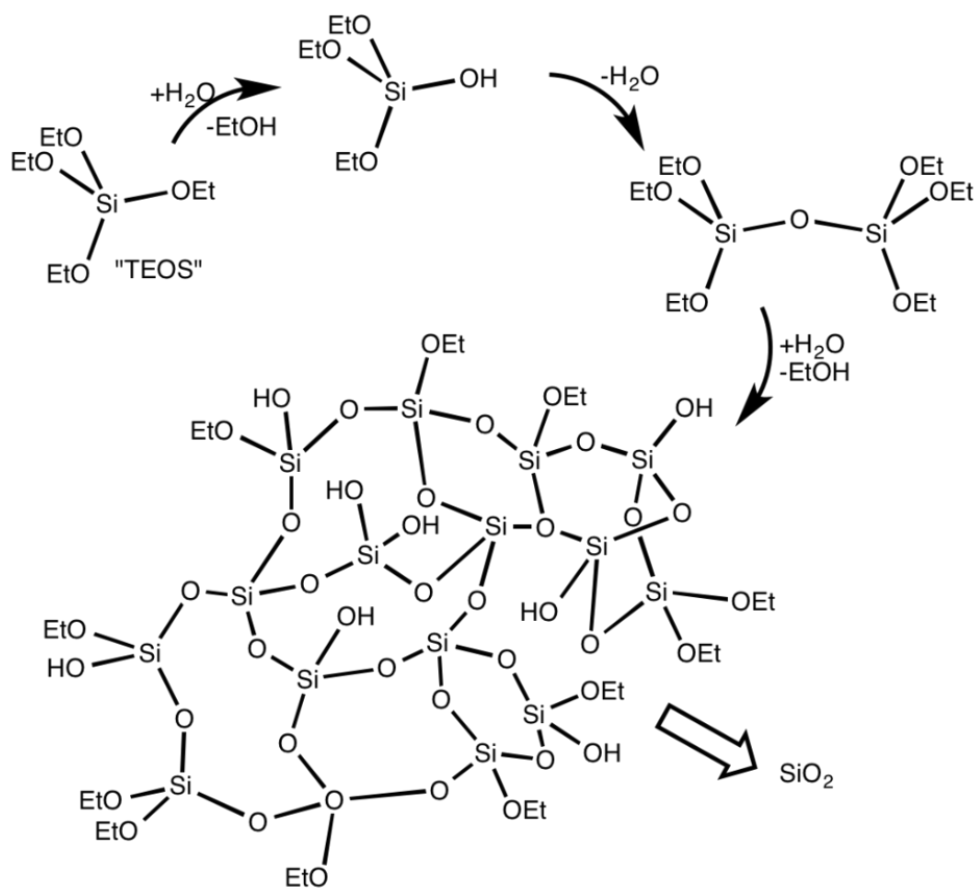


Figure 10: Sol-gel reactions of TEOS silica precursor.

Further hydrolysis of the ethoxy groups and subsequent condensation leads to crosslinking. It is a one-step process as the hydrolysis and condensation reactions occur together in a single reaction vessel [Stöber 1968].

The process affords macroscopic particles of granular silica with diameters ranging from 50 to 2000 nm; particle sizes are fairly uniform with the distribution determined by the choice of conditions such as reactant concentrations, catalysts, and temperature [Bogush 1988]. Larger particles are formed when the concentrations of water and ammonia are raised, but with a consequent broadening of the particle-size distribution [Van Helden 1981]. The initial concentration of TEOS is inversely proportional to the size of the resulting particles; thus, higher concentrations on average lead to smaller particles due to the greater number of nucleation sites, but with a greater spread of sizes. Particles with irregular shapes can result when the initial precursor concentration is too high [Van Helden 1988]. The process is temperature-dependent, with cooling (and hence slower reaction rates) leading to a monotonic increase in average particle size, but control over size distribution cannot be maintained at overly low temperatures [Bogush 1988].

1.5.2 Two-step process

In 1999 Cédric Boissière and his team developed a two-step process whereby the hydrolysis at low pH (1-4) is completed before the condensation reaction is initiated by the addition of sodium fluoride (NaF) [Boissière 1999]. The two-step procedure includes the addition of a nonionic surfactant template to ultimately produce mesoporous silica particles [Boissière 2000]. The main advantage of sequencing the hydrolysis and condensation reactions is the ability to ensure complete homogeneity of the surfactant and the precursor TEOS mixture. Consequently, the diameter and shape of the product particles as well as the pore size are determined solely by the reaction kinetics and the quantity of sodium fluoride introduced; higher relative fluoride levels produces a greater number of nucleation sites and hence smaller particles [Boissière 1999]. Decoupling the hydrolysis and condensation process affords a level of product control that is substantially superior to that afforded by the one-step Stöber process, with particle size controlled nearly completely by the sodium fluoride-to-TEOS ratio [Boissière 1999].

The two-step Stöber process begins with a mixture of TEOS, water, alcohol, and a nonionic surfactant, to which hydrochloric acid is added to produce a microemulsion [Prouzet 2005]. This solution is allowed to stand until hydrolysis is complete, much like in the one-step Stöber process but with the hydrochloric acid replacing the ammonia as catalyst. Sodium fluoride is added to the resulting homogeneous solution, initiating the condensation reaction by acting as nucleation seed [Boissière 1999]. The silica particles are collected by filtration and calcined to remove the nonionic surfactant template by combustion, resulting in the mesoporous silica product.

The selection of conditions for the process allows for control of pore sizes, particle diameter, and their distributions, as in the case of the one-step approach [Boissière 2000]. Porosity in the modified process is controllable through the introduction of a swelling agent, the choice of temperature, and the quantity of sodium fluoride catalyst added. A swelling agent (such as mesitylene) causes increases in volume and hence in pore size, often by solvent absorption, but is limited by the solubility of the agent in the system [Prouzet 2005]. Pore size varies directly with temperature [Boissière 1999], bound by the lower out of the surfactant cloud point and the boiling point of water. Sodium fluoride concentration produces direct but non-linear changes in porosity, with the effect decreasing as the added fluoride concentration tends to an upper limit [Boissière 2001].

1.5.3 Morphological variations: mesoporous silica

Several different structural and compositional motifs can be prepared using the Stöber process by the addition of chemical compounds to the reaction mixture. These additives can interact with the

silica through chemical and/or physical means either during or after the reaction, leading to substantial changes in morphology of the silica particles.

The one-step Stöber process may be modified to manufacture porous silica by adding a surfactant template to the reaction mixture and calcining the resulting particles [Grün 1997]. Surfactants that have been used include cetrimonium bromide [Liu 2006], cetyltrimethylammonium chloride [Kambara 2007], and glycerol [Vacassy 2000]. Calcining the solid leads to removal of the surfactant and solvent molecules by combustion and/or evaporation, leaving mesopore voids throughout the structure, see Figure 11 [Grün 1997].

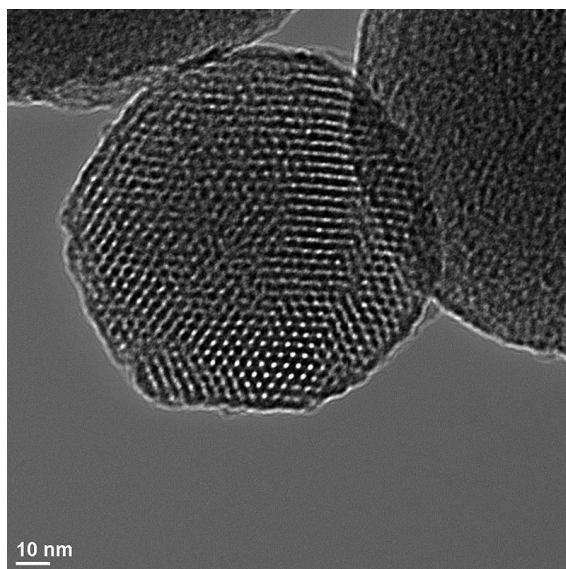


Figure 11: Micrometer- and submicrometer-size spheres of ordered mesoporous oxide [Grün 1997].

Varying the surfactant concentration allows control over the diameter and volume of pores, and thus of the surface area of the product material [Liu 2006]. Increasing the amount of surfactant leads to increases in total pore volume and hence particle surface area, but with individual pore diameters remaining unchanged [Kambara 2007]. Altering the pore diameter can be achieved by varying the amount of ammonia used relative to surfactant concentration; additional ammonia leads to pores with greater diameters, but with a corresponding decrease in total pore volume and particle surface area [Liu 2006]. The time allowed for the reaction to proceed also influences porosity, with greater reaction times leading to increases in total pore volume and particle surface area. Longer reaction times also lead to increases in overall silica particle size and related decreases in the uniformity of the size distribution [Liu 2006].

1.6 Inorganic–Organic Hybrid Materials

One of the major advances of sol–gel processing is undoubtedly the possibility of synthesizing hybrid inorganic–organic hybrid materials, where organic and inorganic building blocks are combined. Sol–gel processing is a very suitable way to make such materials due to the mild processing conditions. The high temperature synthesis route to ceramic materials, for example, does not allow the incorporation of thermally labile organic moieties [Kickelbick 2007].

There are a wide range of possibilities to vary the composition and structure, and thus the properties of hybrid materials:

- chemical composition of the organic and inorganic moieties,
- ratio of the inorganic to organic components,
- kind of interaction between organic and inorganic moieties,
- structure of the building blocks, and distribution of the building blocks (random, block-like, etc.).

Two different approaches can be used for the incorporation of organic groups into an inorganic network by sol–gel processing, namely, embedding of organic molecules into gels without chemical bonding (class I hybrid materials) and incorporation of organic groups through covalent bonding to the gel network (class II hybrid materials).

Embedding of organic molecules is achieved by dissolving them in the precursor solution. The gel matrix is formed around them and traps them, and the organic and inorganic entities interact only weakly with each other. A variety of organic or organometallic molecules can be employed, such as dyes, catalytically active metal complexes, sensor compounds, or even biomolecules or small particles. If sol–gel processing of alkoxides is performed in the solution of an organic polymer, the inorganic network (formed by sol–gel processing) and the organic network interpenetrate but are not bonded to each other. The presence of organic compounds may of course influence gelation because of polarity changes in the system. Very important sol–gel materials are obtained when functional or nonfunctional organic groups are covalently linked to oxide networks (class II materials).

1.7 Aging and Drying

The sharp increase in viscosity at the gel point freezes in a particular network structure. Thus, gelation is structurally related to glass-forming processes. However, this structure may change considerably with time, depending on the temperature, solvent, or pH conditions. It is very

important to realize that the chemical reactions leading to network formation are not finished with gelation, and structural rearrangements take place in the wet gels. This phenomenon increases the stiffness of the gels and is called aging. Controlled aging is an important step when monoliths are prepared. For most practical sol–gel processes, aging plays an indirect role. For example, when films or coatings are deposited, gelation occurs concomitant with or immediately after the deposition process. This is mostly followed by a drying or hardening step. In order to obtain coatings with reproducible properties, the period between deposition and drying/hardening, during which aging occurs, must be kept constant [Hüsing 1998].

2 In Situ Sol-gel Synthesis of Hybrid Inorganic–Polymer Nanocomposites

2.1 Formation of the Organic Network and Crosslinks between the Organic and Inorganic Components in Hybrids

The in situ formation of nanoparticles or an inorganic network via sol–gel methods may occur either in the presence of a preformed polymer (that is already polymerized), or by simultaneous formation of both the organic and inorganic networks, forming an interpenetrating polymer network (IPN) [Zou 2008]. While the inorganic network in hybrids is formed via hydrolysis and condensation reactions, the organic network is formed via polymerization reactions between the monomers, forming macromolecules with repeating units [Gadakh 2016]. The polymers may be classified into two basic types: “addition” and “condensation” polymers.

Figure 12 shows example reactions in the formation of these two types of polymers. Addition polymers are formed by the linking of monomers without the formation of any byproducts. Addition reactions may be initiated by free radicals and propagated by the chain radicals (as shown in Figure 12a). Reactions between radicals or radical transfer reactions can terminate radical polymerization. Alternatively, Ziegler–Natta catalysts may also be used in the synthesis of addition polymers [Adnan 2018]. Polyethylene and polypropylene are common examples of addition polymers. Unlike addition polymers, condensation polymers are typically synthesized using difunctional monomers, or different monomers with end groups that can react with each other to form the chain.

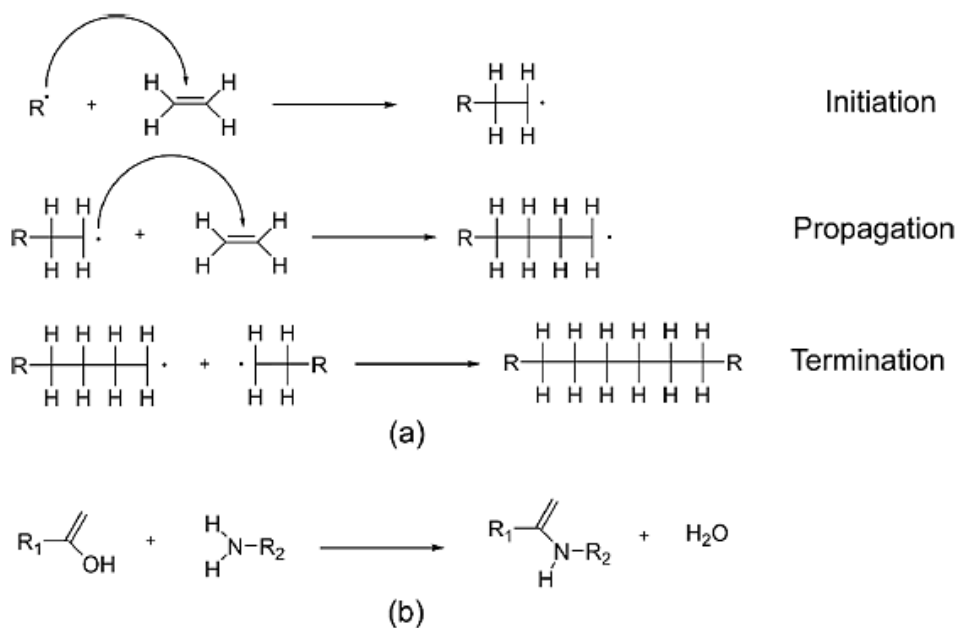


Figure 12: Formation of addition and condensation polymers.

As a result, a small molecular byproduct (e.g., water, methanol, etc.) may also form (as shown in Figure 12b). Branches or crosslinks can form if a trifunctional monomer is present in addition. Polyamides and polyesters are two classes of polymers that form via condensation reactions.

The properties of nanocomposites prepared by the sol–gel process are affected by the size of the particles formed, as well as the interactions between the inorganic and organic components. Strong chemical bonds between the continuous and dispersed phases resulting in the formation of Class II hybrid materials are preferred, since the presence of these bonds will facilitate dispersion and reduce phase separation. However, for these bonds to form, there must be suitable functional groups available on the polymer chains. In some cases, there may be competition for the bonds to form, as these functional groups generally also react with functional groups on other monomers in order to increase the chain length. In other cases, coupling agents may be used to form bridges between the inorganic domains with either the polymer chains or monomer units when there are no suitable functional groups available for bond formation with the inorganic components. Silane coupling agents (SCAs) are one such example and are often used for modifying the surfaces of filler particles in nanocomposites to increase compatibility between the organic and inorganic components [Kango 2013]. These are organosilicon compounds with two different functional groups, typically with the formula $X(CH_2)_nSiR_3$, where X is a functional organic group and R is a hydrolysable group [Mallakpour 2015]. The organic group reacts with the polymer matrix and the hydrolysable group reacts with the surface of the inorganic nanoparticles.

Commonly used SCAs include 3-aminopropyltriethoxysilane (APTS), 3-glycidyloxypropyltrimethoxysilane (GPTMS), 3-isocyanatopropyltriethoxysilane (IPTES), n-decyltriethoxysilane (DTES), and methacryloxypropyltrimethoxysilane (MPTMS) [Kango 2013, Mallakpour 2015].

The SCAs may be introduced to the nanocomposites via several paths, including copolymerization with the monomers and reaction with the preformed polymer or the silicon precursor (or a mixture of the two). Modification of the preformed polymer by the SCA before the sol–gel process is the frequently used approach [Afzal 2011, Jiao 2013, Kango 2013, Mallakpour 2015, Zou 2008], allowing polycondensation reactions between the trialkoxysilyl groups on the SCA bonded to the polymer and the metal alkoxide precursor, forming a covalent bond between the two phases.

In addition to SCAs, other coupling agents include carboxylic acids (e.g., oleic acid, tetrafluorobenzoic acid, etc.), polymer/copolymer chains (e.g., poly(ethylene glycol), polymethyl methacrylate, poly(glycidyl methacrylate), etc.), and organophosphorus molecules (e.g., phosphonic acids, aminophenyl phosphate, etc.) [Afzal 2011, Jiao 2013, Kango 2013, Mallakpour 2015, Zou 2008].

2.2 Nanocomposite Fabrication via Sol–Gel Processes

The inorganic components of the nanocomposites are primarily transition metal oxides (e.g., TiO₂, ZrO₂, etc.) or silica (SiO₂). In the literature, it is common that the authors do not specify the inorganic component in the hybrids as nanoparticles, but instead as nanodomains. This is most likely because the inorganic networks formed are so small and polymer-like that they may not qualify as particles with a defined shape (e.g., spheres). This is more prevalent in the works on polydimethylsiloxane (PDMS) nanocomposites, where the hybrids are called, for example, M–O–PDMS (where M is the transition metal) instead of PDMS–M_xO_y nanocomposites. The previously mentioned inorganic components are based on the assumption that these inorganic networks will form nanoparticles if they grow to an appreciable size. The chemistry behind the synthesis routes, the effect of various parameters on the inorganic structures formed, as well as the resulting properties of the nanocomposites have been deeply investigated [Almeida 2014, Bi 2014].

2.3 Epoxy Nanocomposites

Epoxy is a thermosetting polymer and an excellent choice for high performance composite materials when reinforced with SiO₂ due to the resulting strength, toughness, good chemical and heat resistance, and high thermal stability [Afzal 2011, Almeida 2014, Bi 2014]. Typically, epoxy composites are cured via a condensation reaction with an amine- or anhydride-based curing agent,

forming a copolymer. Epoxy nanocomposites containing titania (TiO_2) are also of interest due to the photocatalytic properties imparted to the polymer by the TiO_2 , as well as increases in the refractive index [Guan 2006, Lü 2009, Sangermano 2006]. Due to the challenges with achieving a homogeneous dispersion of nanoparticles when employing a traditional ex situ blending route, there has been an increased focus on the use of in situ sol-gel techniques instead for nanocomposite synthesis. Diglycidyl ether of bisphenol A (DGEBA) is commonly used as the monomer, and poly(oxypropylene diamine), also known as Jeffamine, is often used as the curing agent in these nanocomposites.

For synthesizing nanoparticles in situ in epoxy, most researchers have attempted either a *one-step* or a *two-step* procedure, as shown in Figure 13.

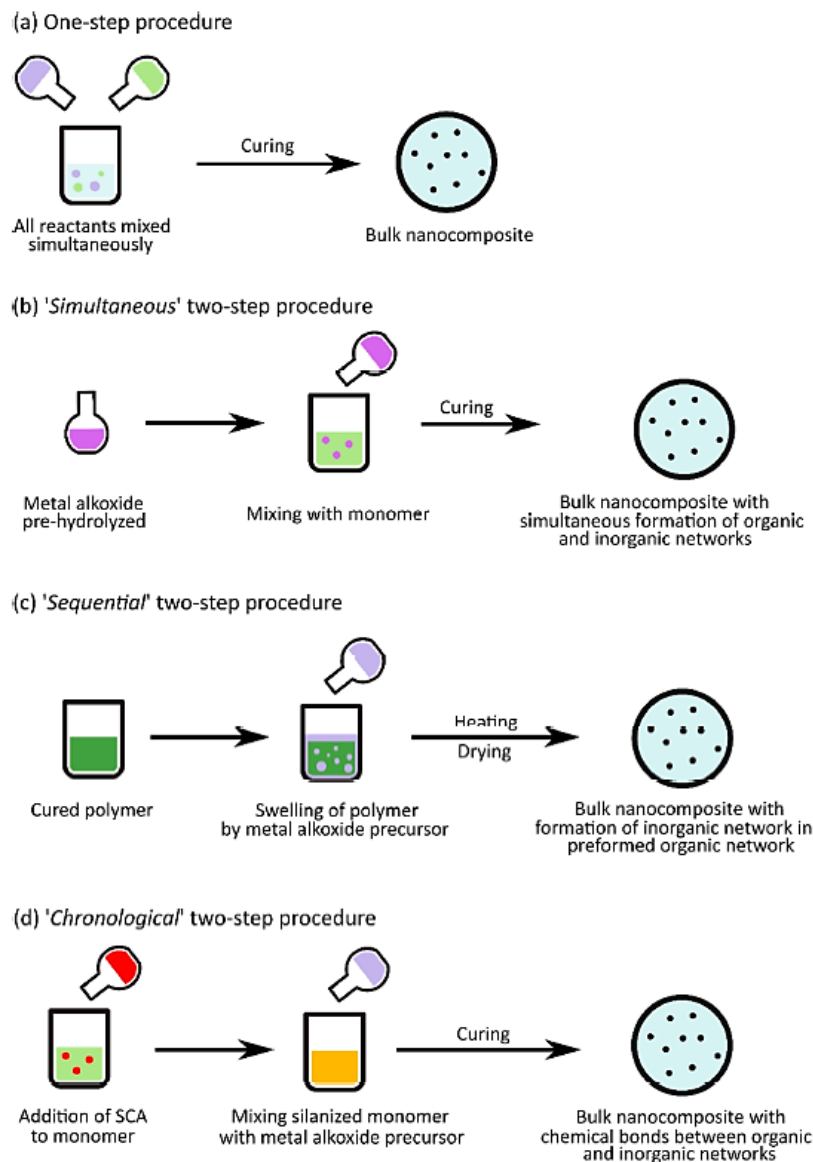


Figure 13: Synthesis of in situ nanoparticles in epoxy resin.

In the one-step procedure, the precursors and reaction components (epoxy resin, coupling agent, inorganic oxide precursor, curing agent, solvent, catalysts, etc.) are all mixed simultaneously and reacted, before being cast into bulk films. There are several variations of the two-step procedure. In a ‘simultaneous’ two-step procedure, the inorganic oxide precursor (TEOS, TIP (titanium (IV) isopropoxide), etc.) is pre-hydrolyzed in the first step using a catalyst (e.g., p-toluenesulfonic acid monohydrate (TSA) or dibutyltin dilaurate (DBTDL)). The second step involves the polymerization of the organic components and the formation of the oxide network simultaneously when the pre-hydrolyzed precursor is mixed with the monomer and curing agent. In a ‘sequential’ two-step procedure, the epoxy resin is cured in the first step, before being swollen by the alkoxide, water, catalysts, etc. in the second step. The inorganic oxide network in this case forms in a preformed organic network, as the epoxy is already cured. Finally, there is also the ‘chronological’ two-step procedure where an SCA is first added to the epoxy to form modified (silanized) monomer chains. In the next step, the inorganic precursors (alkoxide, water, catalyst, etc.) are added sequentially to form the oxide network before the nanocomposite is cured. Since the coupling agents provide a chemical bond between the organic and inorganic networks, this procedure results in the formation of Class II hybrids. One of the advantages with a two-step procedure is that it offers more control over specific reactions, depending on which variation of the procedure is used, since not all of the reactions are occurring simultaneously, as in the one-step procedure.

2.3.1 Effect of Synthesis Procedure and pH on the Structure and Morphology of Nanocomposites

Matějka et al. prepared epoxy–SiO₂ nanocomposites using a one-step procedure [Matějka 1998, Matějka 1999, Matějka 2000], a simultaneous two-step procedure [Matějka 1998, Matějka 1999, Matějka 2000], and a sequential two-step procedure [Matějka 2000]. Differences in the structure of the inorganic domains arose based on whether the reaction was carried out in a one-step or two-step procedure. In the one-step procedure, large SiO₂ aggregates (100–300 nm) were observed through scanning electron microscopy (SEM) [Matějka 2000], which was attributed to the reaction being catalyzed by the amine curing agent (a base) due to its molar excess over the acidic catalyst (TSA).

Base catalysis promotes the condensation reaction and the formation of colloidal (spherical) particles. Small angle X-ray scattering (SAXS) experiments revealed compact silica structures with high fractal dimension ($D_m = 2.7$) [Matějka 2000]. For hybrids prepared using the two-step simultaneous process, smaller SiO₂ structures were observed (50–100 nm) with a lower fractal dimension ($D_m = 1.7$), indicating a more open SiO₂ cluster due to the TEOS being pre-hydrolyzed by an acid [Matějka 1998, Matějka 2000]. The choice of catalyst can also affect the morphology—

DBTDL was seen to be less effective at hydrolyzing TEOS than TSA, resulting in more compact SiO₂ clusters ($D_m = 2.5\text{--}2.7$) [Matějka 1998]. In the two-step sequential process, the distribution of the inorganic phase was not uniform, with a higher SiO₂ concentration on the surface. This was due to the inhomogeneous swelling of the epoxy resin by the TEOS. However, the SiO₂ domains were small (10 nm) and formed an open structure ($D_m = 1.9\text{--}2.2$) due to the acid catalysis of the TEOS hydrolysis [Matějka 1998]. Dynamic mechanical analysis (DMA) showed a larger shear storage modulus for the in situ epoxy-SiO₂ nanocomposites compared to pure epoxy [Matějka 1998]. However, this reinforcement was dependent on the procedure used for preparation. Acid pre-hydrolysis of TEOS resulted in higher modulus in the nanocomposites, compared to those prepared without pre-hydrolysis (e.g., in the one-step procedure or when the TEOS was pre-hydrolyzed by pH neutral DBTDL catalyst). The sequential two-step procedure with pre-hydrolyzed TEOS possessed the largest storage modulus. In addition, the loss factor ($\tan \delta$) also decreased and broadened with the inclusion of SiO₂ in epoxy, with the sequential two-step prepared hybrid showing the largest decrease. The observed reinforcement effects are attributed to increasing interphase interactions in the hybrid systems, resulting in a larger immobilized layer of polymer chains around the nanoparticles [Matějka 1998]. The nanocomposites were determined to have a bicontinuous morphology (the SiO₂ forms a continuous phase in the organic matrix) rather than a particulate composite (with dispersed SiO₂ particles), based on agreement of the data with the two different models [Matějka 2000].

Bauer et al. [Bauer 1996] similarly prepared epoxy-SiO₂ nanocomposites using both a one-step procedure and a two-step sequential procedure, but without any additional catalysts. SAXS data (corroborated by TEM images) showed that the nanocomposites prepared using a one-step procedure had extensive phase mixing (slope of -2 in the Porod region), while those prepared using the two-step sequential procedure (with the pre-cured epoxy) were strongly phase-separated (slope of -4 in the Porod region) [Bauer 1996]. The latter result is contrary to that presented by Matějka et al. [Matějka 1999], where the sequential procedure also led to phase mixing (-2 slope in the Porod region). This difference was attributed by Matějka et al. [Matějka 1999] to differences in the temperature of the synthesis (60°C instead of 90°C), with a higher temperature promoting increased grafting between the organic and inorganic networks. Thermogravimetric analysis (TGA) also showed increased thermal stability for the nanocomposites, with the initial mass loss occurring at 20–50 °C higher temperatures than for pure epoxy resin [Bauer 1996]. A decrease in the slope of the thermogravimetric curves (resembling a small plateau) was observed between 400 and 600 °C for pure epoxy resin, corresponding to char formation. This plateau was shifted to higher temperatures for the nanocomposites, with the inorganic network possibly acting as a barrier to the

decomposition of the organics. The skeleton-like morphology of the SiO₂ remaining after the organic burn-off indicated the formation of an interpenetrating polymer network (IPN), similar to the bicontinuous morphology suggested by Matějka et al. [Matějka 2000].

2.3.2 The Effect of Silane Coupling Agents

Several works have also employed the ‘chronological’ two-step procedure in the preparation of epoxy nanocomposites, using SCAs to improve the dispersion of the nanoparticles formed in situ.

Figure 14 shows a schematic for a possible outline of the reactions occurring during this procedure between the DGEBA monomer, the coupling agent, and the precursor. Nazir et al. [Nazir 2010] prepared epoxy–SiO₂ nanocomposites by first modifying the DGEBA monomer with the SCA APTS, followed by sol–gel reaction with TEOS and water and subsequent curing using Jeffamine.

Nanocomposites were also prepared without the SCA using the same synthesis procedure, minus the addition of the APTS [Torrens 2008].

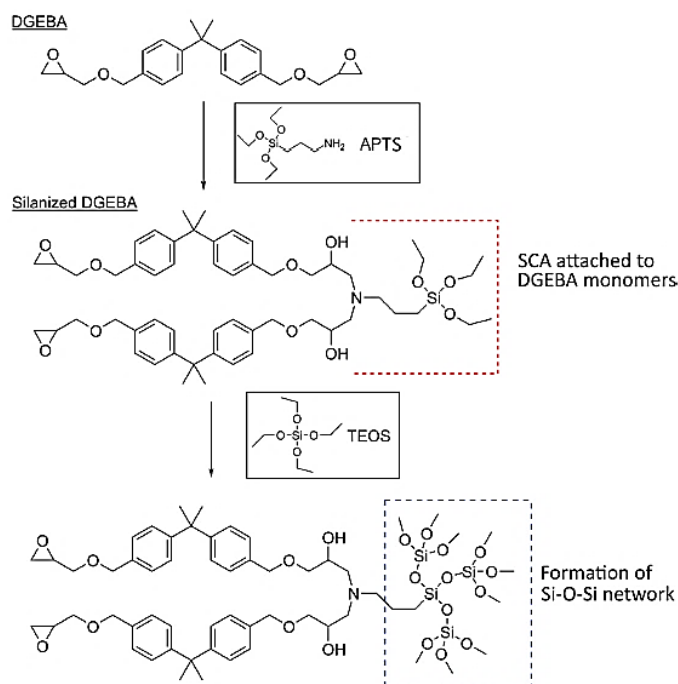


Figure 14 Scheme for a possible outline of the reactions occurring between the DGEBA monomer and the silane coupling agent.

3 Flame retardants (FRs) and thermal degradation of epoxy resin

The term FR subsumes a diverse group of chemicals which are added to manufactured materials, such as plastics and textiles, and surface finishes and coatings. Flame retardants are activated by the presence of an ignition source and are intended to prevent or slow the further development of

ignition by a variety of different physical and chemical methods. They may be added as a copolymer during the polymerization process, or later added to the polymer at a molding or extrusion process or (particularly for textiles) applied as a topical finish [EPA 2005]. Mineral flame retardants are typically additive while organo-halogen and organophosphorus compounds can be either reactive or additive. Plastic combustion process can be stopped by:

- (1) Inhibiting combustion at flame front.
- (2) Removing heat from polymer.
- (3) Preventing polymer decomposition/fuel release.

Each of these approaches can be used alone or combined to generate flame retardancy in a polymeric material. For this reason, each type of flame-retardant falls into a category that fits one or more of the above listed approaches. The general flame-retardant classes can be summarized as follows (see Figure 15):

- Gas phase flame retardants (i.e., halogen, phosphorus): reduce the heat in the gas phase during the combustion by scavenging reactive free radicals (i.e., H and OH radicals), thus inhibiting the degradation process.
- Endothermic flame retardants (i.e., metal hydroxides, carbonates): work in gas phase and condensed phase by releasing non-flammable gases (H_2O , CO_2) which dilutes the fuel and cools the polymer.
- Char forming flame retardants (i.e., intumescent, nanocomposites (containing inorganic oxides as filler for the polymer matrix)): operate in condensed phase by preventing fuel release and providing thermal insulation for underlying polymer.

In the solid phase, the flame retardant forms a carbonaceous layer on the surface of the polymer by dehydration, formation of double bonds, thus initiating cyclization and cross-linking (phosphorous, nitrogen compounds, intumescent systems).

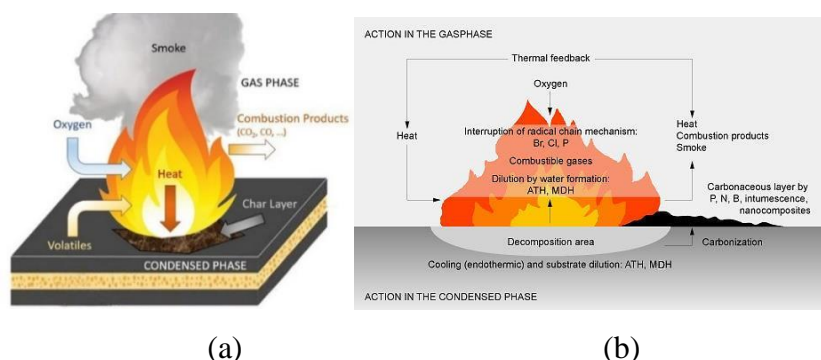
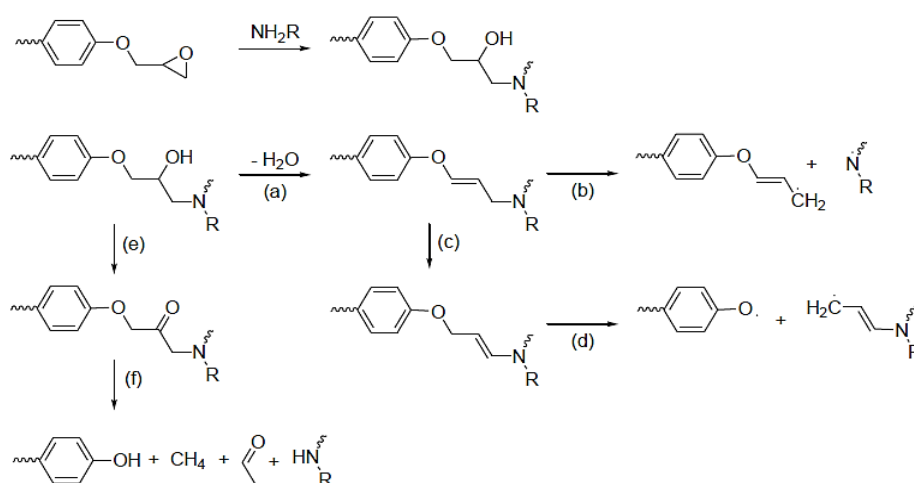


Figure 15: Flame retardant actions (a) and flame retardant classes (b).

3.1 Thermal Degradation of Epoxy Resins

Like other thermoset resins, when exposed to high temperatures (300–400 °C), the organic matrix of the cured epoxy laminate decomposes releasing heat, smoke, soot and toxic volatiles [Vogt 1985]. During the combustion of a polymer, there are generally four different reactions taking place in the condensed phase. The main reactions are end- or random-chain scissions that generate radical species. Simultaneously, various functional groups or atoms that are not part of the polymer backbone can be stripped off. Such a reaction is known as chain stripping. The last dominant reaction occurring is the cross-linking of the different radicals produced during the chain scission to form new thermally stable polymers or char. In the case of epoxy resins, the first step of thermal decomposition is the dehydration or dehydrogenation of the secondary alcohol formed during the cross-linking reaction to yield allylic amides (Scheme 1, a) [Bishop 1970]. The unsaturated moiety can then undergo isomerisation (c) followed by allylic-oxygen bond scission (d) [Bishop 1970]. In the case of amine hardeners the weak C-N bond formed during curing will then undergo allylic-nitrogen bond scission (b) to form volatile particles or contribute to charring [Vogt 1985].



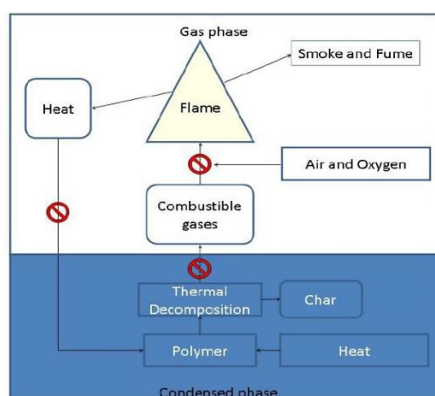
Scheme 1: Thermal degradation paths of an amine cured epoxy resin.

Both the nature of the resin and the hardener determine the thermal stability of the cured resin. When a sample of DGEBA cured with DICY (N,N'-Diisopropylcarbodiimide) is exposed to fire, significant dripping is observed (dripping of molten fuels is a widely observed fire phenomenon, and, by igniting other fuels, it can promote fire spread and increase fire hazards) [Huang 2018], which prevents it from passing UL94 V0 rating (UL94, *Underwriters Laboratories - ISBN 0-7629-0082-2 standard procedure*, is a flammability test used to measure burning rate of standard samples, see chapter 5 for more details) [Laoutid 2009]. UL94 V0 class means that the investigated sample shows a strong tendency to extinguish. However, when novolac epoxy resins are cured using the

same hardener, no dripping is observed. This can be justified by the difference in internal structure of the cured polymer. The high functionality of novolac epoxy resins leads to highly cross-linked structures whereas DGEBA leads to more linear and flexible polymer chains. Hence, under thermal stress, the flexible DGEBA polymer will undergo main chain scission resulting in the formation of smaller polymer chains. The shorter polymer chains formed have lower T_g (glass transition temperature) and will therefore melt and drip off the burning polymer. In contrast, when the highly cross-linked cured novolac epoxy resin undergoes chain scission, the polymer chain length does not endure such a drastic shortening. Hence no dripping is observed.

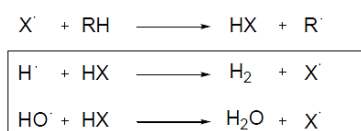
3.2 The Use of Flame Retardants

The fire resistance of the cured resin can however be improved by the addition of a flame retardant. Thus, it is important to know that every application demands a different formulation (using different resins, hardeners and fire retardants). As shown in the flame cycle (Scheme 2) there are different steps where a fire scenario can be stopped.



Scheme 2: Combustion cycle of a polymer fire. Red marks represent the main approaches to extinguish a fire scenario.

A flame retardant can act in the gas phase by inhibition of the exothermic oxidation reaction in the flame via radical scavenging, thus reducing the energy feedback to the polymer surface. Scheme 3 demonstrates how halogenated flame retardants react via radical scavenging [Lewin 2001].



Scheme 3: Gas phase reaction of halogenated flame retardants (X = Cl, Br).

A flame retardant can also promote the formation of a thermal barrier (charring) at the surface of the condensed phase which blocks the release of gaseous fuel and prevents the transfer of heat back to the burning polymer [Vandersall 1971]. An increased char yield results in a reduced amount of

combustible gases reaching the flame which in turn leads to extinction. Flame retardants acting via the latter mechanism are known as condensed phase active because they catalyse the formation of char (see Figure 15).

3.3 Halogenated Flame Retardants

Until recently, the majority of the flame retardants were halogen based and the most widely used one in epoxy resins applications is the reactive tetrabromobisphenol A (TBBPA, see Figure 28). When under thermal stress, bromine based flame retardants such as TBBPA are known to act as flame poisons by releasing volatile bromine radicals that scavenge hydrogen radicals in the flame to form nonflammable hydrogen bromide gas and in turn dilute the flammable oxidants (Scheme 3) [Rakotomalala 2010]. This leads to an interruption in the flame cycle. Such flame retardants are known as gas phase active (Scheme 2).

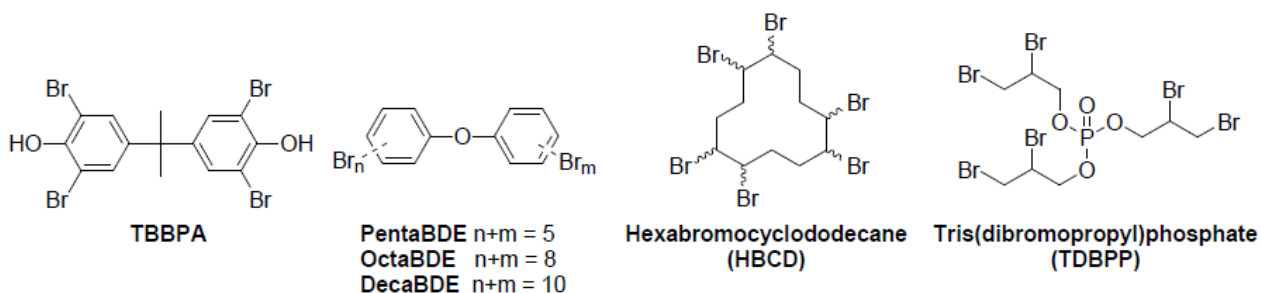


Figure 16: Halogenated flame retardants used for PWB (printed wiring boards).

It should be considered that the primary cause of death in household fires is smoke. The Underwriters Laboratories examined over 20 different combinations of materials found in common households. The result of the study showed that synthetic materials cause hotter fires and an increase in toxic smoke compared to natural furnishings [Rakotomalala 2010]. It is a fact that consumer products, decorations and household objects in general, make home fires distinctively more dangerous. The average escape time for an occupant out of a burning home has dropped from 17 minutes in 1977 to 3 minutes in 2007. A fire retardant system has always limitations which, when exceeded, may lead to a sustained fire. The nature of the flame retardant added has a non-negligible impact on the toxicity of the fumes released [Rakotomalala 2010]. Despite their benefits of slowing down the flame spread or reducing the fire growth, flame retardants can also increase the yield of toxic gases (such as carbon monoxide), or even decompose to toxic gases during a fire scenario (such as hydrogen bromide) [Price 2005]. Halogenated flame retardants in particular are often toxic or even carcinogenic by themselves.

3.4 Alternatives to Halogen Flame Retardants

The alternative compounds to halogen containing flame retardants for will be discussed in this section. They can be separated into three groups:

- Inorganic flame retardants.
- Nitrogen-based flame retardants.
- Phosphorus-based flame retardants.

3.4.1 Metal Hydroxides

Metal hydroxides such as, aluminium hydroxide (ATH) and magnesium hydroxide (MDH) have several positive effects when applied as a flame retardant. They are very cheap, easy to obtain, non toxic and environmentally friendly. Nonetheless very high loadings are required to obtain flame retardancy (~30–60 wt. %). Such high loadings have detrimental effects on the properties of the end product.

They have a strong tendency to react via a condensed phase mechanism. Metal hydroxides decompose to metal oxides and water, which is a highly endothermic reaction detracting energy from the ignition source (Equation 3.1: endothermic reaction of ATH which leads to the release of water).



This flame retardancy mechanism is known as a heat sink. The released water evaporates, thus cooling the surface of the polymer and diluting the burnable gases at the same time [Bourbigot 1999]. The remaining metal oxides form a protective barrier on the polymer surface, shielding it against further decomposition (reducing the heat release rate) and reducing the amount of toxic gases released.

Aluminum-oxide-hydroxide (AlOOH or boehmite) has a much higher thermal stability and can be applied in epoxy systems that undergo lead-free soldering. As mentioned above, lead-free soldering required higher processing temperatures which demands higher thermal stability from the additives used. Prior to lead-free soldering a sample would pass the delamination test at 260°C. However, the currently used system for PWB consisting out of a novolac epoxy resin and DICY as a hardener must endure 288°C without delaminating. Metal hydroxides are often used as synergists with phosphorus based flame retardants (e.g., metal phosphinates).

3.4.2 Melamine Polyphosphate

Melamine polyphosphate (MPP, Figure 17) is mostly used in combination with other flame retardants, such as metal phosphinates, metal hydroxides and phosphates [Hörold 2002]. It is characterised by its good thermal stability and a low impact on the glass transition temperature (T_g). Under thermal stress, melamine derivatives decompose endothermically (heat sink) and release inert nitrogen gases (e.g., ammonia) that dilute oxygen and the flammable gases in the flame. For this reason, melamine and its derivatives have been classified as efficient blowing agent [Bourbigot 2007, Morgan 2013]. Often phosphoric acid is also formed as a decomposition product and promotes the formation of insulating char on the surface of the polymer [Bourbigot 1999, Rakotomalala 2010].

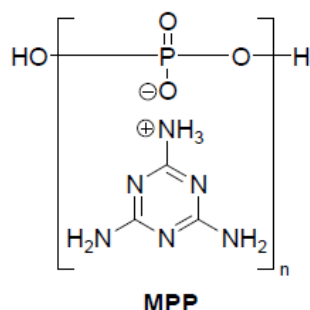


Figure 17: Melamine polyphosphate.

3.4.3 Phosphorus Flame Retardants

Red phosphorus, a long known and very effective fire retardant is mainly used in polyamides, polycarbonates and polyesters [Levchik 1996]. It is nontoxic and thermally stable up to 450 °C. Unlike white phosphorus, red phosphorus is not spontaneously flammable. As a polymer, red phosphorus breaks down during the process of fire to form P_2 molecules that are active species in the gas phase. Red phosphorus reacts with moisture to form toxic phosphine gases, therefore it is important to provide suitable stabilisation and encapsulation. Since red phosphorus has an inherent colour, final products are limited to be brown and red. Toshiba described an adhesive formulation made from a blend of bisphenol A and cresol novolac epoxies using red phosphorus as a flame retardant [Honda 1999]. They achieved UL 94-V0 rating with 4 wt. % red phosphorus (encapsulated in a phenolic resin and coated with ATH) and 25 wt. % ATH as a synergist.

The majority of literature on halogen free flame retardants focuses on phosphorus based products, which are predicted to be the largest growing share of the flame retardant market. Phosphorus flame retardants (organic and inorganic) are in general not harmful and do not tend to form toxic gases

since phosphorus is mostly locked into the char [Rakotomalala 2010]. Under thermal stress, the major part of phosphorus is oxidised to phosphorus pentoxide (P_2O_5) which then hydrolyses to polyphosphoric acid ($H_xP_yO_z$).

Polyphosphoric acid in particular plays an important role in creating carbonaceous char. Phosphorus flame retardants that react via the gas phase form phosphorus containing radicals and gases such as PO and PO_2 derivatives respectively. The newly formed PO and PO_2 derivatives can be rapidly oxidised to P_2O_5 which in turn forms polyphosphoric acid. It was found that non-halogenated phosphorus flame retardants have an environmentally friendly profile [Verbruggen 2006]. The environmental, health and end-of-life properties of 9,10-dihydro-9-oxa-10-phosphaphenanthrene-10-oxide (DOPO, Figure 18), which will be discussed in more detail later on, were investigated very closely [Hu 2017].

In contrast to uncoated red phosphorus, no release of phosphine gases (PH_3) were observed and it was also possible to partly recycle the phosphorus into fertilisers. Nonetheless, there are some reports on toxic and carcinogenic organophosphorus compounds which were used in the past (e.g., tris(dibromopropyl) phosphate) [Prival 1977]. Organophosphorus compounds provide good physical properties and require less loading compared to regular fillers (e.g., ATH). However, a broad application is only gradually taking place since these are still more expensive than conventionally used flame retardants (e.g., ATH or TBBPA see Figure 16). Nonetheless, the production of phosphorus flame retardants on industrial scale will contribute to reduce their price.

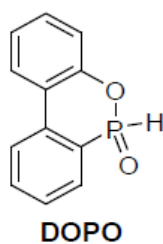
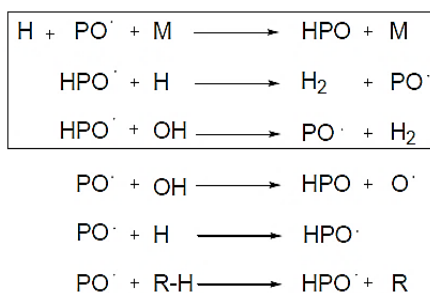


Figure 18: 9,10-dihydro-9-oxa-10-phosphaphenanthrene-10-oxide.

3.4.3.1 Mechanism of Phosphorus Flame Retardants

Although industrial and academic efforts led to numerous phosphorus-based flame retardant solutions, most of the results were based on empirical research. Considering that the degradation of an epoxy resin is strongly dependent on the nature of the resin and the hardener (and other additives) applied, there is no common mechanism of flame retardancy for phosphorus compounds. Phosphorus compounds that promote hydrogen recombination and scavenging of hydroxyl radicals by molecular phosphorus are also classified as gas phase active (Scheme 4) [Rakotomalala 2010].



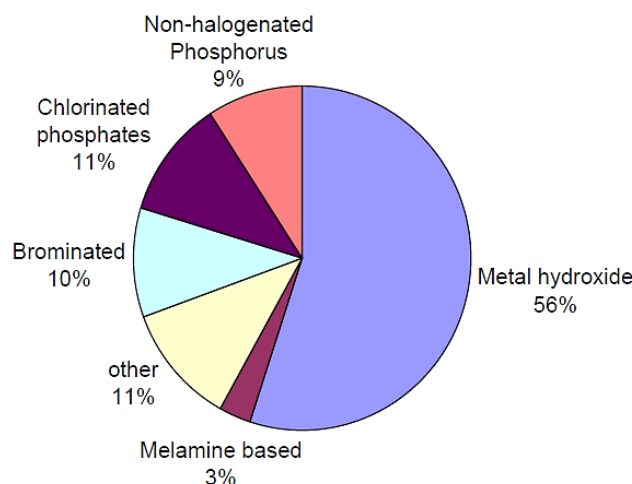
Scheme 4: Elementary steps of the gas phase flame retardation by triphenylphosphine oxide and Exolit OP. The frame is highlighting the process of hydrogen scavenging. M is a third body species [Rakotomalala 2010].

The release of phosphorus-containing volatiles that contribute to the extinction of the flame decreases with oxidation state of the phosphorus [Braun 2006]. Another mode of gas phase activity is the dilution of the flammable gases by the release of inert/non-flammable gases (e.g., H₂O for ATH). Phosphorus based flame retardants tend to form polyphosphoric acids under thermal stress hence promoting the formation of thermally stable polymers (charring). A major benefit of phosphorus flame retardants is that both mechanisms are taking place [Ahmad 2014]. It is possible to promote either mechanism through chemical tailoring. The acid phosphorous compounds [Singh 2009] accelerate the decomposition of char-forming polymers (e.g., epoxy resin); furthermore, the acid character of these compounds altogether with a blowing agent (e.g., melamine or its derivatives) may well produce a swollen multicellular carbonaceous layer [Bourbigot 2007, Morgan 2013]. The acid phosphorus compounds, in fact, are able to promote the dehydration of the epoxy resin producing a carbonaceous layer, which acts as thermal shield and oxygen diffusion barrier [Bourbigot 2007, Liu 2017, Visakh 2015].

There are two ways to render a polymer flame retardant. On the one hand the polymer can be blended with a flame retardant and on the other hand the flame retardant can be introduced to the polymer via a chemical reaction. The main difference between the two pathways is that the flame retardant is either blended as an additive (henceforth referred to as non-reactive FR) or covalently attached to the polymer (henceforth referred to as reactive FR).

3.4.4 Additive Flame Retardants

Both classes of flame retardants, the reactive and the non-reactive have various advantages in different applications. Additives represent the largest market share in flame retarded polymers (see Scheme 5).



Scheme 5: Market shares of different flame retardants for epoxy resin applications (2007) [Rakotomalala 2011].

To reach the desired effect, high loadings are necessary (up to 60 wt. %), which often has a negative impact on the material and mechanical properties of the polymer [Pagliuca 2011]. The use of fillers has the great advantage that most additives (e.g., ATH) are very cheap and widely applicable.

Metal salts of dialkyl phosphinates are known to be effective flame retardants since the late 1970s [Sandler 1979]. Clariant investigated a wide spectrum of zinc, aluminum and calcium salts of dialkyl phosphinates as flame retardants [Kleiner 1998]. Aluminium diethyl phosphinates that were originally developed for glass-fibre reinforced polyamides and polyester achieved UL94 V0 rating in with ~40 wt. % additive [Rakotomalala 2010]. Clariant initiated the production of aluminium salts of diethyl phosphinate, which are commercially available under the brand name Exolit OP 930 and Exolit OP 935 (see Figure 19) [Weferling 2001].

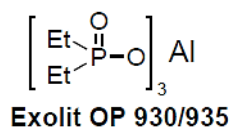


Figure 19: Commercially available aluminium phosphinates.

They now find commercially promising application in PWBs [Hörold 2002]. The flame retardancy of Exolite OP 935 in the phenol novolac epoxy resin commercialised by Dow Chemicals (DEN 438) is summarised in Table 1.

Table 1: Required loading of Exolit OP 935 to achieve UL 94-V0 rating in DEN 438 cured with DICY/Fenuron. Tg measured by Differential Scanning Calorimetry (DSC, see chapter 5) [Huang 2018].

FR	FR-content (wt. %)	Phosphorus-content (wt. %)	UL 94-V rating	Tg (°C)	FR
Exolit OP 935	9.5	2.0	V0	169	Exolit OP 935
Exolit OP 935 + MPP	8 (4+4)	1.6	V0	179	Exolit OP 935 + MPP
Exolit OP 935 + 30% Boehmite	6.1	1.4	V0	171	Exolit OP 935 + 30% Boehmite

Some of the key aspects of metal phosphinates are their high phosphorus content (~17 wt. %), good thermal stability (up to 320 °C) and lower affinity to moisture. Hydrolytic stability is especially important, since the release of phosphoric acids is not tolerated during extrusion or lead-free soldering because of acidic degradation. Schartel et al. investigated aluminium diethyl phosphinates (w/o melamine cyanurate as a synergist) as a flame retardant for polyesters (w/o glass-fibre). The results indicate that diethyl phosphinic acid is released in the gas phase during the decomposition of the polymer. UL94 V0 rating could be achieved with a combined flame retardant loading of 20 wt. % [Braun 2006].

It has been reported that metal phosphinates are most effective in combination with a nitrogen synergist, such as melamine polyphosphate (MPP) [Rakotomalala 2010].

Aromatic phosphates like triphenyl phosphate (TPP) are known to increase the flame retardancy of a polymer. A novolac epoxy resin hardened with DICY/Fenuron passes the UL94 V0 test with only 1.6 wt. % phosphorus (Table 2) [Ciesielski 2008].

Table 2: Synergistic effect of Boehmite and MPP in combination with DOPO in DEN 438 cured with DICY/Fenuron. Tg measured by Differential Scanning Calorimetry (DSC) [Rakotomalala 2010].

FR	FR-content (wt. %)	Phosphorus-content (wt. %)	UL 94-V rating	Tg (°C)
DOPO	11.2	1.6	V0	155
DOPO + MPP	13.0 (6.5+6.5)	2.1	V0	157
DOPO + 30% Boehmite	2.9	0.4	V0	168

A disadvantage of aromatic phosphates is that they are impaired by their reduced hydrolytic stability and often lead to a loss of clarity when blended into a polymer. Thus, they are mainly used

as synergists in combination with bridged aromatic phosphates (e.g., RDP) [Al-Malaika 2001]. Due to its spherical shape, TPP, which is a typical plasticiser, has a negative impact on the physical properties of the cured polymer. Compared to aromatic phosphates, bridged aromatic diphenyl phosphates have found a broad application beyond epoxy resins. The resorcinol and bisphenol A bridged diphenyl phosphates are available under the trade name Fyrolflex RDP and BDP respectively from ICL-IP. In Japan, Daihachi also commercialised RDX, a resorcinol bridged dixylyl phosphate under the trade name PX-200 (Figure 20).

Their main advantages are a good thermal stability (increasing from RDP to RDX), a high flame retardancy and low volatility. However, they are limited by potential plasticising effects and blooming (exudation), which can have a negative influence on electrical properties (current leak). Like TPP, RDP suffers from a hydrolytic instability but BDP and RDX are considerably more stable against moisture due the incorporation of bulkier groups compared to RDP. On the other hand, large groups lead to a lesser phosphorus content. Therefore higher loadings are necessary. UL94 V0 ratings can be achieved with 10 – 20 wt. % additive, depending on the polymer and other synergists applied [Ciesielski 2008]. In the case of BDP UL94 V0 rating could be achieved with 11.5 wt. % flame retardant loading in novolac epoxy resin cured with DICY/Fenuron (Table 3). In contrast to TPP, bridged aromatic diphenyl phosphates are mostly active via a condensed phase mechanism. A strong char yield decreases fuel supply to the flame and reduces the heat release rate.

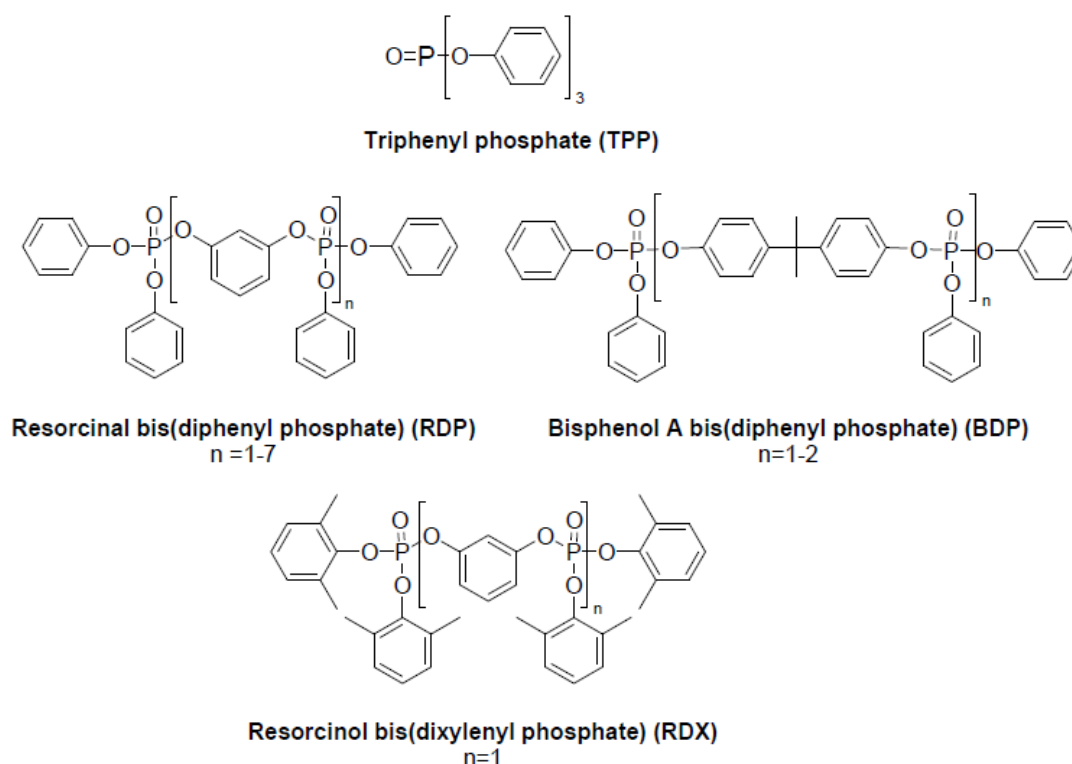


Figure 20: Commercially available phosphates.

Table 3: Tg of the neat resin (DEN 438/DICY/Fenuron) = 181 °C. Tg measured by Differential Scanning Calorimetry (DSC) [Ciesielski 2008].

FR	FR-content (wt. %)	Phosphorus-content (wt. %)	UL94 V rating	Tg (°C)
TPP	16.81	1.6	V0	136
BDP	11.55	2.07	V0	157
BA-(DOP) ₂	10.02	0.99	V0	164
BA-(DOP-S) ₂	15.28	1.41	V0	167
DDM-(DOP) ₂	9.85	0.84	V0	180
DDM-(DOP-S) ₂	12.94	1.22	V0	184

3.4.5 Reactive Phosphorus Flame Retardants

As mentioned above, the use of additive flame retardants, such as MPP, requires high loadings or the addition of a synergist in order to impart flame retardancy to epoxy resins used for epoxy resin applications.

However, it should be specified that similar phosphorus contents are required for DOPO-based additives and for reactive DOPO derivatives to reach UL94 V0 rating. Even though the reactive approach has yet to be adopted in industry, it has been subject to an ever growing interest from the academic community. Indeed, the reactive P-H bond of hydrogen phosphonates or phosphinates enables to covalently bind the flame retardant to the polymer chain by reaction with the epoxy functionality (see Figure 21) [Seibold 2008].

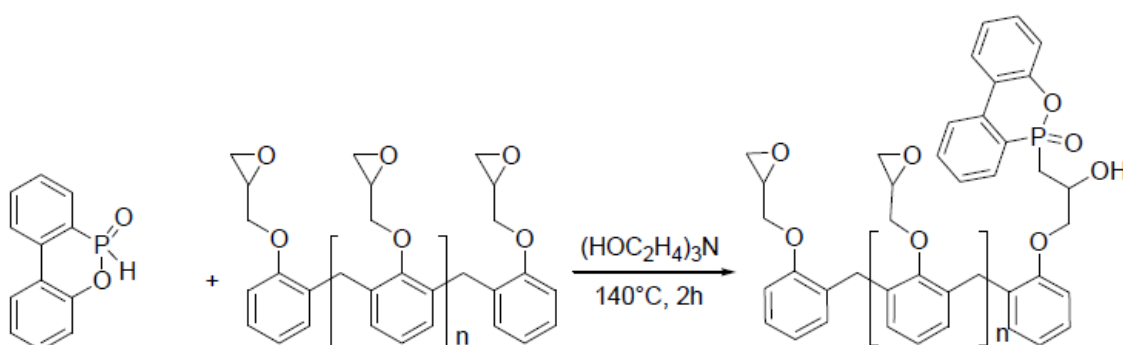


Figure 21: Rendering a novolac epoxy resin flame retardant via chemical incorporation of DOPO [Seibold 2008].

This chemical modification renders the epoxy resin inherently flame retardant. Such an approach could theoretically allow lower phosphorus loadings than the additive approach and also eliminates the risk of flame retardant leaching from the polymer during the polymer processing. There has also

been a growing interest toward phosphorus containing curing agents that would impart flame retardancy while acting as a cross-linker [Hergenrother 2005].

Until now, there has only been a limited amount of industrially relevant reactive phosphorus flame retardants.

9,10-Dihydro-9-oxa-10-phosphaphenanthrene 10-oxide (DOPO, Figure 18), which was developed by Sanko, was successfully pre-reacted with DGEBA (1 – 3 wt. % P) and cured with 4,4'-diaminodiphenylsulfone (DDS, Figure 22) and phenolic novolac (PN, Figure 22) [Rakotomalala 2010]. UL 94 V0 rating was reached with both hardeners with 1.6 and 2.2 wt. % P-loading for DDS and PN respectively.

Only 1.6 wt. % P-loading was necessary in modified novolac epoxy resin cured with DICY/Fenuron to reach a UL 94-V0 rating [Hu 2017, Rakotomalala 2010]. It should be noted that DOPO is the first efficient halogen free flame retardant for novolac-based epoxy systems. It was recently reported that the addition of the inexpensive Boehmit (30 wt. %) significantly reduced the required loading of DOPO (see Table 2) [Hu 2017, Rakotomalala 2010].

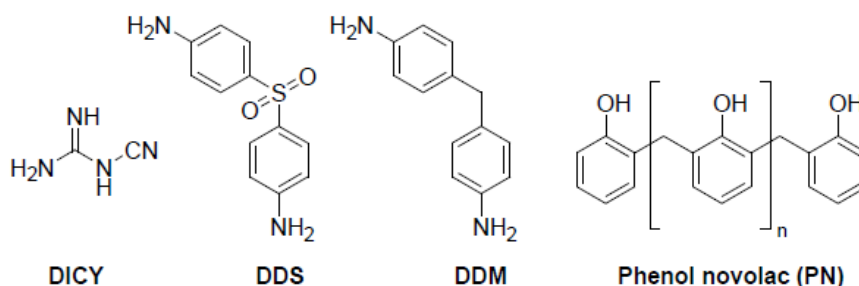
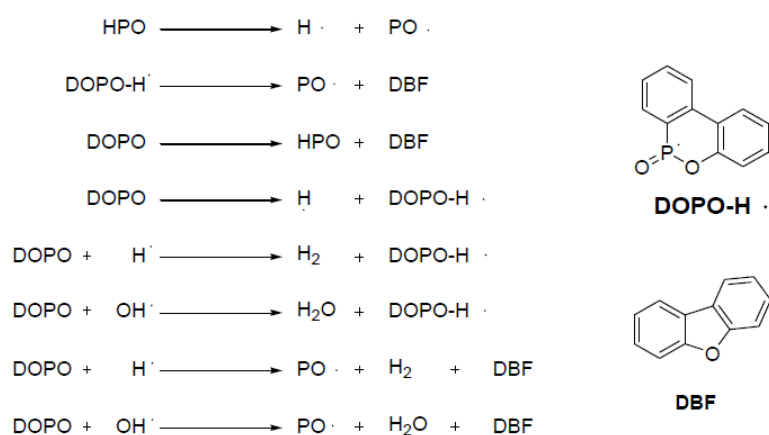


Figure 22: Regularly used hardeners for epoxy resins.

DOPO is thought to act mainly through a gas phase mechanism. To confirm the gas phase activity of DOPO several TD-MS (thermal desorption mass spectroscopy) experiments were carried out and validated by DFT calculations. It indicated that PO and HPO are the gas active specimens (see Scheme 5) [Ciesielski 2009].



Scheme 5: Proposed mechanism for flame retardant reactivity of DOPO in the gas phase.

The reactivity of this mono-functional phosphinates results in a decrease of the functionality of the epoxy resin [Liu 2002]. Such reduction has been shown to have a detrimental impact on the T_g of the cured resin which represent a significant drawback for lead-free soldering that require a T_g over 170 °C.

In order to prevent the reduction of functionality of the epoxy resin, DOPO was reacted with benzoquinone to yield the bifunctional 2-(6-oxido-6H-dibenzo[c,e][1,2]oxaphosphorin-6-yl)1,4-benzenediol (DOPO-HQ, Figure 23) [Wang 1998].

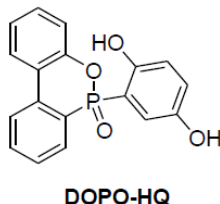


Figure 23: 2-(6-Oxido-6H-dibenzo[c,e][1,2]oxa-phosphorin-6-yl)1,4-benzenediol.

This hydroquinone product is currently commercialised by Sanko in Japan as HCA-HQ. When DOPO-HQ was pre-reacted with DGEBA only 2.1 wt. % P were required to impart flame retardancy. However, the thermal stability of the chain elongated DGEBA is similar to the unmodified cured resin, (T_d (5%, in air)= 397 °C unmodified vs. 401 °C FR). DOPO-HQ was also pre-reacted with a cresol novolac to yield a flame retarded resin with 1.1 wt. % P when cured with phenol novolac [Wang 2001].

4 State of art, major drawbacks and objectives

The sol–gel chemistry offers a flexible approach to obtaining a diverse range of materials. [Dave 2016, Kafshgari 2019, Uche 2013]. For example, scientists have used it to produce the world’s lightest materials and some of its toughest ceramics. It allows differing chemistries to be achieved as well as offering the ability to produce a wide range of nano-/micro-structures. The author of this

PhD thesis wants to show, through the explanation of several research activities, the application of various sol–gel methods. These methods can allow to develop hybrid materials with a significant potential in many industrial fields, because of their unusual composite properties, morphologies and geometries.

This thesis will focus on the peculiar properties in terms of superhydrophobicity and flame retardancy, that can be achieved using suitable sol-gel techniques:

- waterglass silica coating;
- in-situ synthesis of silica nanoparticles;
- functional surface modification by silica-based hybrid systems.

4.1 Sol-gel treatments for the surface modification of natural fibers

4.1.1 Fire retardancy of biocomposite materials

In the last ten years, the interest in natural fiber-reinforced polymer composites exhibited a significant growth as far as fundamental research and their industrial applications are considered: indeed, these materials are not expensive, fully or partially recyclable and also biodegradable [Biagiotti 2004, Puglia 2005, Saxena 2011]. Apart from wood, such plants as flax, jute, sisal, kenaf, cotton, hemp, bamboo, banana, pineapple, ramie, etc., have been utilized as a source of lignocellulosic fibers and very often exploited as the reinforcement of composites. Their convenience, renewability, low density and price, as well as acceptable mechanical features make them very attractive “green” alternatives to glass, carbon and man-made fibers, commonly employed for the manufacturing of composites [Bledzki 1999, Saheb 1999, Wambua 2003].

As compared to synthetic fiber-reinforced composites, the natural fiber-containing counterparts are more environmentally friendly, hence deserving use in a wide range of applications, including transportation (cars, railway coaches, aerospace vehicles), military purposes, building and construction industries (partition boards, ceiling paneling), packaging, consumer products, etc. Among the different natural fibers, despite its current limited availability, hemp is particularly raising interest for green composite manufacturing, as it is an inexpensive renewable resource and shows low density, high specific strength with respect to glass or aramid fibers and good biodegradability, as well [Boccarusso 2016, Szolnoki 2015].

Until the early 1900s, industrial hemp was a valuable crop used all over the world for its strong fibers and oil seeds. Indeed, the Yearbook of the United States Department of Agriculture documents well the significant spread of hemp cultivation all over the world in 1913 [Dewey 1913].

By the 1930s, the commercial cultivation of hemp began to decrease, due to its reduced demand compared to increasingly popular synthetic fibers. Nowadays, hemp is regaining interest for green composite manufacturing, thanks to the ecological and economic advantages over conventional composites.

One of the major drawbacks of the aforementioned composites, including those containing hemp, is their ease of flammability when exposed to a heat flux or a flame source [Kandola 2018]: this behavior can significantly restrict the application fields of these materials, especially when the possibility of the use of the composites is strictly related to specific regulatory fire tests that have to be passed, hence ensuring public safety.

The natural fiber-reinforced composites, when exposed to fire or any other high-intensity heat source, undergo thermal decomposition and combustion processes according to the adopted experimental conditions. In particular, the time to ignition of the composites and the intensity of combustion process are significantly affected by such parameters as heat and mass transfer from and to the composite material, oxygen concentration and the circulation of gas in the area where combustion takes place. Important issues comprise the rate of flame spread, Heat Release Rate (HRR), mass loss and carbonization rates. The ease of the combustibility of a composite material depends on a number of factors, including the nature of the composite and its components (i.e., type of natural fibers and polymer matrices), its density, structure, thermal conductivity, humidity content, and so on.

The fire retardancy of composite materials can be enhanced exploiting different strategies. First, it is possible to add different kinds of fire retardants in liquid or solid form during the manufacturing process: as a result, they are embedded within the composite structure. More specifically [Grexa 2001, Lazko 2013]:

- (1) the natural fibers can be impregnated with a solution of the flame retardant;
- (2) the flame retardant can be incorporated into the adhesive system (e.g., melamine urea formaldehyde condensate, pea protein);
- (3) the fibers can be subjected to a sol-gel surface treatment;
- (4) the fibers can be mixed with the flame retardant before the addition of an adhesive.

In these conditions, the performed treatments should exhibit an acceptable thermal stability that prevents the activation of the flame retardant during the fabrication step of the composite material.

Second, it is possible to apply fire retardant finishing treatments at the end of the fabrication process: this is very often performed when intumescent flame-retardant coatings are exploited [Bourbigot 2007].

The treatment with non-combustible components provides natural fibers or lignocellulosic particles with a fire-retardant coating: in these conditions, fire retardants tend to migrate inside the flammable materials, thus resulting in the fire protection of the latter.

The different flame retardant additives (5–10 wt. % in relation to dry mass) used for lignocellulosic materials comprise ammonium salts of phosphoric acid (i.e., melamine phosphate, ammonium polyphosphate), zinc chloride, boric acid, salts of sulfuric acid, zinc borate, vermiculite, aluminum hydroxide, magnesium hydroxide, expandable graphite and pentaerythritol (as the carbon source for intumescent systems) [Balakrishnan 2013, Durin-France 2000, Grexa 2001, Lazko 2013, Reti 2009].

Unlike thermoplastic matrix-natural fiber composites, for which the open scientific literature reports several nice examples [Bhattacharyya 2015, Suardana 2011], the investigation of the fire behavior of thermosets reinforced with natural fibers has been only partially reviewed.

Manfredi et al. [Manfredi 2006] investigated the thermal and fire behavior of composites based on unsaturated polyester or modified acrylic resins and reinforced with different natural fibers (namely, jute, flax, sisal) at 30 vol. %. It was found that both the polymer matrices showed similar fire behavior, notwithstanding that modified acrylic resin-based composites gave rise to lower smoke as compared to unsaturated polyester-based counterparts, thanks to the char-forming properties of the former. Among the composites with modified acrylic resins, sisal-reinforced materials showed the highest fire risk and the worst fire behavior. Furthermore, jute fiber-containing composites exhibited quick growing, but short-lasting fire and, conversely, flax fiber-containing composites developed long duration, but slow growing fire.

Hapuarachchi and co-workers [Hapuarachchi 2007] assessed the potential application of industrial hemp fiber-reinforced sheet molding compound materials suitable for building applications, with particular emphasis on their fire behavior. The composites were added with aluminum trihydrate and subjected to cone calorimetry tests performed at 25 and 50 kW/m². A significant decrease of the peak of the heat release rate was found for the systems containing aluminum trihydrate: this finding demonstrated that the obtained composites can compete with current building materials in terms of fire behavior.

Chai et al. [Chai 2012] compared the flax-fiber-reinforced epoxy samples to glass-fiber-reinforced counterparts. It was found that glass fibers were able to provide partial protection from ignition, acting as a heat sink, as well as a physical barrier to the heat source; conversely, flax fibers were themselves susceptible to ignition and combustion with a higher peak of heat release rate compared to their glass fiber equivalents. In addition, the glass/flax hybrid laminates showed fairly good fire resistance with respect to flax-reinforced laminates. Their structural integrity and the resistance to fire was found to decrease with increasing the amount of natural reinforcement.

Very recently, Szolnoki et al. [Szolnoki 2015] prepared flame-retarded natural hemp fabric-reinforced epoxy resin composites. For this purpose, the hemp fabrics were treated according to three different methods: (i) immersion of preheated fabric into cold phosphoric acid solution (allowing the penetration into the capillaries of the fibers) and subsequent neutralization; (ii) reactive modification with an aminosilane-type coupling agent; (iii) the combination of the sol-gel surface coating with the first approach. The presence of phosphorus in the hemp fabrics turned out to decrease the flammability not only of the reinforcement, but also of the epoxy composites made thereof. In addition, it was possible to achieve V-0 classification (it means that burning stops within 10 s on a vertical specimen; drips of particles allowed as long as they are not inflamed) according to UL-94 standard (UL is the abbreviation for the Underwriters Laboratories, an independent organization in the United States to control and certificate product safety; furthermore, UL-94 is a flammability test performed on a defined specimen) rating by applying an amine-type phosphorus-containing curing agent in combination with the treated hemp fabrics.

The author of this PhD thesis prepared hemp fabric/epoxy composites by using vacuum bag molding. This technique has minimal impact on tool cost and imposes no limits on the part size process for producing large-scale composites; thus, the reduction in laminate flaws to improve part quality can be obtained at a competitive cost.

In particular, in this thesis, a simple and ecofriendly chemical strategy will be shown. This sol-gel strategy allows to coat hemp fabrics with a silica-based fire retardant layer, obtained by using a waterglass coating prepared in acidic conditions. In parallel, Ammonium Polyphosphate (APP), a very well-known flame retardant, is added to epoxy resin, aiming at assessing the possible joint effects of the flame retardant with the waterglass treatment. Very recently, this additive was used by our group [Boccarusso 2016] for conferring fire retardant properties to hemp/epoxy composites manufactured by the infusion process: the obtained results showed that the epoxy resin added with 16.32 wt. % APP can be used in infusion processes of biocomposites without any impact on the technological feasibility of the process itself and provides significant enhancement as far as the fire

behavior is considered. Pursuing this research, the author investigated the effect on the concurrent presence of surface-treated hemp fabrics and APP on the fire behavior of the obtained composites, assessed through cone calorimetry tests. The effect of the modification of hemp fabrics with the waterglass treatment was assessed through Scanning Electron Microscope (SEM), Fourier Transform Infrared (FTIR) spectroscopy and solid-state Nuclear Magnetic Resonance (NMR). Furthermore, Thermogravimetric Analysis (TGA) performed in nitrogen were exploited for assessing the thermal stability of both the waterglass-treated hemp fabrics and of their epoxy composites.

4.1.2 Production and functionalization of natural fibers

Recently natural fibers such as kenaf, hemp, flax, jute, and sisal became the object of great research interest as green or eco-friendly reinforcement of composites. They may assure weight, cost, and CO₂ release reduction and less reliance on oil sources [Holbery 2006]. The use of fibers derived from natural annually renewable resources may have environmental but also social and economical advantages over other fibers so as demonstrated through life cycle assessment (LCA) method [Alves 2010].

In 1983, for the first time, when passing repeated times in a high-pressure homogenizer wood pulp gave microfibrillated celluloses, MFCs [Herrick 1983, Kelley 2011, Nechyporchuk 2016, Turbak 1983a, Turbak 1983b]. The mechanical action of the homogenizer caused disintegration of the fibers into sub-structural fibrils and microfibrils. Nowadays MFC, also known as nanofibrillated cellulose (NFC) or cellulose nanofibers or nanofibrils (CNF) are produced from various sources in a diameter as small as 5 nm [Kelley 2011, Nechyporchuk 2016]. Four mechanical methods are used are: homogenization, microfluidization, microgrinding and cryocrushing. The drawbacks are fibers entanglement and clogging of the mechanical apparatus and mechanical energy consumption [Kelley 2011, Nechyporchuk 2016]. The currently available techniques generally yield a wide size distribution of produced CNF with, also, some non-fibrillated residual fibers. The mechanical energy consumption is obviously a function of the degree of fibrillation [Kelley 2011]. Recently the detection of biological and chemical pre-treatment methods allowing an easier mechanical disintegration made CNF more attractive for the commercial applications. However, the research keeps on looking for new methods allowing, also, if possible, to have products of superior properties [Nechyporchuk 2016]. One of the applied methods is mild cellulose hydrolysis catalysed by some enzymes that enhances fibrillation [Nechyporchuk 2016]. Chemical routes allow, instead, easier delamination of fibrils by introduction negatively charged groups (carboxylation via

TEMPO-mediated oxidation or via periodate chlorite oxidation, sulfonation, carboxymethylation,) or positively charged groups (quaternization) on the cellulosic fibers [Nechyporchuk 2016].

Another challenge in the use of MFCs comes from the hydrophilic character of cellulose and the tendency to form strong network held together by hydrogen bonds [Hubbe 2008, Kalia 2014, Missoum 2013, Nechyporchuk 2016]. Many methods of surface modification to have them well dispersed in non-polar polymer matrices were proposed and discussed in the literature [Hubbe 2008, Kalia 2014, Missoum 2013, Nechyporchuk 2016].

In this thesis a new pretreatment that allows to have hemp fibers with diameters from tens of microns to tens of nanometers with the aid of a low power mixer will be described. The pretreatment creates, also, a silica layer that allows easy surface modification with the so many organometallic silanes commercially available. The pretreatment method exploits the sol-gel strategy of section 4.1.1. The sol-gel strategy consisted in exposing the hemp fabrics to inexpensive and ecofriendly waterglass solutions that allowed the formation of a silica-based coating, resistant to washing and able to act as a thermal shield and to protect from heat sources. The formation of –C–O–Si– covalent bonds between the coating and the cellulosic substrate was demonstrated through Fourier Transform Infrared (FTIR) and solid-state Nuclear Magnetic Resonance (NMR) analysis. In this thesis will be shown that when properly prolonging this sol-gel and eco-friendly process the fabric becomes brittle and easily gives silica coated hemp fibers with the aid of a low power mixer. The silica based coating present on them allows easy functionalization with 3-Aminopropyl)triethoxysilane (APTS).

4.2 Hybrid epoxy nanocomposites

4.2.1 Thermal and fire behavior of hybrid silica/epoxy nanocomposites

It is well-known that polymeric materials cannot be used for high-performance applications because of their limited properties. This limitation can be overcome by using organic/inorganic composites. Epoxy/silica systems represent one of the most widely utilized organic/inorganic systems. Because of heat, moisture, and chemical resistance and good adhesion to many substrates, epoxy resins are mostly exploited in the field of coatings, adhesives, casting, potting, composites, laminates, and for encapsulating semiconductor devices [Potter 1970, Stöver 1996].

Recently, organic–inorganic polymer hybrids raised great attention. They require nano-level molecular design but are expected to have unique properties that are not simply the sum of those of the composite components: unprecedented materials may be created with the hybrid strategy [Gon 2017]. Aerogels may be strengthened through proper organic–inorganic hybridization strategies

[Shimizu 2017]. Organic-inorganic hybrid perovskites (e.g., $\text{CH}_3\text{NH}_3\text{PbI}_3$), with advantages of easy processing, tunable bandgaps, and superior charge-transfer properties, have emerged as a new class of revolutionary optoelectronic semiconductors promising for various applications [Zhao 2016].

Recently, the attention of the scientific research, is focused on materials for linings in the aerospace field. In this case, the requirements related to the mechanical properties are often limited. On the contrary, severe regulations about the fire resistance must be respected in order use the materials [Matějka 1998]. As it is known, traditional halogen-based flame retardants are persistent organic pollutants of global concern and generate corrosive/toxic combustion products [Dasari 2013]. In this prospect, polymer nanocomposites, i.e., polymer matrices filled with specific, finely dispersed nanofillers, are considered to pave the way for future materials combining physico-chemical and thermo-mechanical performances with enhanced flame-retardant behavior [Laoutid 2009]. However, most of the literature on these materials is qualitative, and often points to conflicting/misleading suggestions from the perspectives of short-term and long-term fire exposure tests [Dasari 2013]. Hence, there is a renewed need to fundamentally understand the fire response of such materials [Dasari 2013]. These findings justify the topic proposed in this PhD thesis, which investigates the structure and fire behavior of new in-situ generated silica/epoxy hybrid materials.

The organic/inorganic hybrid materials usually consist of nanostructured domains of the inorganic filler, homogeneously dispersed in the polymer matrix [Afzal 2013]. Epoxy/silica hybrids may be prepared by simply dispersing preformed silica particles or (better) by promoting the “in-situ” formation of a silicate phase through sol–gel chemistry. The “in-situ” method allows obtaining a wide range of morphologies ranging from the particles dispersion to the formation of co-continuous organic–inorganic networks [Innocenzi 2005, Piscitelli 2013]. Furthermore, the sol–gel process allows tailoring the interface between organic and inorganic phases through the adequate selection of both the silane precursors of the inorganic phase and the sol–gel reaction conditions [Mascia 2005, Piscitelli 2015].

In details, the use of coupling agents allows preventing phase separation phenomena of the epoxy and inorganic components, hence giving rise to the formation of silica/epoxy hybrid networks; therefore, the organic and/or inorganic precursors have to be modified in order to achieve an optimal compatibility between the organic and inorganic components of the resulting hybrid material [Davis 2003, Matějka 1999]. However, the preparation of epoxy hybrid materials is largely empirical and requires an efficient control of the key parameters for the assembly of the organic and inorganic domains into an optimized morphology. Hybrids containing particulate inorganic oxides

are produced under conditions that ensure fast condensation rates: therefore, phase separation takes place by a nucleation and growth mechanism [Mascia 2005].

Mascia et al. [Mascia 2005] thoroughly studied a lot of coupling agents, including APTS, GPTMS, and mercaptosilanes. In particular, APTS has been frequently used, as extensively studied by Bakhshandeh et al. and Seraja et al. [Bakhshandeh 2014, Seraj 2014]. It possesses three hydrolysable ethoxy groups that, thanks to silanols condensation, can be grafted onto the surface of sol-gel silica. Conversely, the aminopropyl group is not hydrolysable and may react with the epoxy rings similarly to amine hardeners; this way, it may promote a very good compatibilization effect. It turns out that the formation of one network can exert a control on the growth of the other, thereby creating conditions that lead to a wide range of morphologies at the nanometer length scale, including the co-continuous morphology [Mascia 2005, Seraj 2014].

Despite the mechanical properties of these hybrid systems (particularly referring to the epoxy/silica systems that exploit APTS as coupling agent) have been deeply investigated, few studies report on the thermal as well as fire behavior of these materials, with and without the addition of a phosphorous-based flame-retardant, that often, because of very severe regulations (i.e., in aerospace engineering), prevents their applicability [Troitzsch 1983]. It is known that the inclusion of silica into epoxy networks favors the char formation and increases its yield, hence improving the thermal stability: in fact, the carbonaceous residue layer acts as a thermal insulator and a barrier to oxygen diffusion [Phonthammachai 2012, Visakh 2015]. Matějka et al. [Matějka 1998] investigated the thermal degradation of epoxy/silica nanocomposites owing to their widespread use as high-performance materials. Thermal analysis results, coming from several experiments [Phonthammachai 2012, Visakh 2015], confirm that silica, being an inherently stable inorganic phase, lowers the degradation rates by favoring the formation of more voluminous and mechanically stronger char; furthermore, it also affects the pyrolytic degradation of amine-cured epoxy networks that proceeds through several overlapping mechanisms, e.g., dehydration, intramolecular cyclization, isomerization, or chain-transfer reactions [Ramirez 2007, Singh 2010, Wu 2010].

The author of this PhD thesis applied an “in situ” sol-gel synthesis procedure to a commercial two-component epoxy resin system. The samples were characterized by means of infrared spectroscopy (FTIR), small-angle X-ray scattering (SAXS), transmission electron microscopy (TEM), dynamic mechanical analysis (DMA), nuclear magnetic resonance (NMR). In this thesis will be shown that the experimental results support the presence of a very fine distribution of silica nanoparticles (at nanometer level) within a hybrid network structure was obtained for all the in-situ prepared

samples. It will be shown as a non-isothermal post curing treatment beyond the T_g (glass transition temperature) of the neat epoxy affects the thermal and mechanical features of the obtained hybrid materials. In vertical flame spread tests, the presence of silica domains, even at very low loadings (2 wt. %), prevented the dripping of incandescent drops. Furthermore, a remarkable reduction (about 40%) of the heat release rate (HRR) was observed in the presence of just 2 wt. % silica in the samples not subjected to non-isothermal post curing treatments (instead of 16% for the fully cured sample). All these findings were mainly ascribed to the nanoparticles clustering derived from the post curing treatments; the hybrids were subjected to.

4.2.2 Fire retardancy of phosphorous-based in-situ generated silica/epoxy composite materials

Phosphorous compounds are considered as potential replacement for halogen based toxic flame-retardants [Lu 2002, Rakotomalala 2010, Salmeia 2015ab, Wendels 2017]. Among the phosphorus based FRs, development of 9,10-dihydro-9-oxa-10-phosphaphenanthrene-10-oxide (DOPO) and its derivatives have gained much attention in the research and industrial community due to their efficient and versatile flame retardant action (see section 3.4.3). They have recently been reported to be harmless for aquatic organisms and human cells [Hirsch 2017, Salmeia 2018, Waaijers 2013].

DOPO and its derivatives:

- 3-(6-oxidodibenzo[c,e][1,2]oxaphosphinin-6-yl)propanamide (DA),
- 6H-dibenz[c,e][1,2]oxaphosphorin,6-[(1-oxido-2,6,7-trioxa-1-phosphabicyclo[2.2.2]oct-4-yl)methoxy]-, 6-oxide (DP),

do not induce acute cytotoxicity in human lung epithelial cell as well as human macrophages [Gustavsson 2017, Hirsch 2017, Salmeia 2018].

Another DOPO derivative 10-(2,5-dihydroxyphenyl)-9,10-dihydro-9-oxa-10-phosphaphenanthrene-10-oxide (DOPOHQ) has also been evaluated for its eco-toxicity and was found to have toxicity markedly lower than commercially prevalent phosphates [Liu 2018, Salmeia 2018]. These studies and experimental results confirm that phosphorous-based flame-retardants can be considered green flame retardant, especially when their preparation occurs taking into consideration the principles of green chemistry [Salmeia 2018].

However, the use of additive flame-retardants, such as DOPO and its derivatives, requires high loadings or the addition of a synergist in order to impart flame retardancy to epoxy resins. It should be specified that 10-20 wt. % of phosphorus contents are required for DOPO-based additives and

for reactive DOPO derivatives to reach V0 rating according to UL-94 standard [Ciesielski 2008, Levchik 2001]. Recently, the reactive approach has been subject to an ever-growing interest from the academic community. Indeed, the reactive P-H bond (contain in DOPO and some DOPO derivatives) of hydrogen phosphonates or phosphinates enables to covalently bind the flame retardant to the polymer chain by reaction with the epoxy functionality [Seibold 2008]. This chemical modification is able to confer flame retardant characteristics to the epoxy resins and allows lower phosphorus loadings than the additive approach and also eliminates the risk of flame-retardant leaching from the polymer during the polymer processing. There has also been a growing interest toward phosphorus containing curing agents that would impart flame retardancy while acting as a cross-linker [Hergenrother 2005, Levchik 1998, Lin 2005, Liu 1997, Wang 1999]. Until now, there has only been a limited amount of industrially relevant reactive phosphorus flame-retardants. Saito et al. [Saito 1981] prepared a pre-reacted DGEBA (bisphenol A diglycidyl ether) with DOPO by curing with 4,4'-diaminodiphenylsulfone (DDS) and phenolic novolac (PN) [Saito 1981]. UL-94-V0 rating was reached with both the aromatic hardeners with 1.6 and 2.2 wt. % of P-loading for DDS and PN respectively. Only 1.6 wt. % of P-loading was necessary in modified novolac epoxy resin cured with DICY/Fenuron (dicyandiamd/dimethyl-3-phenylurea) to reach a UL-94-V0 rating [Döring 2009]. It was recently reported that the addition of the inexpensive Boehmit (30 wt. %) significantly reduced the required loading of DOPO [Döring 2009]. The reactive approach may be a useful method in order to improve the fire behavior of epoxy resins but the reactivity of DOPO, mono-functional phosphinate, results in a decrease of the functionality of the epoxy resin [Liu 2002]. Such reduction has been shown to have a detrimental impact on the glass transition temperature (T_g) of the cured resin which represent a significant drawback [Liu 2002].

Regarding a reactive approach, DOPOHQ may be used to prevent the reduction of functionality of the epoxy resin. Wang et al. [Wang 1998] prepared a pre-reacted DGEBA with DOPOHQ and 2.1 wt. % of P-loading in order to impart flame retardancy, although the thermal stability of the chain elongated DGEBA was similar to the unmodified cured resin [Wang 1998, Wang 2001]. Recently, Salmeia et al. [Salmeia 2018] synthesized, using a green chemistry approach, the phosphorous based flame retardants DA and DP. DA and DP additives were dispersed in polyester films and the fire behavior of the final products was studied. The polyester films containing the FR additives passed the vertical fire tests and exhibited higher LOI (Limit Oxygen Index) values compared to the virgin polyester films. TGA (Thermal Gravimetric Analysis) data and elemental analysis of char obtained for FR formulations indicated possible condensed phase activity of the FR additives. Salmeia et al. [Salmeia 2018] identified phosphorus based volatile species in the evolved gas

analysis performed using DIP-MS (Direct Insertion Probe - Mass Spectrometry). Such phosphorus species were responsible for the gas phase flame inhibition and thus improving the flame retardancy of the polymer.

DA and DP may be used as green flame retardants for epoxy resin cured with aliphatic amine. Based on the results reported in the literature [Salmeia 2018], DA should guarantee an efficient flame inhibition mechanism linked to a strong gas phase activity and DP flame retardant may be efficient through a strong condensed phase activity linked to a production of a large amount of phosphoric acid compounds. DA shows a primary amino chemical functionality which may allow this DOPO-based additive to react with the oxirane rings of the epoxy resins. This reactivity should assure a very good dispersion in the epoxy matrix by improving the fire behavior with lower phosphorus loadings than an additive approach. DP could increase also the char content when used in combination with a char-forming polymer as epoxy resin.

The addition of DA or DP into in-situ generated silica/epoxy materials synthesized by following the methodology of section 4.2.1 may allow to obtain a product showing no dripping phenomena of incandescent drops and improved flame retardancy.

The author of this PhD thesis investigated a new methodology to obtain self-extinguishing in-situ silica/epoxy materials. The in-situ procedure was applied to a commercial two-component (with a cycloaliphatic amine as hardener) epoxy resin system. This new methodology was designed with the collaboration and the experience in the flame retardancy field of the Additive and Chemistry Group (Empa Research Institute, St. Gallen). The author of this PhD thesis spent six months by working on this methodology and characterizing the fire behavior of the prepared materials. The silica/epoxy materials were synthesized by exploiting the in-situ sol-gel synthesis procedure of section 4.2.1 and DA or DP as phosphorous-based flame-retardants were added, even at very low P-loadings (1 - 2 wt. %). The flame-retardant effect due to the addition of a nitrogen source in the nanocomposites was also studied through the dispersion in the batch of a fixed amount of melamine. In this thesis, the above-mentioned methodology and the study of the fire behavior of these phosphorous-based in-situ generated silica/epoxy composite materials will be shown. The samples were characterized by several techniques. The silica structure and the presence of the FRs were assessed through FT-IR. NMR measurements were used to study the reactivity between DA and epoxy resin. The flame retardancy for the composite samples was tested by PCFC, Cone Calorimeter and UL-94 vertical burning measurements (profile temperature for the propagation flame was captured with Infrared Camera during the burning test). Thermal stability and glass transition data together with a preliminary study of the fire behavior were performed through TGA

and DSC. In order to achieve a deep understanding of the decomposition pathway of the FR additives: DIP-MS and PY-GC-MS data were collected, in addition to SEM-EDX (Microscopy and Energy-Dispersive X-ray Spectroscopy) measurements (elemental analysis) of char obtained. Thus, in this research activity, detailed analyses of new in-situ generated silica/epoxy hybrid materials were carried out and all the findings were mainly ascribed to the innovative material design.

5 Experimental and Methods

5.1 Materials

Sodium metasilicate (Na_2SiO_3), hydrochloric acid (37% ACS), ethanol (ACS reagent, anhydrous), 3-aminopropyltrimethoxysilane (APTS, >98% ACS), tetraethyl orthosilicate (TEOS, >99% ACS), ninhydrin (ACS reagent) and Bisphenol A diglycidyl ether (DGEBA) were purchased from Sigma Aldrich (St. Louis, MO, USA).

A two-component epoxy resin system (SX10), consisting of a modified bisphenol A resin and modified cycloaliphatic polyamines, and plain weave hemp fabrics (grammage: 160 g/m²) were purchased by MATES S.r.l. (Milan, Italy). Ammonium Polyphosphate (APP) particles (white free-flowing powder) were supplied by Tecnosintesi S.p.A. (Bergamo, Italy).

A two-component epoxy resin system, consisting of bisphenol A resin (Epikote™ Resin 827) and modified cycloaliphatic polyamines (Epikure™ Curing Agent 943) were purchased by Hexion Specialty Chemicals GmbH (Duisburg, Germany). The phosphorous based flame retardants:

- 3-(6-oxidodibenzo[c,e][1,2]oxaphosphinin-6-yl)propanamide (DA),
- 6H-dibenz[c,e][1,2]oxaphosphorin,6-[(1-oxido-2,6,7-trioxa-1-phosphabicyclo[2.2.2]oct-4-yl)methoxy]-, 6-oxide (DP),

were provided and synthesized by Empa (Swiss Federal Laboratories for Materials Science and Technology, St. Gallen, Switzerland); their synthesis procedure is described and reported in the literature [Salmeia 2018]. 2,4,6-Triamino-1,3,5-triazine, sym-Triaminotriazine (melamine, >99%) and 1,8-Diazabicyclo(5.4.0)undec-7-ene (DBU, >98% ACS) were purchased from Sigma-Aldrich (Switzerland).

5.2 Synthesis of the investigated samples and sol-gel methodologies

5.2.1 Hemp fabric silica coating

A waterglass solution 0.1 M, Na_2SiO_3 , was acidified to pH = 2.5 with hydrochloric acid. Hemp fabrics were repeatedly soaked into this solution for 10 min and dried in an electric oven at 80 °C

for 20 min. The treatment was repeated five times. To the best knowledge of the author, this is the first time that an inexpensive waterglass solution was exploited for obtaining a silica based coating: indeed, the proposed approach can be considered as an application of sol-gel chemistry using a precursor (Na_2SiO_3) that does not need hydrolysis and is performed in water solutions, avoiding the organic solvents usually required by the alkoxy precursors.

5.2.2 Manufacturing of hemp fabric/epoxy composites

The epoxy composite laminates were fabricated by hand lay-up [Amirkhosravi 2017], positioning, on the mold, six layers of plain weave hemp fabric impregnated by the two-component epoxy resin system (SX10, see section 5.1). The hand lay-up process was adopted in order to avoid the filtration of the filler in the resin by the reinforcement layers.

After impregnation, in order to increase the volumetric percent of reinforcement and to eliminate entrapped air, the laminates were enclosed in a vacuum bag, and polymerization was accomplished through a 48h cure cycle at room temperature. The 3 mm-thick laminate contains 25 wt. % of reinforcing agent; the 22 vol. % was obtained as the ratio of the hemp fiber volume (estimated as the ratio of fiber weight and density, 1.4 g/cm^3) to the laminate volume. Four different composites were produced by infiltrating hemp fabric sheets or treated hemp fabric sheets with epoxy or APP-charged epoxy. The obtained samples are coded as reported in Table 4.

Table 4: Samples investigated. APP, Ammonium Polyphosphate; H, untreated hemp fabrics; HT, waterglass-treated hemp fabrics.

Symbol	Hemp fabric and epoxy composite samples	Amount of APP added to the epoxy (wt. %)
H	Hemp fabrics	0
HT	Hemp fabrics treated with waterglass	0
H/E	Hemp fabrics/epoxy composite	0
HT/E	Hemp fabrics treated with waterglass/epoxy composite	0
H/E-15APP	Hemp fabrics/epoxy composite	15
HT/E-15APP	Hemp fabrics treated with waterglass/epoxy composite	15

5.2.3 Hemp particles production

Hemp fabric sheets were submitted to iterated soaking-drying cycles (see section 5.2.1). In each cycle the hemp fabric sheets were soaked, for 20 min, in a diluted (0.01 M) solution of waterglass (Na_2SiO_3) acidified up to pH= 2.5 with hydrochloric acid. After 5 min excess water dripping, the sheets were left to dry for 10' at 80 °C. The concentration of 0.01 M is the only difference with the procedure describes din section 5.2.1.

After 30 cycles the dry sheets could be easily teared and then reduced to powders with the aid of a low power (350 W) mixer. When the aspect was similar to wadding, water was added (20 g of hemp in 100 ml of water) to successfully complete the grinding. The obtained pulp was dispersed in a waterglass solution 0.1 M acidified up to pH= 2.5 with hydrochloric acid and stirred for 24h (20 g of hemp in 500 ml of solution). The suspension was left to settle and the surnatant was substituted with distilled water in stirring condition. This operation was repeated three times. The hemp pulp was washed three times in centrifuge with water/ethanol mixtures (50% in volume). After drying at 80°C, the hemp was reduced, in the 350 W mixer, to a powder. The powders were dispersed in water and ultrasonicated (20 kHz, 900-1000 W, 30'). The final product was washed (three times) with a solution of EtOH/Water (50/50, vol/vol) in centrifuge (10000 rpm, 10') and dried for 24h at 40 °C.

5.2.4 Particles functionalization

The functionalization with silica waterglass solution makes the hemp fibers, with a well distributed presence of silanol groups on the surface, suitable for a chemical reaction with a coupling agent molecule, for example APTS (3-aminopropyltrimethoxysilane). APTS provides amino primary functional groups on the hemp surface. The reaction with the coupling agent has been performed by adding silica coated hemp fibers (Hemp_SiO_2) into a solution of EtOH/Water (80/20, vol/vol), containing APTS (10 % vol.), acidified up to pH= 5 with acetic acid. The functionalization occurs after only one soaking/drying cycle (soaking time/drying time=20'/10'). As long as the final product, it has been washed with a solution of EtOH/Water (50/50, vol/vol) through three centrifugation cycles (10000 rpm, 10'). Finally, amino functionalized microfibers ($\text{Hemp_SiO}_2\text{-APTS}$) has been dried for 24h at 80°C.

5.2.5 Synthesis of epoxy composites epoxy/APTS functionalized hemp fibers

The synthesis was performed in one pot involving the following two steps:

- Mixtures of epoxy (DGEBA, SX10) and amino functionalized microfibers, with weight percentages of hemp particles equal to 1, 2, 5 wt. %, were stirred vigorously at 80 °C for 2h in a closed system to get the reaction between the primary amino groups and oxirane rings.
- The amount of hardener needed for the curing (26 wt. % of the epoxy resin) was then added to the mixture at room temperature and mixed for 5 min. The resulting mixtures were poured into a Teflon® mold. The curing process was carried out at 30 °C for 24 h; then, the curing was completed by treating the samples at 80 °C for 4h.

5.2.6 Preparation of the epoxy/silica hybrid nanocomposites

APTS and TEOS were used as silica precursors and added to the commercial two-component epoxy resin system, hence promoting an “in situ” sol–gel synthesis prior to the addition of the epoxy hardener. Samples from batches containing different TEOS loadings were prepared. The TEOS/epoxy weight ratio was changed in the range 0 - 0.15 at constant TEOS/APTS weight ratio (equal to 3). The synthesis route is inspired to one already reported in the literature [Jiao 2013]. However, in the present research activity, the TEOS/epoxy weight ratio was remarkably increased (0.12 instead of 0.04) and acetone was avoided; this required substantial changes of the synthesis procedure. So as indicated in the second step reported below, silica formation required a higher temperature (80°C instead of room temperature) and reflux conditions. The synthesis was performed in one pot involving the following three steps:

- Mixtures of epoxy (DGEBA, SX10) and APTS with weight ratios epoxy/APTS changing from 100/3 to 100/5 were stirred vigorously at 80 °C for 2h to get a silanized epoxy.
- TEOS, distilled water and ethanol (EtOH) were added to the silanized epoxy and stirred vigorously at 80 °C under reflux for 90 min. The reaction vessel was, then, opened and kept at 80°C for 30 min in order to remove ethanol and water.
- The amount of hardener needed for the curing was then added to the mixture at room temperature and mixed for 5 min. The resulting mixtures were degassed under vacuum and poured into a Teflon® mold. The curing process was carried out at 30 °C for 24h; then, the curing was completed by treating the samples at 80 °C for 4h.

The silica contents estimated from the stoichiometry were 2, 4, 6 wt. %. The typical reaction batches are reported in Table 5 together with their acronyms that will be used throughout the sections.

Table 5: Typical formulations of the investigated systems.

Sample	Epoxy (g)	Coupling agent (g)	Hardener (g)	TEOS (g)	EtOH (g)	Water (g)
EPO	15	0	3.9	0	0	0
EPO_2%Si	15	0.457	3.9	1.060	0.117	0.478
EPO_4%Si	15	0.602	3.9	1.397	0.154	0.629
EPO_6%Si	15	0.752	3.9	1.745	0.193	0.786

A post cure treatment was also performed by thermally treating the samples in a tube furnace, at 3 °C/min from 25 to 100 °C, i.e., 15 °C higher than the neat epoxy glass transition temperature. These samples will be coded by adding “t” to the acronyms: as an example, EPO(EPO is the acronym for the commercial two-component epoxy resin system containing 0 wt.% of silica)_2%Si_t is the post cured hybrid system containing 2 wt. % of silica.

5.2.7 Preparation of the in-situ silica/epoxy composites added by phosphorous based flame retardants

In order to promote an “in-situ” sol-gel synthesis, prior to the addition of the cycloaliphatic hardener, APTS ((3-aminopropyl)triethoxysilane) and TEOS (tetraethyl orthosilicate) were used as silica precursors and added to the commercial two-component epoxy resin system. The TEOS/epoxy weight ratio was kept fixed in the at constant TEOS/APTS weight ratio (equal to 2).

For the synthesis route were followed the same operative conditions which are indicated in the section 5.2.6 with the intention likely to obtain silica domains in a organic–inorganic network [Matějka 1998, Matějka 1999, Matějka 2000], for this reason acetone was avoided and a temperature of 80 °C under reflux was used as required by the silica formation process.

The synthesis was performed in one pot involving the following four steps:

- Mixtures of epoxy, DGEBA (Epikote™ Resin 827) , and APTS with fixed weight ratio epoxy/APTS were stirred at 80°C for 2h, hence obtaining a silanized epoxy.
- TEOS, distilled water and ethanol (EtOH) were added to the silanized epoxy and stirred vigorously at 80 °C under reflux for 90 min. The reaction vessel was, then, opened and kept at 80 °C for 30 min in order to remove ethanol and water.
- After 30 min the temperature was increased up to 100°C and DA/DP (see Figure 24) was added together with melamine (one third in amount respect to the phosphorus-based flame-retardant mass) and stirred vigorously under reflux for 60 min. DA/DP was added to the

mixture in order to have a stoichiometric amount, in terms of P loading, equal to 1 and 2 wt. %.

The amount of hardener (Epikure™ Curing Agent 943) needed for the curing was then added to the mixture at room temperature and mixed for 5 min. The resulting mixtures were degassed under vacuum and poured into a steel mold and taken for curing (40°C/3h) followed by post-curing (150°C/2h).

The synthesis route is the same as the one reported previously in section 5.2.6 but for the third step where the flame retardants are added. Samples devoid of silica were also prepared through, directly, steps 3 and 4.

The silica content estimated from the stoichiometry were 2 wt. %. The typical reaction batches are reported in Tables 6 and 7 together with their acronyms that will be used throughout the thesis. In order to obtain a more precise estimation of the P-loadings percentages, the elemental analysis with ICP-OES (Inductively Coupled Plasma-Optical Emission Spectrometry, see section 5.3.1) was performed for EPO2%Si_DA2%P_Mel, EPO2%Si_DA1%P_Mel, EPO2%Si_DP2%P_Mel and EPO2%Si_DP1%P_Mel epoxy samples (see Tables 7 and 8).

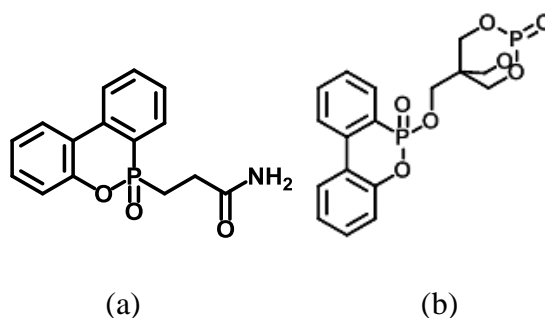


Figure 24: Chemical structure of (a) 3-(6-oxidodibenzo[c,e][1,2]oxaphosphinin-6-yl)propanamide (DA) and (b) 1-oxo-4-hydroxymethyl-2,6,7-trioxa-1-phospha-bicyclo[2.2.2]octane (DP) flame retardants.

Table 6: Typical formulations of the investigated systems with DA additive.

Sample	Epoxy [g]	TEOS [g]	APTS [g]	EtOH [g]	Water [g]	Hardener [g]	DA [g]	Mel [g]
EPO	107.75	/	/	/	/	25.86	/	/
EPO_DA2%P	107.75	/	/	/	/	25.86	41.1	/

EPO_Mel	107.75	/	/	/	/	25.86	/	13.7
EPO_DA2%P_Mel	107.75	/	/	/	/	25.86	41.1	13.7
EPO2%Si	107.75	6.92	3.61	0.85	2.75	25.86	/	/
EPO2%Si_DA2%P	107.75	6.92	3.61	0.85	2.75	25.86	41.1	/
EPO2%Si_Mel	107.75	6.92	3.61	0.85	2.75	25.86	/	13.7
EPO2%Si_DA2%P_Mel	107.75	6.92	3.61	0.85	2.75	25.86	41.1	13.7
EPO2%Si_DA1%P_Mel	107.75	6.92	3.61	0.85	2.75	25.86	27.4	9.13

Table 7: Typical formulations of the investigated systems with DP additive.

Sample	Epoxy	TEOS	APTS	EtOH	Water	Hardener	DA	Mel
	[g]	[g]	[g]	[g]	[g]	[g]	[g]	[g]
EPO	107.75	/	/	/	/	25.86	/	/
EPO_DP2%P	107.75	/	/	/	/	25.86	27.3	/
EPO_Mel	107.75	/	/	/	/	25.86	/	9.10
EPO_DP2%P_Mel	107.75	/	/	/	/	25.86	27.3	9.10
EPO2%Si	107.75	6.92	3.61	0.85	2.75	25.86	/	/
EPO2%Si_DP2%P	107.75	6.92	3.61	0.85	2.75	25.86	27.3	/
EPO2%Si_Mel	107.75	6.92	3.61	0.85	2.75	25.86	/	9.10
EPO2%Si_DP2%P_Mel	107.75	6.92	3.61	0.85	2.75	25.86	27.3	9.10
EPO2%Si_DP1%P_Mel	107.75	6.92	3.61	0.85	2.75	25.86	18.2	6.10

Table 8: %Phosphorus (%P) analyses of EPO2%Si_DA1%P_Mel and EPO2%Si_DA2%P_Mel.

Sample	Average [%]	Standard deviation [%]	Root square deviation [%]
EPO2%Si_DA1%P_Mel	1.58	0.03	1.6
EPO2%Si_DA2%P_Mel	2.23	0.24	10.6

Table 9: %P analyses of EPO2%Si_DP1%P_Mel and EPO2%Si_DP2%P_Mel.

Sample	Average [%]	Standard deviation [%]	Root square deviation [%]
EPO2%Si_DP1%P_Mel	1.64	0.06	3.5
EPO2%Si_DP2%P_Mel	2.42	0.27	11.1

5.3 Analytical techniques for chemical analysis and testing

5.3.1 Scanning electron microscope (SEM-EDX) and inductively coupled plasma optical emission spectroscopy (ICP-OES)

A SEM is a type of electron microscope that produces images of a sample by scanning the surface with a focused beam of electrons (see Figure 25). The electrons interact with atoms in the sample, producing various signals that contain information about the surface topography and composition of the sample.



Figure 25: Photo of the SEM apparatus.

The electron beam is scanned in a raster scan pattern, and the position of the beam is combined with the intensity of the detected signal to produce an image. In the most common SEM mode, secondary electrons emitted by atoms excited by the electron beam are detected using an Everhart-Thornley detector. The number of secondary electrons that can be detected, and thus the signal intensity, depends, among other things, on specimen topography. SEM can achieve resolution better than 1 nanometer [Stokes 2008].

SEM images of HT and HT samples (Table 4) were obtained on a Leica Stereoscan 440 Microscope (20 kV) (Leica Microsystems Cambridge Ltd., Cambridge, UK), equipped with an energy Dispersive Analytical System (EDS) from Inca Energy 200, by using AZtecEnergy EDS Software (v2.1, Oxford Instruments, Abingdon, UK, 2006). A digital Optical Microscope (OM), HIROX (Hirox Co., Ltd., Tokyo, Japan), was employed to observe the morphology of the fractured composites (Table 4) in bending tests. The observations were carried out at room temperature and by using KH-8700 Software (v1.40, Hirox Co., Ltd., Tokyo, Japan, 2013).

Energy dispersive X-ray spectroscopy (EDX) of Hemp_SiO₂_APTS was applied in combination with a scanning electron microscope (SEM) using an Inca X-sight device from Oxford Instruments (EDX) and a S-4800 microscope from Hitachi (SEM). An area of about 100 mm x 100 mm was scanned for the EDX measurements using an acceleration voltage of the electron beam of 20 kV, an emission current of 15 mA and a working distance of 15 mm. Under these experimental conditions, the information depth is in the order of a couple of microns.

EDX spectra of all the prepared samples in Tables 6 and 7 after burned (UL94 test, see section 5.3.10) were recorded on a Hitachi S-4800 Scanning Electron Microscope (SEM) equipped with Oxford INCA Energy 250 energy-dispersive X-ray spectroscopy system. EDX spectra were recorded at accelerating voltages of 20kV and with different magnifications to check the uniformity within one sample. Composite samples were coated with 5 nm Au/Pd prior to analysis.

Inductively coupled plasma optical emission spectroscopy (ICP-OES) is a trace-level, elemental analysis technique that uses the emission spectra of a sample to identify, and quantify the elements present. Samples are introduced into the plasma in a process that desolvates, ionises, and excites them. The constituent elements can be identified by their characteristic emission lines, and quantified by the intensity of the same lines [Fassel 1974]. %Phosphorus analyses of EPO2%Si_DA2%P_Mel, EPO2%Si_DA1%P_Mel, EPO2%Si_DP2%P_Mel and EPO2%Si_DP1%P_Mel (see Tables 8 and 9) were carried out using the inductively coupled plasma optical emission spectrometry method (ICP-OES), on an Optima 3000 (PerkinElmer AG, Rotkreuz, Switzerland) instrument. Sample preparation for ICP-OES consists of mixing of samples (300 mg) with H₂O₂ (1 mL) and HNO₃ (3 mL) followed by digestion using a microwave.

5.3.2 Transmission electron microscope (TEM)

TEM operates in the same basic principle as light microscope, where a beam of high voltage electrons is employed as a light source. Owing to the low de Broglie wavelength of high voltage electrons, it is possible to get a resolution thousands of times better than the light microscope. Modern gadgets have powers of resolution that range from 0.1 nm and the magnification up to 2,000,000 times [Matura 2012]. TEM is composed of an evacuated cylinder of about 2 meters height. A heated tungsten filament at the top of the cylinder (the cathode) will emit electrons when it is heated. The emitted electrons are accelerated to the anode by applying a high accelerating voltage from 100 keV to 1 MeV ranges [Egerton 2011]. Some of the accelerated electrons passed through tiny holes in the anode to form an energetic electron beam which passes down the column.

Electro-magnets are placed at intervals down the column to focus the accelerated electron beam [Pulokas 1999].

The double condenser lenses focus the electron beam onto the sample specimen which is clamped into a removable specimen stage. As the electron beam passes through the sample specimen, some of the electrons are scattered, whilst the remaining are focused by the objective lenses either onto a fluorescent screen or photographic film to get a shadow image of the nanoparticles. The unfocused electrons are blocked out by the objective aperture resulting in an enhancement of the image contrast [Kirkland 2010]. Figure 26 is a schematic diagram of the TEM.

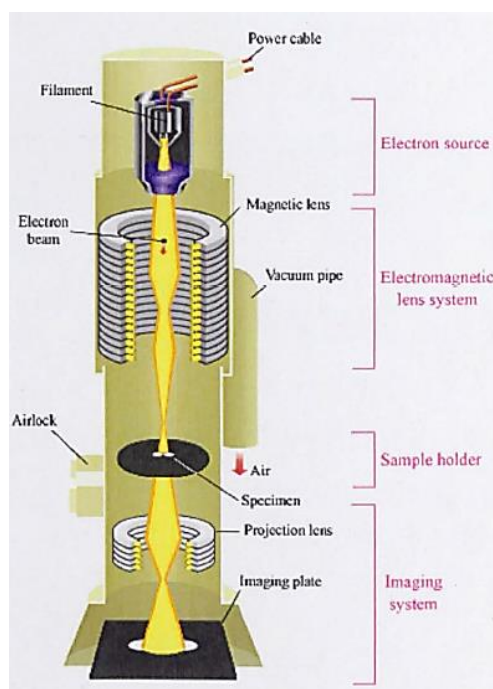


Figure 26: Schematic diagram of TEM instrument.

Bright field TEM analyses of EPO_2%Si, EPO_4%Si and EPO_6%Si (see section 5.2.6) were performed using a FEI TECNAI G12 Spirit-Twin (LaB6 source) equipped with a FEI Eagle-4k CCD camera, operating with an acceleration voltage of 120 kV. High magnification photos for EPO_6%Si were recorded in a TEM/STEM JEOL JEM 2200fs microscope operating at 200 kV. For TEM analysis, all the above mentioned samples were prepared by putting a drop of composite dispersion in ethanol (0.5 mg/ml) on a Lacey Carbon film copper TEM grids. Prior to preparation of composite dispersion, the composites were cryo-milled and fine powders were collected for dispersion.

5.3.3 Nuclear magnetic resonance (NMR)

NMR is a physical observation in which nuclei in a strong constant magnetic field are perturbed by a weak oscillating magnetic field (in the near field and therefore not involving electromagnetic waves [Hoult 1997] and respond by producing an electromagnetic signal with a frequency characteristic of the magnetic field at the nucleus. This process occurs near resonance, when the oscillation frequency matches the intrinsic frequency of the nuclei, which depends on the strength of the static magnetic field, the chemical environment, and the magnetic properties of the isotope involved; in practical applications with static magnetic fields up to ca. 20 tesla, the frequency is similar to VHF and UHF television broadcasts (60–1000 MHz). NMR results from specific magnetic properties of certain atomic nuclei. Nuclear magnetic resonance spectroscopy is widely used to determine the structure of organic molecules in solution and study molecular physics, crystals as well as non-crystalline materials. NMR is also routinely used in advanced medical imaging techniques, such as in magnetic resonance imaging (MRI).

All isotopes that contain an odd number of protons and/or neutrons have an intrinsic nuclear magnetic moment and angular momentum, in other words a non-zero nuclear spin, while all nuclides with even numbers of both have a total spin of zero. The most commonly used nuclei are ^1H and ^{13}C , although isotopes of many other elements can be studied by high-field NMR spectroscopy as well.

A key feature of NMR is that the resonance frequency of a particular simple substance is usually directly proportional to the strength of the applied magnetic field. It is this feature that is exploited in imaging techniques; if a sample is placed in a non-uniform magnetic field then the resonance frequencies of the sample's nuclei depend on where in the field they are located. Since the resolution of the imaging technique depends on the magnitude of the magnetic field gradient, many efforts are made to develop increased gradient field strength.

NMR spectra of H, HT, EPO_2%Si and EPO_2%Si_t (see Tables 4 and 5) were acquired with a 300-MHz (7.0 Tesla) Bruker Avance magnet (Bruker Bio Spin GmbH, Rheinstetten, Germany), composed of a wide-bore system and equipped with a CPMAS (Cross-Polarization Magic-Angle-Spinning) probe, working at ^{29}Si and ^{13}C frequencies of 59.62 and 75.47 MHz, respectively. Samples of hemp and treated hemp fibers (80 ± 1 mg) were loaded into 4-mm zirconia rotors, closed with Kel-F caps and spun at a rate of $10,000 \pm 1$ Hz. ^{13}C NMR spectra were acquired by applying a cross polarization technique and consisted of 1814 time domain points, a spectral width of 300 ppm (22,727.3 Hz), a recycle delay of 2 s, 4000 scans and 1 ms of contact time. The ^{13}C

CPMAS pulse sequence was conducted by using a ^1H Ramp pulse to account for the non-homogeneity of the Hartmann-Hahn condition. ^{29}Si NMR spectra were acquired by using a direct polarization and consisted of 2048 time domain points, a spectral width of 500 ppm (29,762 Hz), 40 s of recycle delay and 2730 scans. Free Induction Decays (FIDs) were processed by BrukerTopSpin (v2.1, Bruker, Billerica, MA, USA, 2006) and MestreNOVA (v9.0, Nanalysis Corp., Mestrelab Research, Calgary, AB, Canada, 2014) Software. Prior to be phase and baseline correction, ^{29}Si and ^{13}C spectra were Fourier transformed by applying a two- and four-fold zero-filling and adopting an exponential filter function with a line broadening of 350 and 50 Hz, respectively.

^1H , $^{31}\text{P}\{^1\text{H}\}$ and $^{13}\text{C}\{^1\text{H}\}$ NMR spectra of (i) EPO (EpikoteTM Resin 827) added by DA and (ii) EPO (EpikoteTM Resin 827) added by DA and DBU were collected at ambient temperature using Bruker AV-III 400 spectrometer (Bruker Biospin AG, Fällanden, Switzerland). ^1H and ^{13}C chemical shifts (δ) in ppm were calibrated to residual solvent peaks. The ^{31}P chemical shifts were referenced to an external sample with neat H_3PO_4 at 0.0 ppm. High-resolution mass spectrometry (HR-MS) was performed by the MS-service of the Laboratory for Organic Chemistry at the ETH Zurich on a Waters Micromass AutoSpec-Ultima spectrometer (EI).

5.3.4 Fourier transform infra-red (FTIR)

FTIR technique is a powerful tool to verify the nanoparticle chemical structure (see Figure 27). It can be employed for qualitative and quantitative analysis [Danzer 2007]. In this technique, the tested sample is mounted in a transparent IR compartment and subjected to IR beam [Coleman 1993]. IR absorption can be ascribed to transitions of molecular vibrational or rotational energy to another state [Coleman 1993].

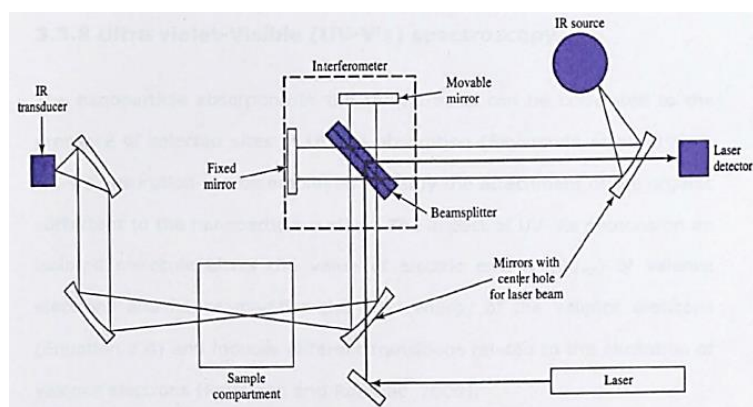


Figure 27: Schematic diagram of FTIR instrument.

FTIR transmittance spectra of hemp fibers were recorded with a Nicolet 5700 FTIR spectrometer (Thermo Fisher, Waltham, MA, USA) using a single reflection Attenuated Total Reflectance (ATR)

accessory with a resolution of 4 cm^{-1} and 32 scans and Thermo Scientific™ OMNIC™ Software Suite (v7.2, Thermo Fisher, Waltham, MA, USA, 2005).

ATR-FTIR (Fourier-Transform Infrared Spectroscopy and Attenuated Total Reflectance) transmittance spectra of H, HT, EPO_WH (not cured epoxy resin, SX10) and all the prepared samples in Table 5, Hemp_SiO₂ and Hemp_SiO₂_APTS were recorded with a Nicolet 5700 FTIR spectrometer (Thermo Fisher, Waltham, MA, USA), using a single reflection Attenuated total reflectance (ATR) accessory with a resolution of 4 cm^{-1} and 32 scans and Thermo Scientific™ OMNIC™ Software Suite (v7.2, Thermo Fisher, Waltham, MA, USA, 2005). All the obtained spectra were normalized to the strong absorption bands at 1607 and 1509 cm^{-1} , related to the C=C bonds of the benzene rings present in the epoxy resin structure, that are not expected to change after the curing reaction.

ATR-FTIR transmittance spectra of EPO_WH (not cured epoxy resin, Epikote™ Resin 827), EPO, EPO_2%Si, EPO2%Si_DA2%P_Mel, EPO2%Si_DP2%P_Mel (see Tables 6 and 7) and the burned material from UL94 test, see section 5.3.10, of EPO, EPO2%Si_DA2%P_Mel, EPO2%Si_DP2%P_Mel were recorded with a Bruker Tensor 27 FTIR spectrometer (Thermo Fisher, Waltham, MA, USA), using a single reflection Attenuated total reflectance (ATR) accessory with a resolution of 4 cm^{-1} and 32 scans and Thermo Scientific™ OMNIC™ Software Suite (v7.2, Thermo Fisher, Waltham, MA, USA, 2005).

5.3.5 Thermogravimetric analysis (TGA)

TGA technique is an essential tool to investigate the thermal stability of nanoparticles and nanocomposites, and to evaluate the surfactant loading level of organic modified nanoparticles. In this technique, the mass of the tested sample was recorded as a function of temperature or time as it is heated at a controlled heating rate in a controlled atmosphere. Modern commercial TGA instrument consists mainly of: (1) sensitive analytical balance, (2) furnace, (3) purge gas system to control the atmosphere, (4) microprocessor for instrument control, and (5) data acquisition (see Figure 28).

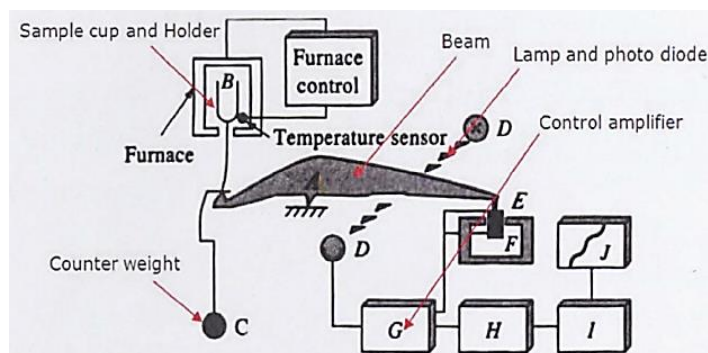


Figure 28: Schematic diagram of TGA instrument.

TGA of all the prepared samples in Table 4 were performed using a Netzsch TG209 (Selb, Germany) apparatus, from room temperature up to 800 °C, at a heating rate of 10 °C/min under a nitrogen atmosphere (experimental error: ± 0.5 wt. %, $\pm 1^\circ\text{C}$) and by using Proteus Software (v4.0, Labcenter Electronics Ltd., Yorkshire, UK, 2000).

TGA of all the samples in Tables 6 and 7 were performed on a NETZSCH TG 209 F1 instrument. Tests were conducted on 2 – 5 mg sample under nitrogen and air atmosphere (flow of 50 mL/min) at a heating rate of 10 °C/min from 25 to 800 °C.

5.3.6 Differential scanning calorimetry (DSC) and dynamic mechanical analysis (DMA)

DSC is a thermoanalytical technique in which the difference in the amount of heat required to increase the temperature of a sample and reference is measured as a function of temperature. Both the sample and reference are maintained at nearly the same temperature throughout the experiment. Generally, the temperature program for a DSC analysis is designed such that the sample holder temperature increases linearly as a function of time (see Figure 29). The reference sample should have a well-defined heat capacity over the range of temperatures to be scanned.

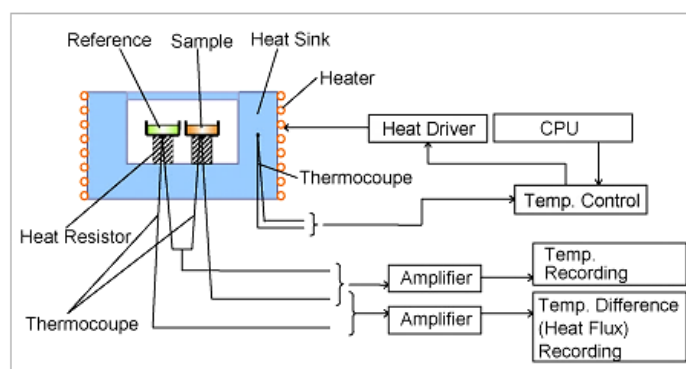


Figure 29: Schematic diagram of DSC apparatus.

The technique was developed by E. S. Watson and M. J. O'Neill in 1962 [Watson 1966], and introduced commercially at the 1963 Pittsburgh Conference on Analytical Chemistry and Applied Spectroscopy. The term DSC was coined to describe this instrument, which measures energy directly and allows precise measurements of heat capacity [Eerikäinen 2005]. Types of DSC:

1. Power-compensated DSC in which power supply remains constant.
2. Heat-flux DSC in which heat flux remains constant.

The result of a DSC experiment is a curve of heat flux versus temperature or versus time. There are two different conventions: exothermic reactions in the sample shown with a positive or negative peak, depending on the type of technology used in the measurement. This curve can be used to calculate enthalpies of transitions. This is done by integrating the peak corresponding to a given transition. It can be shown that the enthalpy of transition can be expressed using the following equation:

$$\Delta H = K \cdot A \quad (5.1)$$

where ΔH is the enthalpy of transition, K is the calorimetric constant, and A is the area under the curve. The calorimetric constant will vary from instrument to instrument, and can be determined by analyzing a well characterized sample with known enthalpies of transitions [Nagy 2013].

Differential scanning calorimetry (DSC) analyses of EPO, EPO2%Si, EPO_DA2%P, EPO_DP2%P, EPO2%Si_DA2%P_Mel, EPO2%Si_DP2%P_Mel, EPO2%Si_DA1%P_Mel, EPO2%Si_DP1%P_Mel (see Tables 6 and 7) were performed on a DSC 214 Polyma instrument (NETZSCH-Gerätebau GmbH, Germany). All DSC experiments were conducted at a controlled heating rate of 10 °C/min under a nitrogen flow of 50 mL/min by running two repeating cycles from 20 °C to 300 °C and back to 20 °C again. The glass transition temperatures were taken as the onset values of the second heating up curve, therefore a first heating up cycle was run in order to verify the completeness of the curing reaction through the absence of any residual exothermic peak.

One of the most fundamental measurements made on polymeric materials is the measurement of the glass transition, T_g (see Figure 30). In general, transitions in materials are associated with different localized or medium-to long-range cooperative motions of molecular segments. The glass transition is associated with cooperative motion among a large number of chain segments, including those from neighboring polymer chains. Although there are several thermal techniques available to make T_g measurements, by far the most sensitive technique is DMA [Pearce 1997]. DMA measures the viscoelastic moduli, storage and loss modulus, damping properties, and tan delta, of materials as they are deformed under a period (sinusoidal) deformation (stress or strain).

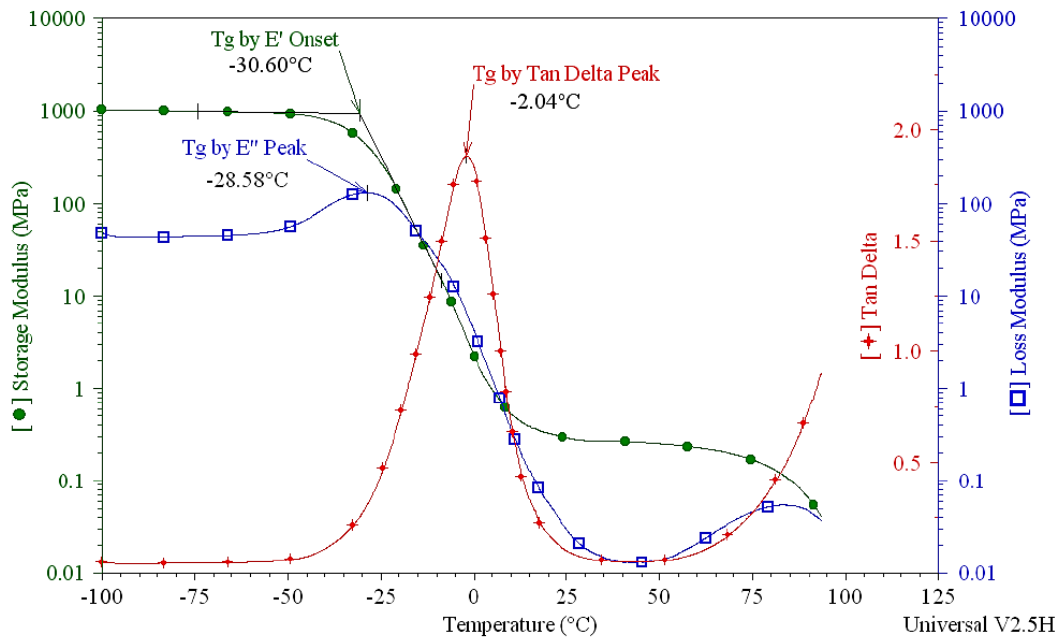


Figure 30: Thermal techniques available to make Tg measurements.

After scanning the sample under test, any of these three viscoelastic parameters can be used to define the Tg. The Figure 30 above shows a scan of a pressure sensitive adhesive run in tension clamps, at a frequency of 1 Hz, an amplitude of 10 microns, and a ramp rate of 5°C/min. This Figure 30 shows the Tg labeled for sample using the following parameters:

- E' Onset: Occurs at the lowest temperature and relates to mechanical failure [Pearce 1997].
- E'' Peak: Occurs at the middle temperature and is more closely related to the physical property changes attributed to the glass transition in plastics. It reflects molecular processes and agrees with the idea of Tg as the temperature at the onset of segmental motion [Pearce 1997].
- Tan Delta Peak: Occurs at the highest temperature and is used historically in literature. It is a good measure of the “leather like” midpoint between the glassy and rubbery states of a polymer. The height and shape of the tan delta peak change systematically with amorphous content [Pearce 1997].

The parameter used to detect the glass transition should be reported along with the frequency of oscillation, the temperature ramp rate, the clamp type used, and the sample dimensions.

DMA of EPO, EPO_t, EPO_{2%Si}, EPO_{2%Si,t}, EPO_{4%Si}, EPO_{4%Si,t}, EPO_{6%Si}, EPO_{6%Si,t} (see Table 5) and epoxy (SX10) composites with 1, 2, 5 wt. %, of Hemp_{SiO₂}-APTS (see section 5.2.5) were carried out on a DMA3300 (TA Instruments). The tests were run in a three-

point bending mode with a span of 40 mm and a frequency of 1 Hz; the width of samples was about 10 mm and the temperature was ramped from 25 to 100 °C at a heating rate of 3 °C/min.

5.3.7 Small-angle x-ray scattering (SAXS)

SAXS is a small-angle scattering technique by which nanoscale density differences in a sample can be quantified. This means that it can determine nanoparticle size distributions, resolve the size and shape of (monodisperse) macromolecules, determine pore sizes, characteristic distances of partially ordered materials, and much more. This is achieved by analyzing the elastic scattering behavior of X-rays when travelling through the material, recording their scattering at small angles (typically 0.1-10°, hence the "Small-angle" in its name). It belongs to the family of small-angle scattering (SAS) techniques along with small-angle neutron scattering, and is typically done using hard X-rays with a wavelength of 0.07 - 0.2 nm [Glatter 1982]. Depending on the angular range in which a clear scattering signal can be recorded, SAXS is capable of delivering structural information of dimensions between 1 and 100 nm and of repeat distances in partially ordered systems of up to 150 nm [Glatter 1982].

SAXS belongs to a family of X-ray scattering techniques that are used in the characterization of materials. In the case of biological macromolecules such as proteins, the advantage of SAXS over crystallography is that a crystalline sample is not needed. Furthermore, the properties of SAXS allow investigation of conformational diversity in polymer materials [Burger 2016].

In an SAXS instrument a monochromatic beam of X-rays is brought to a sample from which some of the X-rays scatter, while most simply go through the sample without interacting with it. The scattered X-rays form a scattering pattern, which is then detected at a detector which is typically a 2-dimensional flat X-ray detector situated behind the sample perpendicular to the direction of the primary beam that initially hit the sample. The scattering pattern contains the information on the structure of the sample. The major problem that must be overcome in SAXS instrumentation is the separation of the weak scattered intensity from the strong main beam. The smaller the desired angle, the more difficult this becomes. The problem is comparable to one encountered when trying to observe a weakly radiant object close to the sun, like the sun's corona. Only if the moon blocks out the main light source does the corona become visible. Likewise, in SAXS the non-scattered beam that merely travels through the sample must be blocked, without blocking the closely adjacent scattered radiation. Most available X-ray sources produce divergent beams, and this compounds the problem. In principle the problem could be overcome by focusing the beam, but this is not easy

when dealing with X-rays and was previously not done except on synchrotrons where large bent mirrors can be used. Therefore, most laboratory small angle devices rely on collimation instead.

Simultaneous small-angle and wide-angle X-ray scattering analyses (SAXS-WAXD) of EPO_2%Si, EPO_2%Si_t, EPO_4%Si, EPO_4%Si_t, EPO_6%Si and EPO_6%Si_t (see Table 5) were carried out using an Anton Paar SAXSpace camera equipped with a 2D imaging plate detector. CuK α X-Rays with 1.5418 Å wavelength were generated by a sealed tube source (40 kV, 50 mA) and slit collimated. All scattering data were corrected for background and normalized for the primary beam intensity. In order to remove the inelastic scattering from the data, SAXS profiles were corrected for both Porod constant and desmearing effect.

5.3.8 Three-point bending test

The three-point bending flexural test provides values for the modulus of elasticity in bending E_f , σ_f , flexural strain ϵ_f and the flexural stress–strain response of the material. The main advantage of a three-point flexural test is the ease of the specimen preparation and testing. However, this method has also some disadvantages: the results of the testing method are sensitive to specimen and loading geometry and strain rate.

The test method for conducting the test usually involves a specified test fixture on a universal testing machine. Details of the test preparation, conditioning, and conduct affect the test results. The sample is placed on two supporting pins a set distance apart.

Calculation of the flexural stress σ_f :

$$\sigma_f = 3 * F * L / 2 * b * d^2 \quad (5.2)$$

$$\sigma_f = 3 * F * L / 2 * b * d^2 \quad (5.3)$$

for a rectangular cross section and a circular cross section [Bandyopadhyay 2013], respectively.

Calculation of the flexural strain ϵ_f :

$$\epsilon_f = 6 * D * d * / L^2 \quad (5.4)$$

Calculation of flexural modulus E_f :

$$E_f = L^3 * m / 4 * b * d^3 \quad (5.5)$$

In these formulas the following parameters are used:

σ_f = Stress in outer fibers at midpoint, (MPa)

ϵ_f = Strain in the outer surface, (mm/mm)

E_f = flexural Modulus of elasticity, (MPa)

F = load at a given point on the load deflection curve, (N)

L = Support span, (mm)

b = Width of test beam, (mm)

d = Depth or thickness of tested beam, (mm)

D = maximum deflection of the center of the beam, (mm)

m = The gradient (i.e., slope) of the initial straight-line portion of the load deflection curve, (N/mm)

R = The radius of the beam, (mm)

Three-point bending tests of all the prepared samples in Table 4 were carried out in a MTS (MTS Systems Corporation, Eden Prairie, MN, USA) Alliance RT/50 universal testing machine in stroke control, setting the crosshead speed at 1 mm/min in accordance with the ASTM 790M standard and by using MTS TestWorks Software (v4, MTS Systems Corporation, Eden Prairie, MN, USA, 2006). The tests were performed on specimens of $60 \times 25 \times 3 \text{ mm}^3$; the sample span-to-depth ratio was 16:1.

5.3.9 Standard test method for tensile properties of plastics

The epoxy mechanical properties were evaluated by mechanical compressive testing according to the ASTM-D638 standard in order to obtain the tensile stress-strain curves, the ultimate tensile strength and tensile modulus of elasticity. The test speed value was chosen in the recommended range between 5 to 500 mm/min (0.2 to 20 in/ min) by using the lowest speed that ruptures the specimen within $\frac{1}{2}$ to 5 minutes. The epoxy samples were left over night at conditioning temperature (room temperature in a dry airborne).

Epoxy nanocomposites samples were prepared in the standard shape and dimensions, which is shown in Figure 31.

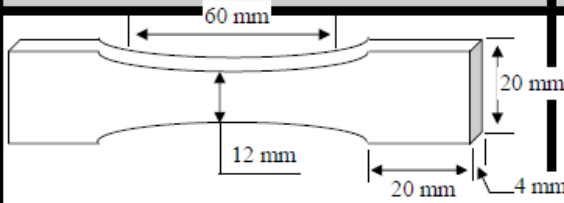
Test Type	Test Specimen Specification	Standardization Code
1. Tensile		ASTM - D638

Figure 31: Standard shape and dimensions of epoxy composites according ASTM-D638 standard.

EPO, EPO_2%Si, EPO2%Si_DA2%P_Mel, EPO2%Si_DP2%P_Mel specimens (see Tables 6 and 7) were tested by ZwickiLine for Flexible Low-Force Testing (see Figure 32). The head speed was 1 mm/minute. The tensile stress of the tested specimens was measured as function of its strain.



Figure 32: Photo of the Flexible Low-Force Testing apparatus.

5.3.10 UL94 VB - vertical burning test

There is a set of standard UL94 tests for the flammability of plastic parts in appliances and devices [Laoutid 2009]. The most commonly employed test is UL-94 VB for measuring the flame spread and ignitability (ease of ignition) of a vertical sample exposed to a small flame. A blue flame with a power of 50 W, and 20 mm height is applied to the bottom of the sample for 10 seconds, and then

removed (see Figure 33). The afterflame time t_1 (the time required for the flame to extinguish) is noted. The flame is then applied again for another 10 seconds. Then, the afterflame time t_2 is noted, and the afterglow time t_3 is noted (the time required for the fire glow to disappear). According to the standards, five samples must be tested [Morgan 2007]. Figure 33 shows the experimental set up for the UL94 flammability test.

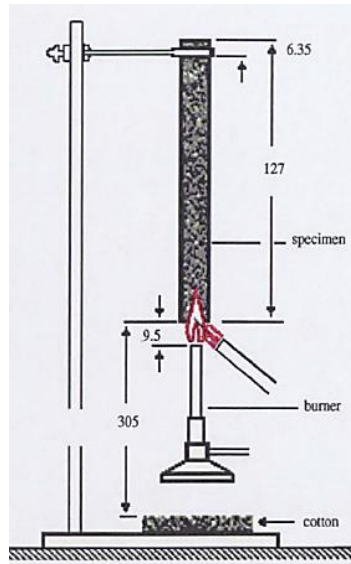


Figure 33: UL94 VB – Vertical Burning Test experimental set up of the apparatus during the flammability test.

The polymer sample is then classified as V0, V1, or V2 according to the values of t_1 , t_2 , and t_3 (see Table 10).

Table 10: Flammability classes according to the UL94 standard test (IEC 60695-11-10).

Fire Classification	
UL-94 V0	<ul style="list-style-type: none"> • t_1 and t_2 less than 10 s for each specimen • $t_1 + t_2$ less than 50 s for the five specimens • $t_2 + t_3$ less than 30 s for each specimen • No after flame or afterglow up to the holding clamp • No burning drops
UL-94 V1	<ul style="list-style-type: none"> • t_1 and t_2 less than 30 s for each specimen

	<ul style="list-style-type: none"> • $t_1 + t_2$ less than 250 s for the five specimens • $t_2 + t_3$ less than 60 s for each specimen • No after flame or afterglow up to the holding clamp • No burning drops
UL-94 V2	<ul style="list-style-type: none"> • t_1 and t_2 less than 30 s for each specimen • $t_1 + t_2$ less than 250 s for the five specimens • $t_2 + t_3$ less than 60 s for each specimen • No afterflame or afterglow up to the holding clamp • Burning drops allowed

UL94 tests of all the prepared samples in Tables 5 (also the thermal treated ones), 6 and 7 were performed according to IEC 60695-11-10 (sample size of 13 x 125 x approx. 3 mm³).

5.3.11 Cone calorimeter

Cone calorimeter is one of the most efficient polymer fire behavior tests. In this test, a sample of dimensions 100 x 100 x 4 mm³ is placed on a load cell and subjected to a given heat flux generally from 10 to 100 kW/m². The sample is uniformly irradiated from above. The measurements of oxygen concentration in the combustion gases are employed to quantify the heat released per unit time and surface area. The basic principle is Huggett's observation that the released heat from most organic materials is proportional to the quantity of oxygen consumed during burning [Babrauskas 1984]. The peak/maximum heat released rate (pKHRR), which is the key point in polymer flame retardancy, can be measured. The average heat released rate (HRR) and the total heat released (THR) can be measured as well. Furthermore, the cone calorimeter test enables the measurements of time to ignition (TTI), time to flame-out (TTF), mass loss rate (MLR), and time of combustion (TOC). During combustion, the quantities of carbon monoxide (CO), carbon dioxide (CO₂), and the released smoke can be quantified. Figure 34 shows the experimental set up for the cone calorimeter testing.

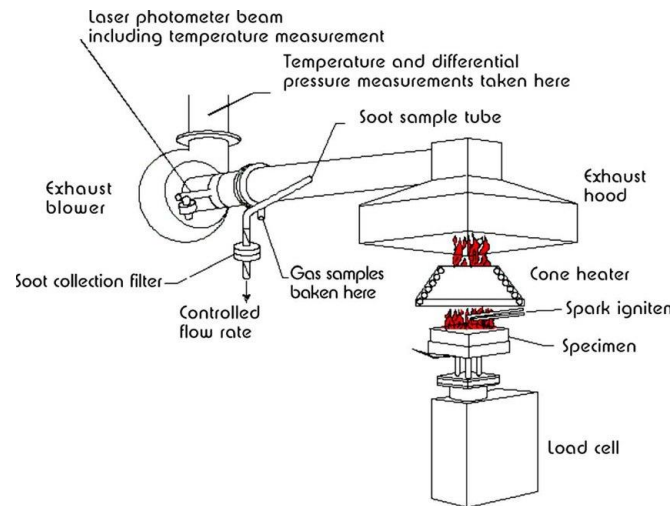


Figure 34: Schematic diagram of Cone Calorimeter apparatus.

To investigate the combustion behavior of all the investigated materials in Tables 4, 5, 6 and 7 subjected to a constant heat flux, cone calorimeter tests (Fire Testing Technology, East Grinstead, London, UK) were performed following the ISO 5660 standard, by using squared samples ($5 \times 5 \times 0.3 \text{ cm}^3$ and $100 \times 100 \times 4 \text{ mm}^3$), with a heat flux of 35 kW/m^2 , in horizontal configuration. Time to ignition (TTI), total heat release (THR), peak of the heat release rate (pkHRR) were measured. Total smoke release (TSR), CO yield, CO₂ yield and specific extinction area (SE) were evaluated, as well. For each sample, the experiments were repeated at least three times in order to ensure reproducible and significant data.

5.3.12 Pyrolysis combustion flow calorimeter (PCFC)

The pyrolysis combustion flow calorimeter (also known as microscale combustion calorimeter, MCC) is a powerful instrument to evaluate the fire behavior of milligram scale (mg-scale) samples [Lyon 2004]. It seems evident that mg-scale analysis will not depict the physical effects occurring at larger mass scale (e.g., dripping or intumescence). Therefore, this analysis should not be used as a tool to describe the fire behavior of a material in real-scale conditions [Lyon 2007]. However, mg-scale analysis can provide valuable information about fire properties of a material [Schartel 2007]. During this measurement, a mg-scale sample is heated up at a constant rate under an inert atmosphere, leading to possible formation of char [Lyon 2007]. The produced volatiles are swept from the pyrolyzer by an inert gas, combined with oxygen, and combusted at high temperature (see Figure 35). The heat release rate is calculated from the measured flow rate and oxygen concentration. Useful parameters can be obtained from this measurement, such as the total heat release per unit initial mass (HR), the heat release capacity (HRC) (HRC; defined as the maximum

heat release rate divided by the constant heating rate), and the temperature at the maximum heat release rate (T_{max}) [Lyon 2004].

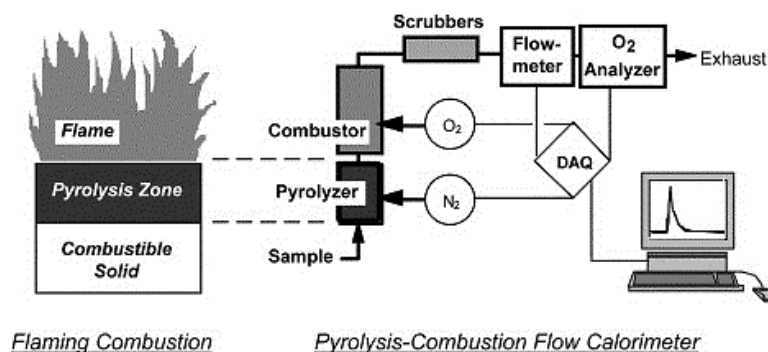


Figure 35: Schematic diagram of Pyrolysis combustion flow calorimeter.

Heat release rates (HRR) of all the samples in Tables 6 and 7 were determined using pyrolysis combustion flow calorimeter (PCFC) (Fire Testing Technology Instrument UK) following ASTM D7309. Each sample (~7 mg) was exposed to a heating rate of 1 °C/s from 150 to 750 °C in the pyrolysis zone.

5.3.13 Pyrolysis–gas chromatography–mass spectrometry (Py-GC-MS) and Direct inlet probe mass spectroscopy (DIP-MS)

Pyrolysis–gas chromatography–mass spectrometry is a method of chemical analysis in which the sample is heated to decomposition to produce smaller molecules that are separated by gas chromatography and detected using mass spectrometry [Schartel 2010].

Pyrolysis is the thermal decomposition of materials in an inert atmosphere or a vacuum. The sample is put into direct contact with a platinum wire, or placed in a quartz sample tube, and rapidly heated to 600–1000 °C (see Figure 36). Depending on the application even higher temperatures are used. Three different heating techniques are used in actual pyrolyzers: isothermal furnace, inductive heating (Curie Point filament), and resistive heating using platinum filaments. Large molecules cleave at their weakest bonds, producing smaller, more volatile fragments. These fragments can be separated by gas chromatography. Pyrolysis GC chromatograms are typically complex because a wide range of different decomposition products is formed. The data can either be used as fingerprint to prove material identity or the GC/MS data is used to *identify individual fragments* to obtain structural information.

To increase the volatility of polar fragments, various methylating reagents can be added to a sample before pyrolysis [Beach 2009].

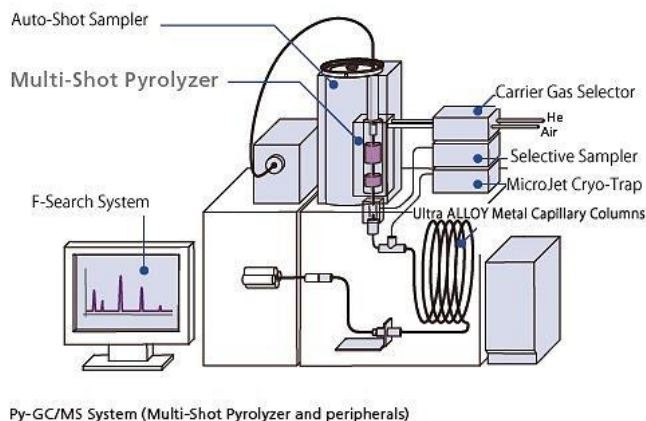


Figure 36: Schematic diagram of Pyrolysis–gas chromatography–mass spectrometry.

Besides the usage of dedicated pyrolyzers, pyrolysis GC of solid and liquid samples can be performed directly inside programmable temperature vaporizer (PTV) injectors that provide quick heating (up to 60 °C/s) and high maximum temperatures of 600-650 °C. This is enough for many pyrolysis applications. The main advantage is that no dedicated instrument has to be purchased and pyrolysis can be performed as part of routine GC analysis. In this case quartz GC inlet liners can be used. Quantitative data can be acquired, and good results of derivatization inside the PTV injector are published as well [Benin 2014].

Pyrolysis gas chromatography is useful for the identification of volatile compounds [Benin 2014]. These materials include polymeric materials, such as acrylics or alkyds [Dumitrascu 2012]. The way in which the polymer fragments, before it is separated in the GC, can help in identification.

Pyrolysis-Gas Chromatography Mass Spectrometry (Py-GC–MS) measurements of all the prepared samples in Tables 6 and 7 were performed by placing 30–100 µg of specimen in a quartz tube (1 mm internal diameter x 25 mm length). The specimen was then loaded in the pyrolysis probe (5200 (CDS Analytical, Inc., Oxford, PA)) and placed in the special inlet at the interface. The specimen was pyrolyzed at 800 °C under helium atmosphere for 30 s. The volatiles were separated by a Hewlett-Packard 5890 Series II gas chromatograph and analyzed by a Hewlett-Packard 5989 Series mass spectrometer.

Together with Py-GC-MS, Direct inlet probe mass spectroscopy (DIP-MS) [Hacaloglu 2011] was used to detect possible volatile products from the combustion of all the samples in Tables 6 and 7. The technique is based on the direct insertion of the sample in the ionization chamber, where the sample is exposed to heating and ionized by electronic impact. The measurement was performed on a Finnigan/Thermoquest GCQ ion trap mass spectrometer equipped with a DIP module. The sample (about 1 mg) is introduced in a quartz cup situated on the tip of the probe, which is inserted into the

ionization chamber through an inlet. The measurement was performed with an ionization voltage of 70 eV, temperature of the ionic source of 200 °C and pressure below 10⁻⁶ mbar. A probe temperature ramp was run from 30 °C to 450 °C at a rate of 50 °C/min.

6 Results and discussion

6.1 Development of a sol-gel method for the improvement of the flame retardancy of hemp fabric/epoxy composites

6.1.1 Characterization of the silica coating

Figure 37 shows the typical ATR-FTIR spectra of hemp fabrics before and after the treatment (two and five soaking/drying cycles) with the acidic waterglass solution by following the procedure described in section 5.2.1. First of all, it is noteworthy that spectra modifications are consistent with the formation of a silica-based coating. In particular, the bands around 1200 and 1135 cm⁻¹ may be assigned to the stretching of the –Si–O–cellulose and –Si–O–Si– bonds, respectively [Abdelmouleh 2004, Britcher 1995].

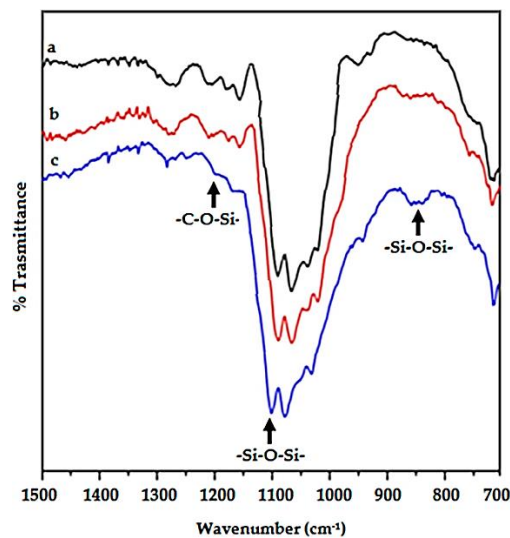


Figure 37: ATR-FTIR spectra of (a) untreated (black line); (b) after two (red) and (c) five (blue) soaking/drying cycles.

Therefore, a silica-based coating probably anchored to the hemp substrate through the formation of covalent bonds should have been formed. This finding may be ascribed to the low pH value (pH = 2.5) of the acidified waterglass solution: indeed, it is well known that when silicates are dissolved in acidic solutions, the formation of silicic acid would be expected, according to the following equation:



However, as soon as the reaction proceeds, the molecular units become larger, slowly giving rise to thickening phenomena that finally lead to the formation of a gel [Brinker 2013, Freundlich 1926, Reddy 2011]. This behavior was explained by Iler [Iler 1979] through a polymerization mechanism according to the following steps:

- (1) formation of the particles from the precursors;
- (2) subsequent growth of the particles;
- (3) creation of links among the particles, which give rise to chains and networks extending throughout the liquid medium.

Harris and coworkers [Harris 1982] hypothesized the formation of very small silica nanoparticles, comprising 3–7 silicon atoms linked through –Si–O–Si– siloxane bonds: this hypothesis was confirmed through NMR spectroscopy in the case of potassium silicate solutions with the K:Si atomic ratio equal to one.

The pH = 2.5 of the acidified waterglass solution, which is slightly higher than the silica isoelectric point (2.0–2.5), but lower than that reported for hemp (>3.0) [Brinker 2013, Islam 2011], is expected to ensure that the silica and hemp surfaces are negatively and positively charged, respectively (see section 1.2.1). This should: (i) favor silica nanoparticles to approach the fiber surface; and (ii) as long as the condensation reactions have a nucleophilic substitution mechanism, make the condensation reaction at the hemp surface preferential with respect to the reaction between silanol groups (Si–OH) in the solution.

Therefore, the formation of a silica-based coating anchored to the hemp surface through covalent bonds is reasonably supported. A mass increase of 5 wt. % was observed after the hemp fabric treatment described in the section 5.2.1 (see chapter 5). In order to further confirm this hypothesis, washing fastness tests have been performed according to the procedure described elsewhere [Cheng 2016]: the silica coating turned out to be resistant to the washing process and to be insoluble in the washing medium.

Figure 38 shows some typical SEM pictures of the hemp fabrics, before and after the treatment with waterglass in acidic condition: it is noteworthy that, after the formation of the waterglass coating, the surface of the fibers becomes smoother.

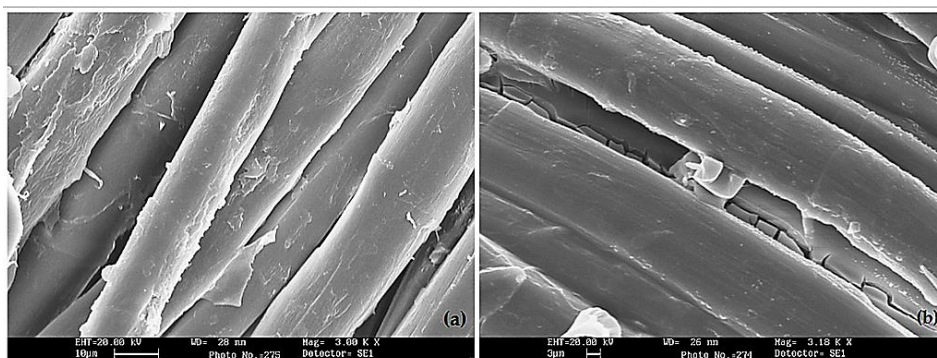


Figure 38: SEM images of: (a) untreated hemp fabric (scale bar: 10 μm); (b) hemp fabric after the waterglass treatment (scale bar: 3 μm).

6.1.2 Solid-state NMR spectroscopy of the hemp fibers

Hemp is commonly composed of cellulose, hemicellulose and lignin. The ^{13}C spectrum of the H sample (Figure 39) showed no evidence of lignin, since no signal was detected in the aromatic-C spectral region.

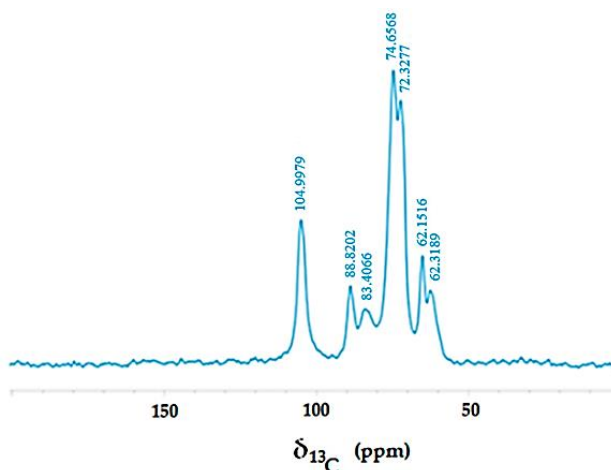


Figure 39: Solid-state NMR spectrum of untreated hemp fabric.

Conversely, oligo- and poly-saccharidic compounds deriving from cellulose and hemicellulose biopolymers were revealed by the intense peaks resonating in the spectral region 54–114 ppm. In particular, the two peaks at 62.45 and 65.07 ppm were ascribed to methylene carbons belonging to different saccharidic structures. The relatively up-field resonances of these carbons were ascribed to the closeness to oxygen nuclei in the carbohydrate molecule. The peaks at 88.81 and 104.85 ppm were attributed to anomeric carbons, either in α or β forms. Their relatively down-field frequencies were explained by the scalar bonding of anomeric carbons to two deshielding oxygen atoms exerting an electron-withdrawing effect. Finally, the peaks resonating in the range 67.54–86.16 ppm

were assigned to the remaining hydroxy-alkyl carbons composing oligo- and poly-saccharidic structures.

The superimposition of the H and HT ^{13}C NMR spectra is shown in Figure 40, revealing that all above-mentioned carbohydrate signals were identified also in the HT sample. However, significant differences between the two carbon spectra are evidenced. In particular, the HT sample showed several shoulders rising slightly up-field and resonating at 104.1, 81.43 and 59.83 ppm, respectively. Moreover, the peaks ranging within 67 and 78 ppm resulted in being more intense in the HT sample than in the H sample, whereas the peak at 62.15 ppm decreased in intensity and was accompanied by a slightly up-field shoulder at 59.9 ppm. These results suggest that part of the treated hemp material reacted with the applied silicate reagent. In fact, the appearance of these newly-formed resonances may be attributed to the formation of $-\text{C}-\text{O}-\text{Si}-$ covalent bonds, such an up-field shift being due to the presence of strong electron-releasing silicon nuclei.

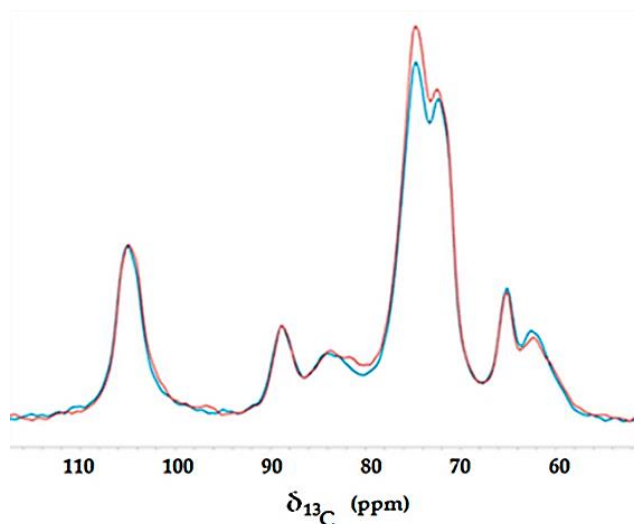


Figure 40: Solid-state NMR spectra of untreated hemp fabric (blue) and hemp fabric after the waterglass treatment (red).

The superimposition of the ^{29}Si spectra of H and HT samples is shown in Figure 41. It is well known, in fact, that plants do uptake from the soil solution some soluble silicates and salts, aiming at strengthening the robustness of their aerial parts. In plants, silica can be up to 10% of the total plant weight [Savvas 2015]. When comparing the curves of Figure 41, significant changes are appreciated as a consequence of the surface treatment. In both samples, two intense and broadened signals were detected at 93.04 and 109.6 ppm and attributed to silicon nuclei forming polysiloxane chains in Q3 and Q4 forms, respectively [Apeloig 1989]. Despite Q3 and Q4 Si nuclei being detected in both the H and HT samples, the intensity of both peaks was significantly higher in the case of the reaction product. In addition, the finding that each of these peaks appeared relatively

broadened is indicative of the coexistence of amorphous and crystalline forms of the polysiloxane network. As shown in Figure 41, the H sample exhibited an intense signal centered at 92 ppm, thus suggesting a relatively large abundance of Q3 Si, which is presumably bound to a single hydroxyl. This resonance almost totally disappeared in the HT sample, whereas a pronounced shoulder emerged up-field at 102.97 ppm. In line with the findings described for carbon spectra, this change can be due to the presence of Q3 Si nuclei, whereby the Si–OH group reacted to form a –C–O–Si–bond.

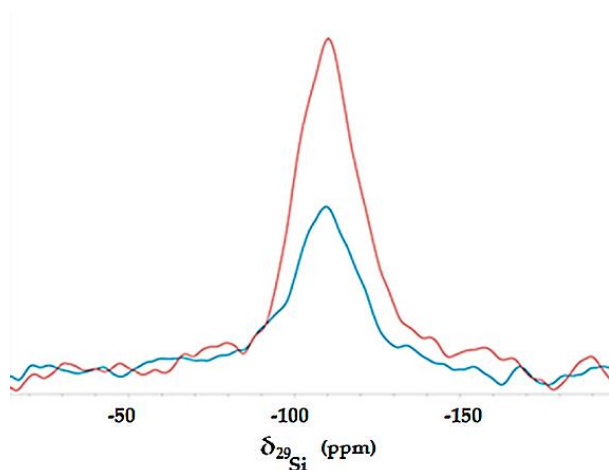


Figure 41: ^{29}Si NMR spectra of hemp (H, blue) and treated hemp (HT, red) samples acquired at a spin rate 10,000 Hz.

6.1.3 Thermogravimetric Analysis of hemp fabric/epoxy composites

Figure 42 shows the thermogravimetry (TG) curves in an inert atmosphere of hemp, before and after the treatment with waterglass in acidic conditions. Table 11 collects the corresponding TG data: $T_{5\%}$, $T_{10\%}$ and $T_{50\%}$ are the temperatures at which 5%, 10% and 50% weight loss are recorded; the residues at 800 °C and at the temperature at which the weight loss rate reaches the maximum are also reported. The thermal behavior of hemp can be interpreted on the basis of the scheme of the thermal degradation mechanism reported in the literature [Alongi 2015], which involves two stages: (1) Stage I (between 300 and 400 °C): this involves two competing pathways that yield aliphatic char and volatiles.

(2) Stage II (between 400 and 800 °C): some of the aliphatic char converts into an aromatic form.

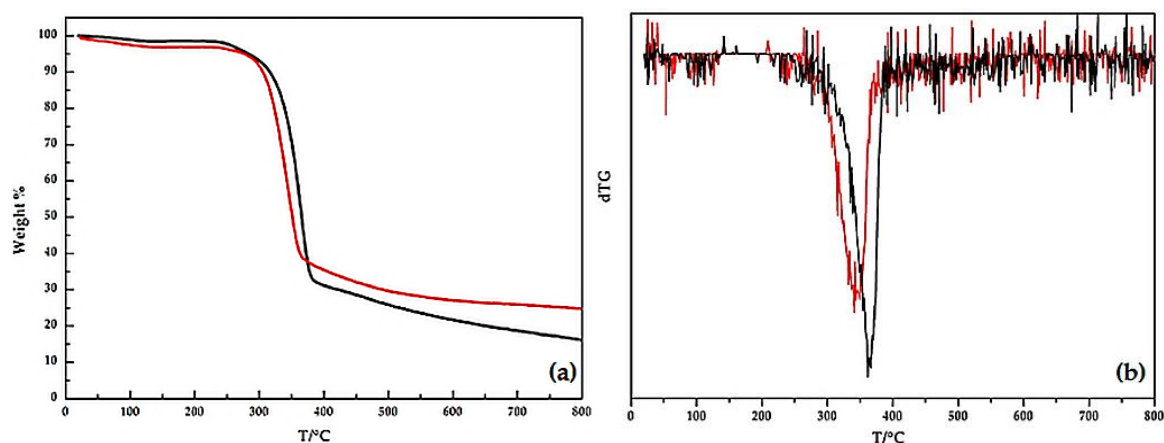


Figure 42: TG (a) and dTG (b) curves in an inert atmosphere for hemp, before (black line) and after (red line) the waterglass treatment.

Table 11: TG data obtained in an inert atmosphere.

Sample	T _{5%} (°C)	T _{10%} (°C)	T _{50%} (°C)	T _{peak} (°C)	Residue at T _{peak} (%)	Residue at 800 °C (%)
H	274	296	338	367	36	22
HT	264	283	324	342	43	30
H/E	221	274	342	357	41	9.9
HT/E	248	289	349	357	40	23
H/E-15APP	203	251	364	328	57	35
HT/E-15APP	264	383	344	319	60	32

According to the reported scheme, the TG curves recorded in an inert atmosphere (Figure 42) show one main degradation step in the temperature range 300–400 °C; furthermore, a slight mass loss is observed in between 80 and 150 °C for both fabrics and could be ascribed to humidity loss.

It is worthy to note that the waterglass treatment, because of the acidic characteristics of the deposited coating, anticipates the thermal degradation of the cellulosic fibers (see the T_{5%} and T_{10%} values of Table 11), but at higher temperatures exerts a protective effect on the substrate, significantly increasing the residue at high temperatures (30.4% vs. 22.1%, for waterglass-treated and pristine hemp, respectively).

When hemp is embedded in the epoxy resin, the waterglass treatment increases the overall thermal stability of the composites, giving rise to a significant increase of the residues at high temperatures (23% vs. 9.9% for HT/E and H/E composites, respectively; Table 11). The TG and dTG curves of the composites are plotted in Figure 43. As far as the composites reinforced with untreated hemp fabrics (i.e., H/E-15APP) are concerned, the presence of 15% of APP in the epoxy matrix determines an anticipation of the degradation phenomena, with respect to H/E counterparts, notwithstanding a significant increase of the final residue at high temperatures. This behavior could be ascribed to the presence of the flame-retardant additive (see section 3.4.3.1), as already reported in the literature [Levchik 1992]. Conversely, the waterglass treatment in combination with the presence of APP turns out to remarkably increase the thermal stability of the obtained composites (compare the last two rows of Table 11): this finding could be ascribed to a joint effect occurring between waterglass and APP during the heating up of the composite material.

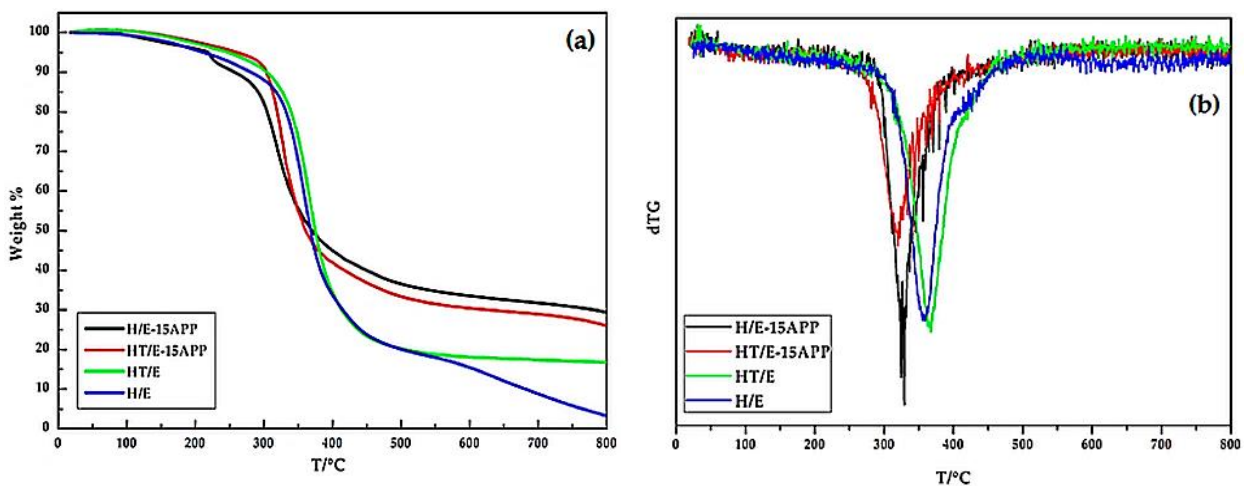


Figure 43: TG (a) and dTG (b) curves in an inert atmosphere for the investigated composite.

6.1.4 Cone Calorimetry Tests of hemp fabric/epoxy composites

Table 11 and Table 12 collect the cone calorimetry data: TTI (s); time to Flame Out (s) (FO); (HRR) (average) (kW/m²); pkHRR (kW/m²); THR (MJ/m²); TSR (m²/m²); mass residue at the end of the cone calorimeter test; SEA(m²/kg); carbon monoxide and dioxide yields (kg/kg). The first two lines refer to untreated (H) and waterglass-treated (HT) fabrics. It is worthy to note that the waterglass coating, despite an anticipation of the ignition of the fabric, is responsible for a slight decrease of HRR, pkHRR and THR and for a limited increase of the final residue, as well, hence further showing its protective effect exerted on the underlying fabric.

Table 12. Results from cone calorimetry tests performed on hemp and on the different composites before and after the waterglass treatment. TTI, Time to Ignition; FO, time to

Flame Out; HRR, Heat Release Rate; THR, Total Heat Released; pkHRR, peak of the Heat Release Rate.

Sample	TTI (s)	FO (s)	HRR (kW/m ²)	pkHRR (kW/m ²)	THR (MJ/m ²)	Residue mass (%)
H	28 ± 7.0	56 ± 2.5	13.2 ± 0.951	57.8 ± 9.77	1.80 ± 0.264	1 ± 0.6
HT	21 ± 2.6	45 ± 4.5	12.3 ± 1.48	51.8 ± 10.4	1.60 ± 0.252	4 ± 0.6
E	78 ± 6.9	166 ± 14.2	507 ± 120	1937 ± 119.3	95.8 ± 8.03	3 ± 0.6
H/E	55 ± 4.0	178 ± 11.9	402 ± 22.6	754 ± 85.7	61.3 ± 1.73	3 ± 0.6
HT/E	39 ± 4.0	187 ± 6.42	260 ± 13.3	642 ± 72.6	64.2 ± 4.65	6.71 ± 0.577
H/E-15APP	46 ± 8.1	336 ± 49.1	90 ± 12	259 ± 16.5	34.4 ± 1.47	28.7 ± 0.577
HT/E-15APP	44 ± 4.2	557 ± 97.1	68 ± 21	232 ± 45.1	40.1 ± 7.59	30.3 ± 0.577

Table 13. Smoke results from cone calorimetry tests performed on hemp and on the different composites before and after the waterglass treatment. TSR, total smoke release; SEA, specific extinction area; ND, not detectable.

Sample	TSR (m ² /m ²)	SEA (m ² /kg)	CO yield (kg/kg)	CO ₂ yield (kg/kg)
H	ND	ND	ND	ND
HT	ND	ND	ND	ND

E	3,276 ± 449	849 ± 55.4	$5.85 \times 10^{-2} \pm 4.91 \times 10^{-3}$	$1.96 \pm 4.27 \times 10^{-2}$
H/E	2,254 ± 77.3	735 ± 22.7	$3.28 \times 10^{-2} \pm 1.08 \times 10^{-3}$	$1.69 \pm 1.01 \times 10^{-2}$
HT/E	2,094 ± 229	667 ± 43.7	$4 \times 10^{-2} \pm 1 \times 10^{-3}$	$1.47 \pm 7.37 \times 10^{-2}$
H/E-15APP	938 ± 68.2	394 ± 33.3	$5 \times 10^{-2} \pm 3 \times 10^{-3}$	$0.87 \pm 2.6 \times 10^{-1}$
HT/E-15APP	1,230 ± 52.6	413 ± 16.3	$5 \times 10^{-2} \pm 2 \times 10^{-3}$	$1.02 \pm 1.94 \times 10^{-1}$

Conversely, the hemp fabric surface treatment seems to be very effective in improving the fire behavior of the prepared composites. Indeed, the presence of the waterglass coating significantly reduces the HRR by 35%, namely from 402 down to 260 kW/m² (see the values for H/E and HT/E, respectively). A similar trend is observed as far as pkHRR is considered: its decrease is as much as -14.9% (from 754 down to 642 kW/m², for H/E and HT/E, respectively). On the other hand, THR does not seem to be affected by the treatment of the fabrics with the waterglass coating, while the latter shows a detrimental effect on TTI, which is reduced from 55 down to 39 s.

A significant role is played by APP: indeed, this flame retardant additive, despite a reduction of TTI, favors a further remarkable decrease of HRR (-77.6% and -73.8%, for H/E-15APP and HT/E-15APP, respectively), pkHRR (-65.6% and -63.8%, for H/E-15APP and HT/E-15APP, respectively) and THR (-43.9% and -37.5%, for H/E-15APP and HT/E-15APP, respectively), with respect to the unfilled composite counterparts (i.e., H/E and HT/E samples).

In addition, the waterglass coating, also in combination with APP, seems to limit the smoke formation of the epoxy composites: in particular, APP turns out to significantly decrease both TSR and SEA parameters. It is noteworthy that the phosphorus additive seems to be more effective when added to the composites where hemp fabrics have not been subjected to the treatment with waterglass. As an example, TSR is decreased by 58.4% and SEA by 46.4%, as well, when 15% of APP is added to the composite (compare the H/E and H/E-15APP samples).

The very high residues after cone calorimetry tests for H/E-15APP and HT/E-15APP (some pictures are shown in Figure 44 and Figure 45) seem to indicate that the acidic character of the waterglass coating, in combination with the presence of APP, could favor the dehydration reactions of the fabric and of the epoxy resin, hence giving rise to the formation of a very stable char (see section 3.4.3.1).



Figure 44: Residue of H/E-15APP after cone calorimetry tests.



Figure 45: Residue of HT/E-15APP after cone calorimetry tests.

6.1.5 Three-Point Bending Tests of hemp fabric/epoxy composites

The hydrophilic behavior of natural fibers has a low compatibility with the hydrophobic polymer matrix; in addition, waxes and other non-cellulosic substances, which determine poor adhesion between matrix and fibers, cover the surface of the latter, as pointed out in the scientific literature [Bismarck 2002, Hautala 2004].

In order to evaluate the effect of the presence of APP in the epoxy matrix and of the waterglass treatment of the hemp fabrics on the mechanical behavior of the obtained composites, three-point bending tests were carried out in accordance with the ASTM 790M standard. Figure 46 plots the stress-strain curves for the different laminates. Table 14 collects the average values of the flexural modulus, flexural strength and maximum strain for the different laminates.

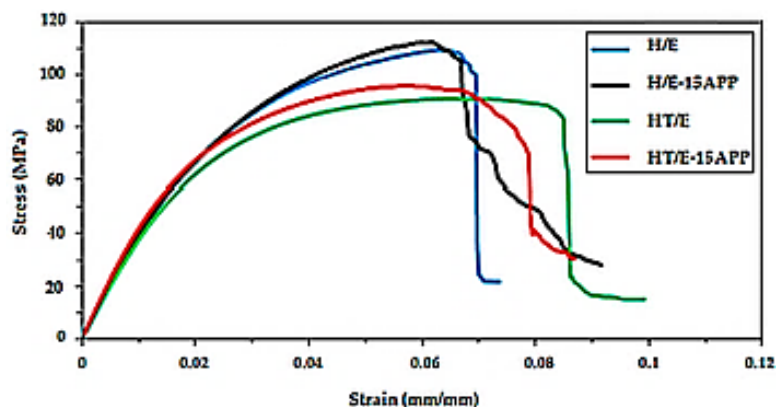


Figure 46: Stress-strain curves for the four types of composites: H/E sample, H/E-15APP sample, HT/E sample, HT/E-15APP sample.

Table 14: Results from the three-point bending tests.

Sample	Flexural modulus (MPa)	Flexural strength (MPa)	Maximum strain (%)
H/E	4550 ± 260.1	109 ± 5.61	7.1 ± 6.7 × 10 ⁻¹
H/E-15APP	4590 ± 324.3	110 ± 6.12	6.9 ± 7.7 × 10 ⁻¹
HT/E	4340 ± 194.1	92 ± 4.8	8.5 ± 8.8 × 10 ⁻¹
HT/E-15APP	4460 ± 258.2	94 ± 5.2	8.2 ± 9.1 × 10 ⁻¹

For all of the tested specimens, an evident pullout, showing a poor fiber/matrix adhesion, characterized the breakage for tensile stress. The photographs of the fracture on the tensile site, in section (140×) and in plane (100×) view, are shown in Figure 47a,b, respectively.

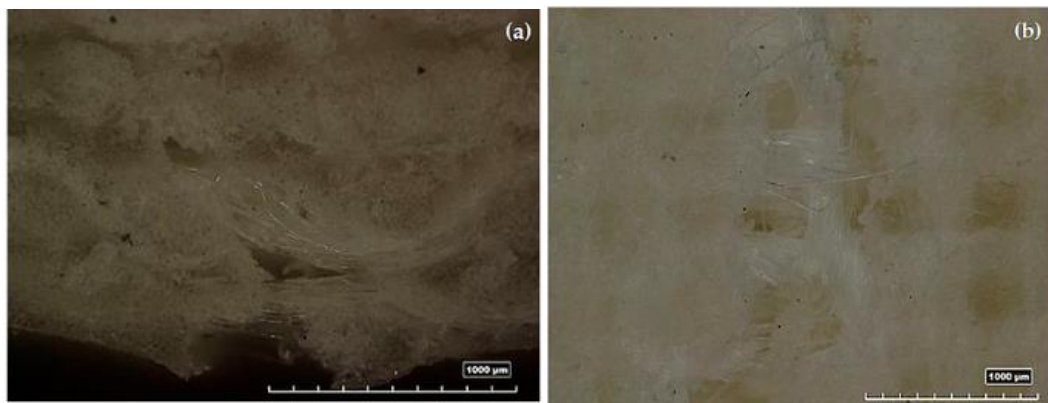


Figure 47: Images of the fracture for the tensile stress in the section (a) (140×) and in the plane (b) (100×) view.

As shown in Figure 46, all of the types of composites show the same initial slope, but, as the strain increases, the behavior is different, according to the treatment the fabrics have been subjected to: in particular, the waterglass treatment of the fibers could give rise to a worse adhesion at the interface fiber-matrix, hence decreasing the maximum stress and increasing of the elongation at break.

Furthermore, the presence of APP in the epoxy matrix does not seem to affect the overall mechanical behavior of the obtained composites.

6.2 A new sol-gel method for the production of hemp fibers through a waterglass based green process

6.2.1 Sol-gel preparation and characterization of hemp fibers

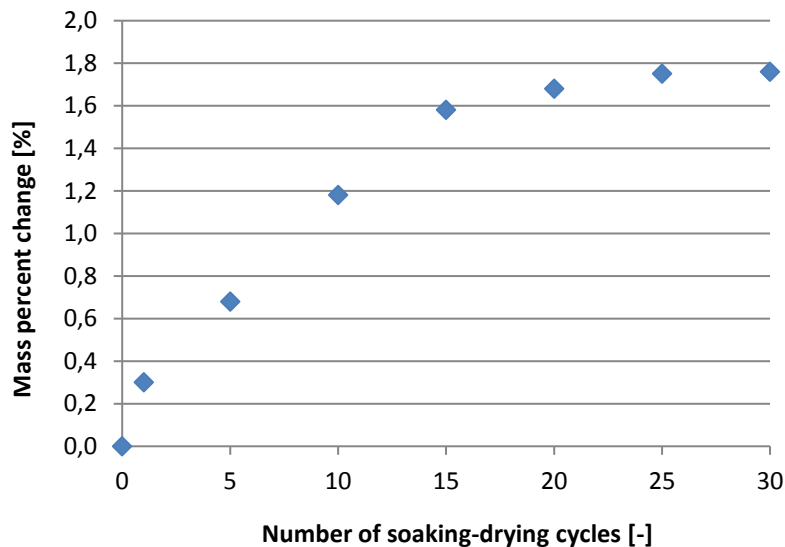
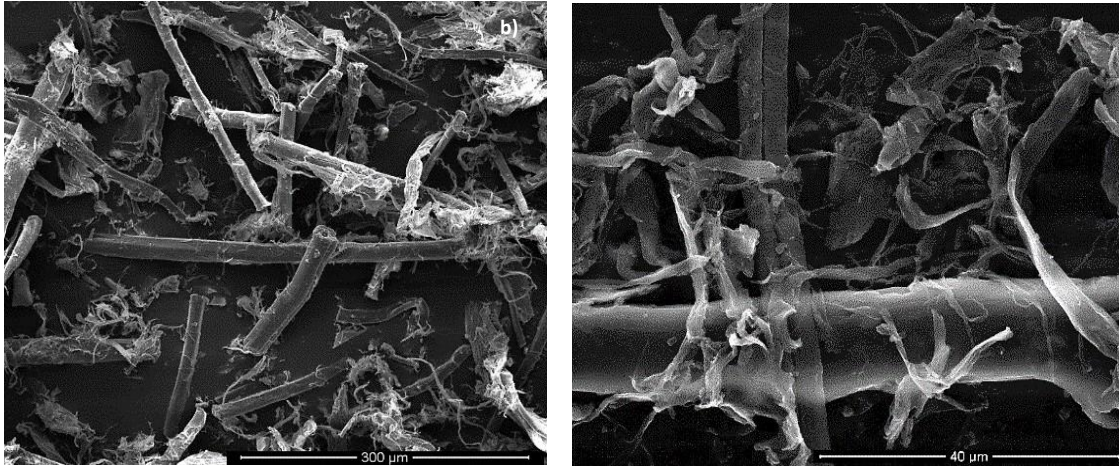


Figure 48: Mass percent change as a function of the number of soaking-drying cycles.

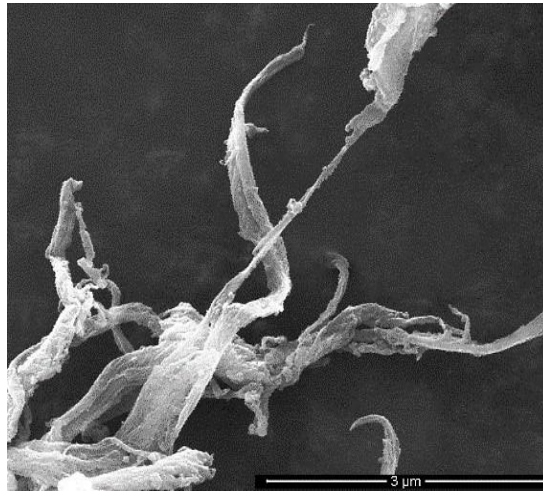
Hemp fabrics were iteratively soaked into acidified waterglass solutions following the procedure described in the section 5.2.3. Figure 48 shows how their mass changes (as wt. %) with the number of soaking-drying cycles. The treatment makes the fabrics to lose progressively softness. After 30 cycles they are *brittle* enough to be easily teared up. They may then be easily reduced to powders with the aid of a low power (350 W) mixer so as previously described.

Figure 49 shows the SEM micrographs of the powders obtained with increasing magnification. As can be seen the fibers obtained have diameter from 10 μm to 10 nm; this result may be explained if we remember the hierarchical structure of plant fibers [Thomas 2011]. They consist of elementary fibers corresponding to single cells of 1-50 μm length and 10-50 μm diameter. The cell has a central lumen, allowing water uptake, surrounded by several cell walls consisting of cellulose microfibrils, 10-30 nm in diameter, embedded in hemicellulose - lignin matrix (see Figure 50). The cell walls differ for the composition of the matrix and the orientation of the microfibrils. Each microfibril consists of 30-100 cellulose molecules in extended chain conformation.



(a)

(b)



(c)

Figure 49: SEM micrographs of the fibers at different magnifications: general overview at 300 μm (a) and increasing details at 40 μm (b) and 3 μm (c).

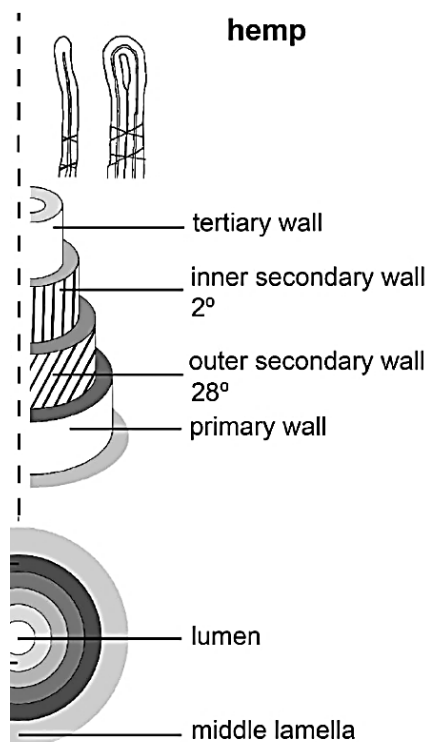


Figure 50: Structure of the hemp elementary fiber [Nytker 2006].

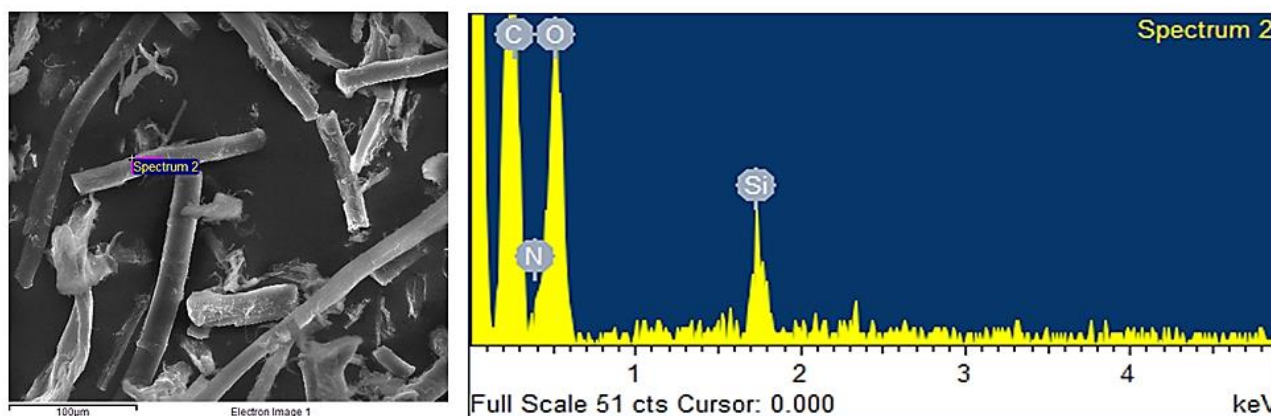


Figure 51: SEM micrograph of hemp fiber after APTS functionalization and EDX spectrum.

In section 6.1, the author showed that the exposition of hemp fabrics to inexpensive and ecofriendly 0.1 M waterglass solutions allowed the formation of a well anchored silica-based coating, resistant to washing. The formation of $-C-O-Si-$ covalent bonds between the coating and the cellulosic substrate was demonstrated through Fourier Transform Infrared (FTIR) and solid-state Nuclear Magnetic Resonance (NMR) analysis. Therefore, the above described results may be explained if we admit that, when reducing the concentration and prolonging the exposure (so as in the present research activity), the waterglass solution deeply penetrates the hierarchical structure of hemp fibers (see section 1.2). The formation of the silicate layer could be responsible of the observed brittleness

and easy reduction, in a low power mixer, to fibers of diameter from microns to tens of nanometers. The hemp fibers were easily functionalized with APTS so as described in section 5.2.4.

Observing hemp fibers again with electron microscopy after APTS functionalization (Figure 51), we can see that they look like those shown in Figure 49. Moreover, the microanalysis EDX confirms the presence of nitrogen on the surface of the fibers.

The presence of amino groups on the surface of the functionalized fibers is well supported also by the ninhydrin test [Ruhemann 1910] and FTIR spectra. In fact, when a small quantity of the treated microfibers was added to a ninhydrin EtOH/Water (80/20, vol/vol) solution the characteristic blue-violet-color appeared.

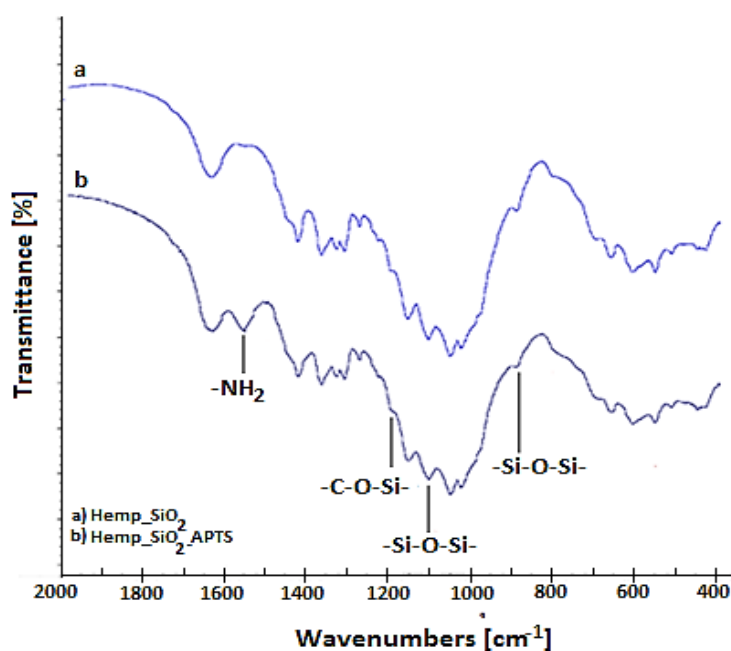


Figure 52: FTIR spectra of a) hemp fabric after functionalization with waterglass (Hemp_SiO₂ sample); b) the spectrum recorded after the functionalization with APTS (Hemp_SiO₂_ APTS sample).

The functionalization is, finally, further confirmed by the FTIR spectra reported in Figure 52 showing the spectra of hemp fibers (Hemp_SiO₂ sample) before (a) and after (b) functionalization with APTS (Hemp_SiO₂_ APTS sample). Spectrum a) proves that the hemp fibers are produced with a silica coating. In fact spectrum a) is similar to the one previously reported and differing from the hemp one for the presence of three bands (see Figure 37 in section 6.1.1); two of them are due to the well known stretching vibration of silicate structure, the third one is due to the condensation reaction between OH of hemp and silanols of silica and the consequent presence of C-O-Si bonds

[Abdelmouleh 2004, Britcher 1995]. As can be seen after exposition to APTS solution a band ascribable to NH_2 stretching vibration appears on the FTIR spectrum.

6.2.2 Scanning Electron Microscopy observations of epoxy/APTS functionalized hemp fibers composites

SEM morphologies of the composites epoxy/APTS functionalized hemp fibers are shown in Figure 53 (a-c) at different magnifications. Figure 53a suggests that the interface with epoxy matrix is very good; this may be the consequence of fibers functionalization with APTS and the consequent presence on their surface of amino groups able to react with epoxy in the same manner as the ones present in the curing agent. The compatibility appears to be very high as shown in 53b, a detail of micrograph 53a. It is so good, in fact, to allow the finer fibers linked to the greater ones to extend in the matrix instead of piling on the surface of the bigger ones. Thanks to this behavior, a *web-like* structure formed by fibrils and microfibrils 53c continuously interconnected from which we can expect particularly good mechanical properties [Nakagaito 2005].

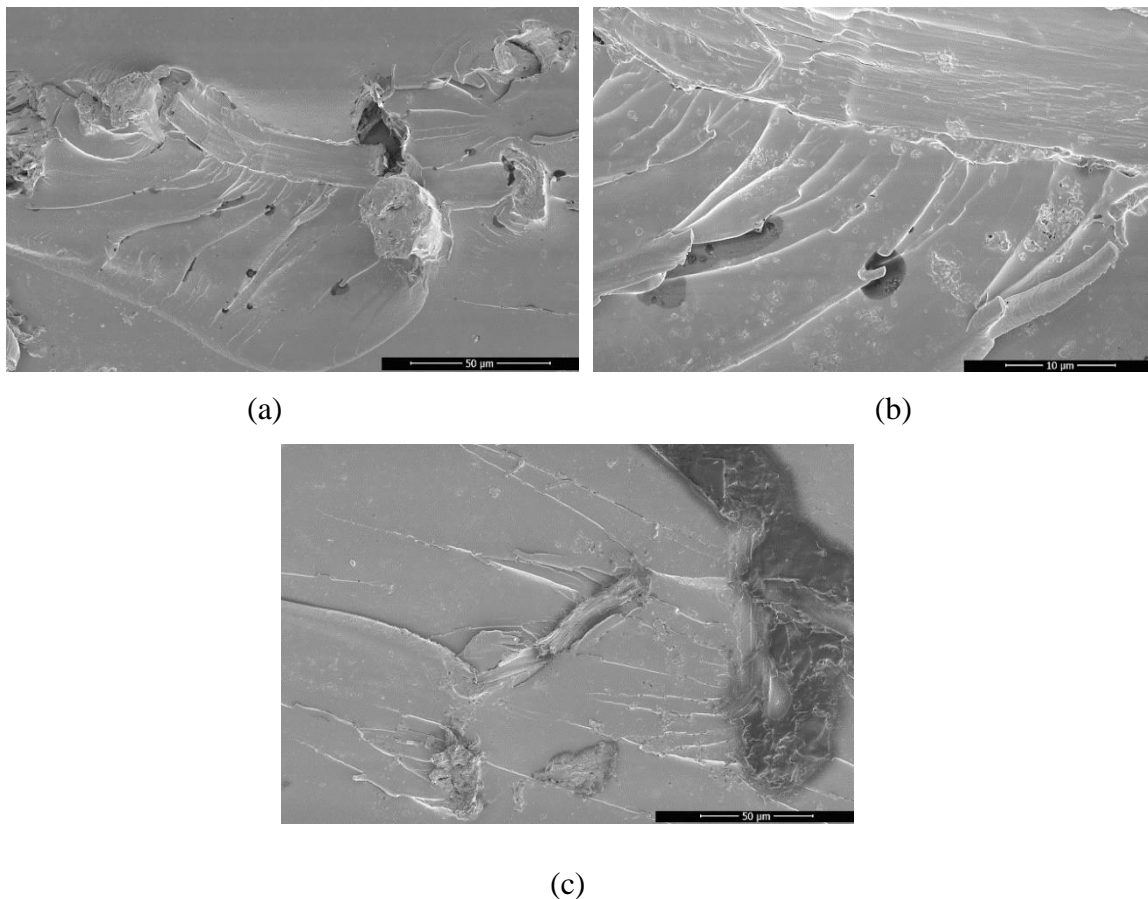


Figure 53: SEM micrographs of the composites epoxy/APTS functionalized hemp fibers at 50 μm scale (a and c) with and a detail of (a) region at 10 μm (b).

6.2.3 Dynamic Mechanical Analysis of epoxy/APTS functionalized hemp fibers composites

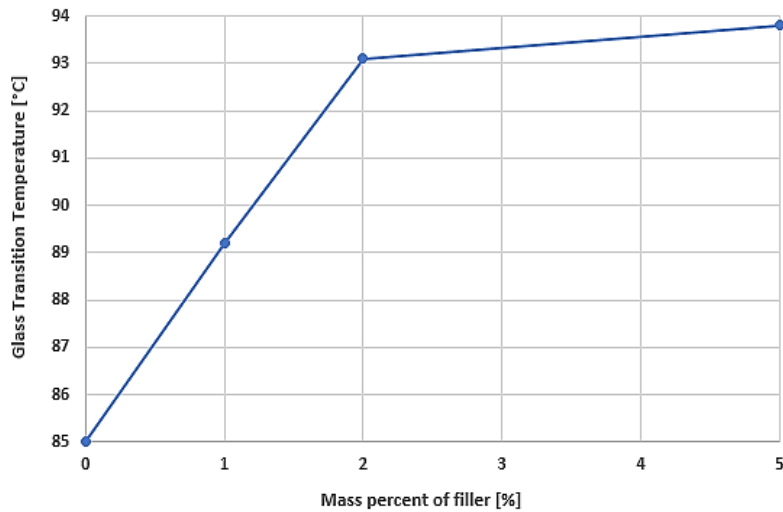


Figure 54: Glass transformation temperature of the composites epoxy/APTS functionalized hemp fibers as a function of composition.

Figure 54 shows the plot of glass transformation temperature, T_g , as a function of composition. The T_g were taken, from DMA results, as the maximum of $\text{Tan}\delta$ vs. temperature curves (see Figure 55). As can be seen the addition the functionalized hemp fibers strongly affects the T_g making it to increase. This is indicative of a good interaction at the interface of fibers with epoxy, consistent with the appearance of SEM micrographs.

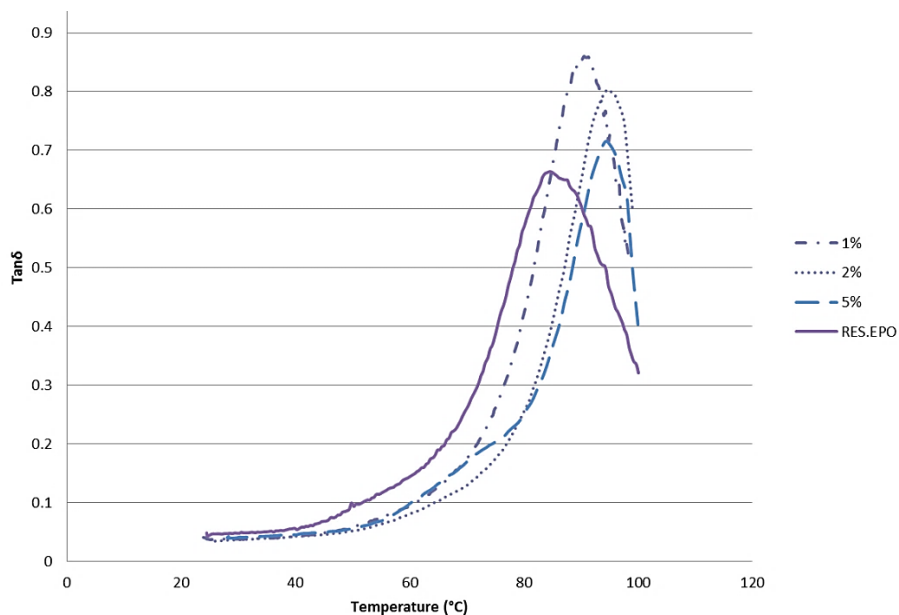


Figure 55: Comparison between the experimental values of $\text{Tan}\delta$ (calculated as storage and loss modulus ratio) for different volumetric percentage.

The values of the storage modulus [Zhang 2007], measured by DMA tests, clearly depict that the incorporation of microfibers for the resin generates an increase of the modulus.

In order to evaluate the influence of hemp microfibers on the storage modulus of composite, two formulae were considered, the analytical formula of “rule of mixtures” [Fragassa 2018, Fukuda 1981, Sideridis 2018] adopted for long unidirectional fibres:

$$E = v_f * E_f + v_m * E_m \quad (6.2)$$

and the formula of “inverse rule of mixtures” adopted in case of short fibers or fillers.

$$1/E = v_f/E_f + 1/(v_m/E_m) \quad (6.3)$$

Where:

- E is composite modulus.
- E_f is fibre or filler modulus.
- E_m is the matrix modulus.
- V_f and V_m are the volumetric percent of fibers and matrix respectively.

In Figure 56 the medium values of storage modulus at environmental temperature is reported for the different values of volumetric content of fibers. In this diagram a comparison with the results of analytical formulae of role of mixture and inverse role of mixture is reported.

For composites reinforced by hemp microfibers, the increase in modulus calculated by the formula of “inverse rule of mixture” for low value of volumetric content (1-2 % vol.) is negligible [Fragassa 2018, Fukuda 1981, Sideridis 2018].

From experimental data, it is possible to note that the increase in modulus starts immediately for low values of volumetric percentage of hemp microfibers and is higher than the values calculated by the formula of inverse rule of mixture (adopted in the case of short fibres).

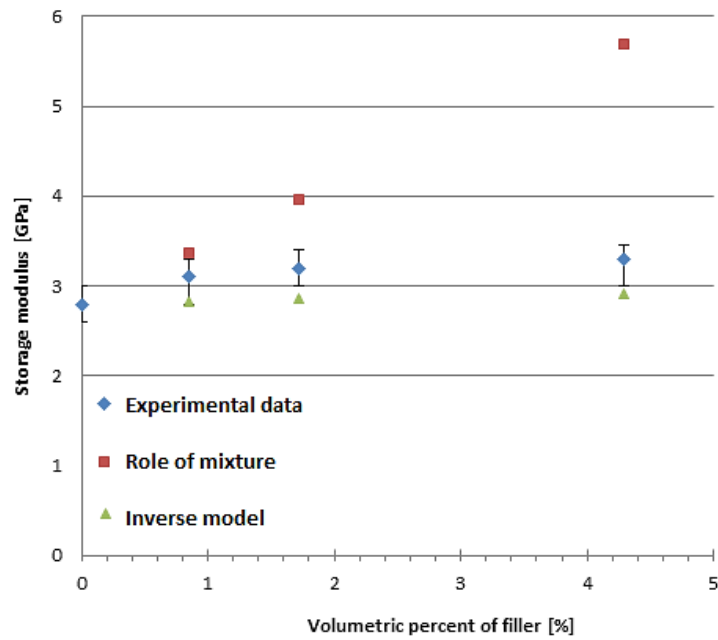


Figure 56: Comparison between the experimental and theoretical values of moduli for different volumetric percentage.

For 1% in weight of microfibers the modulus increases about of 10%. This may be ascribed to the fact that the microfibers effectively could be bonded to macromolecules influencing the rigidity of the resin. Moreover, it is worth reminding that the role of mixture is valid in the case of continuous fibers reinforced composites; the inverse model is, instead, valid for short fibers reinforced composites. The two models might to be both inadequate if, so as SEM micrographs do suggest, a web-like structure [Nakagaito 2005] formed by fibrils and microfibrils continuously interconnected does form.

6.3 Fire behavior study of in-situ generated silica/epoxy hybrids

6.3.1 Characterization of the epoxy/silica hybrid nanocomposites

Figure 57 shows the ATR-FTIR spectra of the different samples listed in Table 5. In the presence of silica, a remarkable evolution of the IR absorption bands in the frequency range between 1050 and 1150 cm^{-1} is observed. The absorption in this frequency range keeps on increasing in the hybrid samples (see the FTIR spectra of EPO_2%Si, EPO_4%Si and EPO_6%Si): this finding can be ascribed to the presence of a progressively higher *silica phase* amount, thus proving its formation from the APTS and TEOS added to the batch through well-known reactions (see Eqs. (1.3), (1.4) and (1.5) in section 1.2.1).

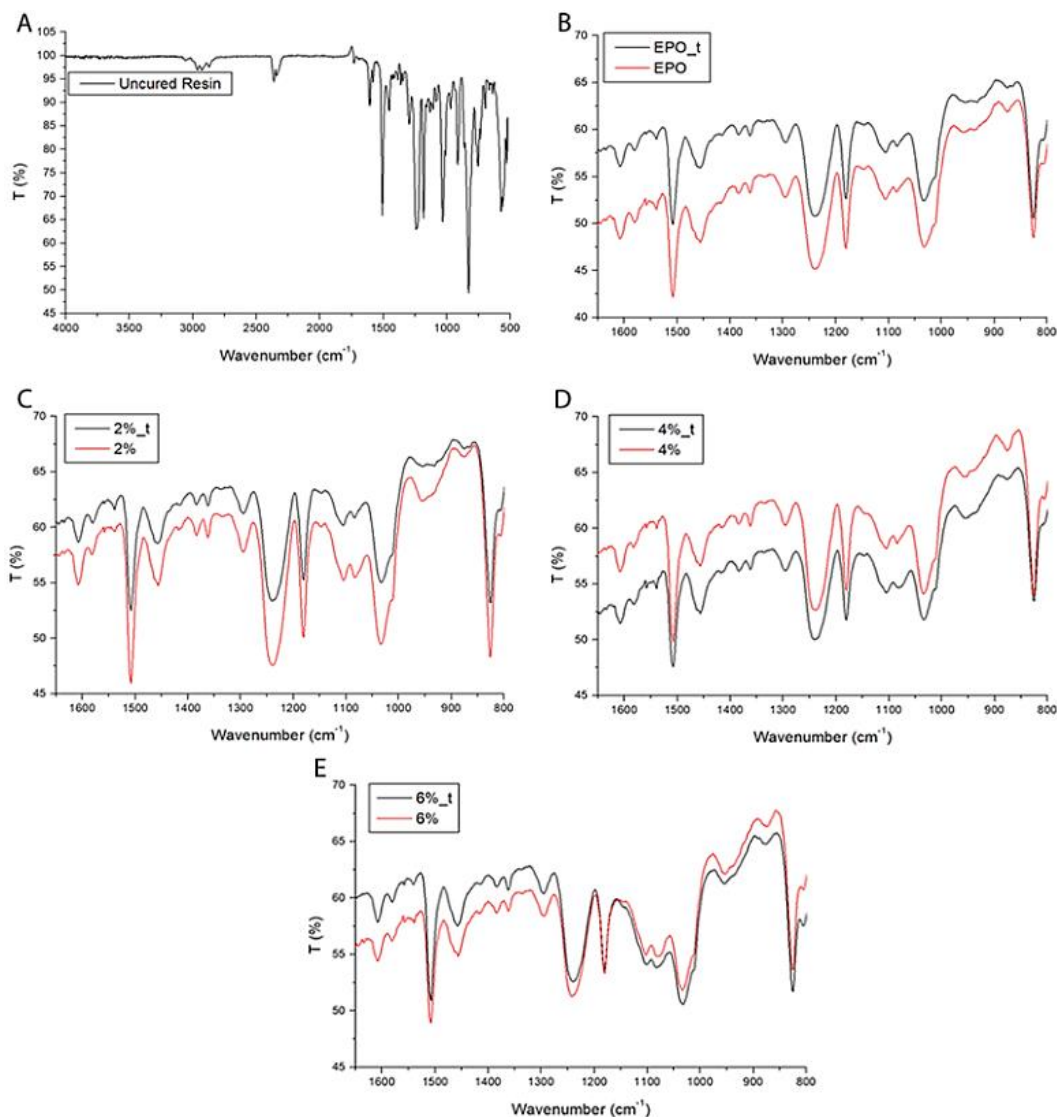


Figure 57: FTIR spectra of the uncured resin (a) and of all the hybrid systems (b–e), either non-thermally treated (red) or subjected to a non-isothermal post curing (dark gray) (color figure online).

It is known, in fact, that SiO_4 stretching vibration modes of fused silica give rise to a sharp band at 1100 cm^{-1} [Šimon 1953, Yu 1999]. When alkaline or earth-alkaline oxides are added, this band gradually shifts towards lower wavenumbers and broadens. This finding is due to the build-up of SiO_4 tetrahedral units bearing a progressively higher number of non-bridging oxygens and therefore to a lack of network connectivity [Šimon 1953, Yu 1999]. In the case of silica gel produced through the sol-gel process, this lack of connectivity may be due to incomplete condensation of silanol groups. Accordingly, the bands appearing at 1070 and 1100 cm^{-1} may be ascribed to partially uncondensed and condensed silica phases, respectively [Mascia 2005, Torrens 2008]. The band at 1070 cm^{-1} may be interpreted also on the basis of the formation of bi-continuous nanocomposites consisting of particles in a hybrid silica-epoxy network (see section 2.1), thus associated with the existence of a “diffused” silica network [Mascia 2006]. It is worth noticing that the characteristic

bands of the epoxy group, located at 970, 913, and 870 cm^{-1} are intense and well defined in the uncured system and disappear in all the other samples. Taking into account that the cure involves the reaction of the oxirane ring with the amine present in the hardener, the disappearance of these bands confirms the completeness of the polymer curing reactions [Jiao 2013].

6.3.2 Morphology of the epoxy/silica hybrid systems

The hybrid systems, before and after the thermal treatment, are transparent, as shown in Figure 58 for EPO_2%Si. TEM micrographs, displayed in Figure 59, show a very fine and even distribution of particles. In all samples, some particles tend to aggregate into clusters or bigger particles. This phenomenon can be very well observed in Figure 60 where a high resolution TEM (HRTEM) of EPO_6%Si sample is shown.

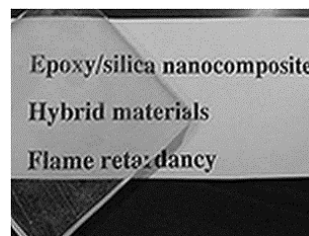


Figure 58: Photograph of an epoxy/silica hybrid material containing 2 wt. % silica.

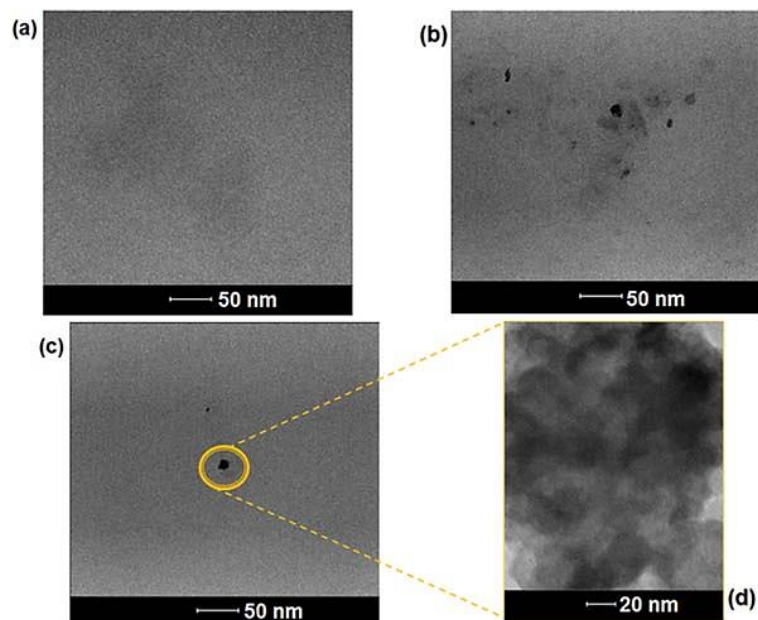


Figure 59: TEM micrographs of EPO_2%Si (a), EPO_6%Si (b), EPO_4%Si (c), and EPO_4%Si at high magnification (d).

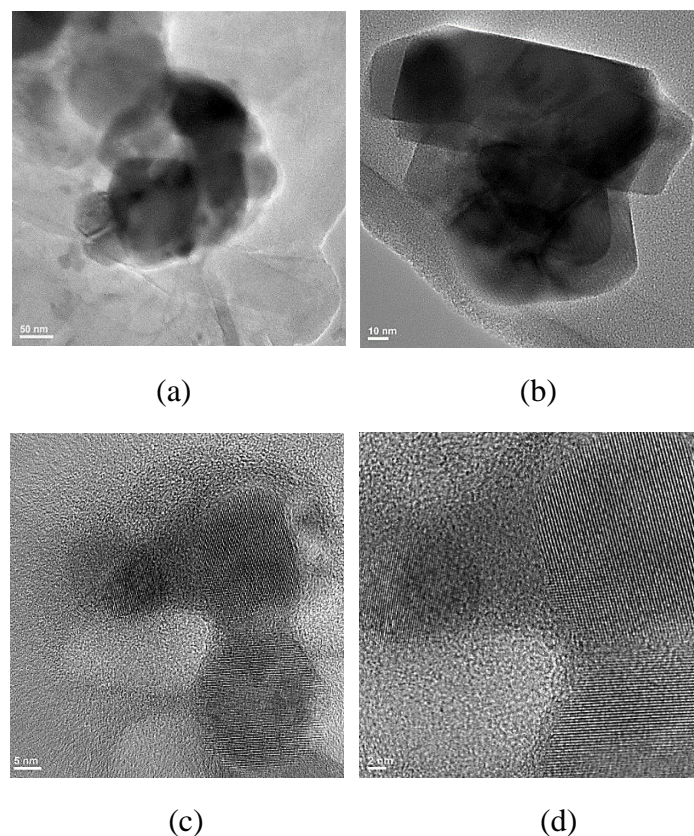


Figure 60: HRTEM micrographs of EPO_6%Si at higher magnifications: general overview at 50 nm (a) and increasing details at 10 nm (b), 5 nm (c) and 2 nm (d).

This clustering effect (see Figure 60) is very limited for the hybrids containing 2 wt. % silica but increases with increasing the filler loading, as observed when comparing TEM micrographs reported in Figures 59a and 59b.

The higher magnification micrograph (Figures 59d and 60) further supports the presence of a hybrid co-continuous structure. This may be attributed [Davis 2003, Matějka 1999] to the first step of the synthesis procedure (see also section 2.3), when epoxy resin and APTS are left to react to form the silanized epoxy through the reaction of the APTS amino group with the epoxy oxirane ring (see Figure 61).

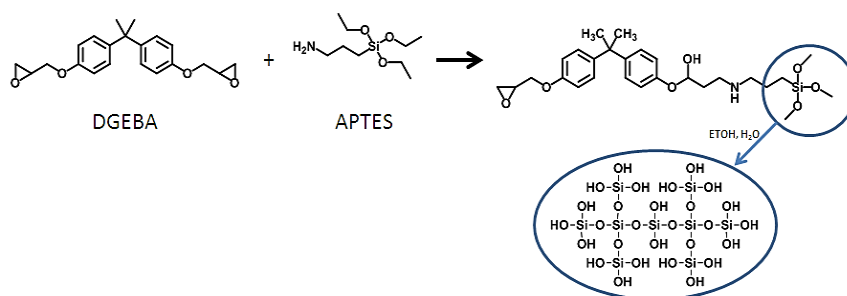


Figure 61: Schema of the synthesis route for the epoxy/silica hybrid nanocomposites.

6.3.3 Small Angle X-ray diffraction analysis of the epoxy/silica hybrid nanocomposites

The WAXD and SAXS results are displayed in Figure 62. In particular, Figure 62a shows for the composite with 6 wt. % of silica the typical epoxy features at q vector equal to 4 and 12 nm^{-1} , which are assigned to local fluctuations of the epoxy network. This confirms that the epoxy network of hybrids is not affected by the functionalization reaction of epoxy resins macromolecules with APTS and silica adducts produced by the sol-gel method. Different results were obtained by some of the authors when 3-glycidyoxypropyl)trimethoxysilane (GPTMS) was used as coupling agent (see section 2.1). In this case, the presence of 3:1 GOTMS:TEOS brought about a significant structural modification of the epoxy network with the disappearance of the peak at q vector equal to 4 nm^{-1} [Piscitelli 2015].

In the SAXS region, at q value lower than 2 nm^{-1} , the spectra of the different hybrids depend on the silica content and the thermal treatment the samples underwent. In details, as can be seen from Figure 62b, the EPO_4%Si and EPO_6%Si SAXS spectra show, before the thermal treatment, a typical Guinier knee feature, which is ascribed to the presence of discrete silica particles homogeneously dispersed in epoxy matrix. After the post cure non-isothermal treatment, this diffraction feature disappears and the diffracted intensity becomes linear with the scattering vector for all samples.

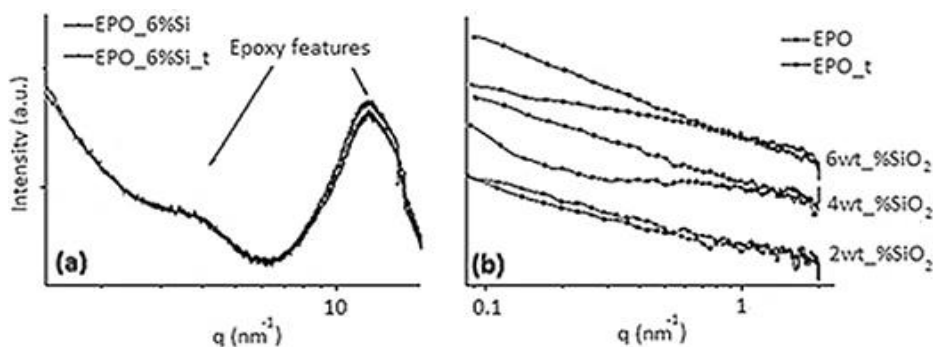


Figure 62: (a) WAXD scattering profiles of epoxy/silica nanocomposites containing 6 wt. % of silica before and after post cure thermal treatment (3 °C/min till 100 °C) and (b) SAXS profile of epoxy/silica nanocomposites before and after post cure thermal treatment.

This evidence may be assigned to the formation of an inorganic fractal structure: its density, which is measured as slope of the diffracted intensity in the $\log I(q)$ - $\log q$ graph, does not depend on the silica content and seems to be approximately similar for all hybrids. The EPO_2%Si shows a SAXS spectrum characterized by a linear diffracted intensity, also before the thermal treatment. This is likely due to the presence of smaller silica particles homogeneously dispersed throughout the

sample, giving rise to a homogeneous co-continuous hybrid morphology. This latter does not change upon the thermal treatment from 25 to 100 °C. From the Guinier feature it is possible to estimate the size of silica particles and the results confirm what is seen from the TEM micrographs: the samples consist of very small particles. In particular, the silica size increases by increasing the silica content from 2% to 6 wt. %, being the geometrical radius equal to 1.15 nm for EPO_4%Si and 1.25 nm for EPO_6%Si. Referring to EPO_2%Si sample, the SiO₂ size is *too small* to be measured.

The SAXS data indicate that the final morphology of the hybrids depends on the silica content and on the effect of post curing thermal treatment. Before this latter, all samples consist of nanostructured particles, whose size increases with TEOS content, which are homogeneously dispersed in an organic–inorganic network made by epoxy resin and diffused epoxy APTS functionalized/siloxane moieties (i.e., not fully condensed). The morphology of the samples with higher silica loadings significantly shifts towards a fractal structure. The silica particles aggregate during the post cure thermal treatment forming a co-continuous hybrid morphology, which appears as a fractal structure in the SAXS analysis [Cao 2010].

6.3.4 Dynamic Mechanical Analysis of the epoxy/silica hybrid nanocomposites

All the prepared samples were subjected to DMA; each test was repeated twice on the same sample. Tan δ vs. temperature curves referring to the first and second DMA runs are shown in Figure 63. Furthermore, the T_g values, calculated as the maximum of Tan δ curve, are plotted as a function of the composition in Figure 64. It is worthy to note that, as the DMA analyses were carried out from room temperature to 100 °C at a heating rate of 3 °C/min, the first repetition of DMA analyses can mimic the non-isothermal “post cure” treatment defined in section 5.2.6. This is the reason, for which in the legend of Figure 63, some curves are coded with “t”, according to the acronyms defined in section 5.2.6.

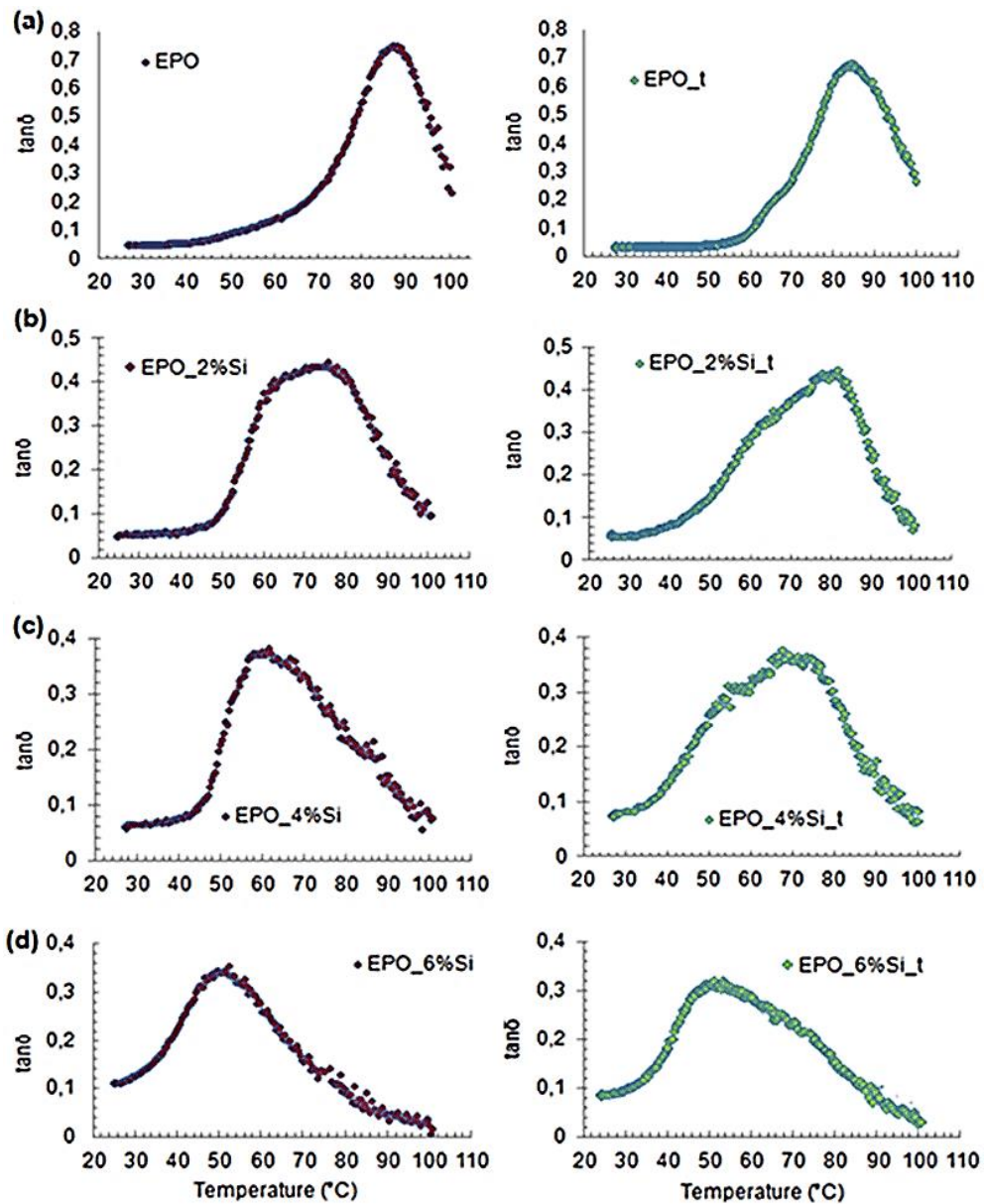


Figure 63: $\tan\delta$ vs. temperature curves of cured epoxy (a) and epoxy/silica nanocomposites (b–d) at different silica content derived from the first (red) and second (dark gray) DMA run.

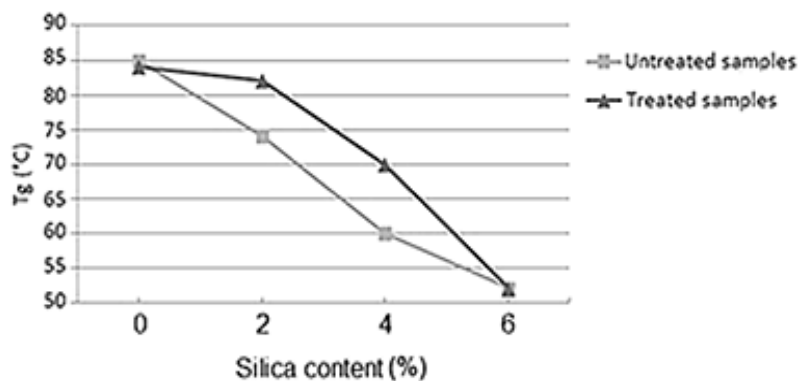


Figure 64: Glass transition temperatures as a function of silica content, for cured epoxy and epoxy/silica hybrid materials: first (squares) and second DMA (triangles) run.

As can be seen, only the cured epoxy curve shows a sharp peak that does not change in the second DMA run, hence indicating that the polymer network is fully cured in the adopted experimental conditions. Conversely, the $\text{Tan}\delta$ peaks for the hybrid samples are broader, possibly showing shoulders; the modifications observed in the successive heating cycles are an indication of the occurrence of structural changes during the second DMA run. This finding can be ascribed to the presence of two co-continuous phases, one consisting of more flexible and the other of more rigid segments [Jiao 2013, Mascia 2005, Mascia 2006], as supported by TEM images of the hybrid system (see Figures 59 and 60), where very fine silica nanoparticles are embedded in a hybrid co-continuous network. According to the FTIR results reported in Figure 57, in all samples the oxirane ring absorption bands almost disappear. This means that the changes should not be related to polymer cure reactions completion. However, two other explanations can be given for the $\text{Tan}\delta$ peaks changes observed in the case of “treated” samples. First, it must be taken into account that the final temperature of the thermal treatment at 3 °C/min (first DMA run) is, for all samples, above the glass transition temperature of the neat polymer network. The mobility that, in the glass transformation range, all the hybrid segments are expected to acquire may well allow silanols ($\equiv\text{Si}-\text{OH}$) or silanols and unhydrolysed $\equiv\text{Si}-\text{O}-\text{C}_2\text{H}_5$ groups to get closer and condensate according to reactions (1.4) or (1.5). This could well explain the changes of $\text{Tan}\delta$ peaks. SAXS results concerning the greater size of silica in the post cured samples may find a similar explanation: taking into account the very low particles diameter (maximum 1.25 nm), when the hybrid segments acquire enough mobility, nanoparticles clustering may easily occur. However, these structural rearrangements may, by themselves, explain the $\text{Tan}\delta$ peaks changes. A third explanation is, by this way, found.

Finally, the trends of T_g curves reported in Figure 64 can be justified as well: in fact, both completion of condensation reaction and/or particles clustering may well justify the T_g increases of the post cure treated samples.

Figure 65 plots the room temperature storage modulus of the samples before and after the post cure non-isothermal treatment. A remarkable increase (+30%) of the modulus is observed, particularly for EPO_6%Si after post curing.

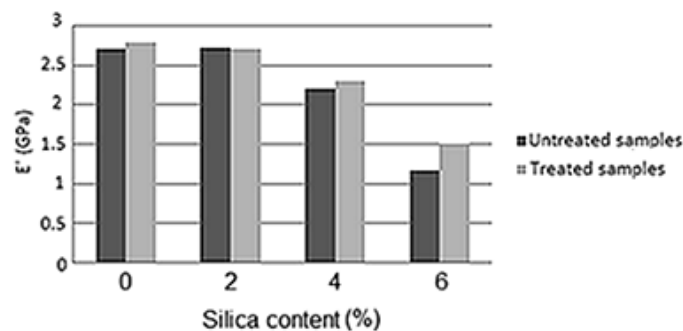


Figure 65: Room temperature storage modulus of untreated and thermal treated samples.

This finding is likely to be ascribed to the nanoparticles clustering occurring in the samples, after the thermal treatment: the clustering may act as a reinforcement for the resin, increasing the mechanical properties with respect to the untreated sample.

6.3.5 Solid-state NMR spectroscopy of the epoxy/silica hybrid systems

The above discussed hypothesis about the occurrence of silicate condensation reactions during the post curing thermal treatment was checked in the case EPO_2%Si by means of solid state NMR spectroscopy. The ^{29}Si NMR and ^{13}C CPMAS NMR spectra are shown in Figures 66 and 67.

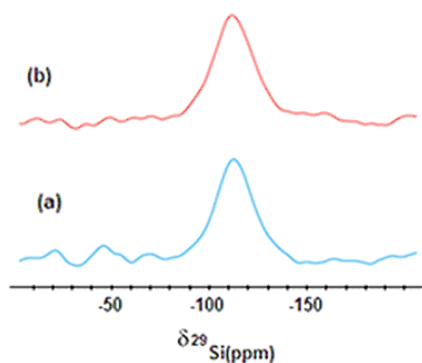


Figure 66: ^{29}Si NMR spectra of hybrid polymer before (a, blue) and after (b, red) the thermal treatment acquired at a spin rate 10,000 Hz (color figure online).

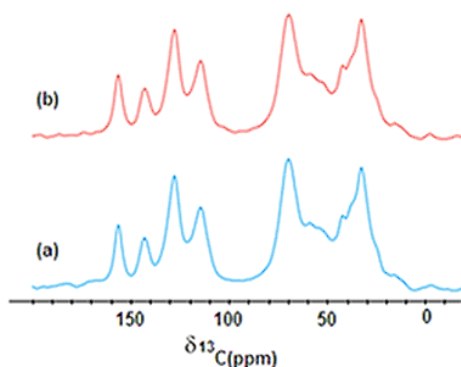


Figure 67: ^{13}C CPMAS NMR spectra of hybrid polymer before (a, blue) and after (b, red) the thermal treatment acquired at a spin rate 10,000 Hz (color figure online).

The ^{29}Si NMR spectrum of studied hybrid material (Figure 66a) shows a relatively broad and intense signal ranging within -95 and -125 ppm and attributable to the Q_4 silicon nuclei. The high-field resonance of this peak is due to the strong shielding-effect resulting for the involvement of observed silicon nuclei in four $-\text{Si}-\text{O}-\text{Si}-$ linkages. Remarkably, the fact any peak was detected in the spectral regions of Q_2 (-85 ppm) and Q_3 (-95 ppm) forms suggests that most of silicon nuclei composing the added TEOS were converted into Q_4 forms during the gel formation. Additionally, the lack of Si peaks in forms different than Q_4 also suggests to exclude a relevant presence of residual APTS, which, depending on the extent of siloxane formation, may polymerize to produce Q_3 forms. However, the comparison with the ^{29}Si NMR spectrum of thermally treated material (EPO_2%Si_t) did not reveal any significant change attributable to the thermal treatment (Figure 66b). The same result was observed when a replicate was analyzed for both sample types. This confirms that the origin of the peculiar properties of studied hybrid material, revealed by other analytical techniques, cannot be explained by a different arrangement of the siloxane network, since most of silicon atoms appear to have been fully involved in the condensation reactions (1.4) and (1.5).

Most signals detected in the ^{13}C CPMAS NMR spectrum of EPO_2%Si (Figure 67a) are attributable to the DGEBA structure. In detail, the alkyl region appears dominated by two peaks corresponding to both the two magnetically equivalent methyls (at 32 ppm) and the quaternary carbon, which the methyls are bound to (at 42 ppm). The four peaks in the range 110–165 ppm correspond to the aromatic carbons of phenol ring. Specifically, the signals at 158 and 143 ppm are due to the two aromatic quaternary carbons which are bound to the oxygen involved in an ether bond and an alkyl quaternary carbon, respectively. The signals at 128 and 143 ppm correspond to protonated aromatic carbons positioned in ortho and meta, in respect of the quaternary aromatic C–O at 158 ppm. The peak at 70 ppm corresponds to the methylene carbon bound to the phenolic oxygen. Finally, the signals at 58, and 44 ppm rise from the methylene and methine carbons composing the DGEBA epoxy group, respectively. The peaks dominating the spectral region 40–60 ppm appear relatively broadened since the methine and methylene signals of unreacted DGEBA resonate at very similar frequencies as compared to the corresponding carbons, which resulting from the opening of the epoxy ring and coupling with APTS or curing agent amino group (Figure 67a). The comparison with the ^{13}C NMR spectrum of EPO_2%Si_t did not reveal any significant difference depending on thermal treatment (Figure 67). Remarkably, the fact that intense ethoxy peaks were not detected in the most shielded alkyl-C region, suggests an approximately complete hydrolysis of ethoxy groups in both APTS and TEOS reagents. This is in agreement with the results

achieved by ^{29}Si spectra about the fully involvement of silicon atoms in the condensation reactions (Figure 66).

Therefore, taking into account the NMR results, the structural changes evidenced by the DMA curves and the T_g changes during the post cure thermal treatment must be, mainly, attributed to the clustering of silica nano-particles evidenced by SAXS analyses.

6.3.6 Fire behavior of the epoxy/silica hybrid systems

The fire behavior of a flame retarded system is usually investigated by performing either flammability (according to UL94 standard, in vertical or horizontal configuration) or forced-combustion (i.e., cone calorimetry) tests: in fact, their combination allows assessing the overall fire performance of the considered system, hence evaluating the reaction of the material towards the application of a flame or a heat flux (see sections 5.3.10 and 5.3.11). In this context, vertical flame spread and cone calorimetry tests were exploited. As far as vertical flame spread tests are concerned, all the samples investigated can not be classified, as they do not achieve self-extinction before the flame reaches the top of the sample. However, the presence of the silica domains in the hybrid structures allows preventing melt dripping phenomena [Matzen 2015], which, at variance, occur in the neat epoxy network. Undoubtedly, melt flow and dripping of the pyrolyzing polymer can be detrimental during a fire, as they often provide an additional ignition source, an additional flame spread process and even favor the starting of a pool fire independent from the original burning item. As clearly reported in the scientific literature [Crompton 2013], the addition of micro- to nano-particles to thermoplastic or thermosetting polymer matrices can prevent these undesired phenomena, because of the increase of the melt viscosity of the burning system: unlike the systems described in the literature, the high homogeneity of distribution of the silica nanoparticles in the epoxy network allows limiting the nanofiller loading to a very small extent that is capable of inhibiting the formation of incandescent drops. Furthermore, it is noteworthy that the flammability behavior of all the samples investigated is not affected by the non-isothermal treatment they possibly underwent. The pictures of the residues after vertical flame spread tests are shown in Figure 68: once again, they demonstrate the high char-forming character of the in situ synthesized silica nanoparticles, which allow achieving a high residue after flammability test.

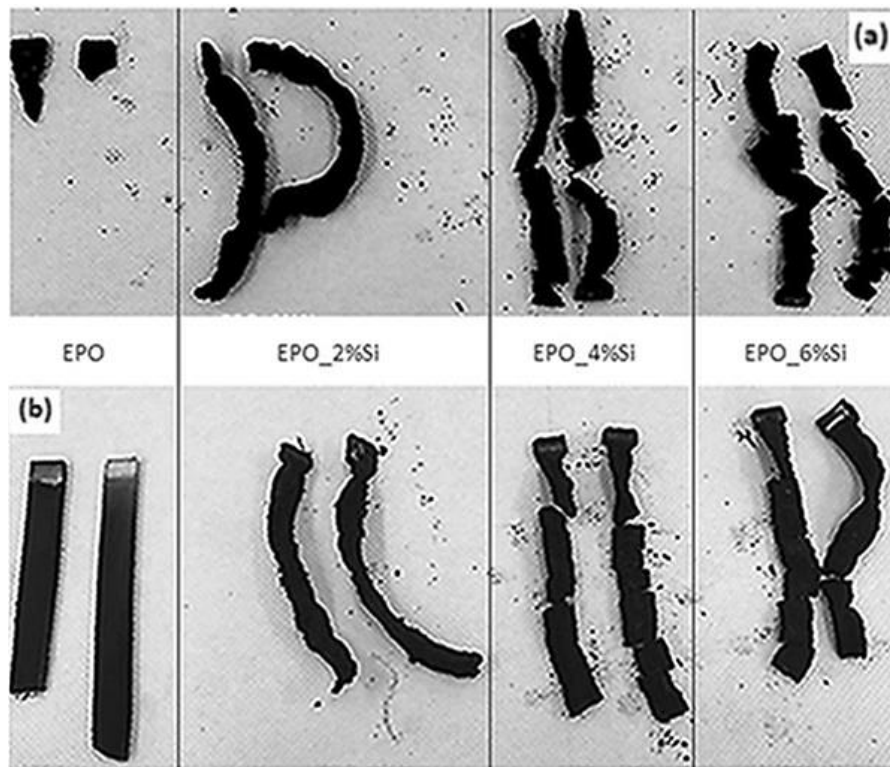


Figure 68: Residues of the different hybrid systems after vertical flame spread tests, before (a) and after (b) the post cure non-isothermal treatment.

As far as forced-combustion tests are considered, Table 15 collects the cone parameters in terms of TTI, HRR, pkHRR, THR and final residue. First of all, it is noteworthy that all the hybrid systems, irrespective of the possible non-isothermal post curing treatment, anticipate the ignition as compared to the neat cured EPO. Conversely, the presence of the silica domains well distributed in the polymer matrix promotes a remarkable decrease of HRR and THR as well: this finding can be explained in terms of formation of a ceramic silica layer, which acts as a thermal shield, hence protecting the underlying materials, slowing down both the diffusion of the volatile flammable degradation products towards the gas phase and the oxygen diffusion towards the degrading material [Malucelli 2016].

Table 15: Results from cone calorimetry tests performed on cured epoxy and epoxy/silica nanocomposites at different silica content before and after thermal treatment. TTI time to ignition, HRR heat release rate, pkHRR peak of the heat release rate, THR total heat released.

Sample	TTI (s)	HRR (kW/m ²)	pkHRR (kW/m ²)	THR (MJ/m ²)	Residue mass (%)
EPO	54 ± 3	504 ± 23	1971 ± 384	84 ± 3	2 ± 0.7
EPO_2%Si	37 ± 4	311 ± 12	991 ± 73	67 ± 9	6 ± 0.5
EPO_4%Si	37 ± 4	308 ± 13	929 ± 102	74 ± 7	7 ± 0.6
EPO_6%Si	32 ± 2	290 ± 15	1231 ± 228	57 ± 6	10 ± 0.6
EPO_t	51 ± 5	423 ± 10	1682 ± 108	77 ± 7	2 ± 0.7
EPO_2%Si_t	43 ± 2	421 ± 15	1791 ± 224	79 ± 6	5 ± 0.4
EPO_4%Si_t	45 ± 1	358 ± 21	837 ± 81	107 ± 3	7 ± 0.6
EPO_6%Si_t	30 ± 1	351 ± 28	1003 ± 32	89 ± 6	10 ± 0.6

The higher reduction of HRR and THR observed for the samples that did not undergo the non-isothermal post curing could be the result of two different phenomena taking place during the thermal treatment: more specifically, this latter can favor further condensation reactions of partially condensed hybrid structures, hence consuming the condensation by-products, which provide an endothermic effect that lowers the heat-related cone parameters.

In addition, the non-isothermal post curing treatment can promote some rearrangements in the silica domains (i.e., silica clustering phenomena, as revealed by SAXS analyses), which, upon the exposure to the heat flux of the cone, give rise to the formation of a less protective ceramic layer that should slow down the heat transfer from the material to the surroundings and vice-versa. Therefore, as a consequence of the silica clustering, the efficiency of the ceramic layer decreases, hence increasing THR and HRR values of the samples subjected to the non-isothermal post curing treatment. It is worth underlining that this effect appears to be particularly strong in the case of EPO_2%Si sample. In fact, for the not post cured sample, the HRR reduction is 40%, whereas it approaches 16% only for the post cured counterpart. NMR results suggest that the second effect is predominant. In addition, the formation of an inorganic phase within the hybrid material is responsible for the increase of the final residue at the end of the tests.

Finally, as far as the smoke parameters (see Table 16) are concerned, the hybrid structure, regardless of the possible non-isothermal post curing treatments, is responsible for an overall slight decrease of the TSR, SEA, CO, and CO₂ yields.

Table 16: Smoke results from cone calorimetry tests performed on cured epoxy and epoxy/silica nanocomposites at different silica content before and after thermal treatment.
TSR total smoke release, SEA specific extinction area.

Sample	TSR (m ² /m ²)	SEA (m ² /kg)	CO yield (kg/kg)	CO ₂ yield (kg/kg)
EPO	3066 ± 206	940 ± 36	0.061 ± 0.03	2.08 ± 0.06
EPO_2%Si	2604 ± 291	941 ± 38	0.060 ± 0.04	1.94 ± 0.03
EPO_4%Si	2851 ± 275	928 ± 3	0.057 ± 0.03	1.91 ± 0.02
EPO_6%Si	2087 ± 355	895 ± 31	0.063 ± 0.01	1.95 ± 0.05
EPO_t	2883 ± 226	937 ± 22	0.066 ± 0.003	1.97 ± 0.04
EPO_2%Si_t	2733 ± 304	839 ± 75	0.057 ± 0.007	1.89 ± 0.2
EPO_4%Si_t	4124 ± 273	607 ± 46	0.034 ± 0.002	1.19 ± 0.04
EPO_6%Si_t	3181 ± 217	472 ± 30	0.029 ± 0.003	1.01 ± 0.06

6.4 Phosphorous-based in-situ generated silica/epoxy materials

6.4.1 Chemical, thermal and mechanical characterization of the in-situ silica/epoxy composites

6.4.1.1 Infrared Spectrophotometry of the in-situ silica/epoxy composites

Figure 69 and Figure 70 show the FT-IR spectra of the different samples. In this analysis, in order to explain the main differences, only the flame retarded samples containing melamine and DA or DP with a P-loading equal to 2 wt. % were taken into account and compared to the blank ones. Additionally, the sample of uncured pristine epoxy (with EPO_WH as acronym) was also considered. It is worth noticing that the characteristics bands of the epoxy group located at 970, 913 and 870 cm⁻¹ are intense and well defined in EPO_WH and disappeared in all the other samples. The disappearance of these bands confirms the completeness of the polymer curing reactions, this because the cure involves the reaction of the oxirane ring with the amine present in the hardener

[Jiao 2013, Torrens 2008]. EPO2%Si shows a slight evolution of the IR absorption bands in the frequency range between 1050 and 1150 cm^{-1} . So as previously reported in section 6.3.1 this may be attributed to formation of the silica phase from APTS and TEOS through the well-known sol-gel reactions (1.3), (1.4) and (1.5).

The addition of the flame-retardant molecules to the in-situ silica/epoxy system, changes several peaks intensities and introduces new characteristic bands. In the case of EPO2%Si_DA2%P, two characteristic strong bands due to the stretching of C-O and to the presence of amide (amide III frequency region) groups at 1090 cm^{-1} and 1260 cm^{-1} are observed. The shoulder at 966 cm^{-1} may be attributed to the existence of P-O-C bonds [Chen 2018] in both phosphorous based flame retardants (see Figure 24). The strong intensity of the band near 1020 cm^{-1} indicates the presence of ortho-disubstituted benzene derivatives [Randle 1956, Tewari 1976]. The band around 760 cm^{-1} can be attributed to the P-C stretching; the 920 cm^{-1} one is reported to be due to the torsional vibration of the acetaldehyde structure in the DA molecule [Beg 1962, Belov 1994, Zhou 2008]. The bands located in the range between 2860 cm^{-1} and 2970 cm^{-1} may be due to the stretching vibration of the C-H bond, and the band around at 800 cm^{-1} could be to the bending vibration of the N-H bond, both present in the molecules of the DA flame retardant and melamine added to the epoxy sample [Mahapatra 2007, Salmeia 2019, Singh 2015].

The ATR-FTIR spectra are, therefore, consistent with the composition of the epoxy samples and show that, in all cases, the resin is well cured.

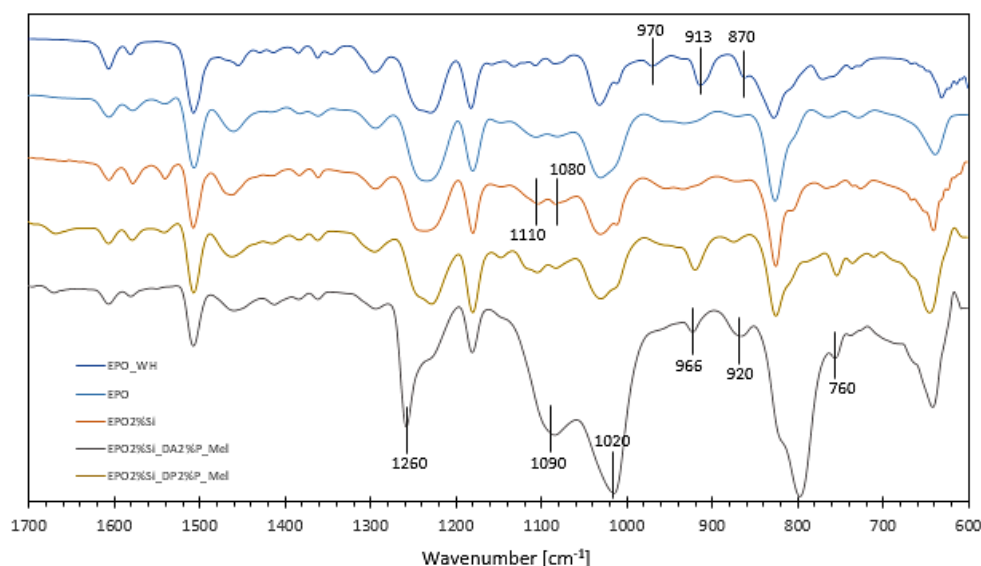


Figure 69: ATR-FTIR spectra of the uncured resin (EPO_WH), cured resin (EPO) and of the in-situ silica/epoxy systems containing 2 wt. % of P-loading and melamine (EPO2%Si_DA2%P and EPO2%Si_DP2%P).

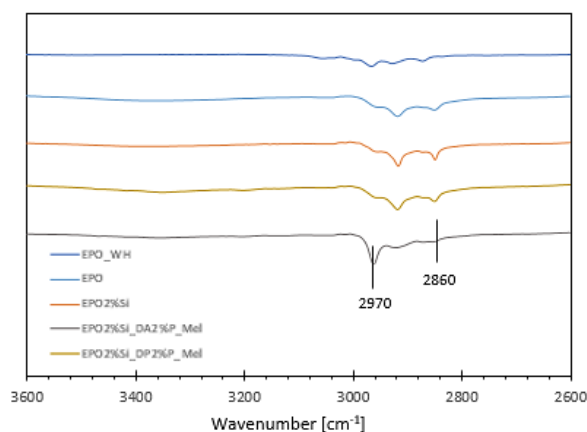


Figure 70: ATR-FTIR spectra (from 2600 to 3600 cm^{-1}) of the uncured resin (EPO_WH), cured resin (EPO) and of the in-situ silica/epoxy systems containing 2 wt. % of P-loading and melamine (EPO2%Si_DA2%P and EPO2%Si_DP2%P).

6.4.1.2 Nuclear Magnetic Resonance analysis of the in-situ silica/epoxy composites

3-(6-oxidodibenzo[*c,e*][1,2]oxaphosphinin-6-yl)propanamide (DA) flame retardant does contain amino groups (see Figure 24) so as the hardener. The reactivity between the DA flame retardant and the epoxy resin was investigated by using ^{13}C -NMR, ^1H -NMR, and ^{31}P -NMR analysis. To this scope DA and the pristine epoxy resin were mixed for 2h at 80°C and left in the heating oven in the same conditions of the curing process ($(40^\circ\text{C}/3\text{h})$ followed by post-curing ($150^\circ\text{C}/2\text{h}$)).

A second sample was prepared by adding 1,8-diazabicyclo[5.4.0]undec-7-ene (DBU), in an amount equal to 5 wt. % of the flame retardant (DA), together with DA and the pristine epoxy resin; the obtained system was mixed for 2h at 80°C and left in the heating oven in the same conditions of the curing process. The reason of this second sample is explained in the following. It is well known, in fact, that the reaction between an epoxy resin and an aliphatic amino hardener leads to a crosslinking reaction and to the synthesis of secondary amino groups in the polymer chain. The formation of secondary amino groups could, further, catalyze the reaction between DA and the pristine epoxy resin. DBU is a chemical compound that belongs to the class of amidine compounds. It is used in organic synthesis as a catalyst (e.g., crosslinking reactions), a complexing ligand, and a non-nucleophilic base [Burckhardt 2018]. Its addition, in the second sample, was intended to completely exclude a reaction between epoxy resin and DA. Both samples were solubilized in DMSO at room temperature without any additional preparation. The two samples were both analyzed through nuclear magnetic resonance spectroscopies.

^{13}C -NMR analysis substantially showed the same result for both the tested epoxy samples. Figure 71 represents the spectrum for the epoxy sample containing DBU. All the peaks usually [Garcia 2003] attributed to the carbon atoms of DGEBA, in particular the ones of the oxirane group (44.2 ppm (C1), 49.9 ppm (C2) and 68.3 ppm (C3)) are clearly visible. We highlight the absence of chemical shifts of carbon atoms linked to OH groups that would form in the case of reaction with DA.

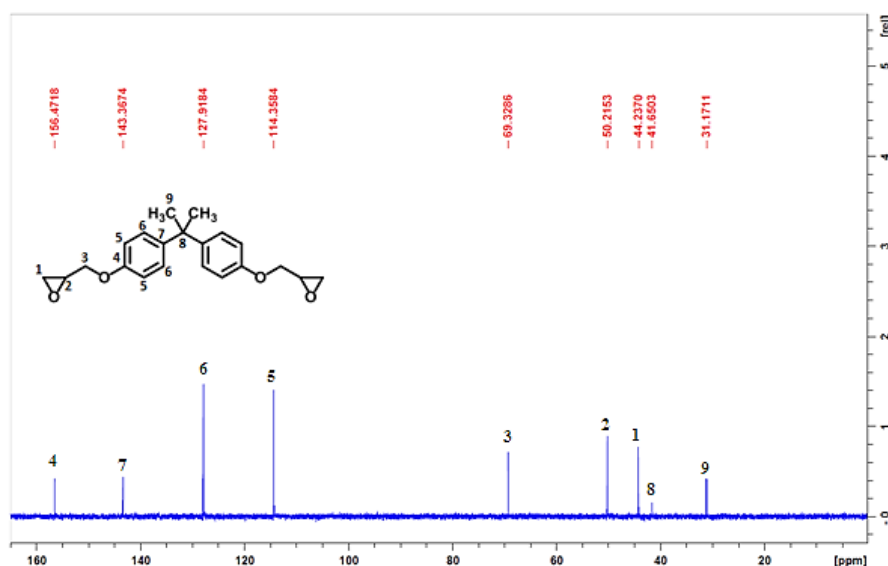


Figure 71: ^{13}C -NMR analysis for the sample composed by DBU, DA and pristine epoxy resin.

^1H -NMR analysis also showed the same result for both the tested epoxy samples. In Figure 72, the ^1H -NMR spectrum for the epoxy sample containing DBU is showed. All the resonance signals have been assigned to the protons present in the basic epoxy resin structure. The “integration values” are also reported in the same Figure. The bisphenol A moiety is responsible for the peaks at 7.1 ppm and 6.8 ppm (aromatic protons) and 1.6 ppm (methyl protons) [Garcia 2003]. The glycidyl terminal group is characterized by fine peaks in the range of $\delta = 2.5\text{--}4.5$ ppm (peaks c, d, e, f and g) [Garcia 2003].

The presence of unreacted DGEBA in ^{13}C -NMR and ^1H -NMR spectra confirms the absence of both direct and catalyzed reaction between DA and polymer resin.

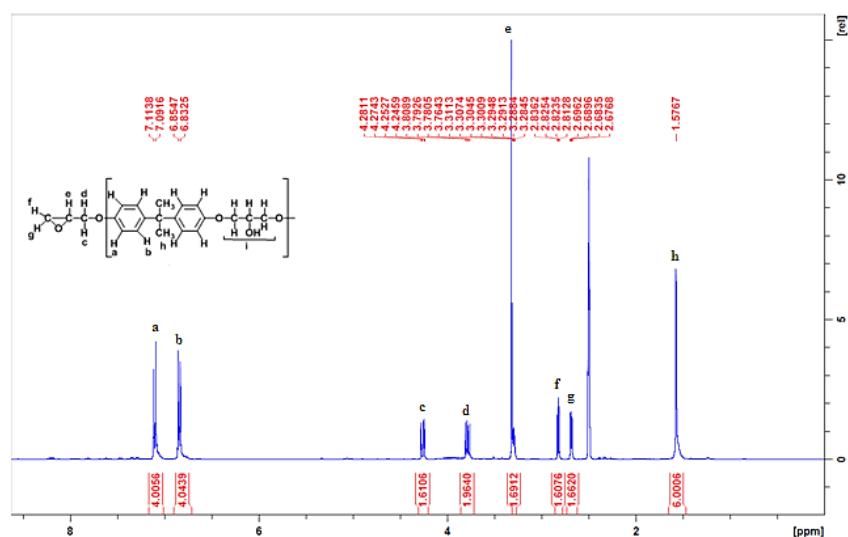


Figure 72: ^1H -NMR analysis for the sample composed by DBU, DA and pristine epoxy resin.

Figure 73 shows the ^{31}P -NMR ($^{31}\text{P}\{^1\text{H}\}$ NMR (162.0 MHz, DMSO- d_6) 1 (ppm): 37.2) spectrum for the epoxy sample containing DBU, representative of both studied epoxy samples. ^{31}P -NMR spectrum shows the characteristic peaks of the unreacted flame retardant, that were attributed by Salmeia et al. [Liu 2017, Salmeia 2018]. The presence of unmodified DA in ^{31}P -NMR spectrum, for the investigated epoxy samples, additionally confirms the absence of both direct and catalyzed reaction between DA and polymer resin.

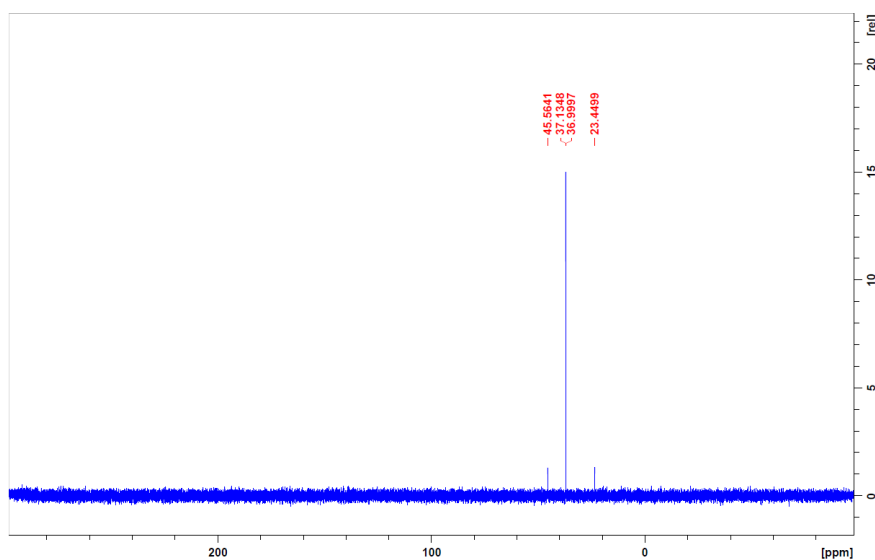


Figure 73: ^{31}P -NMR analysis for the sample composed by DBU, DA and pristine epoxy resin.

Based on the results discussed so far, for both the investigated cases the nuclear magnetic resonance spectra show that there is not reaction between DA and the pristine epoxy resin. These results exclude any possibility of a reactive approach [Döring 2009, Hergenrother 2005, Liu 2002, Saito 1981, Seibold 2008, Wang 1998], therefore DA flame retardant can be considered as a normal additive.

6.4.1.3 Differential Scanning Calorimetry of the in-situ silica/epoxy composites

The glass transition temperatures extracted as the onset values from the DSC thermoanalytical curves of EPO, EPO2%Si, EPO_DA2%P, EPO_DP2%P, EPO2%Si_DA1%P_Mel, EPO2%Si_DA2%P_Mel, EPO2%Si_DP1%P_Mel and EPO2%Si_DP2%P_Mel are shown in Table 17.

Table 17 shows that the addition of DA to the in-situ silica/epoxy network has a detrimental impact on the Tg of the cured resin, working as a plasticizer. Conversely, It is noteworthy that, the incorporation of DP (2 wt.% P) to the in-situ silica/epoxy network increases the Tg of the cured resins. The stiffness effect of DP on the polymer chains is likely due to the formation of hydrogen bonds between the oxygen of DP structure and hydroxyl groups formed because of the cross-linking process. Besides, Table 17 shows that the further addition of melamine together with DP or DA does not appear to have other effects on the Tg.

DA could be able to react through its primary amino groups with the oxirane rings of the epoxy resin (see Figure 24), subtracting reactive cross-linking sites to the cycloaliphatic amino hardener. In this case the excess of curing agent would have a plasticizing effect [Liu 2002]. NMR results do exclude this hypothesis. Alternatively, we may consider [Larin 2016] that the primary amino groups of DA are characterized by a strong chemical affinity toward the oxirane groups of the epoxy resin, although they are not able to react in any specific conditions.

Table 17: Onset values of the glass transition temperature for EPO, EPO2%Si, EPO_DA2%P, EPO2%Si_DA1%P_Mel, EPO2%Si_DA2%P_Mel, EPO_DP2%P, EPO2%Si_DP1%P_Mel and EPO2%Si_DP2%P_Mel.

Sample	Tg [°C]
EPO	127 ± 2
EPO_DA2%P	85 ± 1
EPO_DP2%P	133 ± 1
EPO2%Si	112 ± 1
EPO2%Si_DA2%P_Mel	91 ± 2
EPO2%Si_DA1%P_Mel	90 ± 2
EPO2%Si_DP2%P_Mel	131 ± 3
EPO2%Si_DP1%P_Mel	137 ± 4

6.4.1.4 Tensile properties of the in-situ silica/epoxy composites

Tensile properties for the pure epoxy resin and in-situ silica/epoxy composites were measured according to the ASTM-D638 standard. Figure 74 shows the stress-strain diagrams of pure epoxy resin, in-situ silica/epoxy system and the in-situ silica/resin with the addition of melamine and DA or DP (2 wt. % of P-loading) loaded in tension.

The tensile modulus of EPO, EPO2%Si, EPO2%Si_DA2%P_Mel and EPO2%Si_DP2%P_Mel materials was measured from the slope in the tensile strain range below 0.2%.

The elastic modulus, tensile strength and failure strain of all the considered systems were determined and listed in Table 18.

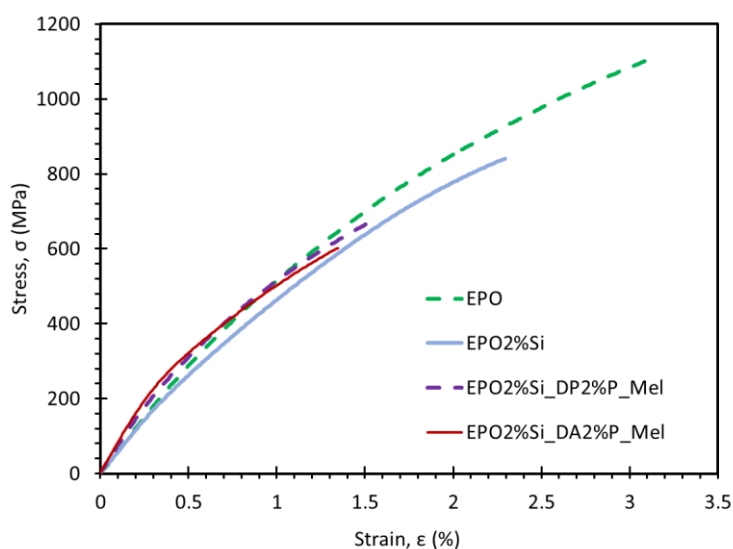


Figure 74: Stress-strain diagrams of pure epoxy resin, in-situ silica/epoxy system and the in-situ silica/resin with the addition of melamine and DA or DP (2 wt. % of P-loading) loaded in tension.

It can be seen that the presence of in-situ silica has a negative effect on the tensile stress-strain behavior of the epoxy polymer. EPO_2%Si exhibited slight lower tensile modulus and lower fracture strength, with respect to pristine epoxy (see Table 18) so as already reported [Johnsen 2007]. The presence of silica has a detrimental effect also on the fracture toughness evaluated as the area under the stress-strain curve.

The addition of melamine and DA or DP has an additional detrimental effect on fracture strength and toughness. On the contrary the young modulus increases by more than around 30%, due to topological constrain effects (e.g., steric hindrance) and chemical interactions between flame retardant and epoxy resin (see section 6.4.1.3).

Table 18: Elastic modulus, tensile strength and failure strain of pure epoxy resin, in-situ silica/epoxy system and the in-situ silica/resin with the addition of melamine and DA or DP (2 wt. % of P-loading).

Sample	E_t [MPa]	$\sigma_{u,t}$ [MPa]	$\epsilon_{f,t}$ [%]
EPO	754 ± 54	1105 ± 144	3.2 ± 0.07
EPO2%Si	712 ± 55	841 ± 170	2.3 ± 0.06
EPO2%Si_DP2%P_Mel	910 ± 60	681 ± 46	1.5 ± 0.05
EPO2%Si_DA2%P_Mel	990 ± 53	601 ± 51	1.3 ± 0.02

6.4.2 Fire behavior of the in-situ generated silica/epoxy materials

The fire behavior was characterized through the UL test and cone calorimeter. An insight into the flame retardancy mechanism was performed through thermogravimetric analysis (TGA), Pyrolysis Combustion Flow Calorimeter (PCFC), Pyrolysis–Gas Chromatography–Mass (PY-GC-MS) and Direct Insertion Probe–Mass Spectrometry (DIP-MS) and ATR-FTIR and EDX analysis of the char produced in the UL test.

UL 94, the Standard for Safety of Flammability of Plastic Materials for Parts in Devices and Appliances testing [UL 94 2013], is a plastics flammability standard released by Underwriters Laboratories of the United States. The standard determines the material’s tendency to either extinguish or spread the flame once the specimen has been ignited.

From lowest (least flame-retardant) to highest (most flame-retardant):

- **HB:** slow burning on a horizontal specimen; burning rate < 76 mm/min for thickness < 3 mm or burning stops before 100 mm
- **V-2:** burning stops within 30 seconds on a vertical specimen; drips of flaming particles are allowed.
- **V-1:** burning stops within 30 seconds on a vertical specimen; drips of particles allowed as long as they are not inflamed.
- **V-0:** burning stops within 10 seconds on a vertical specimen; drips of particles allowed as long as they are not inflamed.
- **5VB:** burning stops within 60 seconds on a vertical specimen; no drips allowed; plaque specimens may develop a hole.
- **5VA:** burning stops within 60 seconds on a vertical specimen; no drips allowed; plaque specimens may not develop a hole.

A cone calorimeter is a modern device used to study the fire behavior of small samples of various materials in condensed phase. It is widely used in the field of Fire Safety Engineering. It gathers data regarding the ignition time, mass loss, combustion products, heat release rate and other parameters associated with the sample's burning properties. The principle for the measurement of the heat release rate is based on the Huggett's principle [Hugget 1980] that the gross heat of combustion of any organic material is directly related to the amount of oxygen required for combustion. Oxygen consumption calorimetry has made the measurement of heat release rate of a fire a routine part of fire testing for both research and for regulatory compliance. Heat release rate is a primary metric of fire size which is foundational in modern fire protection engineering. The device allows a sample to be exposed to different heat fluxes over its surface. Its name comes from the conical shape of the radiant heater that produces a nearly uniform heat flux over the surface of the sample under study [Beyler 2017].

6.4.2.1 Vertical burning test (UL-94) of the in-situ silica/epoxy composites

The fire behavior of a flame retarded system is usually studied by performing either flammability (according to UL-94 standard, in vertical or horizontal configuration) or forced combustion (i.e., cone calorimetry) tests: their combination allows assessing the overall fire performance of the considered system, hence evaluating the reaction of the material towards the application of a flame or a heat flux. In this context, vertical flame spread test (UL-94) was exploited. The results are reported in Table 19 and Table 20. The samples EPO, EPO2%Si, EPO2%Si_Mel, EPO_Mel, EPO2%Si_DP2%P, EPO2%Si_DP1%P_Mel can not be classified, as they do not achieve self-extinction before the flame reaches the top of the sample. Figures 75a and 76a show the residues of EPO sample after the test. They are representative also of sample EPO_Mel. As can be seen the flame has reached the clamp and the coherence of the char is low. The presence of silica, instead, (samples EPO2%Si, EPO2%Si_Mel) gives a quite coherent char after burning so as shown in Figures 75b and 76b for EPO2%Si. Moreover, the presence of the silica domains and DP allow preventing melt dripping phenomena. It is worth underlining that, in the case of DA, for all the studied compositions the presence of silica does appear necessary to not have dripping (see Table 19). Undoubtedly, melt flow and dripping of the pyrolyzing polymer can be detrimental during a fire, as they often provide an additional ignition source, an additional flame spread process and even favor the starting of a pool fire independent from the original burning item. As clearly reported in the scientific literature [Crompton 2013, Malucelli 2016, Matzen 2015], the addition of micro- or nanoparticles to thermoplastic or thermosetting polymer matrices can prevent these undesired phenomena, because of the increase of the melt viscosity of the burning system. It is worth

underlining that the dripping suppression, in the present research activity, occurs at very low silica content so as reported in section 6.3.6. This may be due to formation of silica at very fine size [Crompton 2013, Malucelli 2016, Matzen 2015]. The present synthesis route is, in fact, the same of section 5.2.6. Moreover, the samples added with DA or DP and Mel (melamine) are expected to have a similar silica particles distribution. In fact, the addition of DA or DP and Mel occurs in the third step of the synthesis procedure reported in the experimental and methods section, when silica particles are formed and just before the addition of curing agent. Anyway, as shown by the results listed in Table 19, the use of DA, in the epoxy resin, is crucial in order to obtain V0 or V1 classification. It is worth underlining that, in the case of DP, for all the studied compositions the presence of silica or DP appear necessary to not have dripping (see Table 20). Table 20 shows that, the use of DP, in the epoxy resin, is fundamental in order to obtain V1 or V2 classification.

Table 19: UL-94 VB (vertical burning test) classification and observed dripping phenomenon of all the investigated epoxy samples with DA flame retardant.

Sample	UL-94 Class	Dripping
EPO	NC	Yes
EPO_DA2%P	V0	Yes
EPO_Mel	NC	Yes
EPO_DA2%P_Mel	V0	Yes
EPO2%Si	NC	No
EPO2%Si_DA2%P	V0	No
EPO2%Si_Mel	NC	No
EPO2%Si_DA2%P_Mel	V0	No
EPO2%Si_DA1%P_Mel	V1	No

Table 20: UL-94 VB (vertical burning test) classification and observed dripping phenomenon of all the investigated epoxy samples with DP flame retardant.

Sample	UL-94 Class	Dripping
EPO	NC	Yes
EPO_DP2%P	V1	No
EPO_Mel	NC	Yes
EPO_DP2%P_Mel	V1	No
EPO2%Si	NC	No
EPO2%Si_DP2%P	NC	No
EPO2%Si_Mel	NC	No
EPO2%Si_DP2%P_Mel	V0	No
EPO2%Si_DP1%P_Mel	NC	No

Figures 75c-76c (representative of samples EPO_DA2%P, EPO_DA2%P_Mel, EPO_DP2%P, EPO_DP2%P_Mel) and 75d-76d (EPO2%Si_DA2%P_Mel, EPO2%Si_DP2%P, EPO2%Si_DP2%P_Mel) clearly show that the samples burn only partially producing a very coherent char.

In conclusion the presence of DA and a silica phase appears to be necessary (so as in samples EPO2%Si_DA2%P and EPO2%Si_DA2%P_Mel) to have both V0 classification than no dripping. Conversely, the use of DP makes already possible to obtain no dripping phenomena (so as in sample EPO_DP2%P), nevertheless the addition of melamine and the presence of a silica phase are necessary in order to achieve V0 classification (EPO2%Si_DP2%P_Mel).

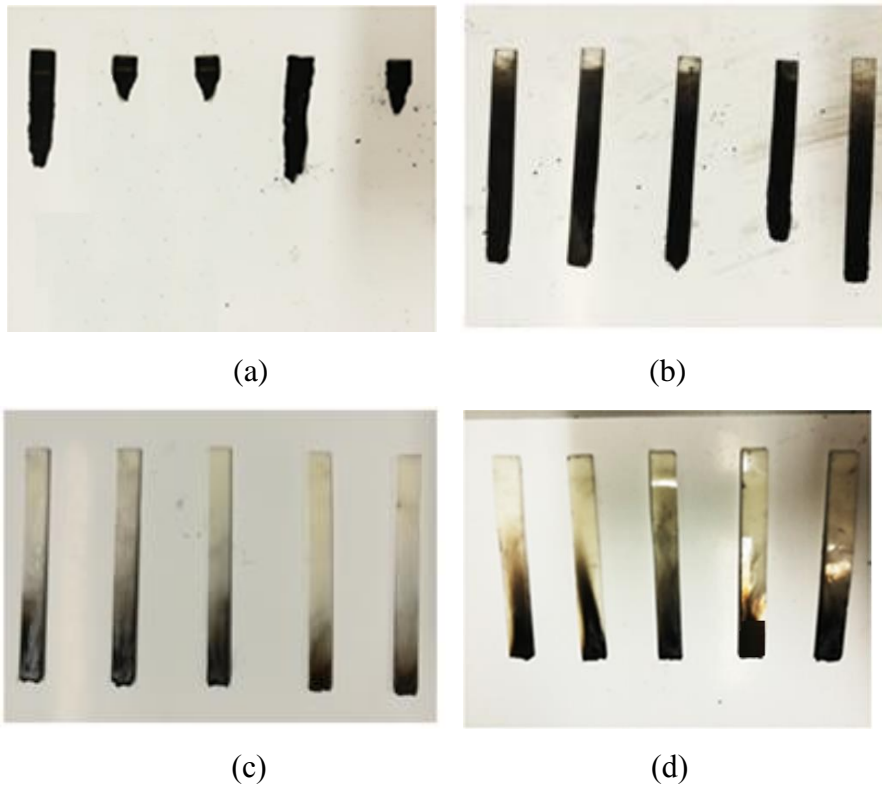


Figure 75: UL-94 VB residues after the burning test of EPO (a), EPO2%Si (b), EPO_DA2%P_Mel (c) and EPO2%Si_DA2%P_Mel (d).

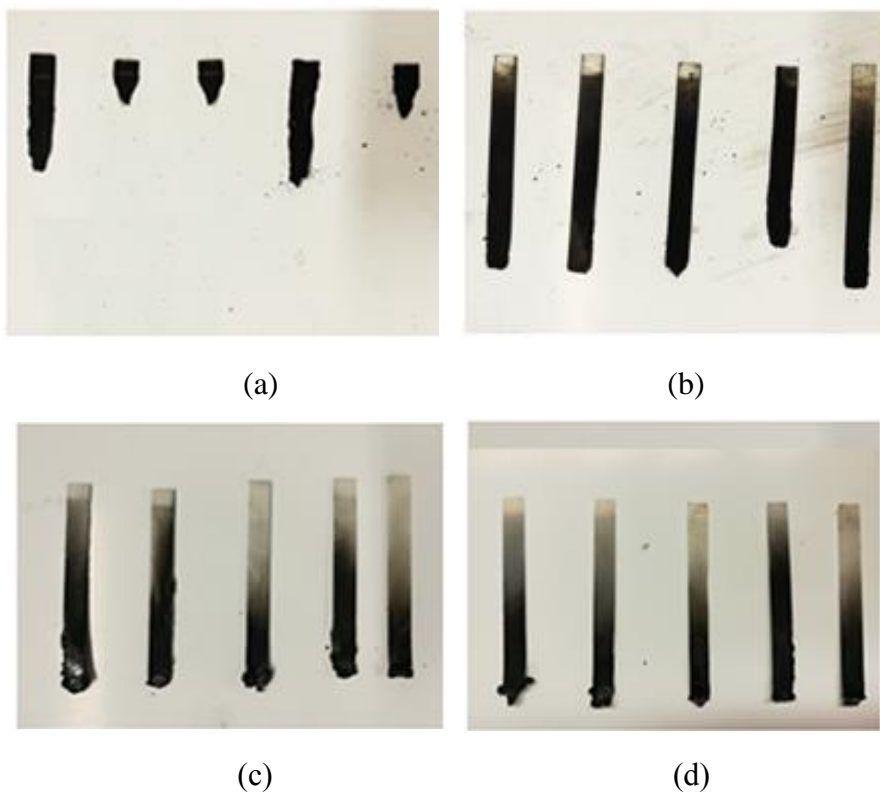


Figure 76: UL-94 VB residues after the burning test of EPO (a), EPO2%Si (b), EPO_DP2%P_Mel (c) and EPO2%Si_DP2%P_Mel (d).

Figures 77 and 78 show some photos taken with the aid of an IR Camera when samples were burned in the same configuration used for UL-94 apparatus. The flame of a “Bunsen burner” was applied to the specimen according to the UL-94 standard. For each sample, the IR video was recorded all along the whole burning up process. The recording started when the Bunsen burner was removed from the sample and was stopped when the flame extinguished or reached the holding sample clamp.

The burning process of EPO and EPO2%Si can be divided in three main phases:

- During the burner flame contact phase, the material captures the flame and the temperature on the surface starts rapidly to increase, depending on the fire behavior of the system.
- During the middle flame phase, the front flame moves and consumes the material; temperature further increases and volatiles are produced which feed the flame in the gas phase.
- During the end flame phase, flashover occurs and the flame envelops the sample.

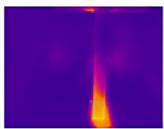
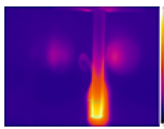
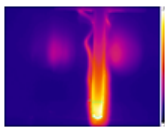
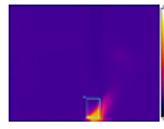
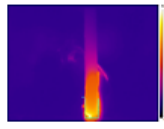
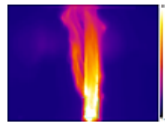
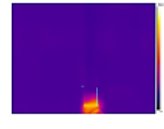
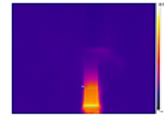
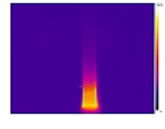
		Contact Flame	Middle Flame	End Flame
EPO	Flame Profile			
	Time [sec]	2	22	42
	T [°C]	164 ± 35	395 ± 52	479 ± 31
EPO2%Si	Flame Profile			
	Time [sec]	0	36	73
	T [°C]	104 ± 23	366 ± 70	471 ± 86
EPO2%Si_DA2%P_Mel	Flame Profile			
	Time [sec]	3	15	27
	T [°C]	63 ± 34	167 ± 50	129 ± 39

Figure 77: IR Camera results: temperature values and flame profiles at “contact”, “middle” and “end” flame phases for EPO (first row), EPO2%Si (second row) and EPO2%Si_DA2%P_Mel (third row).

In the case of EPO and EPO2%Si the temperatures were taken at the end of the burner flame contact phase, when the flame reaches the middle of the sample and when the flashover occurs. As

can be seen the addition of 2 wt. % silica has a strong influence on the fire behavior. All the temperatures are lower, and the effects appear to be retarded.

EPO2%Si_DA2%P_Mel and EPO2%Si_DP2%P_Mel show a completely different behavior as compared with EPO and EPO2%Si. When the burner is removed, the flame propagation is very limited and rapidly extinguishes, especially in the case of DA. The same when the burner flame is newly applied. The first and second temperatures were recorded when the Bunsen burner was removed. The third one is the temperature at the time to flame out. The use of DP allows to achieve lower temperature than EPO and EPO2%Si, nevertheless the effects appear to be retarded as compared with DA.

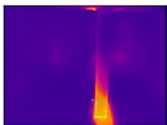
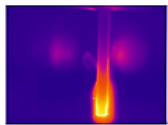
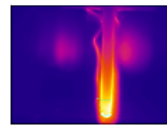
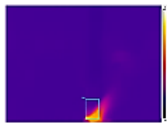
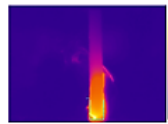
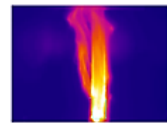
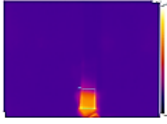
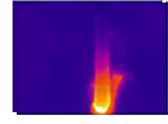
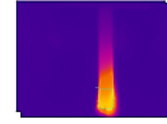
		Contact Flame	Middle Flame	End Flame
EPO	Flame Profile			
	Time [sec]	2	22	42
	T [°C]	164 ± 35	395 ± 52	479 ± 31
EPO2%Si	Flame Profile			
	Time [sec]	0	36	73
	T [°C]	104 ± 23	366 ± 70	471 ± 86
EPO2%Si_DP2%P_Mel	Flame Profile			
	Time [sec]	1	44	60
	T [°C]	102 ± 37	183 ± 29	168 ± 22

Figure 78: IR Camera results: temperature values and flame profiles at “contact”, “middle” and “end” flame phases for EPO (first row), EPO2%Si (second row) and EPO2%Si_DP2%P_Mel (third row).

The overall greater thermal stability caused by the presence of silica may be explained on the basis of a shield effect exerted by the silica particles and the refractory carbonaceous char formed by the epoxy, so as previously observed in the case of section 6.3.6. This means that the flame retarding would be due to a condensed phase action. The efficacy of DA should instead be linked to both a condensed phase than a gas phase actions [Liu 2017, Salmeia 2015ab, Salmeia 2018, Scharrel 2010]. As regards DP, its flame retardant activity should mainly be related to a predominant condensed phase activity [Salmeia 2018, Scharrel 2010].

6.4.2.2 Cone Calorimeter Tests of the in-situ silica/epoxy composites

To investigate the combustion behavior of the pure epoxy resin and in-situ silica/epoxy composites subjected to a constant heat flux, cone calorimeter tests were performed following the ISO 5660 standard. As far as forced-combustion tests are considered, Table 21 and Table 22 collect the cone parameters in terms of TTI (Time to Ignition), TTF (Time to Flame Out), MLR (Mass Loss Rate), HRR (Heat Release Rate), pkHRR (peak of Heat Release Rate), TSR (Total Smoke Release), SEA (Smoke Extension Area), THR (Total Heat Release) and final residue. Figures 79 and 80 show the HRR curves vs time for all the analyzed samples. First of all, it is noteworthy that the in-situ silica/epoxy system EPO2%Si does not anticipate the ignition as compared to the neat cured EPO. This means that the silica domains do not interfere negatively with the curing of the epoxy chains. Conversely, the presence of the silica leads to a remarkable decrease of HRR, MLR and THR as well altogether with an increase of the residual mass. This finding can be explained in terms of formation of a ceramic silica layer, which acts as a thermal shield, hence protecting the underlying materials, slowing down both the diffusion of the volatile flammable degradation products towards the gas phase and the oxygen diffusion towards the degrading material [Malucelli 2016]. It is worth underlining that this barrier effect is obtained at very low silica content so as reported in section 6.3.6 for a similar epoxy system. This may be due to formation of silica at very fine size [Crompton 2013, Malucelli 2016, Matzen 2015]. The present synthesis route is, in fact, the same. Also, the samples added with DA or DP and melamine are expected to have a similar silica particles distribution. In fact, the addition of DA or DP and melamine occurs in the third step of the synthesis procedure reported in the experimental and methods section, when silica particles are formed and just before the addition of curing agent.

The HRR, MLR and THR even more reduce in the case of samples containing DA or DP with or without melamine. In the case of DA, the strong increase of the ratio of CO/CO₂ (see Table 23) may be in agreement with a gas phase activity mechanism [Hull 2008, Salmeia 2015ab, Salmeia 2018, Wendels 2017]. On the other side, the use of DP leads to a slight increase of CO/CO₂ (see Tables 23 and 24) than DA ones, which may be due to a predominant condensed phase activity [Salmeia 2015ab, Salmeia 2018].

The flame retardant actions of DA and DP may involve different phenomena taking place during the thermal degradation:

- 1) the presence of the flame retardants could promote a gas phase activity, especially in the case of DA on the basis of the values of the ratio of CO/CO₂, which follows directly from

the inhibition of the free radical reactions by trapping active radicals particularly the ·OH ones [Hull 2008, Salmeia 2015a, Salmeia 2018, Wendels 2017] (see section 3.4.3.1).

- 2) the use of DA or DP could contribute to strengthen the char-forming character of the epoxy resin through a condensed phase activity [Salmeia 2015a, Salmeia 2018].
- 3) the endothermic decomposition of DA or DP lowers MLR and the heat-related cone parameters [Salmeia 2015ab, Salmeia 2018]. During the thermal degradation process, the two phosphorous based flame retardants can slow down the heat transfer to the epoxy material, because of the endothermic nature of their decomposition into phosphorous related products.
- 4) melamine degradation produces N₂ that lead to a dilution of the flame [Bretterbauer 2012, Salmeia 2015ab].

In Figures 81 and 82 the photos of the residues are reported. As can be seen, according to the results reported in Tables 23-24 and 27-28, the residue mass increases in the case of EPO2%Si and when DA or DP and melamine are added. The use of DP allows to achieve the highest increase of residue mass with respect to EPO2%Si (16% vs. 4% for EPO_DP2%P and EPO2%Si composites, respectively; see Table 24).

More than all, however, the photos in Figures 81 and 82 show char intumescence when melamine and DA or DP are both present. This indicates that DA and DP exert also a flame-retardant effect in the condensed phase (see section 3.4.3.1 for more details about the intumescence phenomenon) [Salmeia 2015ab, Salmeia 2018, Singh 2009]. This intumescence phenomenon proves the formation of acid phosphorous compounds during the decomposition of DA and DP. These acid phosphorous compounds [Salmeia 2015ab, Salmeia 2018, Singh 2009] accelerate the decomposition of epoxy resin (according to the results in Tables 25-26 and 27-28); furthermore, the acid character of these acidic phosphorous compounds and of silica altogether with blowing agent behavior of melamine may well produce a swollen multicellular carbonaceous layer (see Figures 81d and 82d) [Bourbigot 2007, Morgan 2013]. Figure 81c and 82c (EPO_DA2%P and EPO_DP2%P) shows that the use of DA or DP without melamine and silica, already allows to obtain a quite bigger amount of char residue (3% and 16% for EPO_DA2%P and EPO_DP2%P composites, respectively; see Tables 23 and 24) as compared with the EPO one (1%, see Table 23). The acid phosphorus compounds, in fact, are able to promote the dehydration of the epoxy resin producing a carbonaceous layer, which acts as thermal shield and oxygen diffusion barrier [Bourbigot 2007, Liu 2017, Visakh 2015]. Based on the results discussed so far, they support the hypothesis that DP exerts a flame retardant activity mainly linked to a condensed phase mechanism, contrary to what appears for DA.

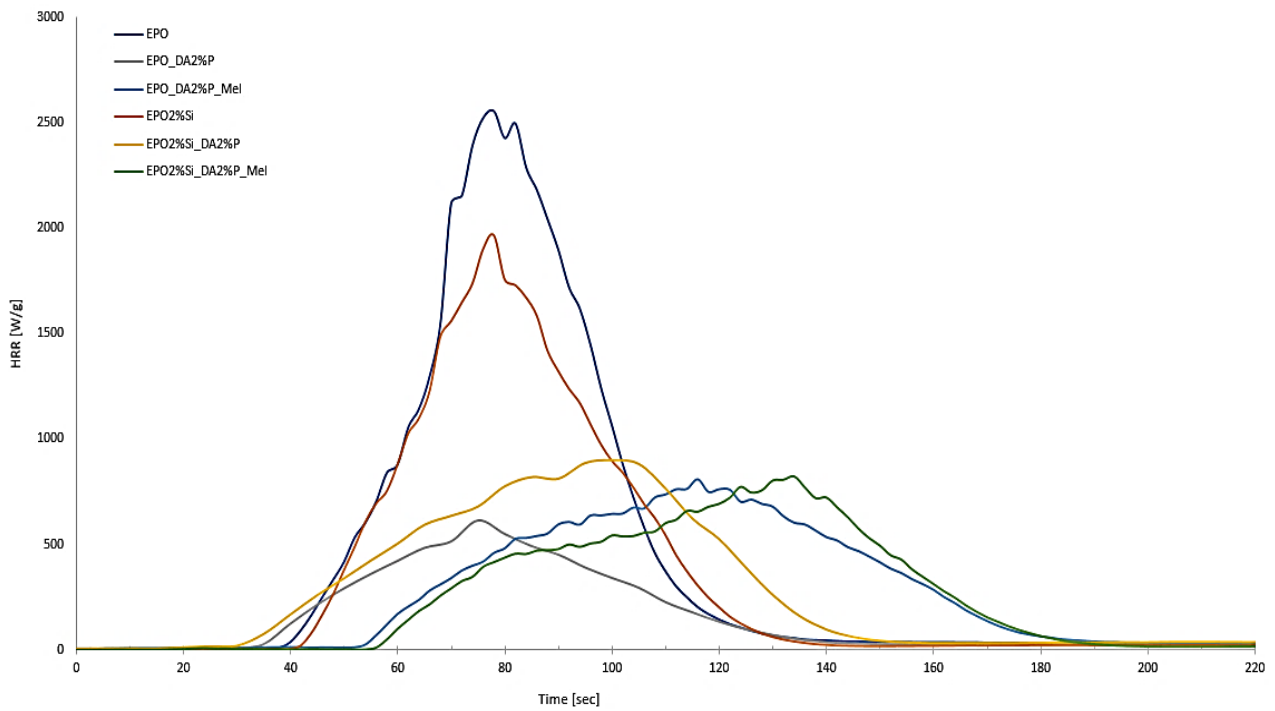


Figure 79: HRR (Heat Release of Rate) curves versus time for EPO, EPO_DA2%P, EPO_DA2%P_Mel, EPO2%Si, EPO2%Si_DA2%P and EPO2%Si_DA2%P_Mel.

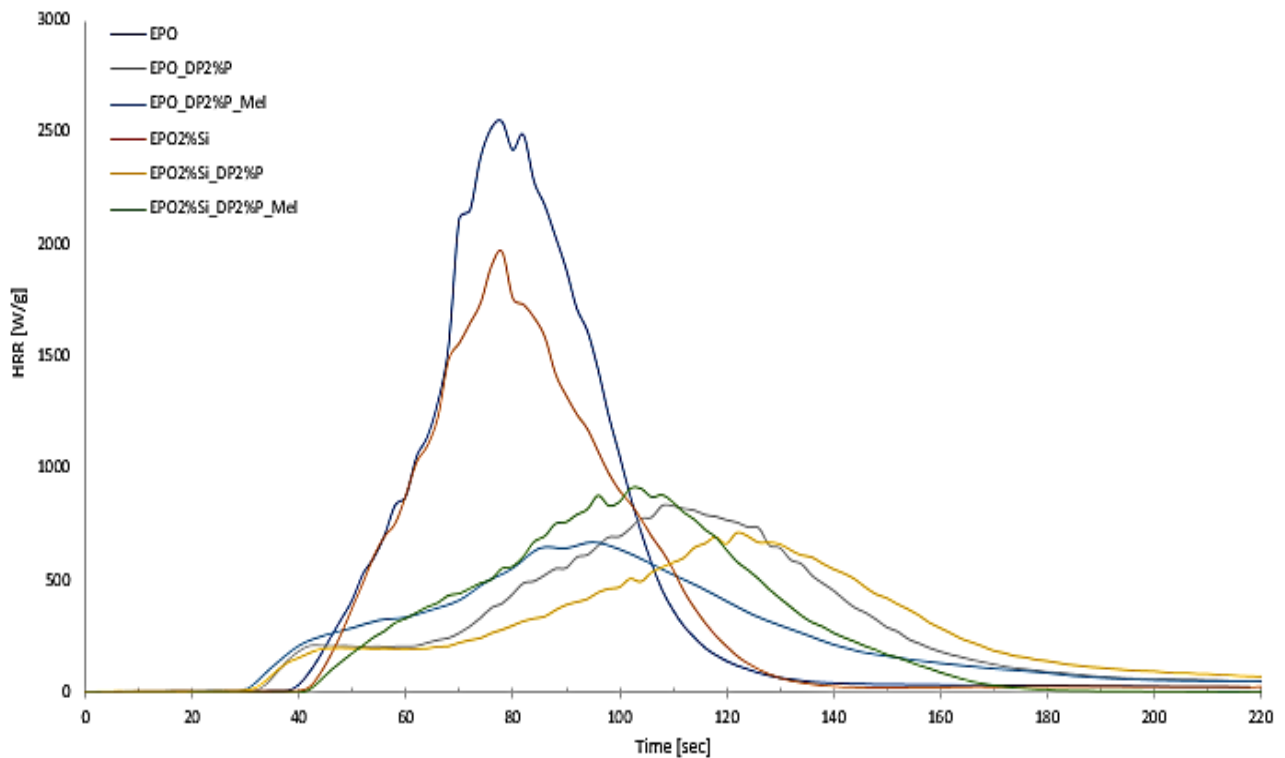


Figure 80: HRR (Heat Release of Rate) curves versus time for EPO, EPO_DP2%P, EPO_DP2%P_Mel, EPO2%Si, EPO2%Si_DP2%P and EPO2%Si_DP2%P_Mel.

Table 21: Results from cone calorimetry tests performed on EPO, EPO_DA2%P, EPO_DA2%P_Mel, EPO2%Si, EPO2%Si_DA2%P and EPO2%Si_DA2%P_Mel. TTI, Time To Ignition; TTF, Time To Flame out; THR, Total Heat Released; HRR, Heat Release Rate; pkHRR, peak of the Heat Release Rate; residue mass.

Sample	TTI [s]	TTF [s]	THR [MJ/m ²]	MLR [g/s·m ²]	HRR [kW/m ²]	pkHRR [kW/m ²]	Residue mass [%]
EPO	38 ± 3	117 ± 3	96 ± 3	77 ± 3	532 ± 23	2550 ± 383.9	1 ± 0.7
EPO DA2%P	34 ± 1	200 ± 0.4	43 ± 3	30 ± 2	160 ± 21	647 ± 81.3	3 ± 0.6
EPO DA2%P Mel	56 ± 4	189 ± 3	61 ± 6	35 ± 3	249 ± 13	823 ± 102	3 ± 0.5
EPO2%Si	40 ± 4	130 ± 5	79 ± 10	42 ± 4	412 ± 12	1964 ± 72.61	4 ± 0.5
EPO2%Si DA2%P	26 ± 5	158 ± 5	64 ± 7	32 ± 5	276 ± 10	773 ± 108	5 ± 0.7
EPO2%Si DA2%P Mel	56 ± 4	189 ± 3	59 ± 7	35 ± 2	249 ± 13	823 ± 102	4 ± 0.6

Table 22: Results from cone calorimetry tests performed on EPO, EPO_DP2%P, EPO_DP2%P_Mel, EPO2%Si, EPO2%Si_DP2%P and EPO2%Si_DP2%P_Mel. TTI, Time To Ignition; TTF, Time To Flame out; THR, Total Heat Released; HRR, Heat Release Rate; pkHRR, peak of the Heat Release Rate; residue mass.

Sample	TTI (s)	TTF (s)	THR [MJ/m ²]	MLR [g/s·m ²]	HRR (kW/m ²)	pkHRR (kW/m ²)	Residue mass [%]
EPO	38 ± 3	117 ± 3	96 ± 3	77 ± 3	532 ± 23	2550 ± 384	1 ± 0.7
EPO_DP2%P	31 ± 2	346 ± 1	61.3 ± 5	18.6 ± 3	135 ± 19	744 ± 76	16 ± 0.6
EPO_DP2%P_Mel	50 ± 6	406 ± 3	61.3 ± 7	17.2 ± 2	158 ± 11	730 ± 128	13 ± 0.5
EPO2%Si	40 ± 4	130 ± 5	79 ± 10	42 ± 4	412 ± 12	1964 ± 73	4 ± 0.5
EPO2%Si_DP2%P	28 ± 4	512 ± 3	67.7 ± 9	13.3 ± 5	106 ± 8	516 ± 111	12 ± 0.7
EPO2%Si_DP2%P_Mel	42 ± 5	172 ± 5	57 ± 5	33 ± 2	247 ± 11	909 ± 121	10 ± 0.6

Table 23: Smoke results from cone calorimetry tests performed on EPO, EPO_DA2%P, EPO_DA2%P_Mel, EPO2%Si, EPO2%Si_DA2%P and EPO2%Si_DA2%P_Mel. TSR, Total Smoke Release; SEA, Specific Extinction Area; CO, Carbon Monoxide; CO₂, Carbon Dioxide.

Sample	TSR [m ² /m ²]	SEA [m ² /kg]	CO yield [kg/kg]	CO ₂ yield [kg/kg]	CO/CO ₂ [-]
EPO	1841 ± 206	131 ± 35	2.85 x 10 ⁻² ± 3.49 x 10 ⁻³	0.49 ± 6.08 x 10 ⁻²	0.06
EPO_DA2%P	4238 ± 217	525 ± 30	6.21 x 10 ⁻² ± 3.12 x 10 ⁻⁴	0.36 ± 5.51 x 10 ⁻²	0.17
EPO_DA2%P_Mel	4255 ± 225	528 ± 22	7.46 x 10 ⁻² ± 3.46 x 10 ⁻³	0.54 ± 4.04 x 10 ⁻²	0.14
EPO2%Si	1981 ± 291	241 ± 38	3.31 x 10 ⁻² ± 4.08 x 10 ⁻³	0.74 ± 2.52 x 10 ⁻²	0.04
EPO2%Si_DA2%P	4626 ± 304	577 ± 75	8.18 x 10 ⁻² ± 7.31 x 10 ⁻³	0.53 ± 1.99 x 10 ⁻¹	0.15
EPO2%Si_DA2%P_Mel	4108 ± 275	508 ± 3	7.14 x 10 ⁻² ± 2.82 x 10 ⁻³	0.51 ± 1.73 x 10 ⁻²	0.14

Table 24: Smoke results from cone calorimetry tests performed on EPO, EPO_DP2%P, EPO_DP2%P_Mel, EPO2%Si, EPO2%Si_DP2%P and EPO2%Si_DP2%P_Mel. TSR, Total Smoke Release; SEA, Specific Extinction Area; CO, Carbon Monoxide; CO₂, Carbon Dioxide.

Sample	TSR [m ² /m ²]	SEA [m ² /kg]	CO yield [kg/kg]	CO ₂ yield [kg/kg]	CO/CO ₂ [-]
EPO	1841 ± 164	131 ± 40	2.85 x 10 ⁻² ± 2.69 x 10 ⁻³	0.49 ± 7.01 x 10 ⁻²	0.06

EPO_DP2%P	2661 ± 278	337 ± 34	5.65×10^{-2} $\pm 4.33 \times 10^{-4}$	0.66 $\pm 6.44 \times 10^{-2}$	0.08
EPO_DP2%P_Mel	2660.6 ± 212	337 ± 26	4.91×10^{-2} $\pm 2.56 \times 10^{-3}$	0.56 $\pm 3.12 \times 10^{-2}$	0.08
EPO2%Si	1981 ± 266	241 ± 35	3.31×10^{-2} $\pm 3.72 \times 10^{-3}$	0.74 $\pm 1.69 \times 10^{-2}$	0.04
EPO2%Si_DP2%P	2722 ± 312	201 ± 81	3.52×10^{-2} $\pm 4.45 \times 10^{-3}$	0.34 $\pm 2.04 \times 10^{-1}$	0.1
EPO2%Si_DP2%P_Mel	2577 ± 281	326 ± 4	4.71×10^{-2} $\pm 2.39 \times 10^{-3}$	0.54 $\pm 1.88 \times 10^{-2}$	0.08



(a)



(b)



(c)



(d)

Figure 81: Cone calorimeter residues after the burning test of EPO (a), EPO2%Si (b), EPO_DA2%P (c) and EPO2%Si_DA2%P_Mel (d).

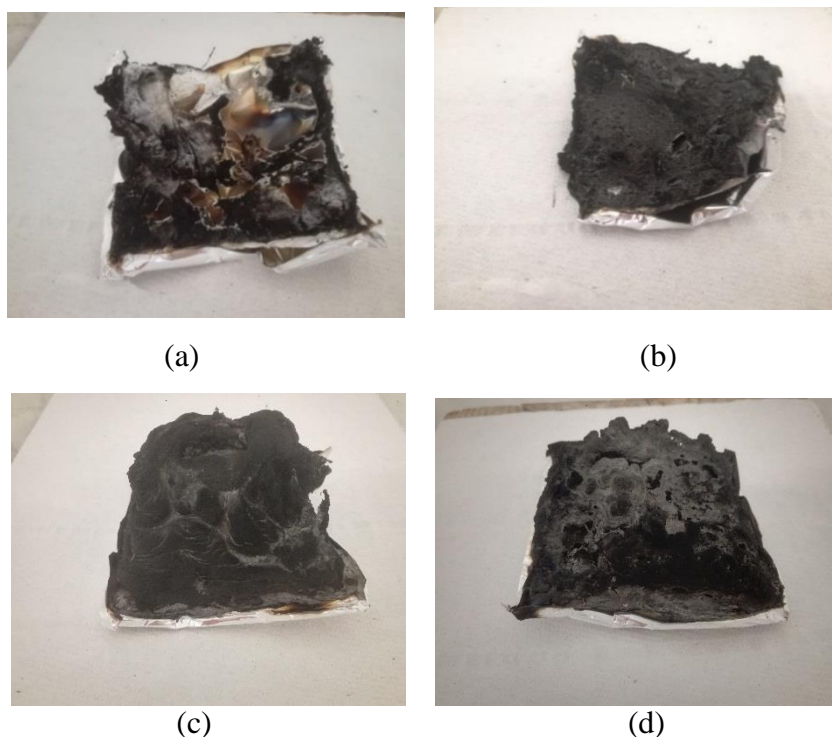


Figure 82: Cone calorimeter residues after the burning test of EPO (a), EPO2%Si (b), EPO_DP2%P (c) and EPO2%Si_DP2%P_Mel (d).

6.4.3 Thermogravimetric Analysis (TGA), Pyrolysis Combustion Flow Calorimeter (PCFC), Pyrolysis–Gas Chromatography–Mass (PY-GC-MS) and Direct Insertion Probe–Mass Spectrometry (DIP-MS) and analysis of the char produced in the UL test

6.4.3.1 Thermal analysis of the in-situ silica/epoxy composites

In Figures 83-84 and 85-86 the thermogravimetric curves recorded, in air, for EPO, EPO_DA2%P, EPO_DP2%P, EPO_Mel, EPO_DA2%P_Mel, EPO_DP2%P_Mel, EPO2%Si, EPO2%Si_DA2%P, EPO2%Si_DP2%P, EPO2%Si_Mel, EPO2%Si_DA2%P_Mel, EPO2%Si_DA1%P_Mel, EPO2%Si_DP2%P_Mel and EPO2%Si_DP1%P_Mel are reported.

The thermal behavior of epoxy resin cured with a cycloaliphatic amine (see section 3.1) can be interpreted on the basis of the scheme of the thermal degradation mechanism reported in the literature [Grassie 1985, Tudorachi 2017, Yan 2014, Zhang 2018]. It is reported that, in nitrogen atmosphere, some principal volatile products, acrolein, acetone and allyl alcohol, are formed at 280°C, although the main decomposition step of the cross-linked resin occurs above 340 °C when phenolic compounds appear together with more complex products with higher molecular weights [Grassie 1985]. In inert atmosphere, in the temperature range between 400 and 600 °C no weight changes are observed because a very stable char is present, which is mainly composed by aromatic

compounds. This is commonly observed for the degradation, in inert atmosphere, of char-forming polymers (e.g., epoxy resin) [Wang 2016].

In air atmosphere, the oxygen attack causes the formation of several oxygenated species, among which aromatic and/or aliphatic aldehydes and ketones, amide groups have been, also, clearly identified [Grassie 1985, Musto 2001, Musto 2003] that are almost completely oxidized at higher temperatures (400-600 °C).

In the present thesis the typical thermogravimetric curves, in the presence of nitrogen or oxygen, reported in the literature for pristine epoxy resins were recorded [Grassie 1985, Tudorachi 2017, Yan 2014, Zhang 2018].

Figures 83, 84, 85 and 86 show the results recorded in air. The typical two previously described steps degradation appear. The presence of the phosphorous based flame retardants affects the curves: the ratio of the mass loss recorded in the second step (400-600 °C) and first step (below 400 °C) increases when the flame retardants are present. This would suggest that the presence of DA or DP increases the overall thermal stability of the composites, giving rise to a significant increase of the residues at high temperatures by promoting the aromatic char formation [Liu 2017].

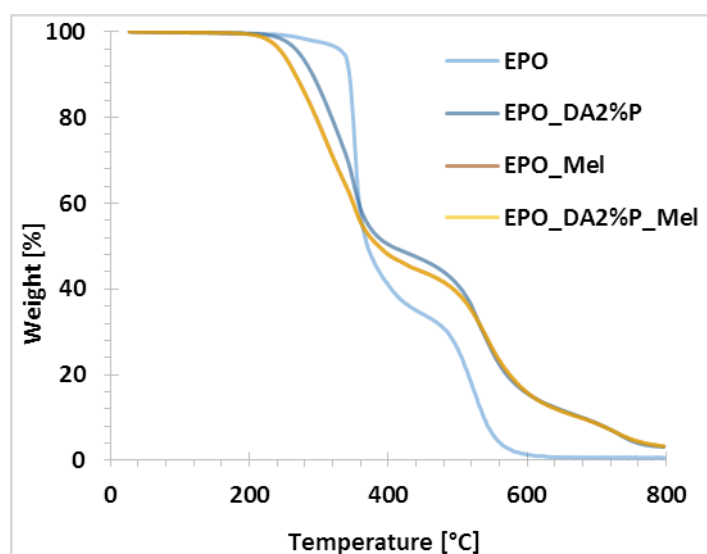


Figure 83: Thermogravimetry (TG) curves in air atmosphere for EPO, EPO_DA2%P, EPO_Mel and EPO_DA2%P_Mel.

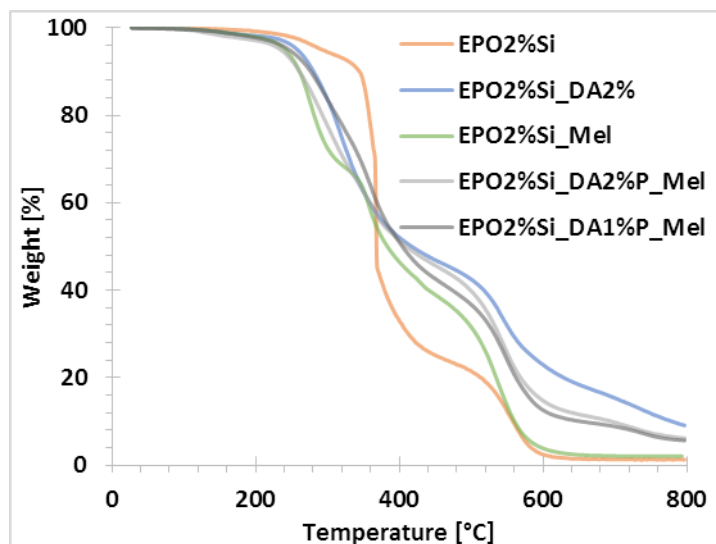


Figure 84: Thermogravimetry (TG) curves in air atmosphere for EPO2%Si, EPO2%Si_DA2%P, EPO2%Si_Mel, EPO2%Si_DA2%P_Mel and EPO2%Si_DA1%P_Mel.

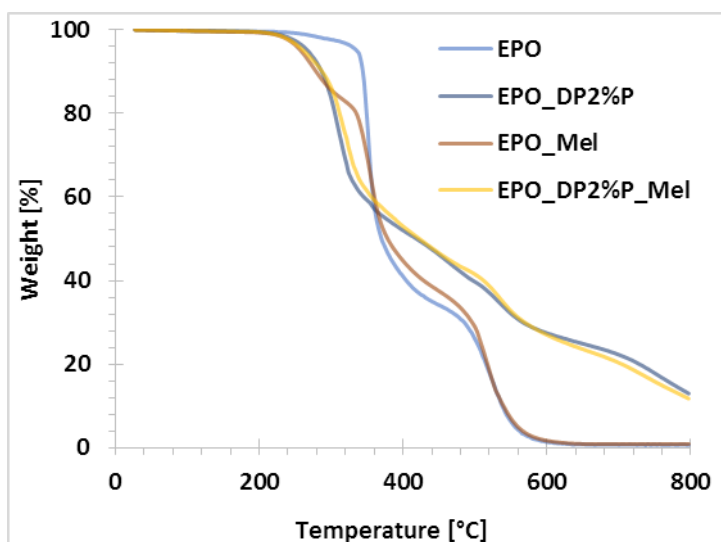


Figure 85: Thermogravimetry (TG) curves in air atmosphere for EPO, EPO_DP2%P, EPO_Mel and EPO_DP2%P_Mel.

Tables 25-26 and Table 27-28 show the thermogravimetric (TG) results in inert and air atmospheres of the different samples. $T_{5\%}$, $T_{10\%}$ and $T_{50\%}$ are the temperatures at which 5%, 10% and 50% weight loss are recorded; the residues at 800°C and at the temperature at which the weight loss rate reaches the maximum (T_{max}) are also reported. The thermal behavior of the epoxy samples is strongly related to the presence of the flame-retardants and the silica phase. EPO2%Si shows a significant increase with respect to EPO (12.1% vs 8.37%) of the residues at high temperatures (at 800 °C); this supports the hypothesis that silica may play a condensed phase activity with formation of a shield exerting a protective effect on the polymer chains so as already reported in section 6.3.6 (for more details, see chapter 3 and section 4.2.1).

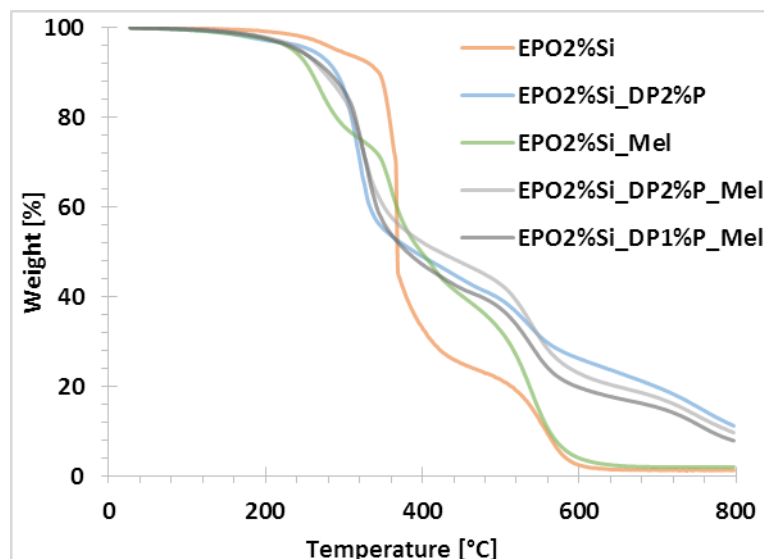


Figure 86: Thermogravimetry (TG) curves in air atmosphere for EPO2%Si, EPO2%Si_DP2%P, EPO2%Si_Mel, EPO2%Si_DP2%P_Mel and EPO2%Si_DP1%P_Mel.

The addition of DA or DP involves an anticipation of the degradation phenomena and, in air atmosphere, a significant increase of the residues at high temperatures, especially in the case of DP, with respect to EPO and EPO2%Si counterparts. The anticipation may be attributed to (i) the formation of acidic phosphorus species during the degradation of the phosphorous based flame retardants (DA and DP), (ii) the acidic characteristics of the in-situ sol-gel silica [Malucelli 2016] and (iii) the production of not flammable volatiles (N_2) [Costa 1988, Zhan 2014], which accelerate the decomposition of the epoxy resin [Liu 2017, Singh 2009]. DP significantly increases the thermal stability of the epoxy composites, in fact, EPO_DP2%P shows a mass residue at 800 °C, in air atmosphere, around four times higher than EPO_DA2%P (12.8% vs. 3.16% for EPO_DP2%P and EPO_DA2%P composites, respectively; see Tables 27 and 28). The effect of DP on the thermal stability of the epoxy resin additionally supports the hypothesis of a strong condensed phase activity [Salmeia 2015ab, Salmeia 2018] for this flame retardant.

Table 25: Thermogravimetry (TG) data collected in an inert atmosphere for all the investigated samples containing DA.

Sample	T _{5%} [°C]	T _{10%} [°C]	T _{50%} [°C]	T _{max} [°C]	Residue at T _{max} [%]	Residue at 800 °C [%]
EPO	338 ± 1.22	344 ± 1.18	367 ± 1.65	354 ± 1.14	73.8 ± 0.13	8.37 ± 0.19
EPO_DA2%P	291 ± 0.65	312 ± 2.15	365 ± 2.33	361 ± 2.66	54.5 ± 0.46	5.75 ± 0.25
EPO_Mel	254 ± 1.17	267 ± 1.13	358 ± 1.26	362 ± 0.59	49.1 ± 0.83	6.29 ± 0.77
EPO_DA2%P_Mel	257 ± 0.89	290 ± 0.79	363 ± 0.88	360 ± 2.31	49.1 ± 0.83	6.29 ± 0.77
EPO2%Si	333 ± 1.12	345 ± 0.33	373 ± 0.52	358 ± 0.26	74.1 ± 0.45	12.1 ± 0.87
EPO2%Si_DA2%P	283 ± 1.31	310 ± 2.01	373 ± 1.16	362 ± 2.14	57.3 ± 0.24	9.85 ± 0.72
EPO2%Si_Mel	250 ± 1.15	278 ± 1.12	367 ± 0.78	355 ± 1.01	61.1 ± 0.78	10.1 ± 0.85
EPO2%Si_DA2%P_Mel	239 ± 0.79	267 ± 2.31	366 ± 1.72	363 ± 0.96	51.8 ± 0.87	8.76 ± 1.45
EPO2%Si_DA1%P_Mel	242 ± 2.12	298 ± 1.15	342 ± 0.48	326 ± 1.25	66.5 ± 0.65	12.2 ± 1.23

Table 26: Thermogravimetry (TG) data collected in an inert atmosphere for all the investigated samples containing DP.

Sample	T _{5%} [°C]	T _{10%} [°C]	T _{50%} [°C]	T _{max} [°C]	Residue at T _{max} [%]	Residue at 800°C [%]
EPO	338 ± 1.22	344 ± 1.18	367 ± 1.65	354 ± 1.14	73.8 ± 0.13	8.37 ± 0.19
EPO DP2%P	295 ± 1.62	302 ± 0.75	333 ± 0.96	318 ± 2.24	67.4 ± 0.98	13.5 ± 0.17
EPO_Mel	258 ± 0.84	320 ± 0.14	366 ± 1.14	359 ± 0.22	59.9 ± 0.62	7.46 ± 0.64
EPO2%Si	333 ± 1.12	345 ± 0.33	373 ± 0.52	358 ± 0.26	74.1 ± 0.45	12.1 ± 0.87
EPO2%Si DP	285 ± 2.33	300 ± 2.37	341 ± 0.71	315 ± 0.42	70.7 ± 0.46	15.6 ± 1.55
EPO2%Si_Mel	245 ± 0.77	291 ± 1.23	374 ± 0.86	360 ± 1.15	64.2 ± 0.65	12.1 ± 0.89
EPO2%Si DP2%P_Mel	270 ± 2.15	307 ± 0.32	343 ± 1.23	324 ± 1.12	70.5 ± 0.33	12.3 ± 1.12
EPO2%Si DP1%P_Mel	250 ± 1.93	289 ± 0.82	372 ± 0.58	366 ± 0.83	56 ± 0.47	9.23 ± 0.57

It is noteworthy reminding that, in the cone calorimeter, the in-situ silica/epoxy systems containing melamine (with or without the addition of the phosphorous based flame retardants) show a significant increase of the ignition time (TTI) as compared to the neat cured EPO and EPO2%Si (see Tables 21 and 22). This means that the early mass loss recorded in the TGA apparatus is also due to formation of not flammable volatiles according to the mechanism reported in the literature [Bretterbauer 2012, Costa 1988, Salmeia 2015ab, Salmeia 2018, Zhan 2014]. Melamine degradation, in fact, is reported to produce ammonia that, in the presence of oxygen, converts to N₂. The increase of the residues, in presence of oxygen, would suggest especially in the case of DP that both flame retardants can promote the formation of a stable char [Bretterbauer 2012, Liu 2017, Salmeia 2015ab, Salmeia 2018, Zhan 2014], which should protect the underlying polymer from the heat, flames, and oxygen, thus leading to improved flame retardancy.

Table 27: Thermogravimetry (TG) data collected in air atmosphere for EPO, EPO_DA2%P, EPO_Mel, EPO_DA2%P_Mel, EPO2%Si, EPO2%Si_DA2%P, EPO2%Si_Mel, EPO2%Si_DA2%P_Mel and EPO2%Si_DA1%P_Mel.

Sample	T _{5%} [°C]	T _{10%} [°C]	T _{50%} [°C]	T _{max_1} [°C]	Residue at T _{max_1} [%]	T _{max_2} [°C]	T _{max_3} [°C]	Residue at T _{max_3} [%]	Residue at 800 °C [%]
EPO	336 ± 1.23	343 ± 1.25	369 ± 0.53	351 ± 1.44	74.9 ± 0.32	519 ± 1.63	/	/	0.71 ± 0.23
EPO_DA2%P	275 ± 1.29	291 ± 0.86	401 ± 0.64	351 ± 1.27	63.7 ± 0.71	526 ± 1.84	/	/	3.16 ± 1.14
EPO_Mel	250 ± 0.55	265 ± 1.42	363 ± 1.19	279 ± 0.53	82.9 ± 0.33	351 ± 0.74	509 ± 0.25	24.3 ± 0.73	1.73 ± 0.18
EPO_DA2%P_Mel	237 ± 1.13	256 ± 1.42	383 ± 0.78	277 ± 0.41	82.3 ± 0.86	364 ± 1.47	534 ± 0.93	20.2 ± 0.26	3.33 ± 1.27
EPO2%Si	293 ± 1.44	341 ± 2.36	368 ± 1.65	367 ± 1.32	60.6 ± 0.42	553 ± 2.55	/	/	1.33 ± 0.88
EPO2%Si_DA2%P	255 ± 2.03	280 ± 0.65	417 ± 0.62	313 ± 1.37	78.1 ± 0.46	536 ± 0.33	/	/	9.02 ± 0.95
EPO2%Si_Mel	241 ± 0.69	261 ± 1.66	379 ± 1.14	274 ± 0.92	83.4 ± 1.24	354 ± 0.61	531 ± 0.45	21.4 ± 0.89	2.08 ± 0.15
EPO2%Si_DA2%P_Mel	232 ± 0.86	261 ± 0.82	409 ± 2.43	297 ± 0.89	78.2 ± 0.78	364 ± 0.78	543 ± 1.45	20.1 ± 1.66	6.16 ± 1.13
EPO2%Si_DA1%P_Mel	245 ± 0.74	276 ± 0.63	401 ± 1.52	289 ± 0.35	86.4 ± 0.31	361 ± 0.85	546 ± 0.96	25.3 ± 2.35	5.68 ± 0.58

Table 28: Thermogravimetry (TG) data collected in air atmosphere for EPO, EPO_DP2%P, EPO_Mel, EPO_DP2%P_Mel, EPO2%Si, EPO2%Si_DP2%P, EPO2%Si_Mel, EPO2%Si_DP2%P_Mel and EPO2%Si_DP1%P_Mel.

Sample	T _{5%} [°C]	T _{10%} [°C]	T _{50%} [°C]	T _{max 1} [°C]	Residue at T _{max 1} [%]	T _{max 2} [°C]	T _{max 3} [°C]	Residue at T _{max 3} [%]	Residue at 800 °C [%]
EPO	336 ± 1.23	343 ± 1.25	369 ± 0.53	351 ± 1.44	74.9 ± 0.32	519 ± 1.63	/	/	0.71 ± 0.23
EPO_DP2%P	266 ± 0.32	283 ± 0.53	421 ± 2.11	308 ± 0.25	77.1 ± 1.27	356 ± 1.55	535 ± 1.37	34.5 ± 0.27	12.8 ± 0.84
EPO_Mel	259 ± 0.82	277 ± 0.42	375 ± 0.89	269 ± 2.07	92.4 ± 2.33	349 ± 0.44	514 ± 0.52	24.2 ± 0.94	0.92 ± 0.12
EPO2%Si	293 ± 1.44	341 ± 2.36	368 ± 1.65	367 ± 1.32	60.6 ± 0.42	553 ± 2.55	/	/	1.33 ± 0.88
EPO2%Si_DP	255 ± 0.92	286 ± 1.57	385 ± 0.71	187 ± 2.41	97.6 ± 0.87	322 ± 0.12	535 ± 0.65	33.7 ± 2.35	11.1 ± 1.14
EPO2%Si_Mel	235 ± 1.72	95.1 ± 2.03	399 ± 1.13	263 ± 0.49	88.3 ± 0.94	353 ± 0.67	536 ± 2.38	20.1 ± 1.17	2.08 ± 0.25
EPO2%Si_DP2%P_Mel	242 ± 1.42	274 ± 1.66	413 ± 1.75	263 ± 1.23	92.1 ± 1.19	320 ± 2.41	541 ± 2.39	33.6 ± 1.69	9.62 ± 1.59
EPO2%Si_DP1%P_Mel	243 ± 0.56	279 ± 0.39	379 ± 0.84	327 ± 0.21	70.5 ± 0.68	536 ± 1.13	747 ± 0.24	11.8 ± 0.41	7.84 ± 0.69

6.4.3.2 Pyrolysis combustion flow calorimeter of the in-situ silica/epoxy composites

As it is known in the the pyrolysis combustion flow calorimeter (also known as microscale combustion calorimeter, MCC) the samples is heated in nitrogen atmosphere in a pyroliser chamber at constant heating rate. The evolved gases are burnt in the combustion chamber. The heat release rate is than plotted as a function of temperature. It is a powerful instrument to evaluate the fire behavior of milligram scale (mg-scale) samples [Lyon 2004]. This analysis can provide valuable information about fire properties of a material [Schartel 2007, Sonnier 2014]. Useful parameters can be obtained from this type of measurement, such as the total heat release per unit initial mass (THR), the heat release capacity (HRC) (HRC; defined as the maximum heat release rate divided by the constant heating rate) [Lyon 2004].

Figures 87 and 88 and Tables 29 and 30 summarize the results corresponding to several PCFC measurements that have been performed in order to study the decomposition of phosphorous-based flame retardants and in-situ generated silica/epoxy materials. It is possible to observe that the EPO2%Si exhibits a smaller heat release capacity and a very strong increase of the residue, with

respect to EPO counterpart, confirming the action of the silica in the condensed phase through a barrier effect [Benin 2014, Malucelli 2016, Matzen 2015, Visakh 2015].

The addition of DA or DP has a strong effect on the heat release capacity confirming the efficacy as flame retardants of epoxy system in agreement with UL-94 test results. However, DA shows a higher reduction of the HRC value (55% vs 19% for EPO_DA2%P and EPO_DP2%P composites, respectively; see Tables 29 and 30) as compared with EPO one. This suggests that the DA has a main action in the gas phase [Bretterbauer 2012, Salmeia 2015ab]

As can be seen, according to the TGA results in inert atmosphere (see Table 26), DP does affect much the residue showing a strong increase of the mass residue (see EPO_DP2%P in Table 30), with respect to the EPO counterpart. These results support that DP has a predominant action in the condensed phase [Liu 2017, Salmeia 2015ab, Salmeia 2018].

Also, the addition of melamine does not affect much the residue, for both flame retardant systems. The increases of the heat release capacity observed when melamine is added to EPO or in combination with DA or DP can be attributed to the exothermic oxidation reaction of ammonia [Zhan 2014]. In fact, the decomposition of melamine in the pyrolyzer chamber produces ammonia [Costa 1988] that afterwards enters the combustion chamber of the MCC, where it burns altogether with the other volatiles produced. In the case of both flame retardants, the presence of melamine increases the time to pHRR through a dilution of the combustible gases.

Finally, it is worth pointing out that the addition of DA or DP has the effect of reducing the pHRR values and making less sharp the curves of Figures 87 and 88.

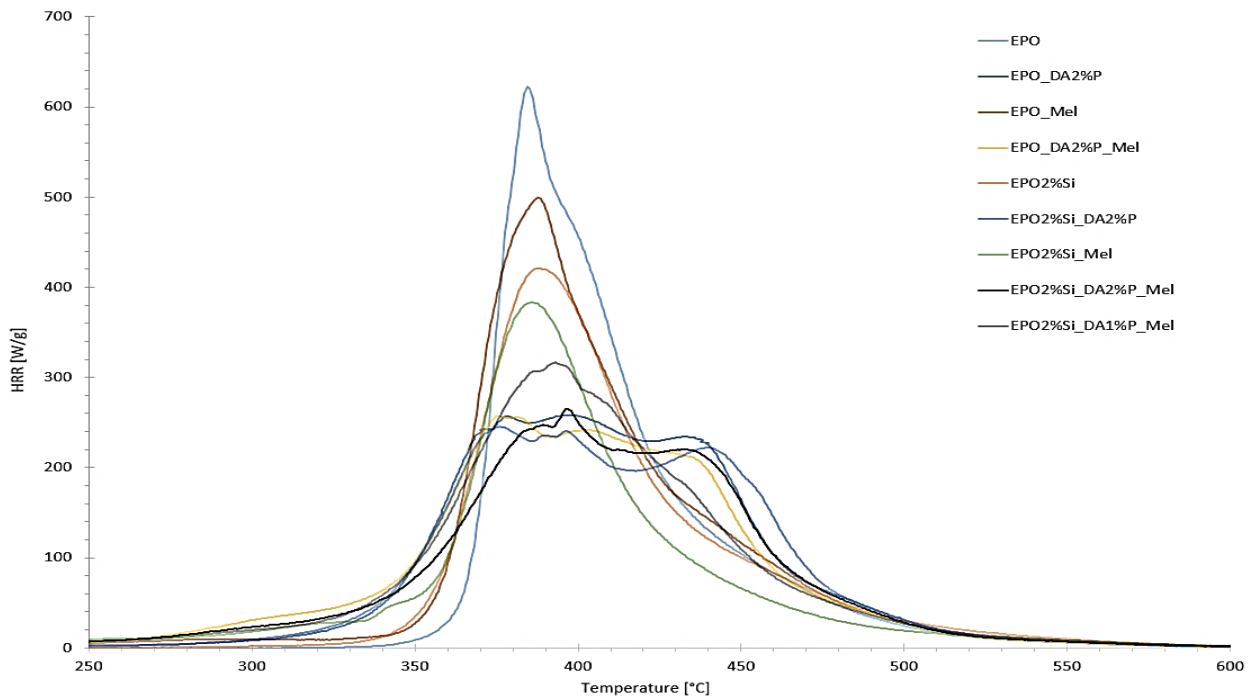


Figure 87: HRR (Heat Release Rate) curves versus temperature for EPO, EPO_DA2%P, EPO_Mel, EPO_DA2%P_Mel, EPO2%Si, EPO2%Si_DA2%P, EPO2%Si_Mel, EPO2%Si_DA2%P_Mel and EPO2%Si_DA1%P_Mel.

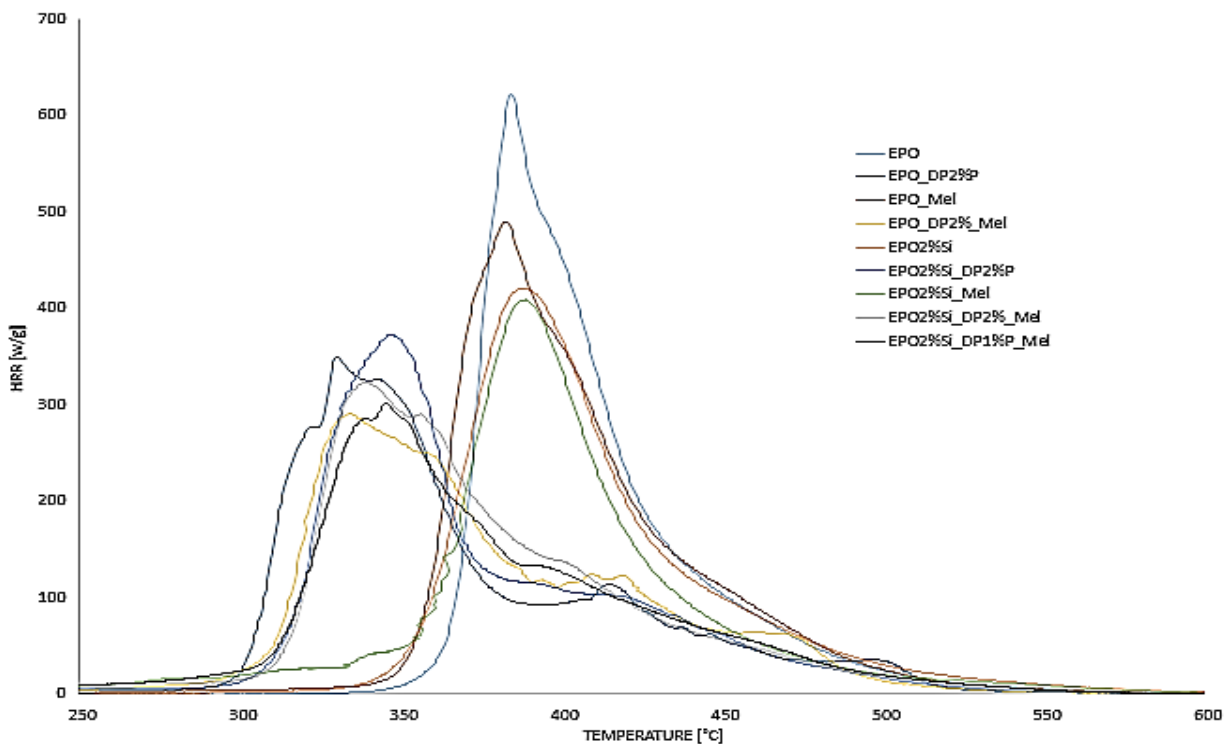


Figure 88: HRR (Heat Release Rate) curves versus temperature for EPO, EPO_DP2%P, EPO_Mel, EPO_DP2%P_Mel, EPO2%Si, EPO2%Si_DP2%P, EPO2%Si_Mel, EPO2%Si_DP2%P_Mel and EPO2%Si_DP1%P_Mel.

Table 29: Pyrolysis Combustion Flow Calorimeter data collected for EPO, EPO_DA2%P, EPO_Mel, EPO_DA2%P_Mel, EPO2%Si, EPO2%Si_DA2%P, EPO2%Si_Mel, EPO2%Si_DA2%P_Mel and EPO2%Si_DA1%P_Mel.

THR: Total Heat Release, HRC: Heat release Capacity, pHRR: (peak of Heat Release Rate)

Sample	THR [kJ/g]	HRC [J/g-K]	pHRR [W/g]	Residue [%]
EPO	30.5 ± 0.29	539 ± 44.5	545 ± 56.8	6.61 ± 0.17
EPO_DA2%P	29.2 ± 0.36	238 ± 11.4	238 ± 4.63	8.12 ± 0.39
EPO_Mel	29.1 ± 0.29	634 ± 102	554 ± 88.6	9.03 ± 2.41
EPO_DA2%P_Mel	30.8 ± 0.51	271 ± 15.2	271 ± 10.6	7.81 ± 0.71
EPO2%Si	28.3 ± 0.12	450 ± 23.9	448 ± 21.6	11.2 ± 0.91
EPO2%Si_DA2%P	28.1 ± 0.05	259 ± 11.6	259 ± 12.5	9.85 ± 0.55
EPO2%Si_Mel	25.8 ± 0.71	393 ± 14.1	393 ± 7.24	9.62 ± 0.56
EPO2%Si_DA2%P_Mel	27.4 ± 0.14	306 ± 4.97	245 ± 1.91	9.06 ± 0.69
EPO2%Si_DA1%P_Mel	28.3 ± 0.43	345 ± 31.7	302 ± 15.8	9.82 ± 0.98

Table 30: Pyrolysis Combustion Flow Calorimeter data collected for EPO, EPO_DP2%P, EPO_Mel, EPO_DP2%P_Mel, EPO2%Si, EPO2%Si_DP2%P, EPO2%Si_Mel, EPO2%Si_DP2%P_Mel and EPO2%Si_DP1%P_Mel.

THR: Total Heat Release, HRC: Heat release Capacity, pHRR: (peak of Heat Release Rate)

Sample	THR [kJ/g]	HRC [J/g-K]	pHRR [W/g]	Residue [%]
EPO	30.5 ± 0.29	539 ± 44.5	545 ± 56.8	6.61 ± 0.17
EPO_DP2%P	24.3 ± 4.20	434 ± 99.3	371 ± 90.8	16.4 ± 0.31
EPO_Mel	34.1 ± 5.31	633 ± 165	630 ± 158	8.72 ± 3.19
EPO_DP2%P_Mel	25.7 ± 0.59	334 ± 21.2	297 ± 13.6	7.43 ± 0.71
EPO2%Si	28.3 ± 0.12	450 ± 23.9	448 ± 21.6	11.2 ± 0.91
EPO2%Si_DP2%P	24.1 ± 3.12	434 ± 99.3	372 ± 91.8	14.4 ± 2.56
EPO2%Si_Mel	26.2 ± 0.82	462 ± 4.03	410 ± 8.01	10.9 ± 0.53
EPO2%Si_DP2%P_Mel	26.3 ± 0.90	316 ± 33.9	270 ± 38.3	15.1 ± 2.34
EPO2%Si_DP1%P_Mel	25.7 ± 0.12	367 ± 16.7	319 ± 23.7	9.82 ± 0.98

6.4.3.3 Pyrolysis–Gas Chromatography–Mass and Direct Insertion Probe–Mass Spectrometry of the in-situ silica/epoxy composites

Pyrolysis–gas chromatography–mass spectrometry (PY-GC-MS) is a method of chemical analysis in which the sample is heated to decomposition (the sample is put into direct contact with a platinum wire, or placed in a quartz sample tube, and rapidly heated to 600–1000 °C to produce smaller molecules, volatiles, that are separated by gas chromatography and detected using mass spectrometry [Beach 2008].

The decomposition products of EPO, EPO2%Si, EPO2%Si_DA2%P_Mel and EPO2%Si_DP2%P_Mel were detected by using PY-GC-MS. The most abundant products were recognized as bisphenol A, 4,4'-(cyclopropane-1,1-diyl)diphenol, 4-isopropylphenol, 4-isopropenylphenol, phenol, benzene, naphthalene, toluene, 2-methylpent-2-en-1-ol, 3-hydroxy-2-methylpentanal, o-cresol, 2-ethylphenol, and 2-allyl-4-methylphenol, along with several tens of other aromatic products observed in lower amounts so as reported elsewhere for similar systems [Grassie 1985, Yan 2013, Zhang 2018]. The presence of dibenzofuran, a decomposition product of DOPO, was observed for EPO2%Si_DA2%P_Mel and EPO2%Si_DP2%P_Mel [Gooneie 2019].

The presence of the above-mentioned compounds was also confirmed through direct insertion probe–mass spectrometry (DIP–MS). In this case, the sample is introduced in a chamber where it is heated, in an inert atmosphere, from 30 °C to 450 °C at a rate of 50 °C/min. The volatiles products are addressed to mass spectrometry [Flego 2012]. The apparatus is considered a proper tool to map pyrolysis mechanism characteristics [Flego 2012].

Figures 89 and 90 show the DIP-MS thermograms for EPO, EPO2%Si_DA2%P_Mel and EPO2%Si_DP2%P_Mel. It is possible to observe that EPO2%Si_DA2%P_Mel has already released a large amount of species at 350 °C, where the volatiles production of EPO is very limited. Moreover, the epoxy sample containing DA and melamine starts its decomposition very early compared to the pristine epoxy, around 200 °C, in agreement with TGA results in inert atmosphere (see section 6.4.3.1). In the case of EPO2%Si_DP2%P_Mel, the relative abundance of the released volatiles follows along the temperature a trend similar to EPO.

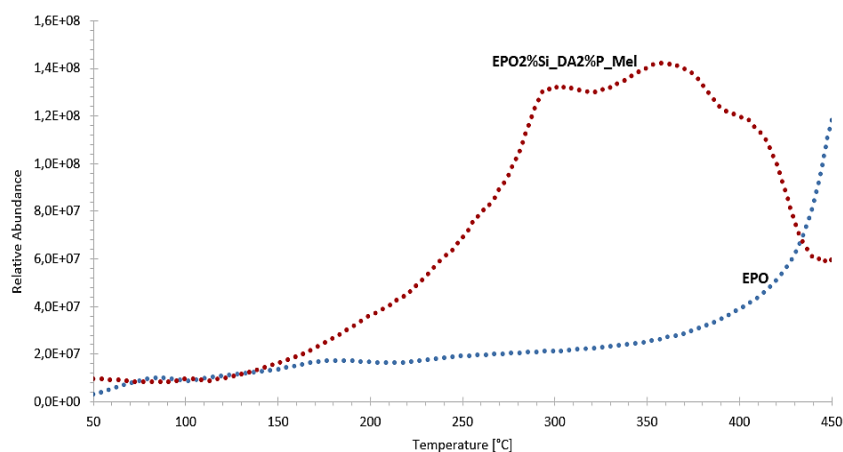


Figure 89: DIP-MS total ion thermograms of EPO2%Si_DA2%P_Mel (red curve) and EPO (blue curve).

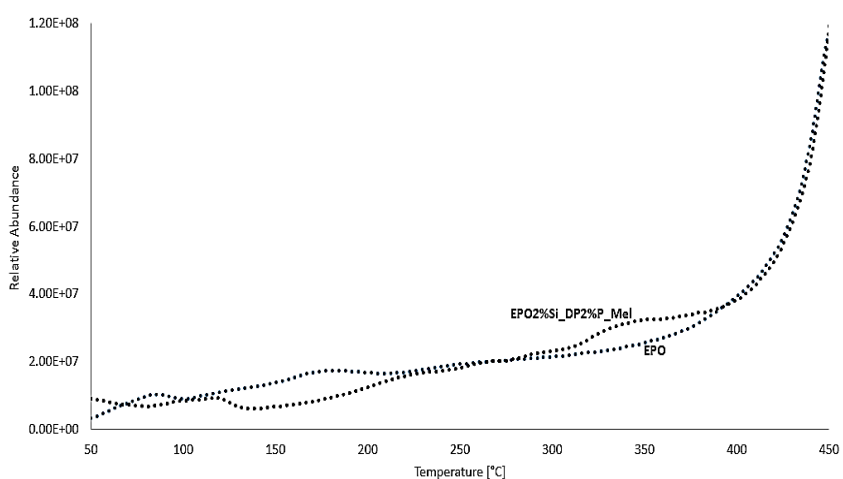


Figure 90: DIP-MS total ion thermograms of EPO2%Si_DP2%P_Mel (green curve) and EPO (blue curve).

Analysis of DIP-MS data for EPO2%Si_DA2%P_Mel and EPO2%Si_DP2%P_Mel suggests the formation of some major decomposition products of DA and DP, which are shown in Figures 91 and 92 together with the m/z ratio used for their detection. The presence of these species was already observed by Salmeia et al. [Salmeia 2018]. Figures 93 and 94 show the thermograms of each species coming from the decomposition of DA and DP.

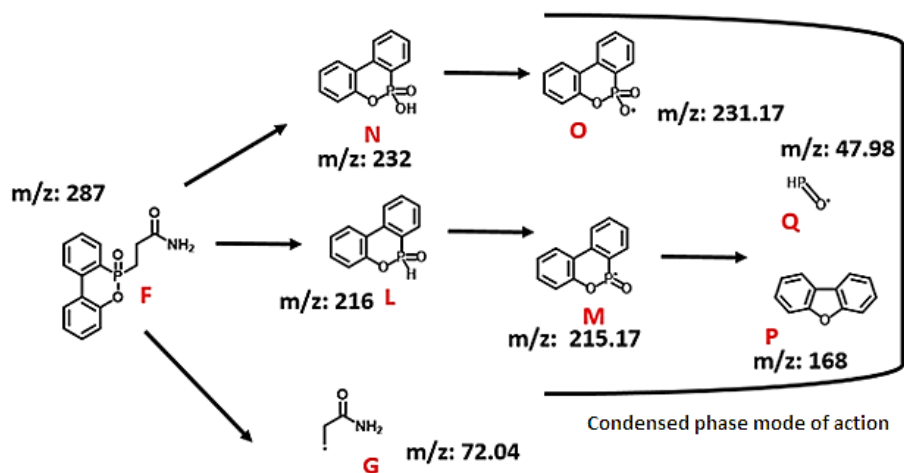


Figure 91: The decomposition pathways of the DA.

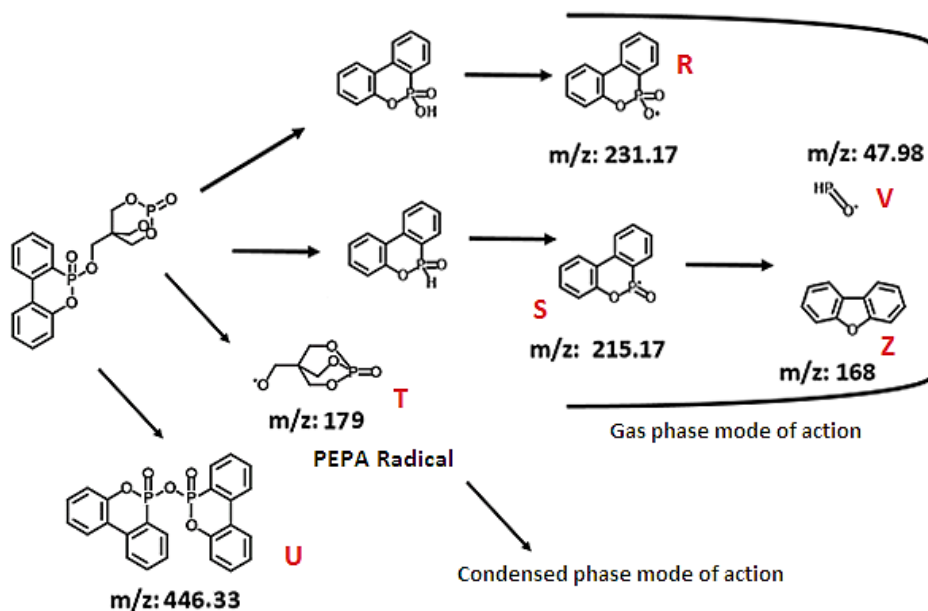


Figure 92: The decomposition pathways of the DP. PEPA is the acronym for the compound 1-(oxo-4-hydroxymethyl-2,6,7-trioxa-1-phosphabicyclo[2.2.2]octane).

According to the DIP-MS results (see Figures 93 and 94), the covalent bond between DOPO (see Figure 18) and acrylamide/PEPA (see Figures 91 and 92) in the flame retardant molecule breaks, and a release of phosphorus decomposition products occurs [Salmeia 2018].

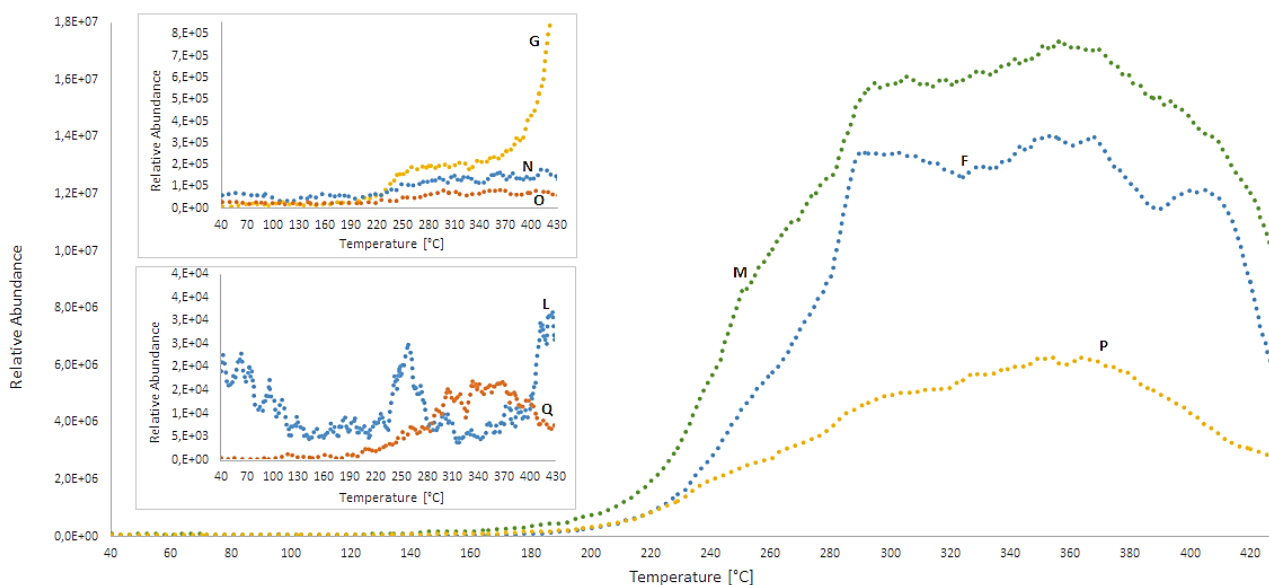


Figure 93: DIP-MS analysis of EPO2%Si_DA2%P_Mel, thermograms for the specified species in Figure 91.

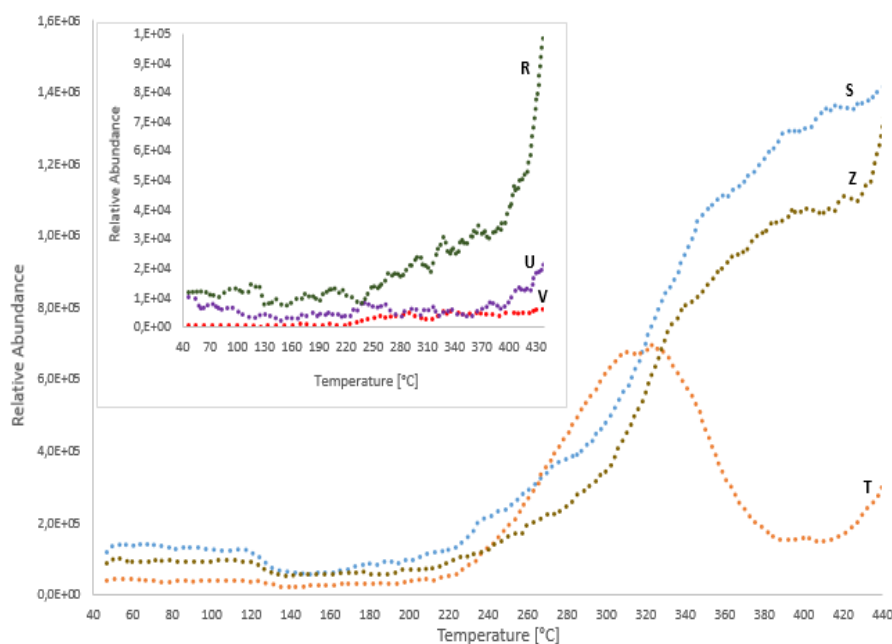


Figure 94: DIP-MS analysis of EPO2%Si_DP2%P_Mel, thermograms for the specified species in Figure 92.

In the literature is reported [Braun 2001, Chin 1995, Levchik 1998, Schartel 2010, Shau 1996, Shirokane 2014, Yan 2013, Yan 2014, Zhang 2018] that the decomposition pathway (see Figure 95), in inert atmosphere and at high temperature, for the epoxy resin begins with the elimination of water from the secondary alcohol group. This was the first reaction which has been recognized when the epoxy resin is heated [Braun 2001, Chin 1995, Levchik 1998, Shau 1996, Shirokane 2014, Yan 2013, Yan 2014]. Subsequently, the resulting allylic bonds, aromatic ether linkages, experienced homolytic cleavage. The homolytic cleavage leads to the formation of a free radical

that can be saturated by an active hydrogen to yield bisphenol A. Alternatively, the intramolecular hydrogen transfer of bisphenol A biradical may generate 4,4'-(cyclopropane-1,1-diyl)diphenol. Figure 95 shows that bisphenol A may undergo homolysis and form free 4-isopropylphenol and phenol radicals. The free phenol radicals could capture hydrogen from the neighboring methyl in the 4-isopropylphenol radical or a hydrogen-donor to generate phenol and 4-isopropenylphenol. On the other hand, the free 4-isopropylphenol and phenol radicals, through H transfer, yield phenol and 4-isopropenylphenol. Analysis of DIP-MS data for EPO, reported in Figure 96, proved the formation of the major decomposition products of pristine epoxy (bisphenol A, 4,4'-(cyclopropane-1,1-diyl)diphenol, 4-isopropylphenol, 4-isopropenylphenol, phenol) considered in the scheme of Figure 95; the m/z ratio used for their detection are also reported in the same Figure. So as reported above the same species were also detected by using PY-GC-MS. Therefore, the collected experimental results are in good agreement with the mechanisms reported in the literature reminded above [Braun 2001, Chin 1995, Levchik 1998, Schartel 2010, Shau 1996, Shirokane 2014, Yan 2013, Yan 2014, Zhang 2018].

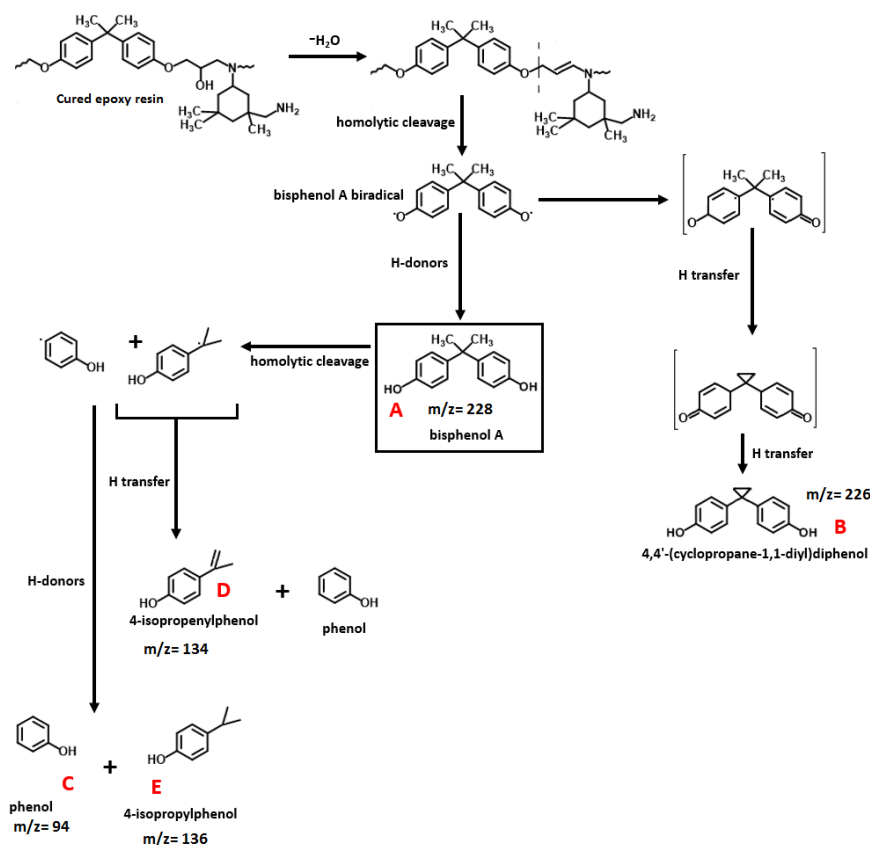


Figure 95: Epoxy resin with cycloaliphatic hardener: degradation mechanism reactions under N_2 (nitrogen) atmosphere [Braun 2001, Chin 1995, Levchik 1998, Schartel 2010, Shau 1996, Shirokane 2014, Yan 2013, Yan 2014, Zhang 2018].

Figure 96 shows the relative abundance along the temperature of bisphenol A, 4,4'-(cyclopropane-1,1-diyl)diphenol, 4-isopropylphenol, 4-isopropenylphenol and phenol released from EPO. It is worth to underline that the decomposition of the DA flame retardant produces a large amount of phosphorous species, in a range of temperature (from 200 to 400 °C), where the epoxy resin shows low relative abundance values of its main volatile compounds (see Figures 93 and 96).

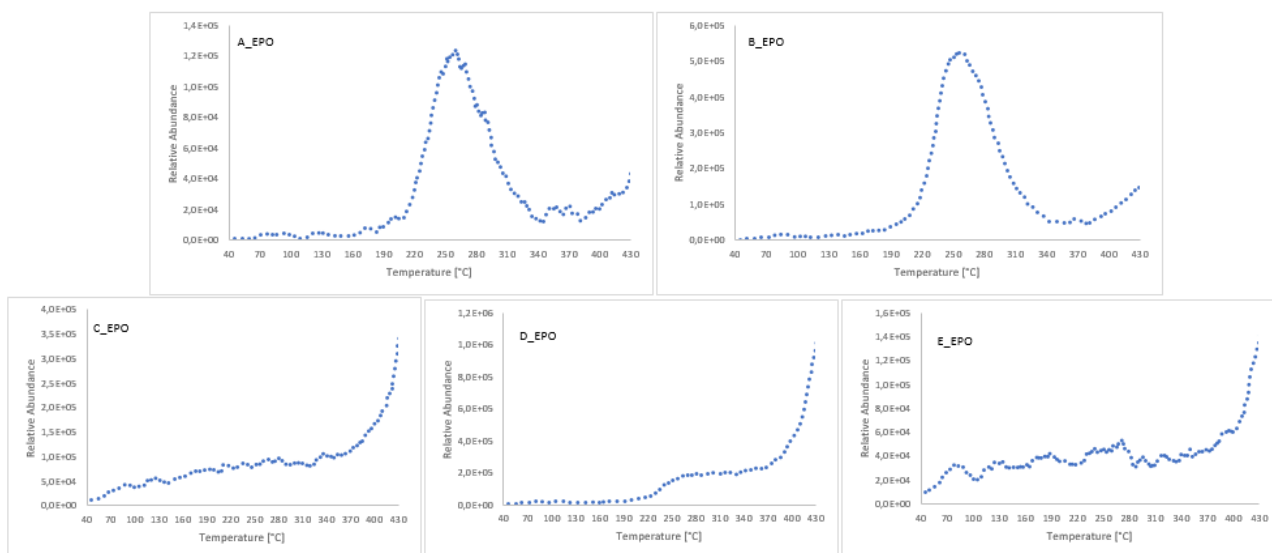


Figure 96: DIP-MS analysis of EPO and EPO2%Si_DA2%P_Mel, thermograms for the specified species in Figure 20.

DIP-MS analysis of EPO2%Si_DA2%P_Mel and EPO2%Si_DP2%P_Mel confirms the presence of dibenzofuran, which is an indirect proof of the formation $PO\cdot$ (see Figures 93 and 94) [Gooneie 2019, Salmeia 2018]. The gas phase activity of DA and DP flame retardants suggested by the PFCF results may be related to the $PO\cdot$ radicals produced during the pyrolysis process. It is well known that, in air atmosphere, $PO\cdot$ radicals can act in the gas phase recombining the active $H\cdot$ and $OH\cdot$ in a flame (see section 3.4.3.1) [Jian 2016, ScharTEL 2010]. The complete consume of the active $H\cdot$ and $OH\cdot$ favors flame extinguishing; otherwise the oxygen attack would cause the formation of several oxygenated species with low molecular weight [Grassie 1985, Musto 2001, Musto 2003]. As already observed by Gooneie et al. [Gooneie 2019] for another polymer system in a previous work, the oxygen may act by extracting a hydrogen radical from the major decomposition products of epoxy resin, and form $HO_2\cdot$ radicals which are later transformed into $HO\cdot$ active oxygen radicals [Gooneie 2019, Nait-Ali 2011, ScharTEL 2010]. However, in the presence of DOPO radicals (species O, M, R and S of Figures 91 and 92) the active oxygen radicals are neutralized and turned into volatile phosphorus species such as $PO\cdot$, $PO_2\cdot$ and $HOPO_2$ (flame inhibitors) [König 2011, König 2012, ScharTEL 2010]. This second effect may strongly contribute to the activity of DA in the gas phase, because of the large amount of DOPO radicals (O and, mainly, M species of Figure 91)

produced during the pyrolysis process of this phosphorous based flame retardant (see Figure 93). The same effect has a lesser intensity in the case of DP, where DOPO radicals (R and, mainly, S species of Figure 92) are produced in a small amount as compared with DA (see Figures 93 and 94). These results suggest that DP has a main action in the condensed phase [Liu 2017, Salmeia 2015ab, Salmeia 2018]. This hypothesis is additionally supported by the release of PEPA radicals (T specie of Figure 92) during the degradation process of DP, which is also consistent with the composition of EPO2%Si_DP2%P_Mel. In fact, it is reported in the literature [Hoang 2015, Salmeia 2015ab, Salmeia 2018, Zhang 2014] that PEPA works in the condensed phase by producing phosphoric acids which can be responsible for condensed phase activity [Bourbigot 2007, Morgan 2013]. These results are in agreement with the data (CO/CO₂ value and mass residue) collected in the case of DP through cone calorimeter, and TGA and PCFC measurements (see Tables 24, 28 and 30).

As regards DA, the formation of a very large amount of flame inhibitors, which subtract active oxygen radicals in the flame zone (see section 3.4.5), clearly indicates that a strong gas phase action of this flame retardant is at the basis of the good performances at UL test and cone calorimeter analysis. All this is in agreement with the significant increase of CO/CO₂ value, recorded when DA is used (see Table 23), that also suggests, as already pointed out, a decrease of the combustion efficiency linked to gas phase activity [Schartel 2010].

It is worth reminding that some condensed phase action, through formation of intumescent char, was recognized in the case of EPO2%Si_DA2%P_Mel and EPO2%Si_DP2%P_Mel (see Figures 81 and 82). This is possible thanks to the earlier decomposition of DA, with respect to the polymer matrix (see Figure 89), and the presence of the PEPA unit [Hoang 2015, Salmeia 2015ab, Salmeia 2018, Zhang 2014]. It is reported in fact that an earlier decomposition of the phosphorous flame retardants than the char-forming polymer matrix (epoxy resin) is necessary to allow intumescent char formation in the presence a blowing agent (melamine) [Bourbigot 2007, Hoang 2015, Morgan 2013, Salmeia 2015ab, Salmeia 2018, Zhang 2014].

6.4.3.4 Char analysis of the in-situ silica/epoxy composites

The chemical composition of the residual chars obtained by the vertical burning test of EPO, EPO2%Si_DA2%P_Mel and EPO2%Si_DP2%P_Mel were qualitatively studied by ATR-FTIR analysis (Figure 97).

As far as the burnt neat epoxy polymer, the peak around 638, 802 and 871 cm⁻¹ are due to aromatic C-H stretching in meta, para and orto, respectively [Grassie 1985, Musto 2001, Musto 2003, Wang 2016]. The combustion of DGEBA epoxy resin produces molecules containing alkoxy C-O and

phenol C-O groups with stretching bands at 1081 cm^{-1} and around 1257 cm^{-1} , respectively [Ciesielski 2009, Grassie 1985, Liu 2012, Musto 2001, Musto 2003, Rakotomalala 2010]. The band at 1510 cm^{-1} may be attributed to the stretching vibrations of the bonds between carbons of the aromatic ring; it was selected as reference peak for the scaling of all the curves in Figure 97, because of the fact that this band shows any modification in the char and original samples [Cholake 2014, Salmeia 2019, Su 2014]. The bands at 2852 cm^{-1} and 2954 cm^{-1} correspond to the stretching vibration of the C-H bond, and the broad band at 1589 cm^{-1} could be due to stretching vibration of the secondary amine N-H bonds produced in the curing reaction [Mahapatra 2007].

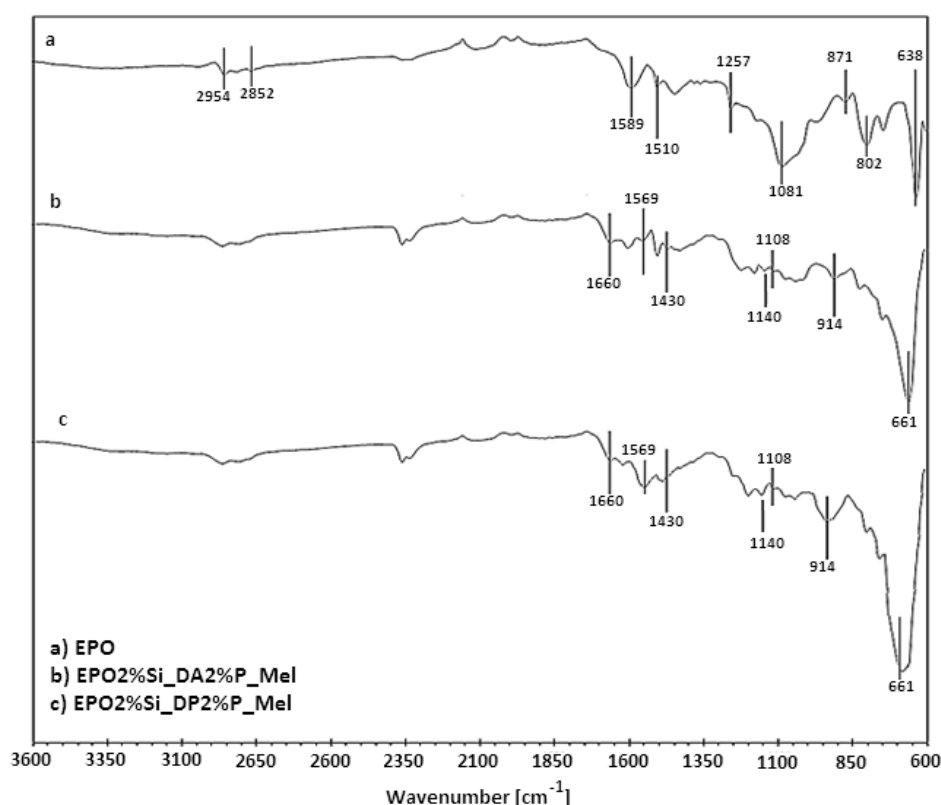


Figure 97: ATR-FTIR spectra for residual chars obtained after the vertical burning test of EPO, EPO2%Si_DA2%P_Mel and EPO2%Si_DP2%P_Mel.

The FTIR spectra of burnt EPO2%Si_DA2%P_Mel and burnt EPO2%Si_DP2%P_Mel show broad peaks at 661 cm^{-1} and 914 cm^{-1} which may be attributed to the existence of stretching vibrations of P-C and P-O-C bonds, respectively [Chen 2018, Meltzer 2015, Salmeia 2019]. EPO2%Si_DP2%P_Mel shows a higher intensity of 661 cm^{-1} and 914 cm^{-1} as compared with EPO2%Si_DA2%P_Mel. This evidence indicates a larger amount of pyrophosphate and polyphosphates (containing P-C and P-O-C bonds) in the char residue of the sample containing DP. The band around 1430 cm^{-1} could be due to the presence of P-N stretching vibrations in the char of both the investigated samples [Salmeia 2019, Su 2014]. The band at 1108 cm^{-1} may be attributed to stretching vibration of silica units

[Branda 2016, Zhi 2019]. Its presence is in agreement with the shield role supposed to be played by silica as reported above (see section 6.3.6).

The presence of C=C stretching band around 1569 cm^{-1} for both the flame retardant samples [North 2014, Wang 2016], which shows higher intensity in the case of DP, gives also proof of carbonization process consequent to dehydration reaction between acid phosphorous compounds and epoxy resin (carbonizing source) [Bourbigot 2007, Liu 2017, Singh 2009], which promotes char formation. This is in agreement with TGA, in air atmosphere, and cone calorimeter results, where an increase of char residue was observed when DA or DP are present (as already observed for another polymer system by Salmeia et al. [Salmeia 2019]). It is worth pointing out the presence of a band around 1660 cm^{-1} which is usually attributed due to the C=O stretching of oxygenated species of low molecular weight that are reported to form [Grassie 1985, Musto 2001, Musto 2003]. The band at 1140 cm^{-1} [Hampton 2010] may be attributed to stretching vibration of P=O, that in the case of DP is mainly due to the condensed phase activity of PEPA through the production of phosphoric acids [Hoang 2015, Salmeia 2015ab, Salmeia 2018, Zhang 2014] and therefore of pyrophosphate and polyphosphates. The flame retardant action of PEPA does not exist for the sample containing DA, hence a lesser intensity of the band at 1140 cm^{-1} appears.

FTIR results for burnt EPO2%Si_DA2%P_Mel and burnt EPO2%Si_DP2%P_Mel, therefore, are consistent with a condensed phase action of DA and DP. Moreover, based on the results discussed so far, it is possible to confirm that a strong condensed phase activity of DP, in combination with silica phase and melamine, is at the basis of the good performances at UL test and cone calorimeter analysis. All this is in agreement with the significant decrease of CO/CO₂ value, recorded when DP is used (see Table 24), that also suggests a decrease of the combustion efficiency linked to a condensed phase action through the formation of a very protective and abundant char (see Table 24 and Figure 82) [Salmeia 2018, Scharrel 2010, Zhang 2014]. The strong condensed phase activity of DP causes the formation of a large amount of intumescent char [Bourbigot 2007], that together with a thermal shield effect of the silica phase [Bifulco 2018] allows to achieve V0 classification (see Table 20).

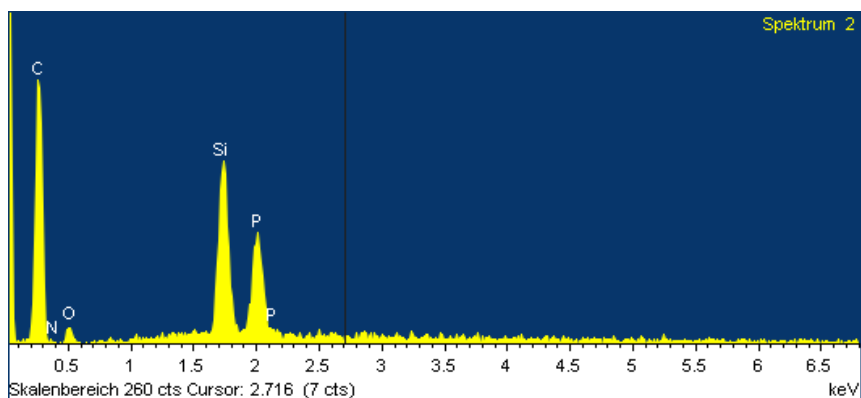


Figure 98: EDX spectrum of residual chars obtained after the vertical burning test of EPO2%Si_DA2%P_Mel.

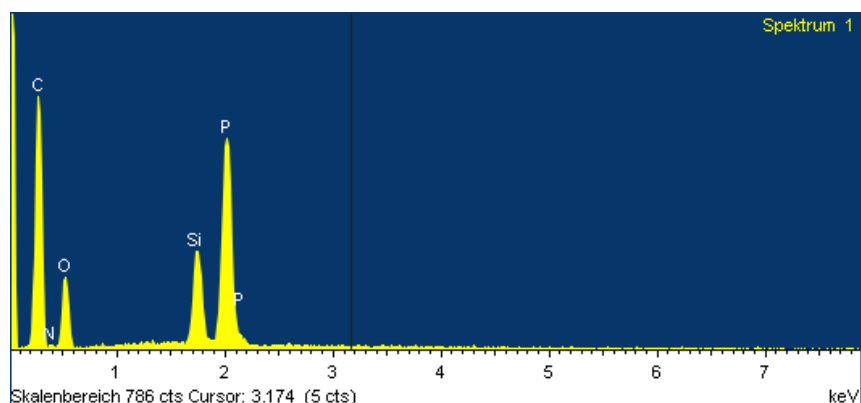


Figure 99: EDX spectrum of residual chars obtained after the vertical burning test of EPO2%Si_DP2%P_Mel.

EDX spectra of residual char obtained after the vertical burning test of EPO2%Si_DA2%P_Mel and EPO2%Si_DP2%P_Mel are reported in Figures 98 and 99. The presence of phosphorus (P) in the char of both samples clearly indicates certain level of condensed phase activity for DA and DP flame retardants. The remarkable improvement in char content for the epoxy resin and higher %P content in the char for DP sample (see Tables 23 and 24 and Figures 98 and 99) clearly indicates higher condensed phase activity of DP compared to DA additive. In fact, in the case of DP sample, the ratio of weight percentage of Si and P is 0.4 much lower than the one of unburned system (0.5). As regards DA sample, the ratio of weight percentage of Si and P is 1.3 much higher than the one of unburned system (0.5), which is in agreement with the strong gas phase activity of the flame retardant through a flame inhibition mechanism (see section 6.4.3.3).

The presence of silicon (Si) in the char residue of both samples is consistent with its role only in the condensed phase whereas DA and DP in both condensed than gas phase.

Conclusions

The sol-gel process has been extensively studied and employed as the most important route in tailoring textile surfaces and in forming new hybrid inorganic-organic materials. This is because this process can modify the chemical nature of material surfaces and introduce ceramic phases into composites through chemistry. Very mild reaction conditions and low reaction temperatures are particularly useful for incorporating inorganic moieties into organic materials or organic materials into inorganic matrices. This thesis has shown some applications that exploit sol-gel methodologies and its advantages to solve industrial and technological problems inherent the use of polymer based bio-composites. These composites can show severe limitations due to the easy flammability of the polymer matrix: this behavior can significantly restrict the application fields of these materials, especially when the possibility of the use of the composites is strictly related to specific regulatory fire tests that have to be passed, hence ensuring public safety (e.g., in the aerospace industry). Additional limitations descend from the mechanical properties of the above mentioned bio-composites, which may be due to a low interfacial adhesion between the filler (e.g., natural fibers) and the polymer matrix. Sol-gel methodologies can improve the fire behavior and the mechanical properties of bio-composites through the in-situ synthesis of ceramic domains in the polymer network or the tailoring of the interphase between filler and matrix.

In this thesis, hemp fabrics have been treated with a new, inexpensive, simple and eco-friendly silica-based coating, able to protect the fabrics from heat sources, hence improving their fire behavior when utilized as reinforcing agent fillers in epoxy-based composites. To the best knowledge of the author, this was the first time that inexpensive waterglass solutions were exploited for this purpose: indeed, the proposed approach can be considered as an application of sol-gel chemistry using a precursor that does not need hydrolysis and is performed in water solutions, avoiding the organic solvents usually required by the alkoxy precursors. FTIR and solid-state NMR spectroscopies have confirmed the formation of $-C-O-Si-$ covalent bonds in between the silica coating and the underlying fabrics. The coating, resistant to washing, allows the fire behavior of hemp fabric/epoxy composites to be improved. In particular, the concurrent presence of hemp surface treatment and APP significantly improves cone parameters HRR, THR, TSR and SEA, which turn out to decrease respectively by 83%, 35%, 45% and 44% as compared to untreated hemp/epoxy composites. At the same time, the formation of a very stable char is promoted, as also assessed by TG analysis performed in an inert atmosphere. Conversely, the low interfacial adhesion between the fibers and the epoxy matrix promotes a brittle behavior of the composites, which show a slightly lower stiffness as compared to the theoretical one. However, the fracture energy absorbed

by the material reinforced by the silica coating is higher. Finally, the presence of APP in the epoxy matrix does not affect the mechanical behavior of the obtained composites.

In this thesis, it has been shown that when properly treated with the above-mentioned waterglass solution, hemp fabric easily gives silica-based coated fibers of diameters from tens of microns to tens of nanometers with the aid of a low power mixer. The silica-based coated fibers can be easily functionalized with APTS and then dispersed in epoxy resin. SEM micrographs of the composites show a tendency to give web-like structure formed by fibrils and microfibrils continuously interconnected, from which particularly good mechanical properties may be expected to descend. DMA analysis shows that the functionalized fibers, till a concentration of 5%, strongly positively affect the glass transformation temperature (10 °C increases) and the storage modulus of the pristine resin.

In this thesis, new hybrid silica/epoxy composites cured with a cycloaliphatic amine have been prepared by using an in-situ sol-gel process. A deep study of the obtained hybrid composites has been performed by means of FTIR, SAXS, TEM, DMA, NMR. The experimental results suggest that the new hybrid structures consist of very fine silica nanoparticles, homogeneously dispersed in an epoxy/silica hybrid network; their size increases with increasing TEOS content (approaching a maximum size of about 1.25 nm). A significant increase of the T_g values is observed for the hybrids, subjected to a non-isothermal post curing treatment up to end temperatures (100 °C) higher than the T_g range temperature of the neat epoxy (85 °C). The FTIR, NMR and SAXS results suggest the following explanation: when entering the glass transformation range, the mobility that all the hybrid segments are expected to acquire may well allow clustering of the very small silica particles, as well evidenced by SAXS; otherwise the clustering may well stiffen the network, hence promoting the T_g increase. The presence of the silica domains in the hybrid organic-inorganic networks prevents melt dripping phenomena in vertical flame spread tests. In addition, as assessed by forced-combustion tests, the inorganic domains act as a thermal protective layer, hence improving the heat and smoke-related parameters. Finally, because of the clustering, the efficiency of the protective ceramic layer decreases after the non-isothermal post curing treatment.

The procedure has been, afterwards, modified by adding DA or DP (two phosphorous-based flame retardants) and eventually melamine just before the addition of the hardener. Melamine has been added as a source of nitrogen that could play a role of blowing agent. UL-94 vertical burning, equipped with an IR Camera, PCFC, TGA and Cone Calorimeter show that the addition of DA or DP with or without melamine strongly improve the fire behavior of the studied epoxy system. UL-94 vertical burning and IR Camera measurements reveal that DA allows to achieve self-

extinguishing capacity for the studied epoxy system, when only 2 wt. % of P-loading is present. Additionally, the presence of only 2% silica guarantees the absence of dripping phenomena during the burning of the epoxy resin. Conversely, DP guarantees absence of dripping phenomena with or without silica but the self-extinguishing is possible only in combination with silica and melamine, and when 2 wt. % of P-loading is present. PCFC, TGA and Cone Calorimeter results show that DA and DP lead to a strong reduction of the HHR values and an increase of the residues in air atmosphere. Cone calorimeter residues show the formation of an intumescent char when the two phosphorous-based flame retardants are used in combination with melamine. DIP-MS and PY-GC-MS support a gas phase activity of DA and DP linked to a flame inhibition mechanism and a simultaneous condensed phase activity. Finally, ATR-FTIR and EDX spectra of the char and the visual analysis of the residual masses of TGA and Cone Calorimeter prove that DA plays a role also in the condensed phase and that the effect of DP on the fire behavior of the epoxy system is mainly due to a condensed phase action through the formation of a very protective and abundant char.

As a future prospective, the above sol-gel functionalized hemp fibers may be used as reinforcement in in-situ silica/polymer bio-composites added with green phosphorous-based flame retardants. This may allow to combine excellent performances in terms of fire behavior with improved mechanical properties.

References

- Abdelmouleh, M., Boufi, S., Belgacem, M. N., Duarte, A. P., Salah, A. B., & Gandini, A. (2004). *Modification of cellulosic fibres with functionalised silanes: development of surface properties. International Journal of Adhesion and Adhesives*, 24(1), 43-54.
- Adnan, M. M., Dalod, A. R., Balci, M. H., Glaum, J., & Einarsrud, M. A. (2018). *In Situ Synthesis of Hybrid Inorganic–Polymer Nanocomposites. Polymers*, 10(10), 1129.
- Afzal, A., & Siddiqi, H. M. (2011). *A comprehensive study of the bicontinuous epoxy–silica hybrid polymers: I. Synthesis, characterization and glass transition. Polymer*, 52(6), 1345-1355.
- Afzal, A., Siddiqi, H. M., Iqbal, N., & Ahmad, Z. (2013). *The effect of SiO₂ filler content and its organic compatibility on thermal stability of epoxy resin. Journal of thermal analysis and calorimetry*, 111(1), 247-252.
- Ahmad, N., Afzali, R., Neupane, Y. R., Amin, S., & Kohli, K. (2014). *Optimization of Gel Based System of Lercanidipine by Statistical Design for Transdermal Delivery; Histopathological Examination and Rheological Characterization. Journal of Biopharmaceutics Sciences*, 2(1), 15-25.
- Al-Malaika, S., Golovoy, A., & Wilkie, C. A. (Eds.). (2001). *Speciality Polymer Additives: Principles and Applications. Blackwell Science*.
- Almeida, J. C., Castro, A. G., Salvado, I. M. M., Margaca, F. M., & Fernandes, M. H. V. (2014). *A new approach to the preparation of PDMS–SiO₂ based hybrids—A structural study. Materials Letters*, 128, 105-109.
- Alongi, J., & Malucelli, G. (2015). *Thermal degradation of cellulose and cellulosic substrates. Reactions and Mechanisms in Thermal Analysis of Advanced Materials; Tiwari, A., Raj, B., Eds*, 301-332.
- Alves, C., Silva, A. J., Reis, L. G., Freitas, M., Rodrigues, L. B., & Alves, D. E. (2010). *Ecodesign of automotive components making use of natural jute fiber composites. Journal of Cleaner Production*, 18(4), 313-327.
- Amirkhosravi, M., Pishvar, M., & Altan, M. C. (2017). *Improving laminate quality in wet lay-up/vacuum bag processes by magnet assisted composite manufacturing (MACM). Composites Part A: Applied Science and Manufacturing*, 98, 227-237.
- Apeloig, Y. (1989). *The chemistry of organic silicon compounds (Vol. 1). John Wiley & Sons*.
- Babrauskas, V. (1984). *Development of the cone calorimeter—a bench-scale heat release rate apparatus based on oxygen consumption. Fire and Materials*, 8(2), 81-95.
- Bakhshandeh, E., Jannesari, A., Ranjbar, Z., Sobhani, S., & Saeb, M. R. (2014). *Anti-corrosion hybrid coatings based on epoxy–silica nano-composites: toward relationship between the morphology and EIS data. Progress in Organic Coatings*, 77(7), 1169-1183.
- Balakrishnan, N., & Mayilsamy, K. (2013). *A study of cotton coated with intumescent flame retardant: Kinetics and effect of blends of used vegetable oil methyl ester. Journal of Renewable and Sustainable Energy*, 5(5), 053121.
- Bandyopadhyay, A., & Bose, S. (Eds.). (2013). *Characterization of biomaterials. Newnes*.
- Bauer, B. J., Liu, D. W., Jackson, C. L., & Barnes, J. D. (1996). *Epoxy/SiO₂ interpenetrating polymer networks. Polymers for Advanced Technologies*, 7(4), 333-339.
- Beach, M. W., Rondan, N. G., Froese, R. D., Gerhart, B. B., Green, J. G., Stobby, B. G., ... & Korobeinichev, O. P. (2008). *Studies of degradation enhancement of polystyrene by flame retardant additives. Polymer Degradation and Stability*, 93(9), 1664-1673.
- Beach, M. W., Vozar, S. E., Filipi, S. Z., Shmakov, A. G., Shvartsberg, V. M., Korobeinichev, O. P., ... & Sick, V. (2009). *Screening approaches for gas-phase activity of flame retardants. Proceedings of the Combustion Institute*, 32(2), 2625-2632.
- Beg, M. A. A., & Clark, H. C. (1962). *Chemistry of the trifluoromethyl group: part v. infrared spectra of some phosphorus compounds containing CF₃. Canadian Journal of Chemistry*, 40(3), 393-398.
- Belov, S., Fraser, G. T., Ortigoso, J., Pate, B. H., & Tretyakov, M. Y. (1994). *Electric resonance optothermal spectrum of the 920 cm⁻¹ ν₁₄+ ν₁₅ torsional combination band of acetaldehyde. Molecular Physics*, 81(2), 359-368.

- Benin, V., Gardelle, B., & Morgan, A. B. (2014). Heat release of polyurethanes containing potential flame retardants based on boron and phosphorus chemistries. *Polymer degradation and stability*, 106, 108-121.
- Berg, J. C. (2010). *An introduction to interfaces & colloids: the bridge to nanoscience*. World Scientific.
- Beyler, C., Croce, P., Dubay, C., Johnson, P., & McNamee, M. (2017). Oxygen consumption calorimetry, William Parker: 2016 DiNenno Prize. *Fire Science Reviews*, 6(1), 1.
- Bhattacharyya, D., Subasinghe, A., & Kim, N. K. (2015). Natural fibers: Their composites and flammability characterizations. *Multifunctionality of Polymer Composites: Challenges and New Solutions*, 1st ed.; Friedrich, K., Breuer, U., Eds, 102-143.
- Bi, Y. T., Li, Z. J., & Liang, W. (2014). Preparation and characterization of epoxy/SiO₂ nanocomposites by cationic photopolymerization and sol-gel process. *Polymers for Advanced Technologies*, 25(2), 173-178.
- Biagiotti, J., Puglia, D., & Kenny, J. M. (2004). A review on natural fibre-based composites-part I: structure, processing and properties of vegetable fibres. *Journal of Natural Fibers*, 1(2), 37-68.
- Bishop, D. P., & Smith, D. A. (1970). Combined pyrolysis and radiochemical gas chromatography for studying the thermal degradation of epoxy resins and polyimides. I. The degradation of epoxy resins in nitrogen between 400 C and 700 C. *Journal of applied polymer science*, 14(1), 205-223.
- Bismarck, A., Aranberri-Askargorta, I., Springer, J., Lampke, T., Wielage, B., Stamboulis, A., ... & Limbach, H. H. (2002). Surface characterization of flax, hemp and cellulose fibers; surface properties and the water uptake behavior. *Polymer composites*, 23(5), 872-894.
- Bledzki, A. K., & Gassan, J. (1999). Composites reinforced with cellulose based fibres. *Progress in polymer science*, 24(2), 221-274.
- Boccarusso, L., Carrino, L., Durante, M., Formisano, A., Langella, A., & Minutolo, F. M. C. (2016). Hemp fabric/epoxy composites manufactured by infusion process: Improvement of fire properties promoted by ammonium polyphosphate. *Composites Part B: Engineering*, 89, 117-126.
- Boday, D. J., Wertz, J. T., & Kuczynski, J. P. (2015). Functionalization of silica nanoparticles for corrosion prevention of underlying metal. *Nanomaterials, polymers and devices: materials functionalization and device fabrication*, 1st edn. Wiley, Hoboken, 121-140.
- Bogush, G. H., Tracy, M. A., & Zukoski Iv, C. F. (1988). Preparation of monodisperse silica particles: control of size and mass fraction. *Journal of non-crystalline solids*, 104(1), 95-106.
- Bogush, G. H., & Zukoski Iv, C. F. (1991). Studies of the kinetics of the precipitation of uniform silica particles through the hydrolysis and condensation of silicon alkoxides. *Journal of Colloid and Interface Science*, 142(1), 1-18.
- Boissière, C., Van Der Lee, A., El Mansouri, A., Larbot, A., & Prouzet, E. (1999). A double step synthesis of mesoporous micrometric spherical MSU-X silica particles. *Chemical Communications*, (20), 2047-2048.
- Boissiere, C., Larbot, A., van der Lee, A., Kooyman, P. J., & Prouzet, E. (2000). A new synthesis of mesoporous MSU-X silica controlled by a two-step pathway. *Chemistry of materials*, 12(10), 2902-2913.
- Boissière, C., Larbot, A., Bourgaux, C., Prouzet, E., & Bunton, C. A. (2001). A study of the assembly mechanism of the mesoporous MSU-X silica two-step synthesis. *Chemistry of materials*, 13(10), 3580-3586.
- Bourbigot, S., & Duquesne, S. (2007). Fire retardant polymers: recent developments and opportunities. *Journal of Materials Chemistry*, 17(22), 2283-2300.
- Bourbigot, S., Le Bras, M., Leeuwendal, R., Shen, K. K., & Schubert, D. (1999). Recent advances in the use of zinc borates in flame retardancy of EVA. *Polymer degradation and stability*, 64(3), 419-425.
- Bourbigot, S., & Duquesne, S. (2007). Fire retardant polymers: recent developments and opportunities. *Journal of Materials Chemistry*, 17(22), 2283-2300.
- Branda, F., Malucelli, G., Durante, M., Piccolo, A., Mazzei, P., Costantini, A., ... & Bifulco, A. (2016). Silica treatments: a fire retardant strategy for hemp fabric/epoxy composites. *Polymers*, 8(8), 313.

- Braun, D., Von Gentzkow, W., & Rudolf, A. P. (2001). Hydrogenolytic degradation of thermosets. *Polymer Degradation and Stability*, 74(1), 25-32.
- Braun, U., Balabanovich, A. I., Schartel, B., Knoll, U., Artner, J., Ciesielski, M., ... & Hoffmann, T. (2006). Influence of the oxidation state of phosphorus on the decomposition and fire behaviour of flame-retarded epoxy resin composites. *Polymer*, 47(26), 8495-8508.
- Bretterbauer, K., & Schwarzinger, C. (2012). Melamine derivatives-a review on synthesis and application. *Current Organic Synthesis*, 9(3), 342-356.
- Brinker, C. J., & Scherer, G. W. (2013). *Sol-gel science: the physics and chemistry of sol-gel processing*. Academic press.
- Britcher, L. G., Kehoe, D. C., Matisons, J. G., & Swincer, A. G. (1995). Siloxane coupling agents. *Macromolecules*, 28(9), 3110-3118.
- Burckhardt, U., & Cannas, R. (2018). U.S. Patent No. 9,988,482. Washington, DC: U.S. Patent and Trademark Office.
- Burger, V. M., Arenas, D. J., & Stultz, C. M. (2016). A structure-free method for quantifying conformational flexibility in proteins. *Scientific reports*, 6, 29040.
- Cademartiri, R., Brook, M. A., Pelton, R., & Brennan, J. D. (2009). Macroporous silica using a "sticky" Stöber process. *Journal of Materials Chemistry*, 19(11), 1583-1592.
- Cao, X. J., Cummins, H. Z., & Morris, J. F. (2010). Structural and rheological evolution of silica nanoparticle gels. *Soft Matter*, 6(21), 5425-5433.
- Chai, M. W., Bickerton, S., Bhattacharyya, D., & Das, R. (2012). Influence of natural fibre reinforcements on the flammability of bio-derived composite materials. *Composites Part B: Engineering*, 43(7), 2867-2874.
- Chen, H., Wang, J., Ni, A., Ding, A., Han, X., & Sun, Z. (2018). The effects of a macromolecular charring agent with gas phase and condense phase synergistic flame retardant capability on the properties of PP/IFR composites. *Materials*, 11(1), 111.
- Cheng, X. W., Guan, J. P., Chen, G., Yang, X. H., & Tang, R. C. (2016). Adsorption and flame retardant properties of bio-based phytic acid on wool fabric. *Polymers*, 8(4), 122.
- Chin, W. K., Shau, M. D., & Tsai, W. C. (1995). Synthesis, structure, and thermal properties of epoxy-imide resin cured by phosphorylated diamine. *Journal of Polymer Science Part A: Polymer Chemistry*, 33(3), 373-379.
- Cholake, S. T., Mada, M. R., Raman, R. S., Bai, Y., Zhao, X. L., Rizkalla, S., & Bandyopadhyay, S. (2014). Quantitative analysis of curing mechanisms of epoxy resin by mid-and near-fourier transform infra red spectroscopy. *Defence Science Journal*, 64(3), 314-321.
- Ciesielski, M., Schäfer, A., & Döring, M. (2008). Novel efficient DOPO-based flame-retardants for PWB relevant epoxy resins with high glass transition temperatures. *Polymers for Advanced Technologies*, 19(6), 507-515.
- Ciesielski, M., Diederichs, J., Döring, M., & Schäfer, A. (2009). Advanced flame-retardant epoxy resins for composite materials.
- Coleman, P. B. (Ed.). (1993). *Practical sampling techniques for infrared analysis*. CRC Press.
- Costa, L., & Camino, G. (1988). Thermal behaviour of melamine. *Journal of thermal analysis*, 34(2), 423-429.
- Crompton, T. R. (2013). *Characteristics and analysis of non-flammable polymers*. Smithers Rapra.
- Danzer, K. (2007). *Analytical chemistry: theoretical and metrological fundamentals*. Springer Science & Business Media.
- Dasari, A., Yu, Z. Z., Cai, G. P., & Mai, Y. W. (2013). Recent developments in the fire retardancy of polymeric materials. *Progress in Polymer Science*, 38(9), 1357-1387.
- Dave, B. C. (2016). *Sol-Gel Coating Methods in Biomedical Systems*. *Medical Coatings and Deposition Technologies*, 373.
- Davis, S. R., Brough, A. R., & Atkinson, A. (2003). Formation of silica/epoxy hybrid network polymers. *Journal of non-crystalline solids*, 315(1-2), 197-205.
- Dewey, L.H. "Hemp". In U. S. Department of Agriculture Yearbook 1913; U.S. Government Publishing Office: Washington, DC, USA, 1914; pp. 283-346.

- Ding, X., Zhao, J., Liu, Y., Zhang, H., & Wang, Z. (2004). Silica nanoparticles encapsulated by polystyrene via surface grafting and in situ emulsion polymerization. *Materials Letters*, 58(25), 3126-3130.
- Döring, M., & Diederichs, J. (2009). Non-reactive-fillers in innovative flame retardants in E&E applications, pinfa: Brussels.
- Drašar, P. (2016). Levy David, Zayat Marcos (ed.): *The Sol-Gel Handbook: Synthesis, Characterization and Applications*. *Chemické listy*, 110(3), 229-230.
- Dumitrascu, A., & Howell, B. A. (2012). Flame retardant polymeric materials achieved by incorporation of styrene monomers containing both nitrogen and phosphorus. *Polymer Degradation and Stability*, 97(12), 2611-2618.
- Durin-France, A., Ferry, L., Lopez Cuesta, J. M., & Crespy, A. (2000). Magnesium hydroxide/zinc borate/talc compositions as flame-retardants in EVA copolymer. *Polymer International*, 49(10), 1101-1105.
- Eerikäinen, H. (2005). Preparation of nanoparticles consisting of methacrylic polymers and drugs by an aerosol flow reactor method.
- Egerton, R. F. (2011). *Electron energy-loss spectroscopy in the electron microscope*. Springer Science & Business Media.
- EPA, U. (2005). Furniture flame retardancy partnership: Environmental profiles of chemical flame-retardant alternatives for low-density polyurethane foam. Environmental Protection Agency, Sep, <http://www.epa.gov/dfe> (last access: 24 September 2013).
- Fassel, V. A., & Kniseley, R. N. (1974). Inductively coupled plasma. *Optical emission spectroscopy*. *Analytical Chemistry*, 46(13), 1110A-1120a.
- Flego, C., & Zannoni, C. (2012). Direct Insertion Probe–Mass Spectrometry (DIP–MS) Maps and Multivariate Analysis in the Characterization of Crude Oils. *Energy & Fuels*, 27(1), 46-55.
- Fragassa, C., Pavlovic, A., & Santulli, C. (2018). Mechanical and impact characterisation of flax and basalt fibre vinylester composites and their hybrids. *Composites Part B: Engineering*, 137, 247-259.
- Freundlich, H., & Hatfield, H. (1926). *Colloid and Capillary Chemistry*, Methuen and Co. Ltd, London, UK.
- Fukuda, H., & Chou, T. W. (1981). A probabilistic theory for the strength of short fibre composites. *Journal of Materials Science*, 16(4), 1088-1096.
- Gadakh, V. S., Shinde, V. B., Khemnar, N. S., & Kumar, A. (2016, December). Application of MOORA Method for Friction Stir Welding Tool Material Selection. In *Techno-Societal 2016, International Conference on Advanced Technologies for Societal Applications* (pp. 845-854). Springer, Cham.
- Garcia, F. G., & Soares, B. G. (2003). Determination of the epoxide equivalent weight of epoxy resins based on diglycidyl ether of bisphenol A (DGEBA) by proton nuclear magnetic resonance. *Polymer Testing*, 22(1), 51-56.
- Glatter, O., & Kratky, O. (Eds.). (1982). *Small angle X-ray scattering*. Academic press.
- Gooneie, A., Simonetti, P., Salmeia, K. A., Gaan, S., Hufenus, R., & Heuberger, M. P. (2019). Enhanced PET processing with organophosphorus additive: Flame retardant products with added-value for recycling. *Polymer degradation and stability*, 160, 218-228.
- Grexa, O., & Lübke, H. (2001). Flammability parameters of wood tested on a cone calorimeter. *Polymer Degradation and Stability*, 74(3), 427-432.
- Gon, M., Tanaka, K., & Chujo, Y. (2017). Creative synthesis of organic–inorganic molecular hybrid materials. *Bulletin of the Chemical Society of Japan*, 90(5), 463-474.
- Grassie, N., Guy, M. I., & Tennent, N. H. (1985). Degradation of epoxy polymers: Part 1—Products of thermal degradation of bisphenol-A diglycidyl ether. *Polymer degradation and stability*, 12(1), 65-91.
- Grün, M., Lauer, I., & Unger, K. K. (1997). The synthesis of micrometer- and submicrometer-size spheres of ordered mesoporous oxide MCM-41. *Advanced Materials*, 9(3), 254-257.
- Guan, C., Lü, C. L., Liu, Y. F., & Yang, B. (2006). Preparation and characterization of high refractive index thin films of TiO₂/epoxy resin nanocomposites. *Journal of applied polymer science*, 102(2), 1631-1636.

- Gustavsson, M. B., Hellohf, A., & Backhaus, T. (2017). Evaluating the environmental hazard of industrial chemicals from data collected during the REACH registration process. *Science of The Total Environment*, 586, 658-665.
- Hacaloglu, J. (2011). Direct insertion probe mass spectrometry of polymers. In *Mass Spectrometry of Polymers—New Techniques* (pp. 69-103). Springer, Berlin, Heidelberg.
- Hampton, C., Demoin, D., & Glaser, R. E. (2010). *Vibrational spectroscopy tutorial: sulfur and phosphorus*. University of missouri, fall.
- Hapuarachchi, T. D., Ren, G., Fan, M., Hogg, P. J., & Peijs, T. (2007). Fire retardancy of natural fibre reinforced sheet moulding compound. *Applied Composite Materials*, 14(4), 251-264.
- Harris, R. K., Knight, C. T. G., & Hull, W. E. (1982). Soluble Silicates. In *ACS Symposium Series* (Vol. 194, pp. 79-93).
- Hautala, M., Pasila, A., & Pirilä, J. (2004). Use of hemp and flax in composite manufacture: a search for new production methods. *Composites Part A: Applied Science and Manufacturing*, 35(1), 11-16.
- Hergenrother, P. M., Thompson, C. M., Smith Jr, J. G., Connell, J. W., Hinkley, J. A., Lyon, R. E., & Moulton, R. (2005). Flame retardant aircraft epoxy resins containing phosphorus. *Polymer*, 46(14), 5012-5024.
- Herrick, F. W., Casebier, R. L., Hamilton, J. K., & Sandberg, K. R. (1983, January). Microfibrillated cellulose: morphology and accessibility. In *J. Appl. Polym. Sci.: Appl. Polym. Symp.:(United States)* (Vol. 37, No. CONF-8205234-Vol. 2). ITT Rayonier Inc., Shelton, WA.
- Hirsch, C., Striegl, B., Mathes, S., Adlhart, C., Edelmann, M., Bono, E., ... & Nyffeler, J. (2017). Multiparameter toxicity assessment of novel DOPO-derived organophosphorus flame retardants. *Archives of toxicology*, 91(1), 407-425.
- Hoang, D., & Kim, J. (2015). Flame-retarding behaviors of novel spirocyclic organo-phosphorus compounds based on pentaerythritol. *Macromolecular Research*, 23(7), 579-591.
- Holbery, J., & Houston, D. (2006). Natural-fiber-reinforced polymer composites in automotive applications. *Jom*, 58(11), 80-86.
- Honda, N., & Sugiyama, T. (1999). U.S. Patent No. 5,994,429. Washington, DC: U.S. Patent and Trademark Office.
- Hörold, S. (2002). U.S. Patent No. 6,420,459. Washington, DC: U.S. Patent and Trademark Office.
- Hoult, D. I., & Bhakar, B. (1997). NMR signal reception: Virtual photons and coherent spontaneous emission. *Concepts in Magnetic Resonance: An Educational Journal*, 9(5), 277-297.
- Hu, Q., Peng, P., Peng, S., Liu, J., Liu, X., Zou, L., & Chen, J. (2017). Flame-retardant epoxy resin based on aluminum monomethylphosphinate. *Journal of Thermal Analysis and Calorimetry*, 128(1), 201-210.
- Huang, X. (2018). Critical drip size and blue flame shedding of dripping ignition in fire. *Scientific reports*, 8(1), 16528.
- Hubbe, M. A., Rojas, O. J., Lucia, L. A., & Sain, M. (2008). Cellulosic nanocomposites: a review. *BioResources*, 3(3), 929-980.
- Huggett, C. (1980). Estimation of rate of heat release by means of oxygen consumption measurements. *Fire and Materials*, 4(2), 61-65.
- Hull, T. R., Stec, A. A., & Paul, K. T. (2008). Hydrogen chloride in fires. *Fire Safety Science*, 9, 665-676.
- Hüsing, N., Schubert, U., Misof, K., & Fratzl, P. (1998). Formation and Structure of Porous Gel Networks from Si (OMe) 4 in the Presence of A (CH2) n Si (OR) 3 (A= Functional Group). *Chemistry of materials*, 10(10), 3024-3032.
- Iler, K. R. (1979). *The chemistry of silica. Solubility, Polymerization, Colloid and Surface Properties and Biochemistry of Silica*.
- Innocenzi, P., Kidchob, T., & Yoko, T. (2005). Hybrid organic-inorganic sol-gel materials based on epoxy-amine systems. *Journal of sol-gel science and technology*, 35(3), 225-235.
- Islam, M. S., Pickering, K. L., & Foreman, N. J. (2011). Influence of alkali fiber treatment and fiber processing on the mechanical properties of hemp/epoxy composites. *Journal of applied polymer science*, 119(6), 3696-3707.

- Jian, R., Wang, P., Duan, W., Wang, J., Zheng, X., & Weng, J. (2016). Synthesis of a novel P/N/S-containing flame retardant and its application in epoxy resin: thermal property, flame retardance, and pyrolysis behavior. *Industrial & Engineering Chemistry Research*, 55(44), 11520-11527.
- Jiao, J., Liu, P., Wang, L., & Cai, Y. (2013). One-step synthesis of improved silica/epoxy nanocomposites with inorganic-organic hybrid network. *Journal of Polymer Research*, 20(8), 202.
- Johnsen, B. B., Kinloch, A. J., Mohammed, R. D., Taylor, A. C., & Sprenger, S. (2007). Toughening mechanisms of nanoparticle-modified epoxy polymers. *Polymer*, 48(2), 530-541.
- Ju, H., Zhang, X., & Wang, J. (2011). Biosensors based on sol-gel nanoparticle matrices. In *NanoBiosensing* (pp. 305-332). Springer, New York, NY.
- Kafshgari, L. A., Ghorbani, M., & Azizi, A. (2019). Synthesis and characterization of manganese ferrite nanostructure by co-precipitation, sol-gel, and hydrothermal methods. *Particulate Science and Technology*, 37(7), 900-906.
- Kalia, S., Boufi, S., Celli, A., & Kango, S. (2014). Nanofibrillated cellulose: surface modification and potential applications. *Colloid and Polymer Science*, 292(1), 5-31.
- Kandola, B. K., Mistik, S. I., Pornwannachai, W., & Anand, S. C. (2018). Natural fibre-reinforced thermoplastic composites from woven-nonwoven textile preforms: Mechanical and fire performance study. *Composites Part B: Engineering*, 153, 456-464.
- Kango, S., Kalia, S., Celli, A., Njuguna, J., Habibi, Y., & Kumar, R. (2013). Surface modification of inorganic nanoparticles for development of organic-inorganic nanocomposites—A review. *Progress in Polymer Science*, 38(8), 1232-1261.
- Kambara, K., Shimura, N., & Ogawa, M. (2007). Larger scale syntheses of surfactant-templated nanoporous silica spherical particles by the Stöber method. *Journal of the Ceramic Society of Japan*, 115(1341), 315-318.
- Kickelbick, G. (2007). *Introduction to hybrid materials. Hybrid materials*, 1, 2.
- Kirkland, E. J. (2010). *Advanced computing in electron microscopy*. Springer Science & Business Media.
- Kleiner, H. J., Budzinsky, W., & Kirsch, G. (1998). U.S. Patent No. 5,780,534. Washington, DC: U.S. Patent and Trademark Office.
- Kolbe, G. (1956). *Das komplexchemische verhalten der kieselsaure.* phdthesis. Friedrich-Schiller-Universität Jena.
- König, A., & Kroke, E. (2012). Flame retardancy working mechanism of methyl-DOPO and MPPP in flexible polyurethane foam. *Fire and Materials*, 36(1), 1-15.
- Kruk, M., Jaroniec, M., & Sayari, A. (1999). Surface heterogeneity analysis of MCM-41 metallosilicates by using nitrogen adsorption data. *Langmuir*, 15(18), 5683-5688.
- LaMer, V. K., & Dinegar, R. H. (1950). Theory, production and mechanism of formation of monodispersed hydrosols. *Journal of the American Chemical Society*, 72(11), 4847-4854.
- Laoutid, F., Bonnaud, L., Alexandre, M., Lopez-Cuesta, J. M., & Dubois, P. (2009). New prospects in flame retardant polymer materials: from fundamentals to nanocomposites. *Materials science and engineering: R: Reports*, 63(3), 100-125.
- Larin, E. A., & Atroshchenko, Y. M. (2016). Epoxide ring-opening approach to the synthesis of diverse trisubstituted cyclopentanes. *ARKIVOC*, 4, 217-226.
- Lazko, J., Landercy, N., Laoutid, F., Dangreau, L., Huguet, M. H., & Talon, O. (2013). Flame retardant treatments of insulating agro-materials from flax short fibres. *Polymer degradation and stability*, 98(5), 1043-1051.
- Levchik, S. V., Costa, L., & Camino, G. (1992). Effect of the fire-retardant, ammonium polyphosphate, on the thermal decomposition of aliphatic polyamides: part II—polyamide 6. *Polymer Degradation and Stability*, 36(3), 229-237.
- Levchik, S. V., Levchik, G. F., Balabanovich, A. I., Camino, G., & Costa, L. (1996). Mechanistic study of combustion performance and thermal decomposition behaviour of nylon 6 with added halogen-free fire retardants. *Polymer Degradation and Stability*, 54(2-3), 217-222.
- Levchik, S. V., Camino, G., Luda, M. P., Costa, L., Muller, G., & Costes, B. (1998). Epoxy resins cured with aminophenylmethylphosphine oxide—II. Mechanism of thermal decomposition. *Polymer degradation and stability*, 60(1), 169-183.

- Levchik, S. V., Bright, D. A., Dashevsky, S., & Moy, P. (2001). *Specialty Polymer Additives. Principles and Applications*.
- Lewin, M., & Weil, E. D. (2001). *Mechanisms and modes of action in flame retardancy of polymers. Fire retardant materials, 1*, 31-68.
- Lin, C. H., Cai, S. X., & Lin, C. H. (2005). *Flame-retardant epoxy resins with high glass-transition temperatures. II. Using a novel hexafunctional curing agent: 9, 10-dihydro-9-oxa-10-phosphaphenanthrene 10-yl-tris (4-aminophenyl) methane. Journal of Polymer Science Part A: Polymer Chemistry, 43(23)*, 5971-5986.
- Liu, Y. L., Hsiue, G. H., Lee, R. H., & Chiu, Y. S. (1997). *Phosphorus-containing epoxy for flame retardant. III: Using phosphorylated diamines as curing agents. Journal of applied polymer science, 63(7)*, 895-901.
- Liu, Y. L. (2002). *Epoxy resins from novel monomers with a bis-(9, 10-dihydro-9-oxa-10-oxide-10-phosphaphenanthrene-10-yl-) substituent. Journal of Polymer Science Part A: Polymer Chemistry, 40(3)*, 359-368.
- Liu, S., Lu, L., Yang, Z., Cool, P., & Vansant, E. F. (2006). *Further investigations on the modified Stöber method for spherical MCM-41. Materials chemistry and physics, 97(2-3)*, 203-206.
- Liu, J., Qiao, S. Z., Liu, H., Chen, J., Orpe, A., Zhao, D., & Lu, G. Q. (2011). *Extension of the Stöber method to the preparation of monodisperse resorcinol-formaldehyde resin polymer and carbon spheres. Angewandte Chemie International Edition, 50(26)*, 5947-5951.
- Liu, J., Tang, J., Wang, X., & Wu, D. (2012). *Synthesis, characterization and curing properties of a novel cycloliner phosphazene-based epoxy resin for halogen-free flame retardancy and high performance. RSC Advances, 2(13)*, 5789-5799.
- Liu, X., Salmeia, K. A., Rentsch, D., Hao, J., & Gaan, S. (2017). *Thermal decomposition and flammability of rigid PU foams containing some DOPO derivatives and other phosphorus compounds. Journal of analytical and applied pyrolysis, 124*, 219-229.
- Liu, M., Yin, H., Chen, X., Yang, J., Liang, Y., Zhang, J., ... & Lu, S. (2018). *Preliminary ecotoxicity hazard evaluation of DOPO-HQ as a potential alternative to halogenated flame retardants. Chemosphere, 193*, 126-133.
- Lu, S. Y., & Hamerton, I. (2002). *Recent developments in the chemistry of halogen-free flame retardant polymers. Progress in polymer science, 27(8)*, 1661-1712.
- Lü, C., & Yang, B. (2009). *High refractive index organic-inorganic nanocomposites: design, synthesis and application. Journal of Materials Chemistry, 19(19)*, 2884-2901.
- Lyon, R. E., & Walters, R. N. (2004). *Pyrolysis combustion flow calorimetry. Journal of Analytical and Applied Pyrolysis, 71(1)*, 27-46.
- Lyon, R. E., Walters, R. N., & Stoliarov, S. I. (2007). *Screening flame retardants for plastics using microscale combustion calorimetry. Polymer Engineering & Science, 47(10)*, 1501-1510.
- Mahapatra, S. S., & Karak, N. (2007). *s-Triazine containing flame retardant hyperbranched polyamines: synthesis, characterization and properties evaluation. Polymer degradation and stability, 92(6)*, 947-955.
- Mallakpour, S., & Madani, M. (2015). *A review of current coupling agents for modification of metal oxide nanoparticles. Progress in Organic Coatings, 86*, 194-207.
- Malucelli, G. (2016). *Surface-engineered fire protective coatings for fabrics through sol-gel and layer-by-layer methods: An overview. Coatings, 6(3)*, 33.
- Manfredi, L. B., Rodríguez, E. S., Wladyka-Przybylak, M., & Vázquez, A. (2006). *Thermal degradation and fire resistance of unsaturated polyester, modified acrylic resins and their composites with natural fibres. Polymer degradation and stability, 91(2)*, 255-261.
- Mascia, L., Prezzi, L., & Lavorgna, M. (2005). *Peculiarities in the solvent absorption characteristics of epoxy-siloxane hybrids. Polymer Engineering & Science, 45(8)*, 1039-1048.
- Mascia, L., Prezzi, L., & Haworth, B. (2006). *Substantiating the role of phase bicontinuity and interfacial bonding in epoxy-silica nanocomposites. Journal of materials science, 41(4)*, 1145-1155.
- Masse, S., Laurent, G., Chuburu, F., Cadiou, C., Déchamps, I., & Coradin, T. (2008). *Modification of the Stöber process by a polyazamacrocyclic leading to unusual core-shell silica nanoparticles. Langmuir, 24(8)*, 4026-4031.

- Masse, S., Laurent, G., & Coradin, T. (2009). Influence of cyclic polyamines on silica formation during the Stöber process. *Physical Chemistry Chemical Physics*, 11(43), 10204-10210.
- Matějka, L., Pleštil, J., & Dušek, K. (1998). Structure evolution in epoxy–silica hybrids: sol–gel process. *Journal of Non-crystalline solids*, 226(1-2), 114-121.
- Matějka, L., Dušek, K., Pleštil, J., Kříž, J., & Lednický, F. (1999). Formation and structure of the epoxy-silica hybrids. *Polymer*, 40(1), 171-181.
- Matějka, L., Dukh, O., & Kolařík, J. (2000). Reinforcement of crosslinked rubbery epoxies by in-situ formed silica. *Polymer*, 41(4), 1449-1459.
- Matura, M., Ettler, V., & Klementová, M. (2012). Transmission electron microscopy investigation of colloids and particles from landfill leachates. *Waste Management & Research*, 30(5), 530-541.
- Matzen, M., Kandola, B., Huth, C., & Scharrel, B. (2015). Influence of flame retardants on the melt dripping behaviour of thermoplastic polymers. *Materials*, 8(9), 5621-5646.
- Meltzer, D., Gottlieb, H. E., Amir, A., Shimon, L. J., & Fischer, B. (2015). Novel crown-ether–methylenediphosphonotetrathioate hybrids as Zn (ii) chelators. *Dalton Transactions*, 44(48), 21073-21080.
- Missoum, K., Belgacem, M. N., & Bras, J. (2013). Nanofibrillated cellulose surface modification: a review. *Materials*, 6(5), 1745-1766.
- Morgan, A. B., & Bundy, M. (2007). Cone calorimeter analysis of UL-94 V-rated plastics. *Fire and Materials: An International Journal*, 31(4), 257-283.
- Morgan, A. B., & Gilman, J. W. (2013). An overview of flame retardancy of polymeric materials: application, technology, and future directions. *Fire and Materials*, 37(4), 259-279.
- Musto, P., Ragosta, G., Russo, P., & Mascia, L. (2001). Thermal-Oxidative degradation of epoxy and epoxy-Bismaleimide networks: kinetics and mechanism. *Macromolecular chemistry and physics*, 202(18), 3445-3458.
- Musto, P. (2003). Two-Dimensional FTIR spectroscopy studies on the thermal-oxidative degradation of epoxy and epoxy– bis (maleimide) networks. *Macromolecules*, 36(9), 3210-3221.
- Mutin, P. H., & Vioux, A. (2013). Recent advances in the synthesis of inorganic materials via non-hydrolytic condensation and related low-temperature routes. *Journal of Materials Chemistry A*, 1(38), 11504-11512.
- Nagy, D., Krassóy, M., Zeke, I., Pásztor-Huszár, K., & Balla, C. (2013). Effects of different freezing methods on some properties of a pasta filata cheese. *Acta Alimentaria*, 42(Supplement 1), 45-52.
- Nait-Ali, L. K., Colin, X., & Bergeret, A. (2011). Kinetic analysis and modelling of PET macromolecular changes during its mechanical recycling by extrusion. *Polymer degradation and stability*, 96(2), 236-246.
- Nakagaito, A. N., & Yano, H. (2005). Novel high-strength biocomposites based on microfibrillated cellulose having nano-order-unit web-like network structure. *Applied Physics A*, 80(1), 155-159.
- Nazir, T., Afzal, A., Siddiqi, H. M., Ahmad, Z., & Dumon, M. (2010). Thermally and mechanically superior hybrid epoxy–silica polymer films via sol–gel method. *Progress in Organic Coatings*, 69(1), 100-106.
- Nechyporchuk, O., Belgacem, M. N., & Bras, J. (2016). Production of cellulose nanofibrils: A review of recent advances. *Industrial Crops and Products*, 93, 2-25.
- Nixon, A., Burchell, M. J., Price, M. C., Kearsley, A. T., & Jones, S. (2012). Aerogel tracks made by impacts of glycine: Implications for formation of bulbous tracks in aerogel and the Stardust mission. *Meteoritics & Planetary Science*, 47(4), 623-633.
- North, G. R., Pyle, J. A., & Zhang, F. (Eds.). (2014). *Encyclopedia of atmospheric sciences (Vol. 1)*. Elsevier.
- Nykter, M. (2006). *Microbial quality of hemp (Cannabis sativa L.) and flax (Linum usitatissimum L.) from plants to thermal insulation*.
- Pagliuca, A. (2011). U.S. Patent Application No. 13/143,696.
- Pearce, E. M. (1997). *Thermal characterization of polymeric materials*, edited by Edith A. Turi, Academic Press, San Diego, CA, 1997, 2420 pp. Price: \$375.00. *Journal of Polymer Science Part A: Polymer Chemistry*, 35(12), 2535-2537.

- Phonthammachai, N., Chia, H., & He, C. (2012). One-step synthesis of oval shaped silica/epoxy nanocomposite: process, formation mechanism and properties. In *The Delivery of Nanoparticles*. IntechOpen.
- Pielichowski, K., Njuguna, J., Janowski, B., & Pielichowski, J. (2006). Polyhedral oligomeric silsesquioxanes (POSS)-containing nanohybrid polymers. In *Supramolecular Polymers Polymeric Betains Oligomers* (pp. 225-296). Springer, Berlin, Heidelberg.
- Piscitelli, F., Lavorgna, M., Buonocore, G. G., Verdolotti, L., Galy, J., & Mascia, L. (2013). Plasticizing and Reinforcing Features of Siloxane Domains in Amine-Cured Epoxy/Silica Hybrids. *Macromolecular Materials and Engineering*, 298(8), 896-909.
- Piscitelli, F., Buonocore, G. G., Lavorgna, M., Verdolotti, L., Pricl, S., Gentile, G., & Mascia, L. (2015). Peculiarities in the structure–Properties relationship of epoxy-silica hybrids with highly organic siloxane domains. *Polymer*, 63, 222-229.
- Pope, E. J. A., & Mackenzie, J. D. (1986). *J. of Non-Cryst. Solids*, 87, 185.
- Potter WG (1970) *Epoxide resins*. Springer-Verlag Inc, New York, NY.
- Price, D., Bullett, K. J., Cunliffe, L. K., Hull, T. R., Milnes, G. J., Ebdon, J. R., ... & Joseph, P. (2005). Cone calorimetry studies of polymer systems flame retarded by chemically bonded phosphorus. *Polymer degradation and stability*, 88(1), 74-79.
- Prival, M. J., McCoy, E. C., Gutter, B., & Rosendranz, H. S. (1977). Tris (2, 3-dibromopropyl) phosphate: Mutagenicity of a widely used flame retardant. *Science*, 195(4273), 76-78.
- Prokop, A., Iwasaki, Y., & Harada, A. (2014). *Intracellular Delivery II*.
- Prouzet, É., & Boissière, C. (2005). A review on the synthesis, structure and applications in separation processes of mesoporous MSU-X silica obtained with the two-step process. *Comptes Rendus Chimie*, 8(3-4), 579-596.
- Puglia, D., Biagiotti, J., & Kenny, J. M. (2005). A review on natural fibre-based composites—Part II: Application of natural reinforcements in composite materials for automotive industry. *Journal of Natural Fibers*, 1(3), 23-65.
- Pulokas, J., Green, C., Kisseberth, N., Potter, C. S., & Carragher, B. (1999). Improving the positional accuracy of the goniometer on the Philips CM series TEM. *Journal of structural biology*, 128(3), 250-256.
- Qiu, B., Xing, M., & Zhang, J. (2015). Stöber-like method to synthesize ultralight, porous, stretchable Fe₂O₃/graphene aerogels for excellent performance in photo-Fenton reaction and electrochemical capacitors. *Journal of Materials Chemistry A*, 3(24), 12820-12827.
- Rakotomalala, M., Wagner, S., & Döring, M. (2010). Recent developments in halogen free flame retardants for epoxy resins for electrical and electronic applications. *Materials*, 3(8), 4300-4327.
- Rakotomalala, M., Ciesielski, M., Zevaco, T., & Doering, M. (2011). New phosphacyclic molecules and their application as flame retardants for epoxy resins. *Phosphorus, Sulfur, and Silicon and the Related Elements*, 186(4), 989-996.
- Ramirez, A., Lopez, B. L., & Sierra, L. (2003). Study of the acidic sites and their modifications in mesoporous silica synthesized in acidic medium under quiescent conditions. *The Journal of Physical Chemistry B*, 107(35), 9275-9280.
- Ramírez, C., Rico, M., Barral, L., Diez, J., García-Garabal, S., & Montero, B. (2007). Organic/inorganic hybrid materials from an epoxy resin cured by an amine silsesquioxane. *Journal of thermal analysis and calorimetry*, 87(1), 69-72.
- Randle, R. R., & Whiffen, D. H. (1956). The infra-red intensities of a band near 1020 cm⁻¹ in mono- and para-substituted benzene derivatives. *Transactions of the Faraday Society*, 52, 9-13.
- Reddy, B. (Ed.). (2011). *Advances in Nanocomposites: Synthesis, Characterization and Industrial Applications*. BoD—Books on Demand.
- Reti, C., Casetta, M., Duquesne, S., Delobel, R., Soulestin, J., & Bourbigot, S. (2009). Intumescent biobased-poly lactide films to flame retard nonwovens. *Journal of Engineered Fibers and Fabrics*, 4(2), 155892500900400206.
- Ruhemann, S. (1910). CXXXII.—Cyclic di- and tri-ketones. *Journal of the Chemical Society, Transactions*, 97, 1438-1449.
- Saheb, D. N., & Jog, J. P. (1999). Natural fiber polymer composites: a review. *Advances in Polymer Technology: Journal of the Polymer Processing Institute*, 18(4), 351-363.

- Saito, T., & Ohishi, H. (1981). U.S. Patent No. 4,280,951. Washington, DC: U.S. Patent and Trademark Office.
- Salmeia, K. A., & Gaan, S. (2015a). An overview of some recent advances in DOPO-derivatives: chemistry and flame retardant applications. *Polymer degradation and stability*, 113, 119-134.
- Salmeia, K. A., Fage, J., Liang, S., & Gaan, S. (2015b). An overview of mode of action and analytical methods for evaluation of gas phase activities of flame retardants. *Polymers*, 7(3), 504-526.
- Salmeia, K. A., Gooneie, A., Simonetti, P., Nazir, R., Kaiser, J. P., Rippl, A., ... & Gaan, S. (2018). Comprehensive study on flame retardant polyesters from phosphorus additives. *Polymer degradation and stability*, 155, 22-34.
- Salmeia, K. A., Neels, A., Parida, D., Lehner, S., Rentsch, D., & Gaan, S. (2019). Insight into the Synthesis and Characterization of Organophosphorus-Based Bridged Triazine Compounds. *Molecules*, 24(14), 2672.
- Sandler, S. R. (1979). U.S. Patent No. 4,180,495. Washington, DC: U.S. Patent and Trademark Office.
- Sangermano, M., Malucelli, G., Amerio, E., Bongiovanni, R., Priola, A., Di Gianni, A., ... & Rizza, G. (2006). Preparation and characterization of nanostructured TiO₂/epoxy polymeric films. *Macromolecular Materials and Engineering*, 291(5), 517-523.
- Savvas, D., & Ntatsi, G. (2015). Biostimulant activity of silicon in horticulture. *Scientia Horticulturae*, 196, 66-81.
- Saxena, M., Pappu, A., Sharma, A., Haque, R., & Wankhede, S. (2011). Composite materials from natural resources: Recent trends and future potentials. In *Advances in composite materials-Analysis of natural and man-made materials*. IntechOpen.
- Schartel, B., Pawlowski, K. H., & Lyon, R. E. (2007). Pyrolysis combustion flow calorimeter: a tool to assess flame retarded PC/ABS materials?. *Thermochimica Acta*, 462(1-2), 1-14.
- Schartel, B. (2010). Phosphorus-based flame retardancy mechanisms—old hat or a starting point for future development?. *Materials*, 3(10), 4710-4745.
- Schubert, U. (2003). Silica-based and transition metal-based inorganic-organic hybrid materials—A comparison. *Journal of sol-gel science and technology*, 26(1-3), 47-55.
- Seraj, S., Ranjbar, Z., & Jannesari, A. (2014). Synthesis and characterization of an anticratering agent based on APTES for cathodic electrocoatings. *Progress in Organic Coatings*, 77(11), 1735-1740.
- Seibold, S., Schäfer, A., Lohstroh, W., Walter, O., & Döring, M. (2008). Phosphorus-containing terephthaldialdehyde adducts—Structure determination and their application as flame retardants in epoxy resins. *Journal of applied polymer science*, 108(1), 264-271.
- Shau, M. D., & Wang, T. S. (1996). Syntheses, structure, reactivity, and thermal properties of new cyclic phosphine oxide epoxy resins cured by diamines. *Journal of Polymer Science Part A: Polymer Chemistry*, 34(3), 387-396.
- Shimizu, T., Kanamori, K., & Nakanishi, K. (2017). Silicone-based organic-inorganic hybrid aerogels and xerogels. *Chemistry—A European Journal*, 23(22), 5176-5187.
- Shirokane, K., Wada, T., Yoritake, M., Minamikawa, R., Takayama, N., Sato, T., & Chida, N. (2014). Total Synthesis of (±)-Gephyrotoxin by Amide-Selective Reductive Nucleophilic Addition. *Angewandte Chemie International Edition*, 53(2), 512-516.
- Sideridis, E., Venetis, J., & Kytopoulos, V. (2018). The Stiffness of Short and Randomly Distributed Fiber Composites. *WSEAS Transactions on Applied and Theoretical Mechanics*, 13, 85-91.
- Šimon, I., & McMahon, H. O. (1953). Study of some binary silicate glasses by means of reflection in infrared. *Journal of the American Ceramic Society*, 36(5), 160-164.
- Singh, H., & Jain, A. K. (2009). Ignition, combustion, toxicity, and fire retardancy of polyurethane foams: a comprehensive review. *Journal of Applied Polymer Science*, 111(2), 1115-1143.
- Singh, D., & Narula, A. K. (2010). Studies on the curing and thermal behaviour of diglycidyl ether of bisphenol-A (DGEBA) in the presence of aromatic diimide-diacids. *Journal of thermal analysis and calorimetry*, 100(1), 199-205.
- Singh, V. B. (2015). Spectroscopic signatures and structural motifs in isolated and hydrated theophylline: a computational study. *RSC Advances*, 5(15), 11433-11444.

- Sonnier, R., Dorez, G., Vahabi, H., Longuet, C., & Ferry, L. (2014). FTIR–PCFC coupling: A new method for studying the combustion of polymers. *Combustion and Flame*, 161(5), 1398-1407.
- Spence, K. L., Venditti, R. A., Rojas, O. J., Habibi, Y., & Pawlak, J. J. (2011). A comparative study of energy consumption and physical properties of microfibrillated cellulose produced by different processing methods. *Cellulose*, 18(4), 1097-1111.
- Stöber, W., Fink, A., & Bohn, E. (1968). Controlled growth of monodisperse silica spheres in the micron size range. *Journal of colloid and interface science*, 26(1), 62-69.
- Stokes, D. (2008). *Principles and practice of variable pressure/environmental scanning electron microscopy (VP-ESEM)*. John Wiley & Sons.
- Stöver HDH (1996) *Polymeric materials encyclopedia*. CRC Press, Boca Raton.
- Su, X., Yi, Y., Tao, J., Qi, H., & Li, D. (2014). Synergistic effect between a novel triazine charring agent and ammonium polyphosphate on flame retardancy and thermal behavior of polypropylene. *Polymer degradation and stability*, 105, 12-20.
- Suardana, N. P. G., Ku, M. S., & Lim, J. K. (2011). Effects of diammonium phosphate on the flammability and mechanical properties of bio-composites. *Materials & Design*, 32(4), 1990-1999.
- Szolnoki, B., Bocz, K., Soti, P. L., Bodzay, B., Zimonyi, E., Toldy, A., ... & Marosi, G. (2015). Development of natural fibre reinforced flame retarded epoxy resin composites. *Polymer Degradation and Stability*, 119, 68-76.
- Tewari, K. S., & Vishnoi, N. K. (1976). *A textbook of organic chemistry*. Vikas Publishing House.
- Thomas, S., Paul, S. A., Pothan, L. A., & Deepa, B. (2011). Natural fibres: structure, properties and applications. In *Cellulose fibers: bio-and nano-polymer composites* (pp. 3-42). Springer, Berlin, Heidelberg.
- Torrens, F., Solar, L., Puchol, V., Latorre, J., Abad, C., & Campos, A. (2008). Incorporation of silica nanospherical particles into epoxy-amine crosslinked materials. *Polymers and Polymer Composites*, 16(2), 139-151.
- Troitzsch, J. (1983). *International plastics flammability handbook: principles-regulations-testing and approval*. Hanser.
- Tudorachi, N., & Mustata, F. (2017). Curing and thermal degradation of diglycidyl ether of bisphenol A epoxy resin crosslinked with natural hydroxy acids as environmentally friendly hardeners. *Arabian Journal of Chemistry*.
- Turbak, A. F., Snyder, F. W., & Sandberg, K. R. (1983a, January). Microfibrillated cellulose, a new cellulose product: properties, uses, and commercial potential. In *J. Appl. Polym. Sci.: Appl. Polym. Symp.:(United States)* (Vol. 37, No. CONF-8205234-Vol. 2). ITT Rayonier Inc., Shelton, WA.
- Turbak, A. F., Snyder, F. W., & Sandberg, K. R. (1983b). U.S. Patent No. 4,374,702. Washington, DC: U.S. Patent and Trademark Office.
- Uche, D. O. V. (2013). Sol-gel technique: A veritable tool for crystal growth. *Advances in applied science research*, 4(1), 506-510.
- UL 94. (2013). *The standard for safety of flammability of plastic materials for parts in devices and appliances testing*.
- Vacassy, R. R. J. F., Flatt, R. J., Hofmann, H., Choi, K. S., & Singh, R. K. (2000). Synthesis of microporous silica spheres. *Journal of colloid and interface science*, 227(2), 302-315.
- Van Blaaderen, A., Van Geest, J., & Vrij, A. (1992). Monodisperse colloidal silica spheres from tetraalkoxysilanes: particle formation and growth mechanism. *Journal of colloid and interface science*, 154(2), 481-501.
- Van Helden, A. K., Jansen, J. W., & Vrij, A. (1981). Preparation and characterization of spherical monodisperse silica dispersions in nonaqueous solvents. *Journal of Colloid and Interface Science*, 81(2), 354-368.
- Vandersall, H. L. (1971). Intumescent coating system, their development and chemistry. *J Fire Flamm*, 2, 97-140.
- Verbruggen, E. M. J., Rila, J. P., Traas, T. P., Posthuma-Doodeman, C. J. A. M., & Posthumus, R. (2006). *Environmental Risk Limits for several phosphate esters, with possible application as flame retardant*. RIVM rapport 601501024.
- Visakh, P. M., & Yoshihiko, A. (2015). *Flame retardants: Polymer blends, composites and nanocomposites*. Springer.

- Vogt, J. (1985). *Thermal analysis of epoxy-resins: identification of decomposition products*. *Thermochimica Acta*, 85, 411-414.
- Wambua, P., Ivens, J., & Verpoest, I. (2003). *Natural fibres: can they replace glass in fibre reinforced plastics?*. *Composites science and technology*, 63(9), 1259-1264.
- Wang, C. S., & Lee, M. C. (1998). *Synthesis and modification of a naphthalene-containing trifunctional epoxy resin for electronic applications*. *Journal of applied polymer science*, 70(10), 1907-1921.
- Wang, C. S., & Lin, C. H. (1999). *Properties and curing kinetic of diglycidyl ether of bisphenol A cured with a phosphorus-containing diamine*. *Journal of applied polymer science*, 74(7), 1635-1645.
- Wang, C. S., & Shieh, J. Y. (2001). U.S. Patent No. 6,291,626. Washington, DC: U.S. Patent and Trademark Office.
- Wang, D. Y. (Ed.). (2016). *Novel fire-retardant polymers and composite materials*. Woodhead Publishing.
- Waaijers, S. L., Hartmann, J., Soeter, A. M., Helmus, R., Kools, S. A., de Voogt, P., ... & Kraak, M. H. (2013). *Toxicity of new generation flame retardants to Daphnia magna*. *Science of the total environment*, 463, 1042-1048.
- Watson, E. S., & O'Neill, M. J. (1966). U.S. Patent No. 3,263,484. Washington, DC: U.S. Patent and Trademark Office.
- Weferling, N., & Schmitz, H. P. (2001). U.S. Patent No. 6,242,642. Washington, DC: U.S. Patent and Trademark Office.
- Wendels, S., Chavez, T., Bonnet, M., Salmeia, K. A., & Gaan, S. (2017). *Recent developments in organophosphorus flame retardants containing PC bond and their applications*. *Materials*, 10(7), 784.
- Wu, Q., Zhang, C., Liang, R., & Wang, B. (2009). *Combustion and thermal properties of epoxy/phenyltrisilanol polyhedral oligomeric silsesquioxane nanocomposites*. *Journal of Thermal Analysis and Calorimetry*, 100(3), 1009-1015.
- Yan, H., Lu, C., Jing, D., & Hou, X. (2013). *Chemical degradation of TGDDM/DDS epoxy resin in supercritical 1-propanol: Promotion effect of hydrogenation on thermolysis*. *Polymer degradation and stability*, 98(12), 2571-2582.
- Yan, H., Lu, C. X., Jing, D. Q., & Hou, X. L. (2014). *Chemical degradation of amine-cured DGEBA epoxy resin in supercritical 1-propanol for recycling carbon fiber from composites*. *Chinese Journal of Polymer Science*, 32(11), 1550-1563.
- Yu, P., Kirkpatrick, R. J., Poe, B., McMillan, P. F., & Cong, X. (1999). *Structure of calcium silicate hydrate (C-S-H): Near-, mid-, and far-infrared spectroscopy*. *Journal of the American Ceramic Society*, 82(3), 742-748.
- Zhan, G., Zhang, L., Tao, Y., Wang, Y., Zhu, X., & Li, D. (2014). *Anodic ammonia oxidation to nitrogen gas catalyzed by mixed biofilms in bioelectrochemical systems*. *Electrochimica Acta*, 135, 345-350.
- Zhang, R. X., Ni, Q. Q., Natsuki, T., & Iwamoto, M. (2007). *Mechanical properties of composites filled with SMA particles and short fibers*. *Composite Structures*, 79(1), 90-96.
- Zhang, W., He, X., Song, T., Jiao, Q., & Yang, R. (2014). *The influence of the phosphorus-based flame retardant on the flame retardancy of the epoxy resins*. *Polymer degradation and stability*, 109, 209-217.
- Zhang, W., Fina, A., Ferraro, G., & Yang, R. (2018). *FTIR and GCMS analysis of epoxy resin decomposition products feeding the flame during UL 94 standard flammability test. Application to the understanding of the blowing-out effect in epoxy/polyhedral silsesquioxane formulations*. *Journal of analytical and applied pyrolysis*, 135, 271-280.
- Zhao, Y., & Zhu, K. (2016). *Organic-inorganic hybrid lead halide perovskites for optoelectronic and electronic applications*. *Chemical Society Reviews*, 45(3), 655-689.
- Zhi, M., Liu, Q., Chen, H., Chen, X., Feng, S., & He, Y. (2019). *Thermal Stability and Flame Retardancy Properties of Epoxy Resin Modified with Functionalized Graphene Oxide Containing Phosphorus and Silicon Elements*. *ACS Omega*, 4(6), 10975-10984.

- Zhou, S., Song, L., Wang, Z., Hu, Y., & Xing, W. (2008). Flame retardation and char formation mechanism of intumescent flame retarded polypropylene composites containing melamine phosphate and pentaerythritol phosphate. *Polymer Degradation and Stability*, 93(10), 1799-1806.
- Zou, H., Wu, S., & Shen, J. (2008). Polymer/silica nanocomposites: preparation, characterization, properties, and applications. *Chemical reviews*, 108(9), 3893-3957.